Harvesting the weak angular reflections from the fundus of the human eye

On Measuring and Analyzing the Light wasted by the Retina

Jan van de Kraats

Harvesting the weak angular reflections from the fundus of the human eye

On Measuring and Analyzing the Light wasted by the Retina

Jan van de Kraats

Jan van de Kraats
Harvesting the weak angular reflections from the fundus of the human eye
Utrecht University, Faculty of Medicine, The Netherlands

ISBN: 9789039345962

Cover illustration:
Part of the spectrometer optics of the ProfSpec 3 instrument

Cover design: Pieter Smit, Jan van de Kraats

Printed by: Torendruk, Nijkerk, The Netherlands

Harvesting the weak angular reflections from the fundus of the human eye

On Measuring and Analyzing the Light wasted by the Retina

Het oogsten van het zwakke en hoekafhankelijke licht gereflecteerd aan het menselijke netvlies

Over het meten en analyseren van het licht dat ongebruikt
door het netvlies het oog weer verlaat
(met een samenvatting in het Nederlands)

Proefschrift

ter verkrijging van de graad van doctor aan de
Universiteit Utrecht op gezag van de rector magnificus,
prof. dr. J. C. Stoof, ingevolge het besluit van het
college voor promoties in het openbaar te verdedigen op
dinsdag 16 oktober des middags te 4.15 uur

door

Jan van de Kraats

geboren op 17 oktober 1949 te Putten

Promotor: prof. dr. D. van Norren

Co-promotor: dr. T. T. J. M. Berendschot

This thesis was financially supported by:

dr. F.P. Fischer Stichting,
Advanced Medical Optics, Inc (AMO) USA,
HOYA MEDICAL EUROPE GMBH,
NTS Optel BV.

Contents

Chapter 1

Introduction

Outline of the thesis
Anatomy of the Eye

Outline of the thesis

The main aim of this thesis was to increase the knowledge on the pathways of light in the eye as used in fundusreflectometry. I spent most of my career in the challenging development of fundusreflectometers. The complex spectral shape of the light reflected from the fovea, measured with these instruments, intrigued me for a long time. In that shape, it was possible to recognize elements like the strong absorption at short wavelengths caused by the eye lens. The macular pigment and blood obviously left an imprint, and with more difficulty, absorption by melanin was recognizable. But could this all be explained in a quantitative way? In 1996, I published my first extensive optical model of the spectral reflection from the fundus (Chapter 4). This thesis ends with an updated version of that model (Chapter 9), fully incorporating the angular properties of the light reflected by the fovea, in particular by the cone receptors. The parameters in the model represent the main reflecting layers in the eye, and the main losses of light in ocular absorbers.

After the Introduction, first a historical overview is presented of the electronics, the computers and the scientific instruments I was involved in during my almost 40 year with the Ophthalmology Department (Chapter 2). In Chapter 3 a more elaborate overview is given of the instruments used for this thesis. In between the chapters of the optical models (Chapter 4 and 9) Chapter 5 contains a pre-study for the final model work in Chapter 9. In this pre-study an extensive analysis of nearly the complete literature on the eye media is made. This was aimed to develop spectral templates and a formula for describing the optical losses in the eye media of a ‘mean subject’ for all wavelengths, at all ages. The (large) resulting formula was incorporated in the final optical model, replacing the more simple formula, taken from the literature, used in Chapter 4. The results from the study of the eye media also enabled to find the optimal balance between light protection and light reception in the optical filters of intraocular lenses (IOLs), implanted in cataract surgery (Chapter 6). The concept of ‘virtual age’ for IOLs might become a practical tool for the cataract surgeon (Chapter 7). A description of the last instrument that was developed, the Macular Pigment Meter follows in Chapter 8. The thesis ends with a summary and conclusions, samenvatting in het Nederlands, about the author / Curriculum Vitae, dankwoord , and a list of publications (Chapter 10).

Anatomy of the eye

The anatomy of the eye, with emphasis on the optical aspects, is briefly described here. Light enters the eye through the cornea (Fig. 1). The cornea is spherically shaped and it forms the first and most important refracting surface due to the large change in index of refraction encountered from air to the corneal tissue. In a spectral sense it heavily attenuates optical radiation below 320 nm, such that at about 300 nm the eye is virtually opaque to optical radiation. Next, the light passes the aqueous humor, which is optically very transparent, except in the far infrared. The lens is another optically important component. It forms the second largest refracting element, and it further spectrally filters the light, mainly as an additional block of the short wavelengths that are dangerous to the retina. The lens is optically limited in size by the circularly shaped pupil, the diameter of which depends on the intensity of the light falling on the retina. The diameter of the pupil can also be changed by pharmaceutical agents. In the measurements used in this thesis, the pupil was often fully dilated to have the most unobstructed view to the retina.
Light passing the lens enters the vitreous, like the aqueous humor an almost optically transparent element. The refraction of light by both the cornea and the lens forms an image of the world outside at the retina. The lens can adjust its shape to have a sharp view nearby, or at a distance; a property called accomodation. This property decreases with age and is lost at middle age. This is what calls for the need of reading spectacles, or other optical artifacts. Pharmaceutical agents for pupil dilation can also paralyze accomodation, which is often helpful during a measurement, because it stabilizes the focus.

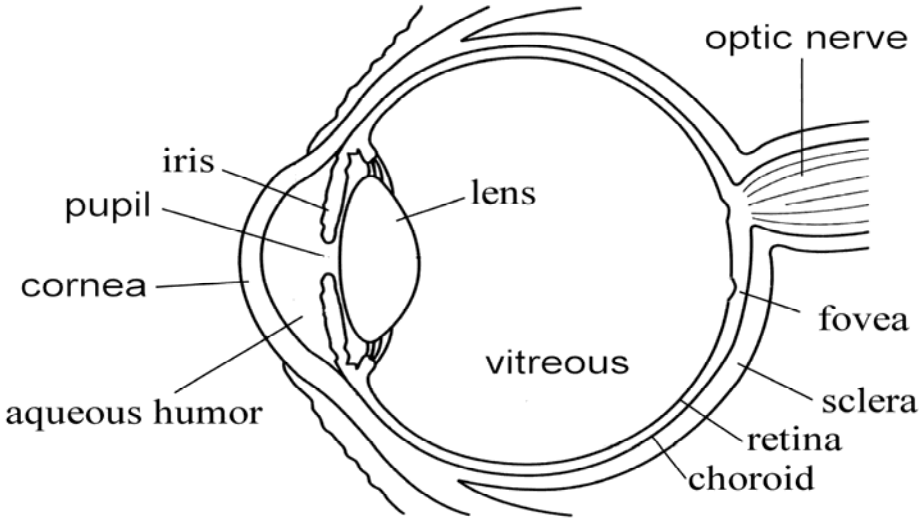

Fig. 1 Anatomical structures of the eye.

The most important part of the eye is the retina, as it contains the light receiving elements, the cones and the rods. The cones are most densely packed in a central area used for vision with the highest acuity, called the fovea. A somewhat larger central area is called the macula. The rods are absent in the central fovea, but very abundant

in the peripheral retina. Linked to the spatially peaked cone distribution is a layer of a yellow substance, the macular pigment. It gives the macula its other name, the yellow spot. Macular pigment mainly consists of lutein and zeaxanthin. The main function of macular pigment probably is its antioxidant property in the fight against free radicals, generated by the combination of high oxygen tension and light. Optical effects are the spectral filtering of dangerous blue light passing the cornea and eye lens filters, and possibly, reducing chromatic aberration in this area of very detailed vision.

The cone receptors are very important elements in the framework of this thesis. They are in fact optical antennas utilized to receive the light. Cones consist of a tapered inner segment which funnels the light to the cylindrically shaped outer segment. The outer segment contains a stack of discs which are rather transparent by nature, but it can be assumed that the discs have very tiny Fresnell reflections due to the small difference in the index of refraction between the discs and the interspaces. In the very center of the fovea cones are the only type of receptor being present, and they are so thin and tightly packed that their shape is almost cylindrical.
The optical antenna property of a cone has a preferred directional sensitivity in the forward direction. This was discovered in 1933 by Stiles and Crawford.[1] They found, with psychophysical means, that light entering the center of the pupil was about 5 times more efficient capturing light than light entering near the pupil's edge. This effect was later named the Stiles-Crawford effect (SCE1). Much later in 1965, Krauskopf[2] discovered that the optical antennas not only receive light, but they also reflect a tiny part of the incoming light back into the direction of the pupil. The shape of the directionality on entrance is, due to the reciprocity of light, also functional on emitting the light. The angular directionality at the retina forms a Gaussian shaped intensity distribution at the plane of the pupil. This is nowadays referred to as the Optical Stiles-Crawford Effect (OSCE). It plays an important role in this thesis.

The discs are also the locations were the visual pigments reside. Visual pigments are the first in the chain of converting light to an electrical signal send to the brain. There are three types of cones, each filled with a spectrally different visual pigment, the long wave sensitive (LWS), the medium wave sensitive (MWS), and the short wave sensitive (SWS) one. The amount of visual pigment present in the cones depends on the light history; a long time in the dark maximizes the amount, while high intensities bleach the visual pigments, making them virtually transparent in the visual spectral region. The outer segments are planted in the retinal pigment epithelium (RPE) like carrots in the soil. There, the receptors exchange their supply and waste products. If this contact is lost in a retinal disease, the receptor will eventually die. The outer segments are continuously renewed (disc shedding). New discs are continuously formed at the anterior end.

The RPE is a thin layer containing the pigment melanin, a substance with very strong light trapping properties. It screens the receptors at the back side from stray light from deeper layers. The RPE is attached to Bruch's membrane, a mechanically strong structure. The blood-brain barrier is formed by close contacts (so called tight junctions) between RPE cells. Posterior to Bruch's membrane is first a thin fenestrated layer of blood vessels, the choriocapillaris. Apart from supplying nutrients, it also serves to stabilize the temperature in case of high levels of illumination absorbed by the RPE. The sclera is a very strong structure at the outside of the eye; it

has a whitish appearance. Between the sclera and the choriocapillaris, we find the choroidal space filled with blood vessels, melanin particles, and tissue. In this thesis, layers posterior to the receptors are often referred to as the “deeper layers”

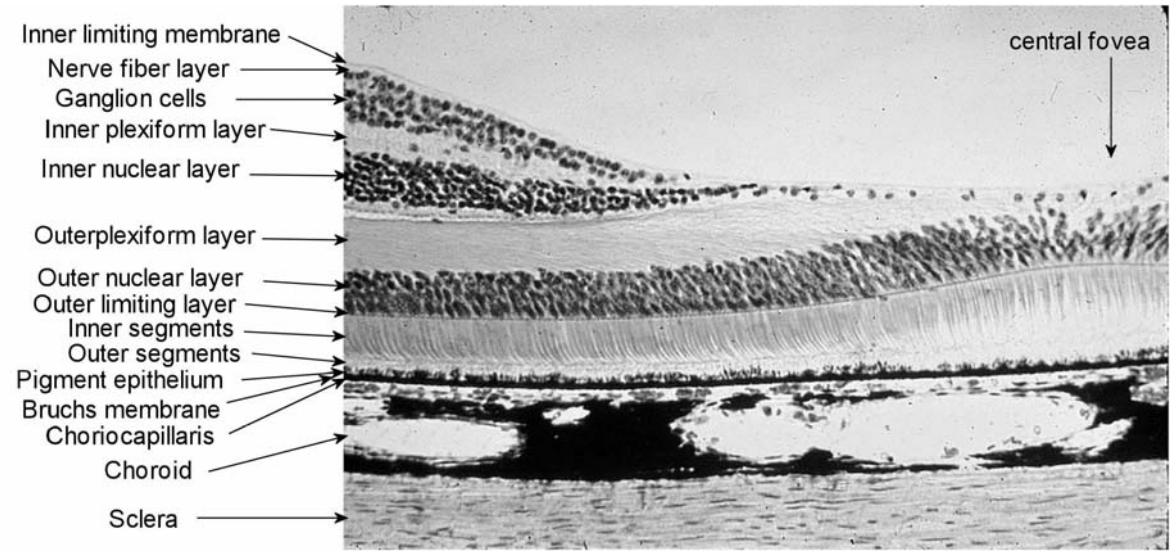

Fig 2 Details of the fovea; inner segments and outer segments are part of the photoreceptors. The central fovea is near the right of the image where the photoreceptors are the longest and neural layers the thinnest. The picture shows an area of 0.5 mm wide.

References

1. W. S. Stiles and B. H. Crawford, "The luminous efficiency of rays entering the eye pupil at different points," Proc. R. Soc. Lond. [Biol]. **112**, 428-450 (1933).

2. J. Krauskopf, "Some experiments with a photoelectric ophthalmoscope," in *Excerpta Medica, International Congress Series*, M. A. Bouman and J. J. Vos, eds., (Excerpta Medica, Amsterdam, 1965), pp. 171-181.

Chapter 2

Historic overview of Instruments developed in the Ophthalmic Physics Group

Evolution of the electronics.

I started in 1967 as an electronic designer in the group Medische en Physiologische Fysica led by Prof. M. A. Bouman, at the Ooglijdersgasthuis in Utrecht. At that time working with electronic tubes, which required heating power and a high voltage power supply, was common. Transistors just became available. They were mounted with other components on printed circuit boards. The boards had islands of copper traces and drilled holes, and connections were made with lead solder and a soldering iron. Philips at that time developed nice building blocks with small encapsulated circuit boards containing for instance a flipflop, a one-shot, or different gating functions.

An important (and very expensive) commercial instrument at that time was the Computer of Average Transients (CAT). It enabled averaging noisy responses from the retina (ElectroRetinoGram, ERG), the brain (Visual Evoked Potentials, VEP's), the pupil, or the eye lens etc., to less noisy traces. The CAT had a memory storage of 400 addresses containing 20 bits in the form of magnetic cores. Offline storage was on paper tape with the help of an electro-mechanical device called a teletype, a kind of telex machine. Calculation of, for instance, the Fourier Transform for estimating the frequency response, had to be done at the Control Data computer of the Medical Physics department, located at the Eisenhouwerlaan. Analog measurement data were also stored directly on a 50 Kg, 7 channel analog tape recorder (Philips Analog7).

Later, integrated circuits became available, both analog and digital. The analog operational amplifiers (OpAmp's) like the T52, and later the famous 741, made the design of amplifiers, filters, comparators, integrators, and voltage-to-frequency converters much easier. Digital functions of the well-known Transistor-Transistor-Logic (TTL) 7400 series had complete decade counters, buffers, and multiple gates in a 14 or 16 pin dual in line package. They were rather power hungry; a large board could easily draw several Amperes at 5 Volts. For the experimental designs, connections were made with a wire wrapping technique.

The microprocessor was introduced around 1971. The very first one was the 4 bits Intel 4004, which escaped my attention. But the second one, the 8 bits Intel 8008 from 1972 was used in one of our optical setups to generate psychophysical stimuli. To illustrate its simplicity, and thereby its complexity in handling, the booting program had to be initiated each time by feeding a code, by setting 8 switches, and pushing a button to single step it. This booting program then could read the rest of the program from paper tape with the help of a teletype. No hard coded memory was available, only a few hundred bytes of volatile RAM.

Later the Motorola 6800 microprocessor became popular. Non volatile memory in the form of EPROM contained the program, enabling to switch the instrument on and be functional. Developing that program was another matter. The program was typed in on a teletype; then the paper tape was taken to the Medical Physics Department at the Uithof to burn the program in EPROM. The EPROM was then put in the instrument located in the Ooglijdersgasthuis for testing. Debugging tools were limited to single stepping and displaying the address and data codes on a hexadecimal display. Single stepping a real time instrument was often not very helpful, so studying the program code was the only way left to solve a problem.

Storage on paper tape was followed by magnetic tape, followed by storage on rotating magnetic discs. Studying the software of very expensive commercial development stations (my first software piracy), enabled the development of software by own means. The first densitometer was possible due to this kind of technique. Its RAM memory size was 256 bytes. As a next step, TV boards enabled (together with editors

of own design) programming on a keyboard and viewing the program on a TV monitor.
The Atari 1040 personal computers were a big advance. They were used for development, for controlling the optical setup, for analyzing and storing the measurement data, and finally for writing scientific papers. The Ataries were succeeded by Microsoft based personal computers. The measuring instruments itself still contained a small microcomputer (e.g. of the type Motorola 6811) to deliver the quick responses needed for the real time functionality. They communicated with the personal computer by means of a serial connection like RS232.

Overview of instruments.

In the mid nineteenth century, Von Helmholtz introduced the principle of ophthalmoscopy. It opened the possibility of observing of the retina in the living eye through the natural pupil. Around 1950 the first attempts were made to quantify the retinal reflection by the application of sensitive detectors, in particular photomultiplier tubes. The electronics involved at that time were all analog; general amplifiers, lock-in amplifiers that only amplified a single frequency, and the output device was often a simple analog meter, or more sophisticated, a pen writer. With the introduction of digital electronics, more stable measurements became possible. At the same time the appearance of computers made real time calculations of the wanted end results feasible.

Reflectometer instruments that measured the reflection of a spot on the retina, with the aim of determining the optical density of the visual pigments, were called densitometers. In Chapter 3 I will discuss the latest model. Reflectometer instruments of the type that combined the spectral analysis of the light reflected from the spot on the retina, with the measurement of the angular properties, are also discussed in Chapter 3, together with a stripped down version specially designed for the measurement of macular pigment.

Since the end of the sixties I built, or helped to build, the following instruments.

1. Refractometer (thesis work of Gerjan van der Wildt).[1] This instrument was basically a two point Hartman-Shack device, although this name was not yet coined at that time. It measured the infrared reflection from a spot on the peripheral retina to obtain the refractive state of the eye lens, varying in real time, together with the pupil diameter, and horizontal eye movement. Detection was by scanning the reflected image over pairs of differential connected silicon photocells. The signals were amplified by electronic tubes.
2. Pupillometer (Aart Kooijman). This instrument was in fact an opto-mechanical television camera to image and measure the diameter of the pupil. It was based on a Nipkov disc made at TNO Soesterberg, which produced a raster by means of a fast scanning spot. The raster (only 100 lines) was imaged on the eye pupil, and the reflection was measured by a photomultiplier. The amplified video signal produced an image of the pupil on an oscilloscope and the connected electronics produced at the end an analog signal representing the pupil diameter. It was used to study the frequency and phase response of the pupil. Later setups, containing an infrared television camera, were used to study automatic perimetry, the response to jumps in wavelengths, and to alternating checkerboards presented on TV screens. It was the subject of my first paper.[2] The alternating checkerboard stimuli were later used for the thesis work of Jan Slooter.[3,4]
3. VEP meter. The VEP setup of Daan van Hoek was an outlier, as it did not use any detection of light reflected by the eye.[5] The stimuli were color steps produced on one of the first prototype color TV screens made by Philips. The TV tube was even not yet rectangular, but of circular shape. At first, responses were amplified by a chopper stabilized tube amplifier. A frequency modulator enabled storage on a commercial tape recorder. The data were analyzed at the Eisenhouwerlaan facility. Later, transistor amplifiers were used. The CAT was used for averaging the responses, and the data put on paper tape for further analysis.
4. Fluorophotometer. This was a device measuring fluorescence in a scan from the cornea to the retina, in order to quantify leakage from the retina. It was

started by Lo Bour, using a modified slitlamp. Later Jan Kees IJspeert put much effort in a completely self-supporting design.

5. Scanning reflectometer (thesis Gijsjan van Blokland).[6,7] This instrument had an Argon-Krypton mixed gas laser as the light source to illuminate a spot on the retina. The reflection profile in the pupil plane, bell-shaped because of the directional reflection of the foveal cones, was measured by scanning the sensitive area of a photomultiplier detector. A (primitive) model of the optical pathways in the retina was developed at that time (mid eighties).
6. Scanning Laser Ophthalmoscopes (SLOs). To obtain an image of the retina, instead of just the reflection from a small spot, an SLO was build. As originally invented by Robert Webb, the SLO (a kind of flying spot raster scanner, much like the Nipkov disc in our pupillometer) was not yet confocal. This means that the detector used all the light reflected from the retina. From our densitometer background we realized that by scanning the sensitive spot detector simultaneously, and in pace with the illuminated spot on the retina, much unwanted scattered light could be avoided. The first design (with much effort from Luuk Tiemeijer) was build according to this idea. It used lenses in a mirrored setup with separate scanning for the illumination part and the detection part. It was not performing very well because it was almost impossible to keep the detector area right on the illuminated spot during the whole scan. Robert Webb than introduced spherical mirrors instead of lenses.[8] It simplified the setup and alignment enormously, because now the scanning part could be used both for illumination and detection. We took his idea and build a setup which by clever positioning of the spherical mirrors cancelled astigmatism by large. This instrument was used for measuring visual pigment maps, and later for the obtaining Stiles-Crawford maps (thesis work Peter Jaap DeLint).[9,10] During the evolution of our SLOs, four different versions numbered SLO1 to SLO4 were developed.
7. Stiles-Crawford instrument. This was a device for psychophysical measurements of the Stiles-Crawford effect. The task was to minimize the contrast in a grating presented in a circular patch. Because of the lengthy measurements, it was not used very often.
8. The flicker macular pigment meter. This was an instrument for psychophysical assessment of the macular pigment by means of heterochromatic flicker photometry (HFP). Again, measurements were difficult to perform, especially for older subjects. Tos Berendschot used the instrument in comparing macular pigment values with different techniques.[11] The HFP results were taken out of the paper during the review process, because details were different from proven designs from the literature. It was not used thereafter.

References

1. G.J.van der Wildt and M.A.Bouman, "An accommodometer: an apparatus for measuring the total accommodation response of the human eye," Appl. Opt. **10**, 1950-1958 (1971).

2. J. van de Kraats and J. H. Slooter, "Objective measuring techniques with the aid of pupillography," Ophthalmologica **175**, 51-52 (1977).

3. J. Slooter and D. van Norren, "Visual acuity measured with pupil responses to checkerboard stimuli," Invest. Ophthalmol. Vis. Sci. **19**, 105-108 (1980).

4. J. Slooter, "Clinical use of visual acuity measured with pupil responses," Doc. Ophthalmol. **50**, 389-399 (1981).

5. L. D. van Hoek, "Multivariate vectorial analysis of the visual evoked response," Kybernetik. **15**, 65-72 (1974).

6. G. J. van Blokland, "Directionality and alignment of the foveal receptors, assessed with light scattered from the human fundus in vivo," Vision Res. **26**, 495-500 (1986).

7. G. J. van Blokland and D. van Norren, "Intensity and polarization of light scattered at small angles from the human fovea," Vision Res. **26**, 485-494 (1986).

8. R. H. Webb, G. W. Hughes, and F. C. Delori, "Confocal scanning laser ophthalmoscope," Appl. Opt. **26**, 1492-1499 (1987).

9. P. J. DeLint, T. T. J. M. Berendschot, and D. vanNorren, "Local photoreceptor alignment measured with a scanning laser ophthalmoscope," Vision Research **37**, 243-248 (1997).

10. P. J. DeLint, T. T. J. M. Berendschot, and D. van Norren, "A comparison of the optical Stiles-Crawford effect and retinal densitometry in a clinical setting," Invest. Ophthalmol. Vis. Sci. **39**, 1519-1523 (1998).

11. T. T. J. M. Berendschot, R. A. Goldbohm, W. A. Klöpping, J. van de Kraats, J. van Norel, and D. van Norren, "Influence of lutein supplementation on macular pigment, assessed with two objective techniques," Invest. Ophthalmol. Vis. Sci. **41**, 3322-3326 (2000).

Chapter 3

The three instruments used in this thesis

The Densitometer.

Four reflectometer instruments with the name densitometer were successively developed. Densitometer 1 occupied half a room in the Ooglijdersgasthuis. It was based on a Zeiss fundus camera, modified to run from the light from an optical bench with a Xenon arc source, optical channels with a special chopper wheel, beam splitters, interference filters etc. Measuring a complete spectrum was very time consuming. About 14 wavelengths could be selected, but only one at a time. The reflection of the fovea, the periphery, and the optic disc was used by Van Norren and Tiemeijer to develop a model of the optical reflection of the human eye containing reflection at the ILM, the RPE, and the sclera.[1] Absorption was supposed to occur in the eye lens, macular pigment, blood, and melanin. More clinically oriented was the thesis work of Gerard van Meel[2] and Jan Keunen[3] with this instrument.
The latest densitometer, number 4, was used for the 1996 model paper in Chapter 4. Clinical work for the thesis of Albert Liem[4,5] and Peter Jaap DeLint[6,7] was also done with this densitometer. A copy was exported to the USA, and used by prof. Joel Pokorny and prof. Vivianne Smith at the University of Chicago.[8] It has the size of a fundus camera, and is easily moved in front of the patient's eye with a joystick. The light source is a small 30 W halogen lamp (Fig 1a). It again contains a specially designed chopper wheel, in this case loaded with 16 interference filters from 410 to 740 nm. It spins at 14 revs per minute enabling quasi-simultaneous measurement of a complete spectrum. The spot on the retina from which the reflection is measured is selectable from 4 sizes (1.6, 2.4, 3.4, and 5.3 deg.). The illuminated spot on the retina is also selectable and is normally somewhat larger in size (1.9, 2.8, 4.2, and 6.3 deg.) compared to the measuring area, to avoid non-illuminated parts in case the retina not precisely in focus.
The detector is, as in all previous versions, a photomultiplicator tube (PMT), or photomultiplier. Light falling on the photocathode generates secondary electrons which, attracted by a large voltage difference, generate multiple secondary electrons on a nearby dynode. Ten of these multiplying steps enable gains of about 10^6, enough to generate micro-Amps with one detected photon. Counting photons instead of directly using the analog current has the advantage of neglecting leakage currents, and drift in analog amplifiers. Counting with a microprocessor in storage bins separately for the measuring wavelengths and dark periods supplied by the chopper wheel (Fig 1b), enables direct calculation of the log signal amplitudes, and double density of the measured visual pigment changes. The longest wavelength (740 nm), where visual pigment is virtually transparent, is used as a reference, compensating for sensitivity changes in the instrument. Finally, the signal counts measured in dark periods are used to compensate the 'measure' counts for changes in room light, and dark current of the photomultiplier. The microprocessor sends once a second a complete time averaged spectrum to a PC for further processing, viewing and storage.

To optimize the instrument for the measurement of the directional reflection of the cones, small and close together illumination and detection pupil areas were used (Fig 1c). This whole, so called pupil configuration, fits in a 2.5 mm eye pupil.
To keep the retina in an unbleached state, the total light was kept to the low value of 1200 Trolands (Td). For bleaching the retina a separate channel can be opened to deliver an unpleasantly high 5.8 log Td. Filtering with a Schott OG495 prevents light damage to the retina with long viewing times, and reduces photophobia. The field size of this channel is large (30 deg.) to enable viewing the retina at the viewing port on top of the instrument when the bleach is on.

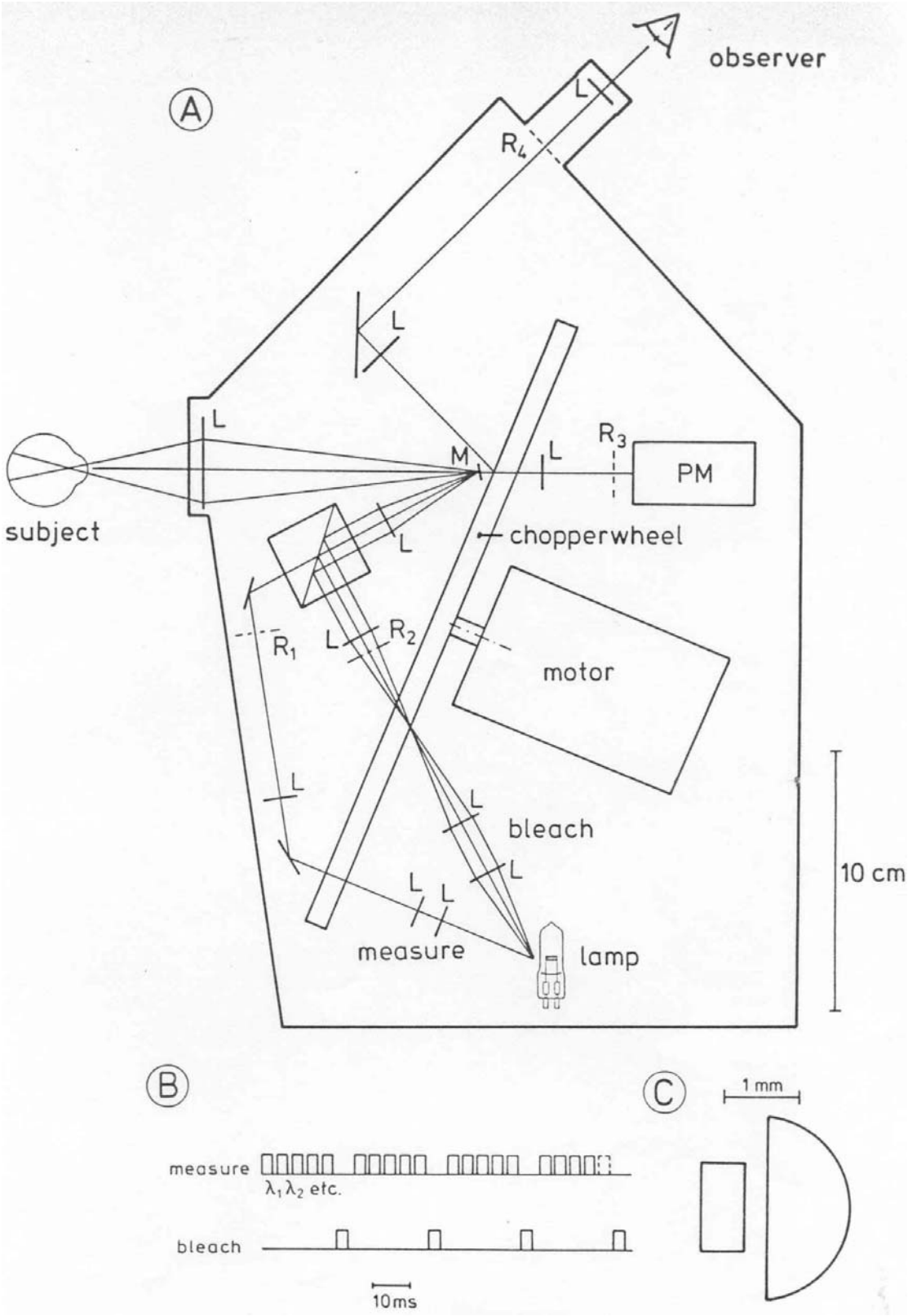

Fig 1. (a) Optics of densitometer 4. L Lenses; R planes conjugate to the retina; M little pupil separating mirror for separating illumination and detected light; PM photomultiplier.
(b) Sequence of the illumination periods for measuring at the different wavelengths, and for bleaching and viewing, provided by the chopper wheel. (c) Pupil configuration at the subjects pupil; rectangle is for illumination; semi-circle is for detection.

The densitometer, and all succeeding reflectometer instruments, are calibrated to provide reflection values relative to a 100% diffusely scattering retina. A device called the white reference has a white reflecting surface (Eastman 6080 white paint). Positioned at 10 times the focal length of the eye (230 mm) from the instruments pupil plane it delivers counts representing 1 % reflection. A second device called the dark reference, or "black hole", contains a photon destructor in the form of two tapered surfaces of shiny reflecting black Perspex. Positioned at the pupil plane of the instrument where illumination and detection beams are separated, light bounces between the tapered surfaces, each reflection destroys about 97% of the light, leaving virtually nothing to escape.

The Profile Spectrometer (ProfSpec) also called the Fundus Reflection Analyzer (FRA)

This reflectometer instrument is described in some detail in Chapter 9. It was designed for combining the spectral resolution of the Delori instrument[9] and the resolution in the pupil plane of the Van Blokland instrument.[10] A first prototype of the optical setup was build by Zagers on an optical bench, he called it the Fundus Reflection Analyzer (FRA).[11] Two later versions were desktop instruments aligned by a joystick. Their properties will be summarized below.

Delori illuminated a spot on the retina with white light. The reflected light was spectrally decomposed with a grating on to a CCD detector. Van Blokland also illuminated a (laser) spot on the retina with the entrance pupil optimized for the Stiles-Crawford 1 effect (SCE1). The detector was scanned along a line running over the pupil and near the entrance pupil. The ProfSpec again illuminated a spot of white light on the retina optimized for SCE1. A slit of 15 by 1 mm near the entrance pupil sampled with a resolution of 0.05 mm the directional and non-directional light reflected from the retina. Light passing through the slit was spectrally decomposed by a prism in a range from 400 to 950 nm. The resulting two-dimensional image was detected by a CCD camera with an integration time in the order of a second, and the instrument needs no scanning at all.

The high illumination levels of about 6 log Td will bleach the visual pigments in seconds. Dark adapted measurements are difficult in the current design. Perhaps the easiest way would be to present the illumination light in flashes with large intervals, simultaneously grabbing the data from the CCD.

The instrument is provided with two extra CCD cameras, one for viewing and focusing the spot on the retina, and another for viewing the pupil of the subject for aligning purposes.

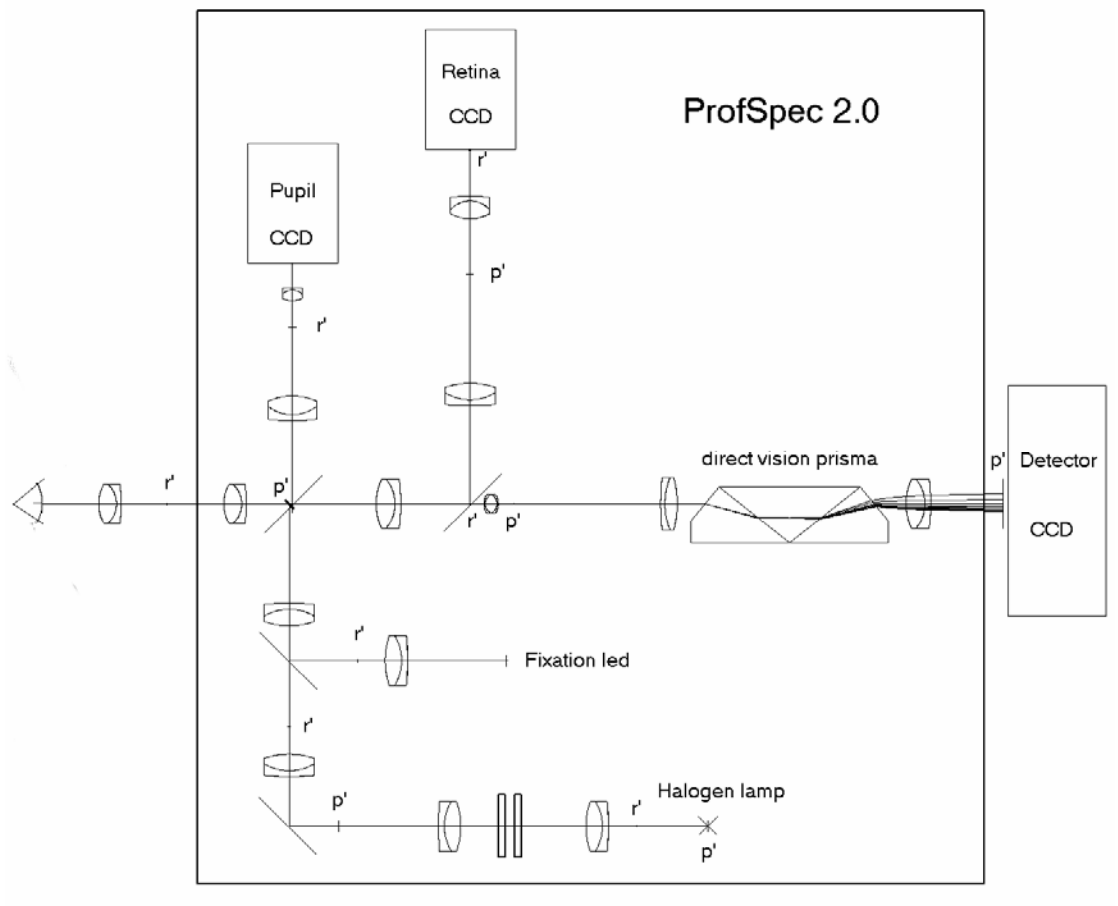

Fig. 2. The optical scheme of ProfSpec 2. The illumination channel starts at the halogen lamp at the bottom of the figure and goes towards the eye (left). The right part at the center line with the direct vision prism and the detector CCD forms the imaging spectrometer. At the top are the channels for viewing the subjects' pupil and retina. Planes conjugate to the pupil are marked with p, and planes conjugate to the retina with r.

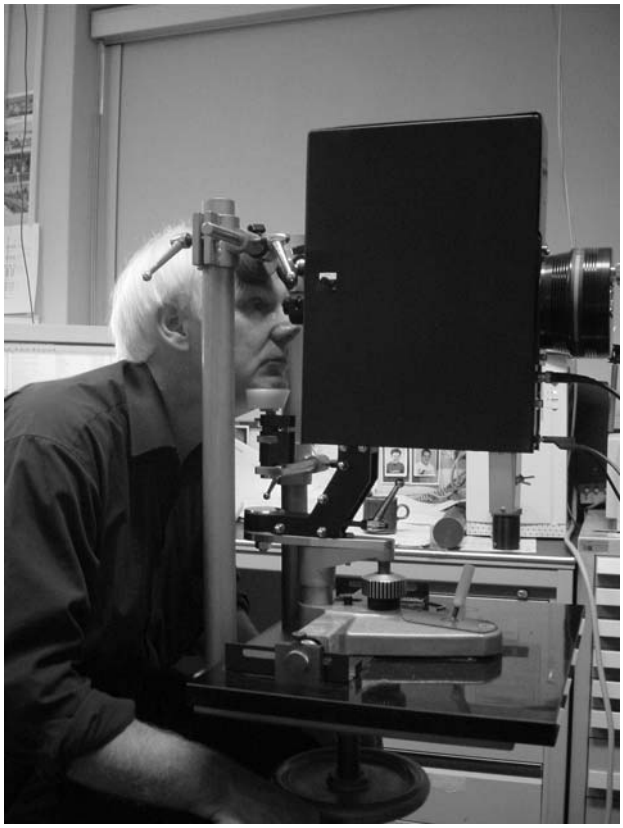

Fig 3. The author as a subject for ProfSpec 2. The extension on the right is the scientific CCD camera for detection of the retinal reflection in both angular and spectral sense.

The development of the compact ProfSpec 2 and later instruments was aided by using an optical design program; Zemax. The trial and error needed in earlier designs could thus be almost eliminated; a big advantage, where time and costs for the machine shop of the Hospital became more important. For larger retinal field sizes, ProfSpec 2 was plagued by ghost reflections in the Badal front lenses. Therefore the more complex setup in ProfSpec 3 was designed with an Offner optical relay containing 3 spherical mirrors. The function of this relay was to move the image of the subject's pupil to a location inside the instrument where, by means of a mirror, the illuminating light was separated from the detected light. Ghost images were indeed eliminated, but focusing the retina by moving one of the two front lenses in the Badal setup was eliminated too. Two Badal systems, one for the illumination channel, and one for the detection channel were included for this purpose. The path lengths of both were adjusted by four mechanically linked mirrors angled at 45 degrees, forming kind of retroreflectors in one plane.

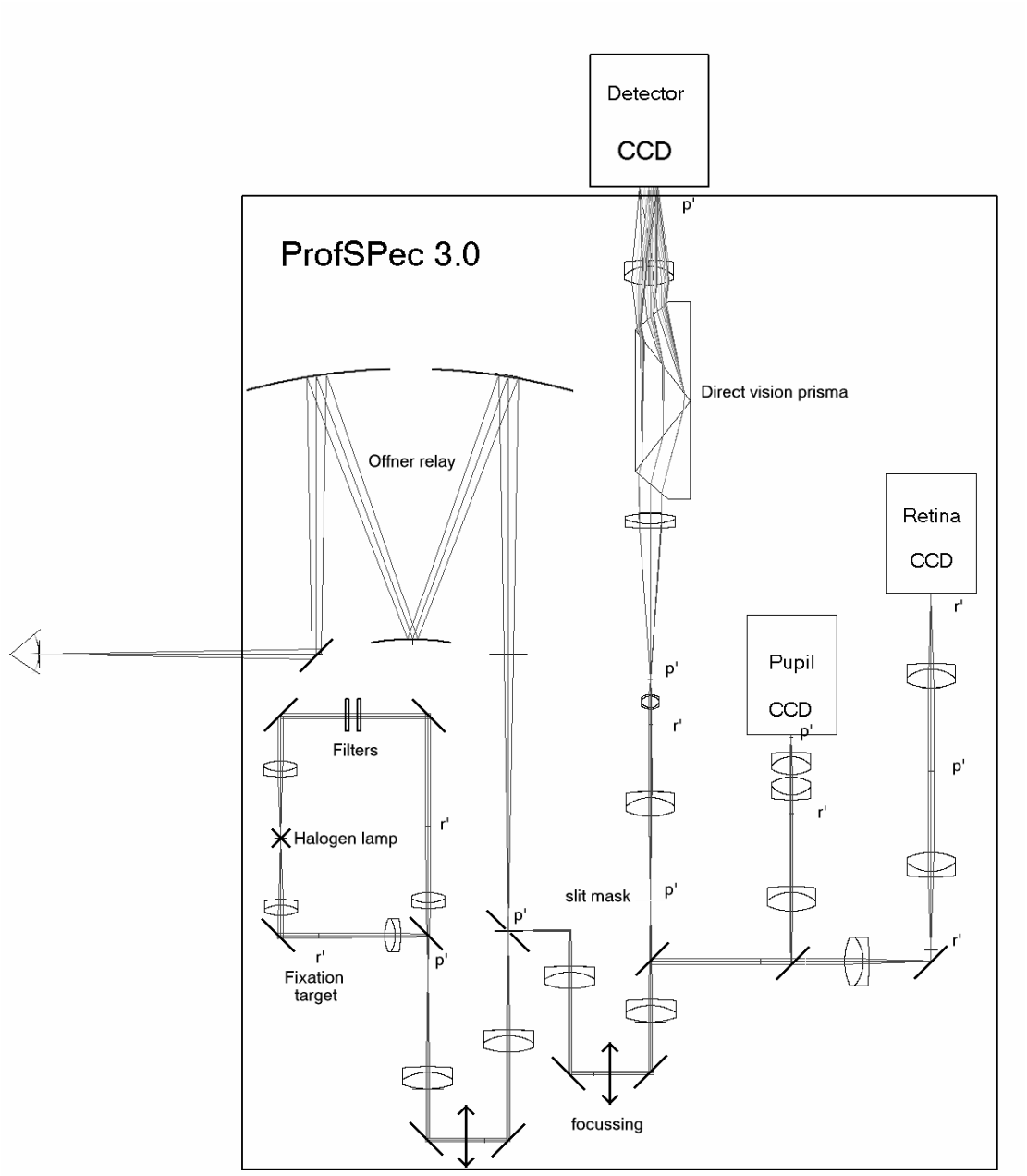

Fig. 4. The optical scheme of ProfSpec 3. See the text for explanation. Later, the complex direct vision prism in the spectrometer channel was replaced by a single 60 degree dispersion prism for less light absorption near 400 nm (see cover). At the right are two channels for observing the subjects pupil and retina. Planes conjugate to the pupil are marked with p, and planes conjugate to retina with r.

The Macular Pigment Reflectometer (MPR)

This instrument is described in detail in Chapter 8. It is a spin-off of the ProfSpec providing the full spectral detail, but not the detail in the pupil profile. It is also lacking the cameras for watching the retina and pupil. It was designed mainly for measuring macular pigment in the undilated eye. It is also known under the name MacPig. The Intellectual Properties (IP) of this instrument were sold by the UMC Utrecht to Zeavision Inc. Patents are pending.

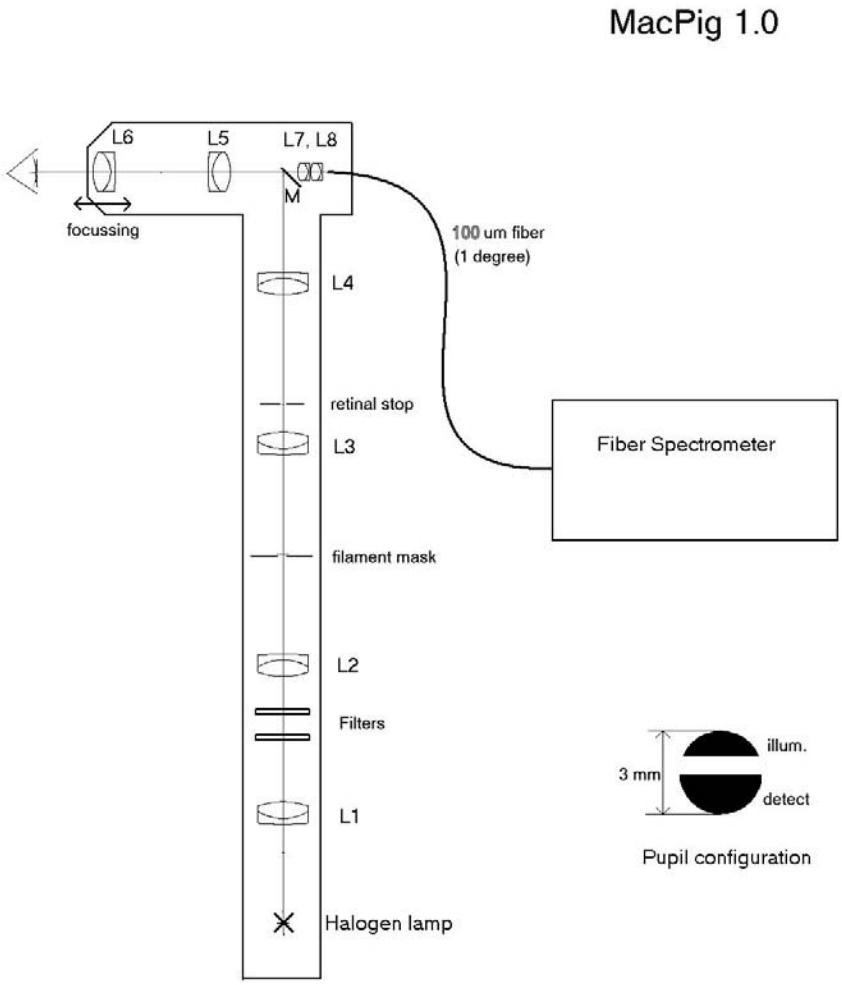

Fig 5. A schematic drawing of the Macular Pigment Reflectometer. The vertical light channel starting with the halogen lamp is for illuminating a spot on the retina. A small mirror in a plane conjugate to the pupil bends the light to the eye through the Badal front lens system for focusing the retina. Light reflected from the fovea passes the same Badal system, and than goes over the top of the small mirror towards an optical fiber connected to a commercial fiber optic spectrometer. The configuration of the illumination beam and the detection beam in the pupil of the eye is shown at the lower right.

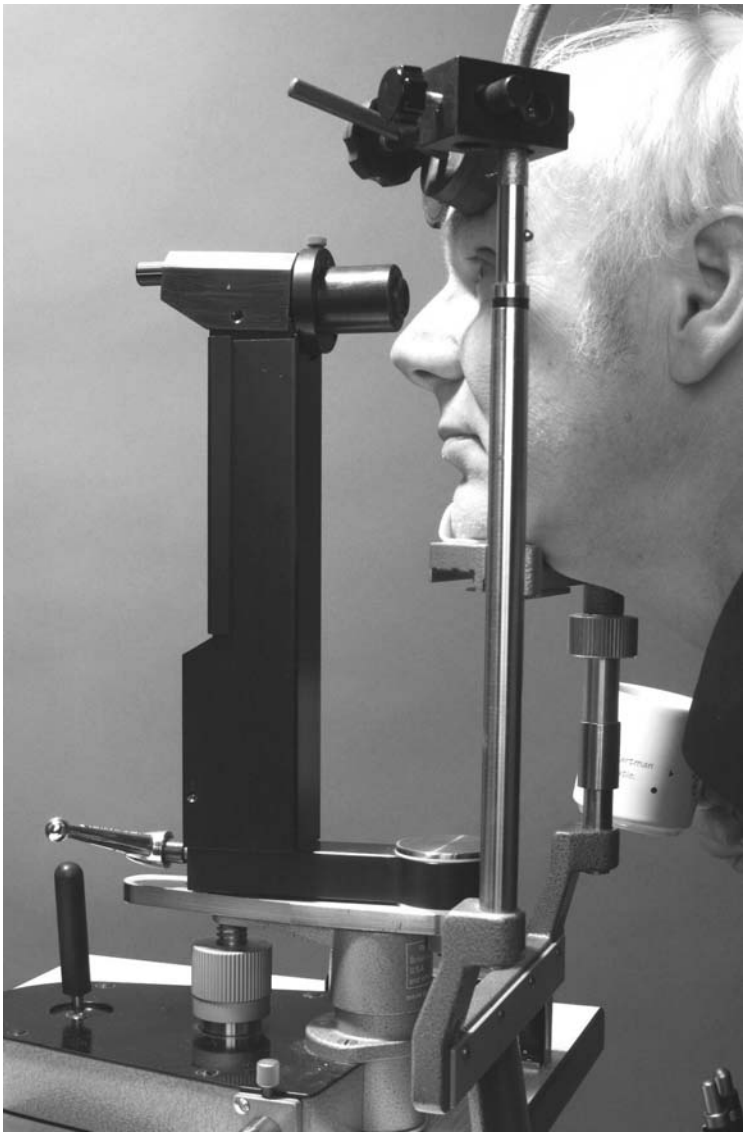

Fig 6. The Macular Pigment Reflectometer.

References

1. D. van Norren and L. F. Tiemeijer, "Spectral reflectance of the human eye," Vision Res. **26**, 313-320 (1986).

2. G. J. van Meel and D. van Norren, "Foveal densitometry as a diagnostic technique in Stargardt's disease," Am. J. Ophthalmol. **102**, 353-362 (1986).

3. J. E. Keunen, D. van Norren, and G. J. van Meel, "Density of foveal cone pigments at older age," Invest. Ophthalmol. Vis. Sci. **28**, 985-991 (1987).

4. A. T. Liem, J. E. Keunen, D. van Norren, and J. van de Kraats, "Rod densitometry in the aging human eye," Invest. Ophthalmol. Vis. Sci. **32**, 2676-2682 (1991).

5. A. T. Liem, J. E. Keunen, and D. van Norren, "Clinical applications of fundus reflection densitometry," Surv. Ophthalmol. **41**, 37-50 (1996).

6. P. J. DeLint, T. T. J. M. Berendschot, J. van de Kraats, and D. van Norren, "Slow optical changes in human cones," Invest. Ophthalmol. Vis. Sci. **38**, 4731 (1997).

7. P. J. DeLint, T. T. J. M. Berendschot, and D. van Norren, "A comparison of the optical Stiles-Crawford effect and retinal densitometry in a clinical setting," Invest. Ophthalmol. Vis. Sci. **39**, 1519-1523 (1998).

8. J. Xu, J. Pokorny, and V. C. Smith, "Optical density of the human lens," J. Opt. Soc. Am. A **14**, 953-960 (1997).

9. F. C. Delori and K. P. Pflibsen, "Spectral reflectance of the human ocular fundus," Appl. Opt. **28**, 1061-1077 (1989).

10. G. J. van Blokland and D. van Norren, "Intensity and polarization of light scattered at small angles from the human fovea," Vision Res. **26**, 485-494 (1986).

11. N. P. A. Zagers, T. T. J. M. Berendschot, J. van de Kraats, and D. van Norren, "A new type of reflectometer: Foveal reflection analyzer," Invest. Ophthalmol. Vis. Sci. **42**, S702 (2001).

Chapter 4

The Pathways of Light measured in Fundus Reflectometry

Jan van de Kraats, Tos T.J.M. Berendschot
and Dirk van Norren

Vision Research 36, 2229-2247 (1996)

Abstract

We measured the spectral reflectance of the fovea of ten normal subjects in four conditions, i.e. under dark-adapted and bleached conditions and at two retinal angles of incidence. The objective was to study optical pathways through the photoreceptor layer resulting in a model that simultaneously explains spectral, directional and bleaching properties of the fovea. On theoretical grounds, we propose that small reflections from the stack of discs in the cone outer segments are the origin of the directional component of foveal reflection. Non-directional reflection occurs at the inner limiting membrane and at all layers posterior to the outer segments. With four reflectance spectra as input, the model allows determination of the density of the photostabile absorbers, the lens, macular pigment, melanin and blood. Because of the simplified modeling of the layers posterior to the photoreceptor layer, the values for the density of melanin and blood are not necessarily comparable to physiological data. The density of the visual pigment calculated with this model is consistent with psychophysical data, with estimates for the ten subjects ranging from 0.41 to 0.80. The long wavelength sensitive cone fraction is calculated as 0.56.

Key words: Density Directional Photoreceptor Reflectometry Stiles-Crawford

Introduction

Knowledge of the pathways light takes through the photoreceptor layer is important for understanding a number of phenomena such as the psychophysical Stiles-Crawford effect and the related directional reflex. Also, light that is not guided through the outer segments of the receptor does not lead to a catch in visual pigment. Retinal densitometry, a technique to assess the amount of visual pigment in vivo, is based on a comparison between the optical reflectance of the fundus in light- and dark adapted states. The pathways light takes through the receptor layer influences the calculation of the real amount of visual pigment. Rushton (1965) and Ripps & Weale (1965) made an early attempt to construct models to calculate the amount of visual pigment. The simplest model assumes (1) a homogeneous layer of light-absorbing visual pigment in the dark-adapted eye, (2) that this layer is transparent in the light-adapted state, (3) and that all light is reflected from a layer posterior to the pigment layer. The light thus passes the visual pigment in the outer segments of the photoreceptor twice. An important development of the simple model was the addition of light reflected anterior to the pigment layer, for instance at the internal limiting membrane (ILM). Rushton (1965) called this "superficial stray-light". A second type of stray-light, traveling through parallel pathways in the receptor interspaces, was called "fundal stray-light". The simple model, which ignores stray-light, underestimates the density of the visual pigment. However, the assessment of the amount of stray-light, and consequently the true density of the visual pigment, has remained a problem for 30 years. Low fractions of stray-light (2% at 500 nm) were found by Rushton (1965), whereas higher fractions of stray-light were reported by Ripps and Weale (1965) (33%) and King-Smith (1973a, 1973b) (57%). The model of van Blokland and van Norren (1986), that is based on measurements of the directional reflection of the retina, added pathways of light in and around the receptor layer. This model predicted 50 % stray-light.

Pathways of light can also be derived from models describing the absolute optical reflectance of the fundus. With the assumption that there are certain reflecting layers and a limited number of absorbers with known spectral extinction in the eye, these models try to quantify these layers by decomposing the measured spectrum. For reasons of simplicity, existing models used light levels that were high enough to bleach the visual pigments. The implicit assumption is that the receptor layer is then completely transparent and can be ignored. Van Norren and Tiemeijer (1986) proposed a model with reflectance at two layers, the retinal pigment epithelium (RPE) and the sclera. Delori and Pflibsen (1989) expanded the model, incorporating more complex light scattering in the choroid.

The optical coherence technique applied to the retina provides a more direct way to study optical pathways (Huang et al., 1991; Hitzenberger, 1991; Puliafito et al., 1995; Hee, et al., 1995). Strong reflections (high amplitudes) are supposed to originate in the region of the choriocapillaris and the RPE. However, structures that scatter diffusely over a certain depth-range are less pronounced. We think that the present interpretation of OCT data leaves room for alternatives (cf. Discussion).

Our aim was to derive a foveal reflection model that simultaneously explains spectral and directional reflection and bleaching effects. Within this rather complicated framework, it serves to first outline our main assumptions, and point out where they differ from existing models. Cone photoreceptors have a directionality that expresses itself in both the psychophysical Stiles-Crawford effect (Stiles & Crawford, 1933) and directional reflection (van Blokland, 1986). How do the directional properties of the receptor layer influence light reflected from deeper layers? On the basis of the nature of the diffuse

white sclera and the multiple scattering of light by the choroidal tissues, we assume that the deeper layers taken together act to some extent as a diffuser with non-directional properties. Optical theory states that looking at a perfect diffuser through refracting optics (for instances a lens or in our case bleached photoreceptors), yields the same apparent reflectance as there would be without these optical elements (Longhurst, 1973). This is because the concentration (amplification of vergency) of light at entry is exactly nullified in the reverse pathway. The reflectivity of the perfect diffuser is constant for all angles, only for very large angles the amplification of vergency yields angles over 90 degrees, and prevents light from reaching the diffuser.
Another approach leading to the same conclusion is that all light from a certain retinal angle, either going (partly) through the bleached outer segment or going through the interspaces, enters the deeper layers, forming a three dimensional cloud of diffuse deeper light. Whereas with different retinal angles, the fractions of light traveling through the outer segments and the interspaces may change, the intensity of the deeper cloud of light remains constant. If a fixed relation exists between entrance light and light posterior to the receptor layer, this relation also must hold for the reverse pathway (reciprocity principle), and consequently emerging light going back from the deeper layers to the direction of the entering light cannot show directionality. This view eliminates the difficult problem of how to divide light entering the receptor layer from the sceral side, into a part entering the outer segments (with strong directionality) and a part entering the receptor interspaces (with, at first sight, non-directional behavior).
If, as argued above, the structures beyond the (bleached) receptor layer do not show directional effects, there must be other sources for the origin of light with directional behavior. As we know from the measurements of van Blokland and van Norren (1986), dark adaptation of the eye (resulting in increased absorption in the visual pigments) greatly reduces the magnitude of the directional component. This eliminates all sources of the directional reflex anterior to the outer segments of the receptors. The only remaining candidate for the origin of the directional reflex, in our view, then lies in the outer segment layer itself, in particular in the cone photoreceptor discs. For anatomical and optical reasons, we are unable to identify other structures that could fulfill this function. The index of refraction of the disc material (1.43) is higher than the fluid around it (1.36) (Piket-May, Taflove & Troy, 1993). Fresnel reflection for this index of refraction step cannot be directly applied due to the small dimension of the thickness of the discs (about 15 nm) compared to the wavelength. More appropriate in this case would be thin film reflection theory (Longhurst, 1973), whereby interference of the reflection at the back of the disc would largely compensate for the reflection at the front, leaving a very small residual reflection. However, the cumulation of about a thousand of these tiny disc reflections may be substantial. Evidence for reflection from the stack of discs comes from a technique which shows the existence of a standing wave pattern in a receptor model, by solving the time integrated Maxwell equations. This technique, however, is still in its infancy and calculations require considerable time on a super computer (Piket-May, Taflove & Troy, 1993). As the magnitude of the reflection of the discs depends on many questionable and unknown variables, the only assumption we make for our model is that there is a given reflection from the discs.

The model presented here is the first to our knowledge to incorporate the receptor layer into a reflection model of the human fovea, assuming directional reflection from the stack of discs in the outer segments and non directional reflection from pre-retinal and post-retinal layers. Our approach thus differs from previous studies that relied on a directional reflection from origins posterior to the receptor layer (van Blokland and van Norren, 1986; Delori and Pflibsen, 1989; Gorrand and Delori, 1995). We used the model to estimate the proportions of light in the optical pathways passing the photolabile visual pigments twice, partly twice or not at all. Estimates for the density of the visual pigments were obtained that are consistent with psychophysical data**.**

Methods

Experimental setup

Fundus reflection measurements were performed with a slightly modified version of the Utrecht Retinal Densitometer (van Norren & van de Kraats, 1989). A few essential details are presented below. The instrument enables, in contrast with older type densitometers, investigation of the directional effects of the photoreceptors, by moving a fixed configuration of small, and closely spaced entry and exit pupils, over the subjects pupil. The small entry and exit pupils further ensured minimal contribution of reflections from the instrument's output lens and the anterior parts of the eye. The apparatus contains two channels that deliver light to the retina. The first channel illuminates the measuring field (1.9, 2.8 or 4.2 degree) on the retina. In this path, a rotating wheel (14 rev./sec.) offers a sequence of 14 interference filters in the range 410-740 nm (bandpass 7 nm) to enable quasi-simultaneous measurement of reflectances across the visual spectrum. Interspaced are 6 stops to retrieve dark counts of the photomultiplier and (roomlight) background level. The mean intensity over time was 1200 Td, ensuring that the bleaching of the visual pigment due to illumination of the measuring field is kept at a low level.

The second channel (30 degree) is used for bleaching. A Schott OG495 and a neutral density (ND) filter were used to limit the bleach intensity to a safe level of 5.8 log Td. For dark adaptation an ND filter was inserted which lowered the level to 200 Td. This level still enabled fixation at the crosshair in the bleach channel.

Light reflected from the fundus in a detection field (1.6 degree) concentric to the illumination field was measured with a photomultiplier in photon count mode. Within the detection field the retina was assumed to be homogeneous. A microcomputer in the instrument accumulated (dark corrected) counts for each interference filter and sent them, once a second, to a desktop computer for further processing.

Calibration.

A surface painted with Eastman 6080 white was used to calibrate reflectance. The spectral reflectance of this paint was tested to be similar (± 4%) to the spectral flatness of a BaSO4 surface. Using the 4.2 degree illumination field, the reflectance measured at 220 mm from the pupil plane of the instrument was set at 1 %, assuming a focal distance of the eye of 22 mm and Lambertian reflectance.

The instrument's stray-light for the different illumination fields was measured with a 'black hole'. This 'black hole' consists of a polished black perspex plate, placed at a 45 degree angle in the pupil plane of the instrument. At this position there is a maximum separation between illumination and detecting beams. The minimal specular stray-light at the surface is further absorbed by the matt black anodized inner surface of an aluminum enclosure tube that tightly fits around the exit lens to prevent room light entering the instrument. The reflectance of the 'black hole' itself was estimated to be less then 0.001%.

Maximum stray-light of the densitometer (0.03% of a white retina) was measured at the shortest wavelength (410 nm). The percentage reflectance R(λ) from the eye, for each illumination field (illum), was calculated from the (instrument corrected) counts measured from the eye and the (instrument corrected) counts from the white surface as follows:

$$R_{(illum,\lambda)} = \frac{N_{meas(illum,\lambda)} - N_{instr(illum,\lambda)}}{N_{white(4.2\,\deg,\lambda)} - N_{instr(4.2\,\deg,\lambda)}} \qquad (1)$$

Protocol.

Both the retinal angle of the reflected light and the bleach state of the visual pigments were varied, in order to test their influence on pathways of light through the receptor layer. All measurements were obtained from the fovea by setting the fixation target at the center of the illumination field. A bite-board and temple pads were used to maintain head position. A mydriatic was used to dilate the pupil. Reflection measurements to test directionality were performed with the instrument's entry and exit pupils aligned to the peak of the Stiles-Crawford (SC) function (van Blokland & van Norren, 1986). The position of the SC peak is slightly nasal in most subjects (about 1 mm in the pupil plane). A second pupil position 2.5 mm temporal to the SC peak and thus closer to the edge of the pupil was chosen to lower the light guided into the receptors. We shall refer to these two pupil positions in terms of retinal angle, calling the peak SC position 'perpendicular' and the temporal position 'oblique'. The densitometer was aligned to the peak of the SC function by carefully monitoring both the measured counts and the retinal image, while making slight adjustments to the pupil position. The retinal image was optimized for brightness and contrast, thereby avoiding reflections from the cornea and lens. In most subjects perimacular reflections appear concentric when the entrance and exit pupils are at the SC peak. Photon counts were maximized for the medium and long wavelengths (> 550 nm), while at the same time keeping the reflection for 410 nm below 0.05 %. At 410 nm the retinal signal is very low, mainly due to the high density of the lens at this wavelength. Low counts at this wavelength are a good indication for the absence of corneal reflections. The interception of entrance or exit light by the pupil, as indicated by a sharp decrease in measured counts, was avoided.

The amount of visual pigment was controlled by the radiance of the bleach light. The decrease in bleach efficiency for the oblique pupil entry position compared to the perpendicular position was calculated as 0.3 log unit (Coble & Rushton, 1971). We used the Rushton equation (Wyszecki & Stiles, 1982) to calculate the unbleached fraction of visual pigment in the four conditions: perpendicular bleached, 0.03; perpendicular dark, 0.93; oblique bleached, 0.06; and oblique dark, 0.97.

To obtain an adequate signal-to-noise ratio, the densitometer outputs were first averaged at 10 second intervals. Twelve of the 10 second averages were again averaged to give a final reflection data point (block of 2 minutes). The standard deviation was calculated from the twelve; 10 second averages and mainly reflects photon noise and minor disturbances caused by short-term movements of the subject. Alignment with the bleach light on took a few minutes. Data recording was then started with the bleach light on for an additional 2 minutes, to obtain an initial bleached spectrum. The dark period lasted at least 10 minutes, the last 2 minutes being used to obtain the dark-adapted spectrum. The spectrum obtained in the last 2 minutes of a second bleach period, lasting at least 5 minutes, was considered the (final) bleached spectrum. If the 560 nm point of the final bleached spectrum differed by more than 0.03 log unit from the initial bleach

spectrum, the run was rejected. Each experimental run lasted 15 to 20 minutes for one alignment.

Subjects

All subjects were Caucasian and had normal color vision, as assessed from their Rayleigh Matches. Two experienced subjects with normal vision, the first two authors, took part in the pilot experiments. More extensive data were obtained for ten subjects, including the authors. The purpose of the experiment was explained and written informed consent was obtained.

Experimental results

Experiment 1 : Directionality

Fig. 1a shows spectra (for subject JK) measured in a bleached retina under 'perpendicular' and 'oblique' conditions (cf. Methods). Continuous lines are fits from the model discussed later; symbols represent experimental data. The visual pigments were bleached away, and the 1.9 degree illumination field was used. Both spectra showed the following features. Reflectance was highest (about 5%) in the long wavelength part of the spectrum (above 600 nm). Melanin is virtually the only absorber in this spectral region (see Fig. 2 for the absorbers used in later analysis). Below 600 nm the sudden decline in reflectance was caused by absorption by blood. Reflectance decreased to a level equal to what we assume to be the reflectance from the outer segment layer. Reflectance between 510 nm and 430 nm was further reduced because of absorption by the macular pigment. At 430 and 410 nm reflectance decreased sharply due to lens absorption. As a consequence small residual reflections from the cornea had a relatively large influence on the data. Therefore, in this and subsequent figures all data points and model curves below 0.01% were omitted (as being not relevant). In the middle of the spectrum there was a marked difference between the two conditions, the reflection for light perpendicular to the retina being about three times higher than for oblique light. We attribute this completely to directional effects in the cone photoreceptors.

In Fig. 1a the spectra are plotted on a logarithmic scale, as is usual to account for the large dynamic range. However, an interesting aspect is overlooked this way. On a logarithmic scale the greatest difference between the spectra (showing in fact the greatest ratio) is seen around 500-550 nm. This is lost when the reflectance spectra are plotted on a linear scale (Fig. 1b). Instead, there is little difference in reflectance for wavelengths higher than 540 nm. This difference in reflectance (in our opinion representing the directional reflectance from the receptors) gained when going from oblique to perpendicular angle, is plotted in Fig. 1c. The steep increase in absorption by blood at wavelengths below 610 nm is not, or at most to a very minor extent, seen in the directional spectrum, in particular when compared to the substantial influence of absorption by blood on the original reflection data shown in Fig. 1a. The decline below 560 nm coincides with increasing absorption by the macular pigment and below 450 nm with absorption by the lens. As will be shown later, the decline at the longest wavelengths is largely due to absorption by water. This experiment suggests that the directional reflection from the receptors has a constant magnitude over a broad range of wavelengths and the spectral shape shown in Fig. 1c is only due to pre-receptor absorbers. This experiment supports the suggestion (cf. Introduction) that the deeper, blood rich layer reflects light non-directional.

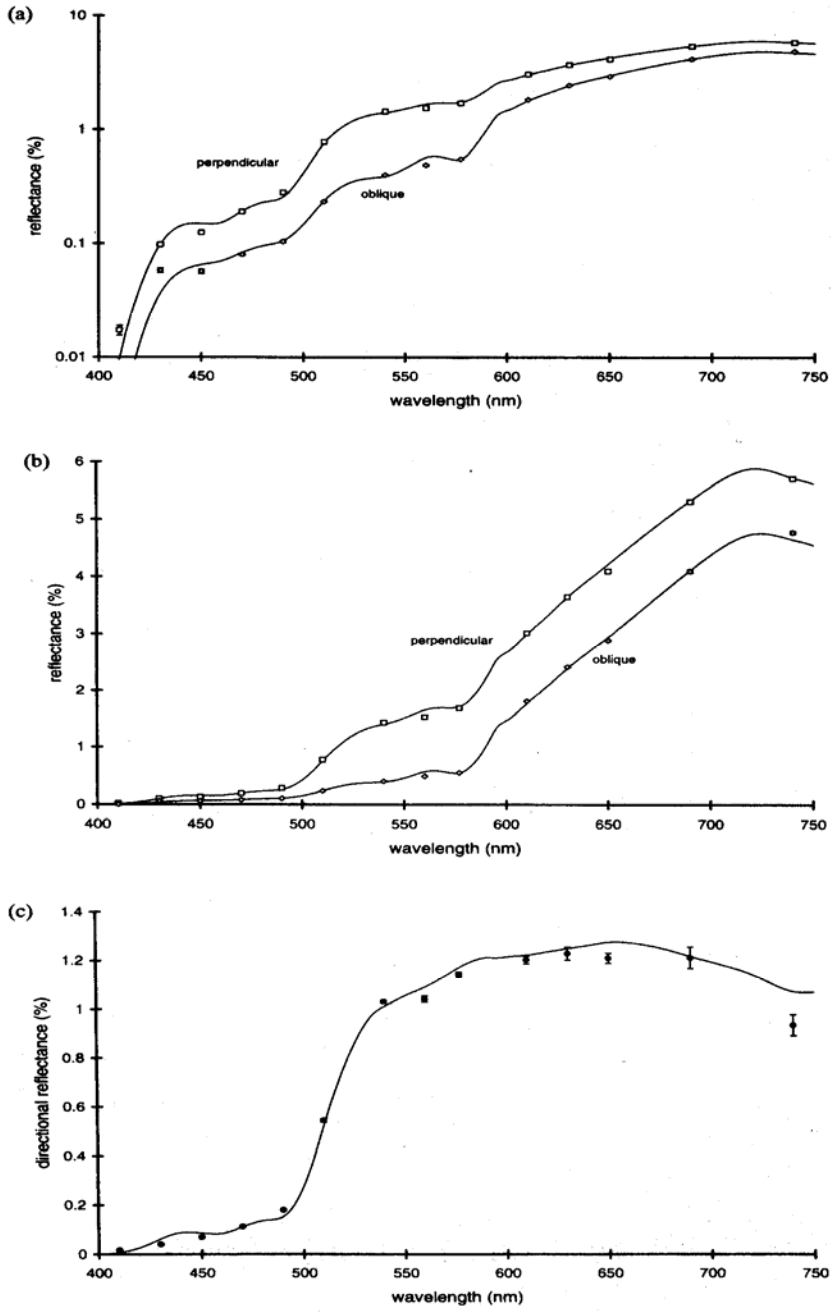

Fig. 1 (a) Reflectance spectra of a bleached fovea for perpendicular and oblique measuring angles. Continuous lines are results from model fitting; points are data obtained from the first author (JK). In this and subsequent figures all data points and model curves below 0.01% were omitted as being not relevant. Illumination field size is 1.9 degrees; detector field size 1.6 degrees. Reflectance is referred to a white diffuse retina. (b) Identical data as in Fig. 1a, but now plotted on a linear scale. (c) The directional reflectance, being the difference in reflectance between the model spectra and data points from Fig. 1b. Although the model curve is a secondary result of the global fitting to the four primary spectra and not a direct fit to the data points in this figure, the fitting is still acceptable. At 540 nm and higher, the directional component is fairly constant. At the shorter wavelengths (below 540 nm), the double pass of lens and macular pigment reduces the magnitude of the difference. At the long wavelengths absorption by water is involved.

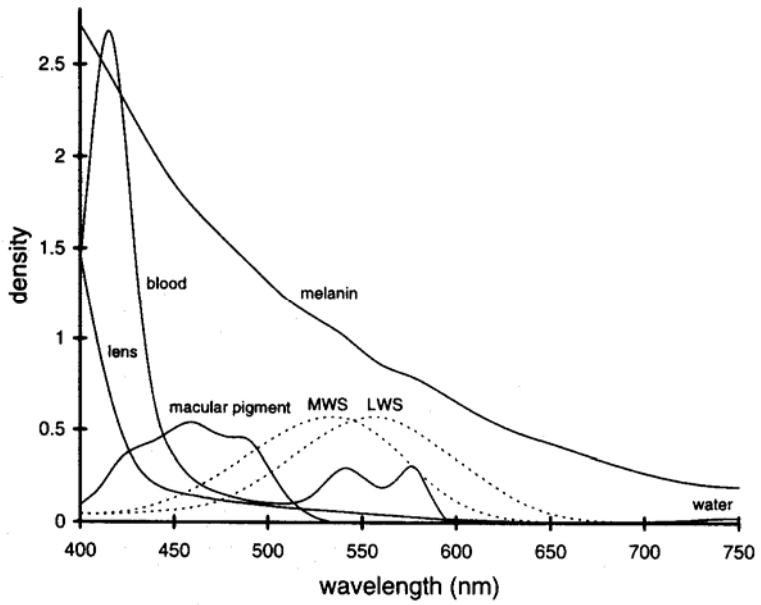

Fig. 2. Absorption spectra of blood, melanin, macular pigment, the lens and water in the eye for a single pass. Mean results of model fitting are used to give representative densities for an average subject. For sources of the spectral shape see text. The thickness of the blood layer is 23 μm, with an oxygenation of 95%. Melanin density is 1.32 at 500 nm; macular pigment density is 0.54 at 460 nm; lens density at 420 nm is 0.54; water density is 0.025 at 740 nm (24 mm). Visual pigment densities are equal, 0.57 at the peak both for LWS and MWS cones, and are shown by the dotted lines.

Experiment 2 : Varying visual pigment.

The impact of the visual pigment on the foveal reflection is illustrated in Fig. 3a. Two 'perpendicular' spectra are presented, one for the bleached and one for the dark-adapted condition. The difference between these logarithmic plots is the well-known result of retinal densitometry (Fig. 3b). This curve is traditionally ascribed to the double traverse of the measuring light through the visual pigments. According to the simple model (cf. Introduction), spectral aspects of posterior reflectors and anterior absorbers do not influence this type of result, and only the spectral density of the visual pigment is assumed to be relevant. For comparison, the absorption spectra of the long and medium wavelength-sensitive visual pigments (DeMarco, Pokorny & Smith, 1992) are also shown. The model curve in this figure is a secondary result of the later described fit to the four original spectra and is not a result of a separate fit applied directly to the data points in this figure.

The absolute linear difference between the perpendicular spectra from Fig. 3a is plotted in Fig. 3c. This difference in reflectance reveals details that go unnoticed in the logarithmic difference of Fig. 3a (that shows in fact ratios). These data represent the absolute reflectance gained when going from the dark-adapted to the bleached state. The maximum appears at 610 nm, instead of 550 nm as seen in Fig. 3b. There is an abrupt decrease at wavelengths below 610 nm, indicative of absorption by blood. The retinal

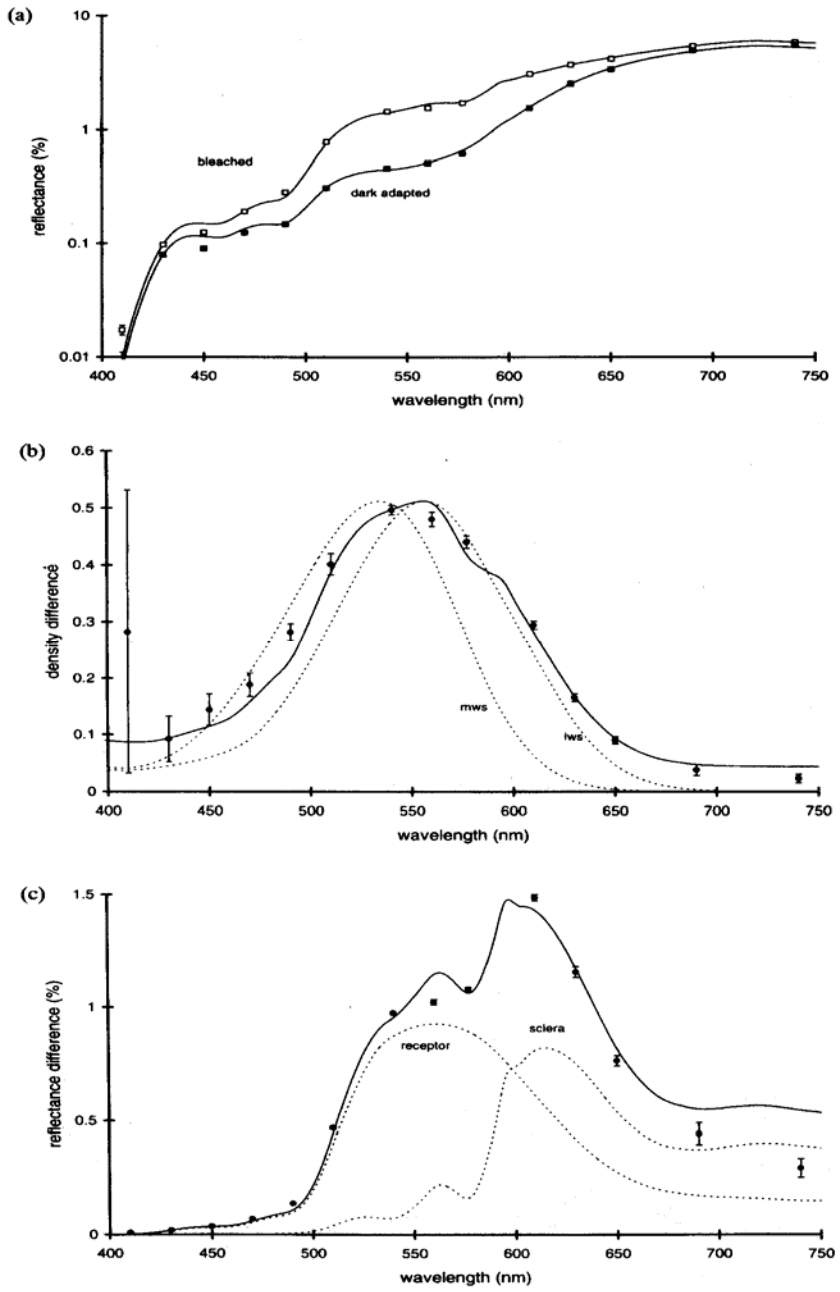

Fig. 3. (a) Reflectance spectrum for the perpendicular measurement angle, measured for the bleached retina (copy of upper curve in Fig. 1a), together with the spectrum measured for the dark-adapted retina. Continuous lines are the results of the model fitting; points are experimental data. (b) Measured density difference spectrum (data points) and a model curve (continuous line), defined as the difference between the logarithmic scaled spectra in Fig. 3a. Although the model curve is a secondary result of the global fitting to the four primary spectra and not a direct fit to the data points in this figure, the result is still acceptable. For comparison, dotted lines show visual pigment absorption curves (DeMarco, Pokorny & Smith, 1992) for LWS and MWS cones. Their peak densities were set equal to the peak of the measured data. (c) Absolute reflectance difference between the spectra in Fig. 3a on a linear scale. This represents the light gained when a dark-adapted fovea is bleached. The continuous line is the model fit. Again this is a secondary result of the global fit to the four primary spectra. Dotted lines show the components from the model fit for light reflected at the receptor discs and the sclera.

vascular system is unlikely to have a great influence as it did not affect the results of experiment 1, and there are no indications of such absorption in the psychophysical spectral sensitivity curves of the fovea. This experiment proves the existence of a pathway of light that traverses the photoreceptors and also the deeper, blood-rich layers. To illustrate this, the results of the two underlying components (sclera and receptor discs) obtained by the model fitting are also shown (dotted lines in Fig. 3c). Again, the model curves in this figure are a secondary result of the later described global fitting.

Experiment 3 : Directionality of light from deeper layers

A more complex experiment provided additional evidence for the non-directionality of the light reflected by the deeper layers. When illumination and detection fields do not overlap in the retinal plane, there is no reflection from receptor- and superficial retinal layers and only laterally diffused light from the deeper layers remains. This was achieved by subtracting the spectrum measured with an illumination field of 4.2 degrees from the spectrum measured with an illumination field of 2.8 degrees. In this way light entering in an annulus with borders at 4.2 and 2.8 degrees and emerging from the retina from the central detection area of 1.6 degrees diameter is obtained. Measurements in the bleached condition showed that very little light emerges at wavelengths below 610 nm (Fig. 4, subject JK). It is difficult to make an absolute comparison with the other spectra because more light entered the eye (reflectance is only clearly defined for local light). This result proves that the light has indeed traveled through the deeper layers and that there was strong absorption by blood and melanin. There was virtually no difference in reflection at the long wavelengths when the results for the perpendicular and oblique conditions were compared. For shorter wavelengths, the amplitude of the difference was low and even negative due to noise, because of the subtraction of almost identical data from the original measurements with 4.2 and 2.8 degree illumination field. From this experiment we can conclude that the light reflected from the deeper layers is non-directional, even after passing the receptor layer with strong directional properties.

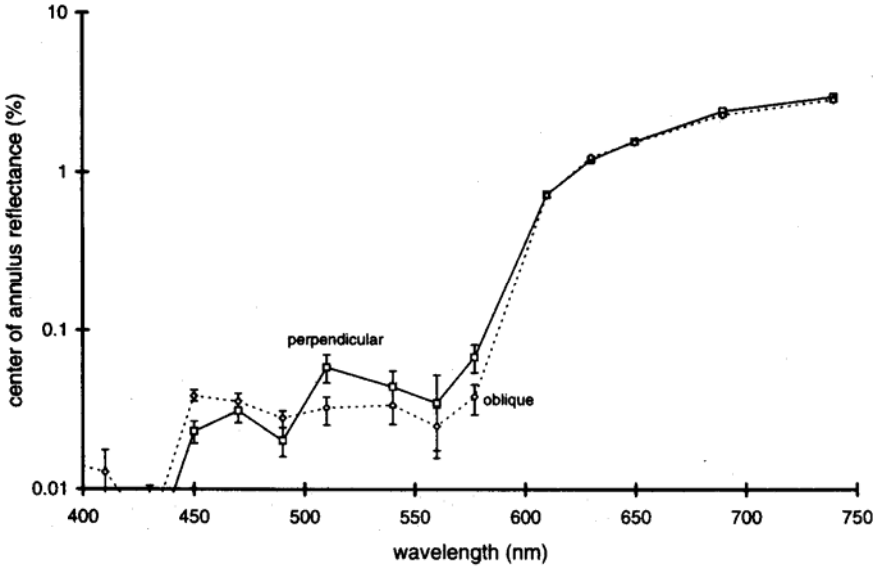

Fig. 4. Reflectance spectra (subject JK) measured from the central 1.6 degree fovea, with an annulus with borders of 4.2 and 2.8 degrees as illumination (see text). Shown are the perpendicular and oblique conditions measured in a bleached retina. Data points below 610 nm are noisy due to the subtraction of low values (see 3.3). Lines in this figure are not based on model prediction, they just connect the data points for visibility. The data in this figure represent the spectral shape of the 'deep' reflected light. The similarity between the two curves, especially at the long wavelengths, indicates the absence of directional effects in this deeper light.

Model

General introduction.

Our starting point was the model developed by van Norren and Tiemeijer (1986), with some of the modifications suggested by Delori and Pflibsen (1989). Our model includes the receptor layer, which was ignored by van Norren and Tiemeijer (1986) and Delori and Pflibsen (1989). The model (Fig. 5) is divided into three main parts, the pre-receptor (mainly eye media), the receptor, and the post-receptor part (all deeper layers). Light entering the eye is represented by a vertical thick line (left) with a downward pointing arrow and light emerging from the eye is represented by a vertical thin line (right) with an upward pointing arrow. In Fig. 5 the absorbing layers are represented as horizontal boxes. Spectral data for these layers were convoluted with the 7 nm bandwidth of the filters used in the measurements (Table 1). The spectral data with densities for an average subject are shown in Fig. 2. Single horizontal lines in Fig. 5 represent reflecting layers. The receptors are depicted as vertical funnel shaped objects. Reflecting layers are assumed to be spectrally neutral, as is the case for Fresnel refraction on layer boundaries with a small difference in the refractive index. An exception is the reflectance of the sclera, that was assumed to decrease slightly in the long wavelength part of the spectrum (see section 4.1). Secondary reflections at the back of reflecting layers (when going upward in the drawing) do not contribute to the measured signal. The model is discussed in detail below. We start at the scleral side because the reflectances of posterior layers are components in the calculation of anterior reflectances. Only those parameters that are allowed to vary in the process of fitting the experimental data are numbered.

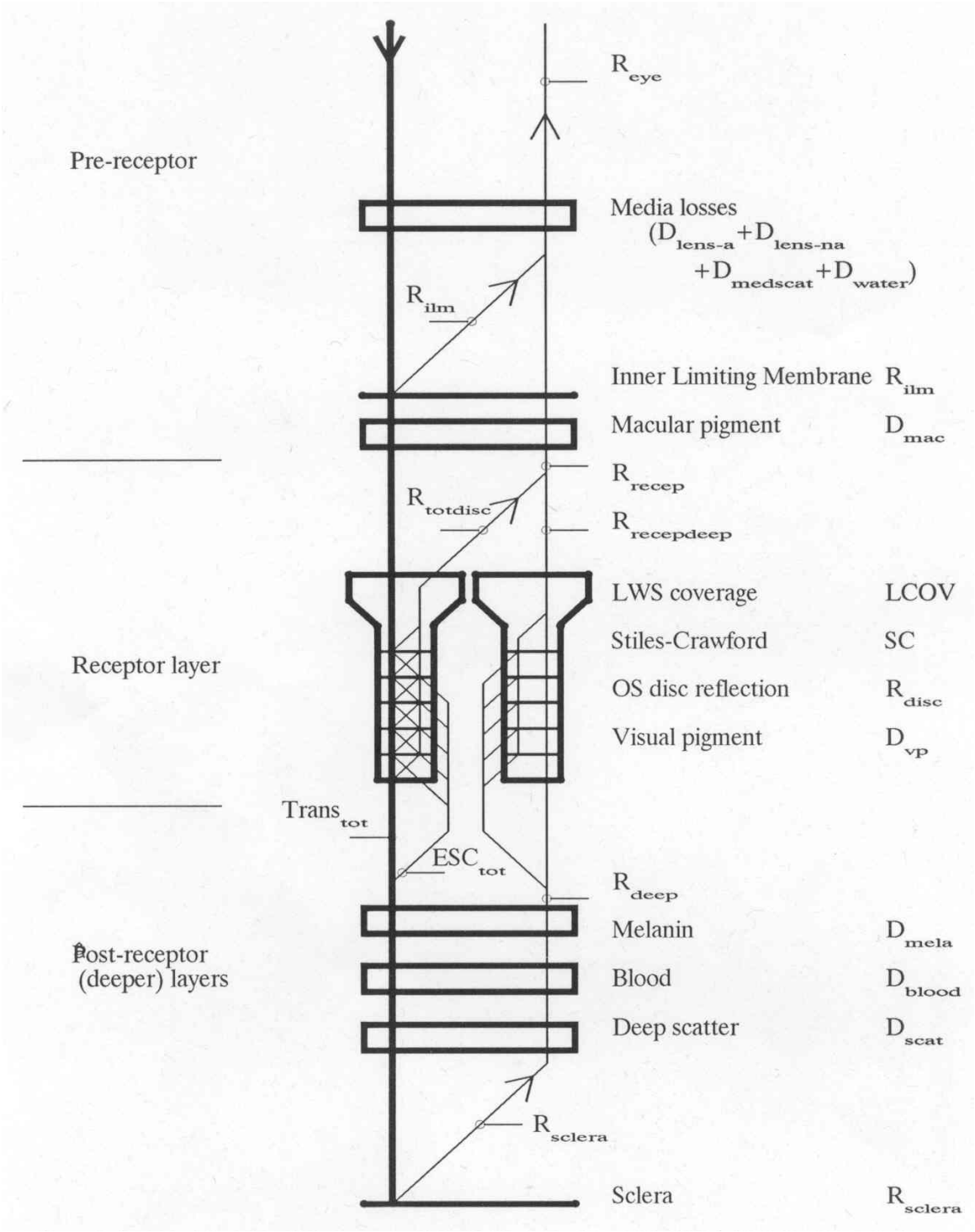

Fig. 5. Model of optical reflectance of the fovea, with pathways through the receptor layer and reflections from the ILM, the receptor discs and the sclera. Reflectors are indicated by horizontal lines. Absorbing pigments are drawn as horizontal boxes. Cones are depicted as funnel-shaped objects. In the dark-adapted condition the cones are filled with visual pigment. Light enters the eye from the top, as indicated by the downward pointing arrow. Upward pointing arrows represent light detected by the instrument, emerging from the eye after reflection from the different layers. Secondary reflections are assumed to be lost elsewhere. Only the reflection from the cone receptor discs is directional. For a complete description of the model see Model section.

Table 1 Spectral data from the literature that were used for the model fitting; for sources see text.

wave	Lens-a	Lensna	Water	Mac	MWS	LWS	Mela	Blood	Sclera
410	0.4388	0.66473	0.0002	0.1642	0.0806	0.0730	0.7695	0.10793	0.999
430	0.3240	0.10332	0.00018	0.3643	0.1206	0.0875	0.66	0.06089	0.948
450	0.2537	0.00453	0.00018	0.4596	0.2309	0.1164	0.5604	0.01564	0.9
470	0.2007	0	0.00018	0.4467	0.4112	0.1796	0.49	0.00764	0.854
490	0.1607	0	0.00022	0.4037	0.6423	0.3421	0.4298	0.00518	0.81
510	0.1267	0	0.00039	0.1326	0.8694	0.5828	0.3705	0.00448	0.769
540	0.0920	0	0.00059	0	0.9902	0.9310	0.3094	0.01296	0.711
560	0.0688	0	0.00075	0	0.8076	0.9958	0.2605	0.00834	0.675
577	0.0492	0	0.00103	0	0.5330	0.8803	0.2395	0.01350	0.646
610	0.0232	0	0.00302	0	0.1212	0.4733	0.1801	0.00027	0.592
630	0.0112	0	0.00334	0	0.0346	0.2356	0.1501	0.00017	0.562
650	7.40E-04	0	0.00366	0	8.27E-03	0.0902	0.1299	0.00012	0.534
690	0	0	0.00525	0	4.30E-04	0.0068	0.09	0.00009	0.481
740	0	0	0.02458	0	1.52E-05	2.63E-04	0.06	0.00012	0.422
	420 nm	420 nm		460			500nm		
	0.3724	0.3080		0.495			0.40		

'wave' is the wavelength, 'Lens-a' is the aging part of lens density, 'Lensna' is the non-aging part of lens density, 'Water' is the density of 24 mm water, 'Mac' is the density of the macular pigment, 'MWS' and 'LWS' are normalized (energy) sensitivities of the medium and long wavelength sensitive visual pigments, 'Mela' is melanin density, 'Blood' is the density of one micrometer of 95% oxygenated blood, 'Sclera' is the reflectance of the sclera. Data were interpolated by a polynomal to 1 nm resolution and convoluted with the 7 nm bandwidth of the interference filters. The 740 nm MWS and LWS data were extrapolated by fitting a straight line through the last original data points. Where applicable, at the bottom of the column, the wavelength and value of normalization are given.

Post receptor (deeper) layers.

We modeled the deeper layers in a very simplified way similar to that of van Norren and Tiemeyer (1986), with absorption by melanin and blood and reflection from the sclera. Delori and Pflibsen (1989) presented a more complex model of the deeper layers. They used fixed values for epithelial melanin and blood in the choriocapillaris and added a more complex reflection in the choroid, using Kubelka-Munk scattering with a fixed tissue scatter term. This resulted in an estimate of the density of choroidal melanin and the thickness of the blood layer. The numbers for blood and melanin are higher (and more realistic in a physiological sense) than the van Norren and Tiemeyer data, but this is at the expense of the three extra parameters. In addition, the results are (1) quite sensitive to the tissue scattering term, which was fixed at a very weak optimum, and (2) the Kubelka-Munk scatter model is only one dimensional and ignores sideward scattering. We think that a more complex three dimensional model, including reflection from Bruch's membrane, and parallel and serial pathways through blood, melanin and tissue, is needed to obtain more precise parameter estimates. As our main interest was not in the deeper layers, but in the behavior of the receptor layer, we did not employ Kubelka-Munk modeling. We only needed a short and simple characterization of the reflection from the deeper layers. By ignoring the details of choroidal parallel pathways and scatter, the values for blood layer thickness and melanin density are underestimated.

The reflectance of the sclera was assumed to decrease in the long wavelength part of the spectrum (Delori & Pflibsen, 1989). It is described by a fixed parameter:

$$R_{sclera(\lambda)} = 0.5 \times \exp(-0.00261(\lambda - 675)) \qquad (2)$$

Parameter 1. Density of deep scatter losses: D_{dscat}

To allow for spectrally neutral losses at the deeper layers (for instance light scattering out of the detection field), a free parameter D_{dscat} was added (Delori & Pflibsen, 1989).

Parameter 2. Thickness of bloodlayer: Th_{blood}

We assumed the oxygenated fraction to be 0.95 (Delori & Pflibsen, 1989). Blood absorption data (both HB and HBO_2) were taken from van Assendelft (1970). The free parameter, $Th_{blood,\lambda}$, represents the thickness of an equivalent layer of blood in micrometres. This value was converted to the optical density of blood $D_{blood,\lambda}$ by using the extinction values from Assendelft (see Table 1 for densities of 1 mm blood). The concentration used was 150 mg/l and the molecular weight was 16.1 mg/mmol.

Parameter 3. Density of melanin: D_{mela}

The shape of the melanin absorption curve was taken from Gabel, Birngruber and Hillenkamp (1978) with the density at 500 nm as the free parameter D_{mela}.

Calculating reflectance of the deeper layers.

The formula for sclera reflectance gives unrealistic values near 100% reflectance for the shorter wavelengths (Table 1). Fortunately, these high values are not important, because the high absorption of blood and melanin in this spectral region virtually eliminates any influence of deeper reflected light compared to the influence of reflection from the photoreceptor discs.
The reflectance of the deeper layers is calculated as:

$$R_{deep(\lambda)} = R_{sclera(\lambda)} * 10^{-2(D_{mela}(\lambda)+D_{blood}(\lambda)+D_{scat})} \qquad (3)$$

Receptor layer.

The receptors in this layer are depicted by the vertical funneling elements in Fig. 5 (two cones are shown rather than one, to avoid crowding of the entering and emerging light paths). Because of their small dimensions, receptors can be considered as optical waveguide antennas (Snyder & Pask, 1973). Antennas are reciprocal, the lobes that describe the directional reception also apply when they radiate. Antennas usually have a pronounced forward lobe, making reception most effective for a perpendicular angle. At oblique angles, less energy is captured and more escapes to the surroundings. With knowledge of the directional forward lobe, the so-called antenna gain and the effective capture area can be determined (Jessop, 1971). The antenna gain is defined as the ratio of the area of a hemisphere and the weighted cross-sectional area of the lobe at the hemisphere. The capture area is defined as the effective reception area and may be larger than the physical dimensions of the antenna. The antenna gain is high and the capture area is large when the directionality of the receiving pattern is high (see Appendix). If the foveal receptors are considered as antennae, the capture area for perpendicular light is

calculated to be larger than the area covered by the receptor itself. This means that we can assume that all the light is captured by the inner segments of the receptor and then travels on to the outer segments. In conclusion, for our detection field we assume light not to enter the receptor interspaces in this perpendicular condition.

For oblique angles, light has to enter the interspaces between the outer segments in order to explain the decreasing psychophysical Stiles-Crawford efficiency. Psychophysical experiments (King-Smith, 1973b; Burns & Elsner, 1993) show an apparent decrease in the thickness of the visual pigment layer at oblique angles. This apparent decrease also narrows the absorption spectra of the visual pigment. Considering the case where light already escapes at the inner segment level instead of escaping along the outer segment, then the fraction of light still guided through the outer segment always encounters the full length of the visual pigment layer. In that case there would be no spectral narrowing of absorption spectra. We therefore assume, as proposed earlier by Walraven and Bouman (1960) that, for oblique angles, light gradually escapes along the outer segment into the receptor interspaces. This results in an exponential decay of guided light within the outer segment.

Parameter 4. Stiles-Crawford effect: SC.

To quantify the captured light as a function of retinal angle, we implemented a Stiles-Crawford parameter (SC) fixed at 1 for the perpendicular condition and between 0 and 1 for the oblique condition. We defined parameter SC as the transmission of the total outer segment due to the apparent absorption of the escaping light. The escaping fraction is then 1 minus SC. For the uniformity of later calculations we converted the free parameter SC to the density of the apparent absorption; D_{esc} defined as:

$$D_{esc} = -\log(SC) \qquad (4)$$

Parameter 5. Receptor disc reflectance: R_{disc}

For an array of receptors with overlapping capture areas (see Appendix) and reflection at the outer segment discs, the apparent reflectance for the whole array equals the apparent reflectance of a single outer segment, although the latter has a smaller diameter. At an oblique angle, light escaping from the outer segment lowers the apparent disc reflectance, as only the light remaining in the outer segment 'sees' the discs. This is the basis for directional reflection according to our view (cf. Introduction).

The free parameter, R_{disc}, is taken to represent the total reflectance of the discs in the absence of other factors. Again, we converted this reflectance for the uniformity of later calculations into an apparent density of a single pass through the outer segment. D_{disc} is calculated as:

$$D_{disc} = -\log(1 - R_{disc}) \qquad (5)$$

Parameter 6. LWS cone coverage fraction: LCOV.

We distinguish between medium (MWS) and long (LWS) wavelength sensitive cones. Short wavelength-sensitive cones are so sparse that they can be neglected (Curcio, Allen, Sloan, Lerea, Hurley, Klock & Milam, 1991). The ratio of the numbers of long and medium sensitive cones is represented by their average coverage fractions, LCOV and MCOV. We argued before that, based on the capture area of the receptors, no light enters directly into the interspaces. We therefore took the sum of LCOV and MCOV as unity.

Parameter 7 Density of the visual pigment D_{vp}

The peak visual pigment density, D_{vp}, was assumed to be equal for LWS and MWS cones (SWS cones were ignored) and was a free parameter. The spectral shapes were taken from DeMarco, Pokorny & Smith, (1992). In Fig. 5 each cone can contain only one visual pigment. The density as a function of wavelength of LWS visual pigment, $D_{lws}(\lambda)$, is obtained by multiplying the normalized LWS density spectrum and D_{vp}. Substituting MWS for LWS gives $D_{mws}(\lambda)$for the MWS visual pigment.

Calculating the reflectance of the receptor layer.

The reflectance of the receptor layer in our model consists of two components, (1) the direct reflectance from the discs and (2) the reflectance of light which has traversed the receptors (either the full outer segment, or partly when escaping along the outer segment) and the deeper layers.

Reflectance of the discs.

Macroscopically we view the reflection from the individual discs as a homogeneously distributed reflectance over the full depth of the outer segment. This distributed reflection (seen from the inner segment) is influenced by (1) losses due to the absorption of visual pigment, (2) losses due to light escaping along the outer segment for oblique angle and (3) losses due to light reflected from the discs. We already assumed that the losses 2 and 3 act as homogeneous distributed optical filters, and we used a similar assumption for visual pigment. Consequently, measured light from discs near the inner segment has a higher amplitude than that of measured light from discs near the end of the outer segment. The pathlengths, from zero to the full length of the outer segment through the homogeneous optical filter, act as a graded (wedge shaped) filter. The resulting transmission from such a filter of maximum density D is described by:

$$T_{graded} = \frac{1-10^{-D}}{D*\ln(10)} \qquad (6)$$

The density of visual pigment and densities due to escaped light and disc reflection losses are substituted for D in equation (6). Pathways for escaped light run from the inner segment to the position of escape along the outer segment and back. So do the pathways for visual pigment (going in and out the receptor). We ignored secondary reflection losses at the back of the discs, permissible if the reflectance is in the order of a few percent. Multiplication by a normalizing factor $D_{disc} * \ln(10)$ is needed to arrive at the definition for reflectance R_{disc}, when D_{lws} and D_{esc} are zero. We then find for the total reflectance of the discs of LWS cones:

$$R_{lwsdisc}(\lambda) = \frac{D_{disc}(1-10^{-(2D_{lws}(\lambda)+2D_{esc}+D_{disc})})}{2D_{lws}(\lambda)+2D_{esc}+D_{disc}} \qquad (7)$$

and a similar expression for the MWS cones $R_{mwsdisc}(\lambda)$.

The total reflectance from the discs of both LWS and MWS cones is:

(8)

$$R_{totdisc(\lambda)} = LCOV * R_{lwsdisc}(\lambda) * MCOV * R_{mwsdisc}(\lambda)$$

Light transmitted through the outer segment.

The transmission of the total length of the LWS cone outer segment, $Trans_{lws}$ is simply determined by the addition of the underlying densities as:

$$Trans_{lws}(\lambda) = 10^{-(D_{lws}(\lambda)+D_{esc}+D_{disc})} \qquad (9)$$

and similarly for the MWS cones $Trans_{mws}(\lambda)$.

The total transmission of LWS and MWS cones is:

$$Trans_{tot}(\lambda) = LCOV * Trans_{lws}(\lambda) + MCOV * Trans_{mws}(\lambda) \qquad (10)$$

Light escaping along the outer segment.

For the escaped light we have to account (in a similar way as for the calculation of reflectance of the discs in equation 7) for the graded density of visual pigment, the density due to light already escaped, and the density due to light already reflected from the discs. Only the pathways from the first disc (inner segment side) to the position along the outer segment where the light escapes into the interspace have to be considered. Multiplication by a normalizing factor $D_{esc} * \ln(10)$ is needed to arrive at the definition for the escaped fraction in the absence of losses from visual pigment and disc reflection. For the LWS cones the escaped fraction is:

$$ESC_{lws}(\lambda) = \frac{D_{disc}(1-10^{-(D_{lws}(\lambda)+D_{esc}+D_{disc})})}{D_{lws}(\lambda)+D_{esc}+D_{disc}} \qquad (11)$$

and similarly for the MWS cones $ESC_{mws}(\lambda)$.

For the total escaped light fraction of LWS and MWS cones we find:

$$ESC_{tot}(\lambda) = LCOV * ESC_{lws}(\lambda) + MCOV * ESC_{mws}(\lambda) \qquad (12)$$

Reflectance of the receptor layer including light paths traversing the deeper layers.

Light entering the deeper layers consists of a fraction that has been transmitted through the outer segments and a fraction that has escaped from the outer segments. The reflectance for pathways traversing the deeper layers and the receptor layer is:

$$R_{recepdeep}(\lambda) = (Trans_{tot}(\lambda) + ESC_{tot}(\lambda))^2 * R_{deep}(\lambda) \qquad (13)$$

The total reflectance at the level of the receptor layer is given by:

$$R_{recep}(\lambda) = R_{totdisc}(\lambda) + R_{recepdeep}(\lambda \qquad (14)$$

Pre-receptor part.

It is assumed that pre-receptor reflection and transmission is non-directional, ignoring minor inhomogeneities in lens absorption over the pupil (Vos & van Os, 1975). Specular reflections from the eye media are avoided in our fundus reflectance measurements.

Parameter 8. Density of macular pigment: D_{mac}

Spectral absorbance by the macular pigment was taken from DeMarco, Pokorny and Smith (1992). As the spatial distribution is not flat, the free parameter D_{mac} represents the average density at 460 nm over our measuring field (1.6 degree).

Parameter 9. Reflectance of the inner limiting membrane: R_{ilm}

The free parameter ILM reflectance (R_{ilm}) is assumed spectrally neutral. We also assume non-directional diffuse reflection, as in our measurements, except for the tiny reflex that was sometimes present at the very center of the fovea, specular reflection was not visible. Minor backscatter in the vitreous cannot be distinguished from the ILM reflectance and is included in this parameter.

Parameter 10. Lens aging part: $D_{lens\text{-}a}$

The density of the media consists of four components, the fixed spectral density of the non aging lens part ($D_{lens\text{-}na}$), the spectral density of the age dependent lens part ($D_{lens\text{-}a}$), which we allowed to vary, the fixed density of the spectrally neutral scatter losses ($D_{medscat}$), and the fixed spectral density of 24 mm of water (D_{water}), representing the vitreous. The parameter values for $D_{lens\text{-}a}$ and $D_{lens\text{-}na}$ are the densities at 420 nm. Spectral data were from the van Norren and Vos (1974) standard observer with the aging algorithm from Pokorny, Smith and Lutze (1987). Since our measurements were not restricted to the center of the pupil, the 0.86 correction term for large pupils was applied to $D_{lens\text{-}a}$ and $D_{lens\text{-}na}$. The term $D_{medscat}$ represents scatter losses in the media (mainly lens, but also some loss due to the corneal reflectance). Delori and Pflibsen (1989) suggested a fixed value of 0.1 for this parameter, $D_{medscat}$. We used 0.15, the value provided by van Norren and Vos (1974) for non spectacle wearers and an additional 0.05 for spectacle wearers. Absorption by the vitreous, taken to be that of pure water (Smith & Baker, 1981), was only significant at the longest wavelengths (0.025 at 740 nm).

Calculating the reflectance at the level of the cornea.

Finally, we have to account for reflection and absorption by the media in order to determine the reflectance of the whole eye.

$$R_{eye}(\lambda) = 10^{-2(D_{lens-na}(\lambda)+D_{lens-a}(\lambda)+Dmedscat+D_{water}(\lambda))} * (R_{ilm} + (1-R_{ilm})^2 * 10^{-2D_{mac}(\lambda)} * R_{recep}(\lambda)) \quad (15)$$

Fitting experimental data

Fitting procedure

Parallel channels in the model call for a fitting algorithm capable of handling non-linear parameters. We therefore applied the Marquardt-Levenberg fitting algorithm (Press, Flannery, Teukolsky & Vettering, 1989). The model has 10 free parameters (3 pre-receptor, 4 receptor layer and 3 post-receptor). To allow optimal fits, we allowed an extra correction density D_{ct}, giving 11 free parameters (see below). The freedom of fitting was limited because in the four spectra, measured for perpendicular and oblique retinal angle and both in fully bleached and dark adapted conditions, 48 data points had to be fitted simultaneously. From the total of 11 free parameters, only 3 parameters were allowed to vary between the four spectra, namely, the Stiles-Crawford parameter SC, the amount of visual pigment density D_{vp} and the correction term D_{ct} . D_{vp} was set at zero for the bleached condition. SC equaled 1 for the perpendicular condition (no leakage) and had a positive value lower than 1 for the oblique condition. The free correction parameter, D_{ct}, was required only in the perpendicular condition. Most spectral absorbers we used tend to become zero at the long wavelengths; this limits the degrees of freedom we have for the fitting process. This was in particular a problem when small reflectance differences occurred between dark and bleached spectra that could not be fully explained by the low visual pigment absorption at the long wavelengths. The visual pigment parameter, being the only free parameter allowed for fitting the difference here, was then strongly influenced. The differences are considered to originate from small alignment disturbances between runs, from small changes in corneal reflection caused by suppression of the blink reaction during long periods of fixation, or from yet unknown processes. D_{ct} (either positive or negative) was therefore added to the media scatter term, $D_{medscat}$, in the perpendicular, dark adapted condition.

The measured data for 410 and 430 nm were excluded from the fitting process, because these low reflection values were liable to small, and in some subjects due to changes in head fixation, variable amounts of back-scattered light from the cornea or lens. The data are included in the spectral plots however, for comparison with the model results (see also experimental results).

The standard deviations (see Protocol) were used for weighting the data during the fitting process and are shown as error bars in the spectral plots of Figs. 1 and 3. Note that these errors bars are minimum estimates, mainly expressing photon noise; errors due to long-term effects, for instance shifts in alignment between blocks, are not included. This is one reason for the model curves missing some data points. Another reason is that model curves as in Fig. 1c, 3b and 3c are not the result of separate fits to the data points in those figures, but secondary results from only one global fit to the four primary spectra. The

reflectance data averaged over the group of ten subjects, together with the standard deviation for the group and the mean of the relative error in each subject, are shown in Table 2. The standard deviation for the group shows the inter-individual differences. The average of the relative errors, calculated from single measurement standard deviations, represents the average stability of a measurement. The parameters obtained from fitting the data for the ten subjects are shown in Table 3.

Table 2. Mean spectral reflectance data for the ten subjects in four conditions

Wave (nm)	Perpendicular bleached			Perpendicular dark			Oblique bleached			Oblique dark		
410	0.027	0.496	0.216	0.021	0.59	0.334	0.019	0.656	0.809	0.023	0.538	0.244
430	0.097	0.344	0.075	0.081	0.313	0.077	0.067	0.353	0.097	0.066	0.371	0.127
450	0.118	0.364	0.050	0.091	0.333	0.050	0.078	0.337	0.074	0.081	0.414	0.069
470	0.170	0.350	0.040	0.122	0.295	0.037	0.099	0.270	0.048	0.100	0.323	0.056
490	0.219	0.365	0.033	0.140	0.277	0.039	0.114	0.265	0.051	0.108	0.297	0.052
510	0.645	0.312	0.023	0.289	0.211	0.034	0.249	0.219	0.041	0.202	0.213	0.045
540	1.230	0.275	0.016	0.451	0.185	0.023	0.443	0.194	0.024	0.318	0.200	0.031
560	1.334	0.259	0.016	0.489	0.186	0.025	0.509	0.195	0.024	0.357	0.203	0.031
577	1.413	0.243	0.015	0.586	0.199	0.019	0.568	0.170	0.020	0.414	0.206	0.024
610	2.073	0.240	0.012	1.196	0.203	0.016	1.198	0.264	0.017	0.960	0.291	0.019
630	2.386	0.254	0.012	1.748	0.226	0.014	1.533	0.277	0.016	1.342	0.296	0.015
650	2.715	0.242	0.012	2.277	0.233	0.011	1.843	0.282	0.015	1.728	0.308	0.013
690	3.461	0.253	0.014	3.270	0.248	0.014	2.639	0.274	0.018	2.574	0.294	0.017
740	3.926	0.229	0.014	3.793	0.235	0.012	3.202	0.251	0.015	3.118	0.262	0.014

Data are percentages referred to a white Lambertian reflector, followed by the relative standard deviation. The relative standard deviation expresses mainly the intra-individual differences in reflectance. The average of individual relative errors is given in each last column, as an indication of the relative error in one subject. This is mainly the result of photon noise and small movements of the subjects.

Results from the fitting process.

The parameters obtained after the fitting process are now shortly discussed and compared with data found in the literature.

Deeper layers

Note that we simplified the model for the deeper layers. Parameters for blood and melanin are therefore not necessarily comparable with physiologically data (cf. Post-receptor (deeper) layers section).

Parameter 1. Density of deep scatter losses.

The deep scatter loss D_{dscat} (0.23), was higher than in the model of Delori and Pflibsen (1989) who found 0.1. This is because we used smaller fields. Delori and Pflibsen found reflectance in the long wavelength part of the spectrum, stemming mainly from deeper layers, to be higher than 10% for lightly-pigmented subjects. This is only partly explained by the large (5 degree) illumination field they used. Van Norren and Tiemeyer (1986) did not use a D_{dscat} term, but allowed the sclera reflectance to change. Converted to the density of deep scatter losses and corrected for not having implemented media scatter losses, we found a density of 0.17.

Table 3. Free and fixed parameters used in the model.

		Method 1			Method 2	
free parameter,	Abbrev.	mean,	sd,	range	mean,	sd
Deep scatter loss	D_{dscat}	0.23	0.06	0.14 - 0.30	0.225	0.006
Blood layer (mm)	T_{hblood}	22.7	16.9	7.3 - 63.2	17	4.5
Melanin density	D_{mela}	1.32	0.23	0.98 - 1.68	1.274	0.028
Stiles-Crawford eff.	SC	0.21	0.11	0.07 - 0.41	0.193	0.022
OS disc reflectance(%)	R_{disc}	2.75	0.73	1.64 - 3.80	2.773	0.095
LWS cone coverage	LCOV	0.56	0.11	0.41 - 0.71	0.525	0.048
Visual pigment dens.	D_{vp}	0.57	0.11	0.41 - 0.80	0.587	0.026
Macular pigment dens.	D_{mac}	0.54	0.12	0.42 - 0.83	0.525	0.025
ILM reflectance (%)	R_{ilm}	0.26	0.09	0.12 - 0.44	0.26	0.024
Lens dens.	$D_{lens\text{-}a+lens\text{-}na}$	0.54	0.11	0.42-0.83	0.533	0.03
Media correction dens.	D_{ct}	0.018	0.009	0.003-0.036	0.0194	0.0028

The free parameter results are for a group of ten subjects. Two methods were used to calculate the averages. In the first method the spectral data from each individual were fitted, and the resulting parameters were averaged to give a group mean and standard deviation. The column 'range' gives the lowest to highest result of the fits. In the second method all corresponding spectra of the ten subjects were averaged to give data for an 'average subject' (Table 2), and subsequently fitted, resulting in a second mean and standard deviation for the 'average subject'. For lens density the results are the sum of the free lens aging parameter and the fixed lens non-aging parameter.

Fixed parameters:

Density of media scatter losses	$D_{medscat}$	0.15 (+0.05)
Density of non aging lens part	$D_{lens\text{-}na}$	0.31 at 420 nm
Density of 24 mm water	D_{water}	0.025 at 740 nm
Reflectance of the sclera	R_{sclera}	0.5 at 675 nm

Parameter 2. Thickness of blood layer.

The thickness of the equivalent blood layer, Th_{blood}, was 23 μm. The mean value from van Norren and Tiemeyer (1986) is given as a density of 0.18 at 500 nm, corresponding to a thickness of 37 μm. Delori and Pflibsen (1989) obtained higher values (60 to 304, average 168 mm) when assuming Kubelka-Munk scattering in the choriodal space, but at the expense of introducing several parameters (cf. Model section).

Parameter 3. Density of melanin.

The density of melanin (1.32 at 500 nm) is mainly determined by the fit to wavelengths above 600 nm. At shorter wavelengths absorption by blood dominates. In addition, at the foveal site, our model shows that the reflection in the receptor layer strongly masks the reflection from deeper layers at wavelength less than 570 nm. Melanin densities ranged from 0.98 to 1.68. This is in the lower end of the range found by Delori and Pflibsen (1989) (0.79 to 8.5). Van Norren and Tiemeyer (1986) reported a value of 0.98.

Receptor layer.

Parameter 4. Stiles-Crawford factor.

The Stiles-Crawford parameter, SC, depends on the setting of the retinal angles (adjustment). In the present context SC as such is not important but is needed only to determine the other parameters. The maximum value of 0.41 ensures that the fitting process can successfully discriminate the directional cone reflection from the non-directional reflection of the pre-receptor and the deeper layers. Note that our definition of SC was slightly different from the psychophysical convention, where it is a measure of light absorbed by visual pigment.

Parameter 5. Receptor disc reflectance.

The combined reflectance from the discs over the full length of the outer segment (2.75 %) can best be compared with the reflectance at the RPE assumed in the models of van Norren and Tiemeyer (1986) (1.18%) and Delori and Pflibsen (1989) (2.3%). The design of the entry and exit pupils of the apparatus influences the directional reflection. If van Norren and Tiemeyer (1986) had used media scatter in their model, their value converts to 2.36% (correction with twice 0.15 D).

Parameter 6. LWS cone coverage fraction.

The coverage fraction of the LWS cones (0.56) is often expressed as the ratio of LWS to MWS cones. Converted to LWS coverage fraction, values of about 0.66 are reported (Vos & Walraven, 1970; Cicerone & Nerger, 1989; Kraft, Makino, Mathies, Lugtenburg, Schnapf & Baylor, 1990).

Parameter 7. Density of the visual pigment.

The visual pigment densities we calculated (0.57 for single traverse) are comparable with psychophysical results. In our calculations, we did not take into consideration whether the visual pigment was fully bleached or fully dark adapted (see section 2.3), so the value D_{vp} is a low estimate. The final result could be about 10 percent higher (0.63) if the Rushton equation is valid (see section 2.3). Visual pigment densities decrease with field size. Smith and Pokorny (1973) found 0.3 for the MWS cone and 0.4 for the LWS cone, using a 2.5 degree test field. Miller (1972) reported 0.5-0.6 for LWS and 0.4-0.5 for MSW cones (1.6 degree test field). Burns and Elsner (1993) reported 0.3 for the MWS cone and 0.5 for the LWS cone, using 2 degree fields. Pokorny and Smith (1976) presented a formula to calculate the densities in relation to field size. For our 1.6 degree field, this would result in 0.52 for LWS and 0.42 for MWS cones. Walraven and Bouman (1960) reported 0.7, based on changes in self-screening of the visual pigments due to changes in Stiles-Crawford effect (2 degree field).

Pre-receptor part.

Parameter 8. Density of macular pigment.

The density of macular pigment (0.54 at 460 nm) differs substantially between subjects and also decreases with increasing field size. Bone, Landrum and Cains (1992) found 0.57 for a spot size of 1.6 degrees (identical to our detection field size). Delori and Pflibsen (1989) used larger fields (illumination 5 degrees, detection 1.2-1.6 degrees) and found 0.21. The mean value from van Norren and Tiemeyer (1986) is 0.24; they also used larger fields (3.5 degrees illumination, 2.5 degrees detection).

Parameter 9. ILM reflectance.

The ILM reflectance appeared to be low (0.26 percent). As judged from direct observation, the inner limiting membrane reflectance for this foveal site must be low compared to the high specular reflections in the perimacular region, that are particularly visible in young subjects. This is partly due to the surface being curved, which results in at most a very small specular reflection at the foveal pit. Values about 0.09 times the total outer segment disc reflection are indicative of low superficial stray-light at wavelengths greater than 500 nm.

Parameter 10. Media density.

The lens density (0.54 at 420 nm, age dependent plus age independent part) for our group of subjects (average age 32, range 20 to 51) was lower than that reported by Pokorny, Smith and Lutze (1987) (0.73, also average age 32). The mean value from van Norren and Tiemeyer (1986) for four young subjects was 0.38 at 419 nm. Delori and Pflibsen (1989) found 0.66 for a group of 10 subjects aged between 22 and 38 years. Minor addition of media back-scatter to the data accounts for the data points at 410 and 430 nm being generally higher than the model fit. This back scatter also partly compensates for media losses when using reflection techniques, yielding lower values for the lens density than those obtained by using psychophysical techniques.

Absorption by water was responsible for the lower predictions for directional reflectance at long wavelengths (Fig. 1c). Absorption of water is hardly recognized in the logarithmic representation of the original reflectance spectra.

Parameter 11. Media correction term.

The media correction term, D_{ct}, was used only in the perpendicular, dark-adapted condition and is a measure of (for instance head position) stability during the measurement. Although generally positive, its value (0.018) is sufficiently low that no further comment need to be made. This leaves 10 important free parameters.

Statistical analysis.

Analysis of covariances between the 11 fitted parameters from a fit to the average subject spectral data yields insight into the degree of independence of the parameters. In addition, each parameter was stepped one by one over a range of fixed values, while the other parameters were allowed to vary. This cross-sectioning of the multi-dimensional parameter space yields (limited) insight into the occurrence of multiple minima. No multiple minima were found.

Only two covariances were significant, $D_{lens\text{-}a}$ with R_{disc} (0.75) and D_{mela} with D_{dscat} (-0.83). The aging lens density hardly changed at wavelengths between 500 and 600nm, where the (by definition) spectrally neutral R_{disc} is the most important component. It is yet unknown how this covariance is influenced by an underestimated lens density due to media back scatter. The negative covariance between melanin density, D_{mela}, and the density of deep scatter losses, D_{dscat} , means that the model is inclined to substitute the spectrally neutral density of D_{dscat} with the almost flat melanin spectrum at long wavelengths. As these are both parameters in our simplified modeling of the deeper layers, effects on receptor and pre-receptor layer parameters should be minimal.

Correlations between the fitted parameters were found by analyzing the parameters for the ten subjects. Age was added as an extra variable in the analyses. Only three correlation coefficients were higher than 0.7. The correlation between $D_{lens\text{-}a}$ and age (0.78) was expected. The correlation between SC and LWS coverage fraction LCOV (0.72) predicts lower directional sensitivity when a subject has a relatively high fraction of LWS cones. This is not very likely. In the long wavelength part of the spectrum, the model probably trades directly reflected light from LWS cones for deeper reflected light. The latter is also influenced by visual pigment changes but does not show directional sensitivity. The last high correlation (0.76) was R_{disc} with D_{vp}. This could simply mean that a longer outer segment has more discs, resulting in both higher total reflection and more visual pigment.

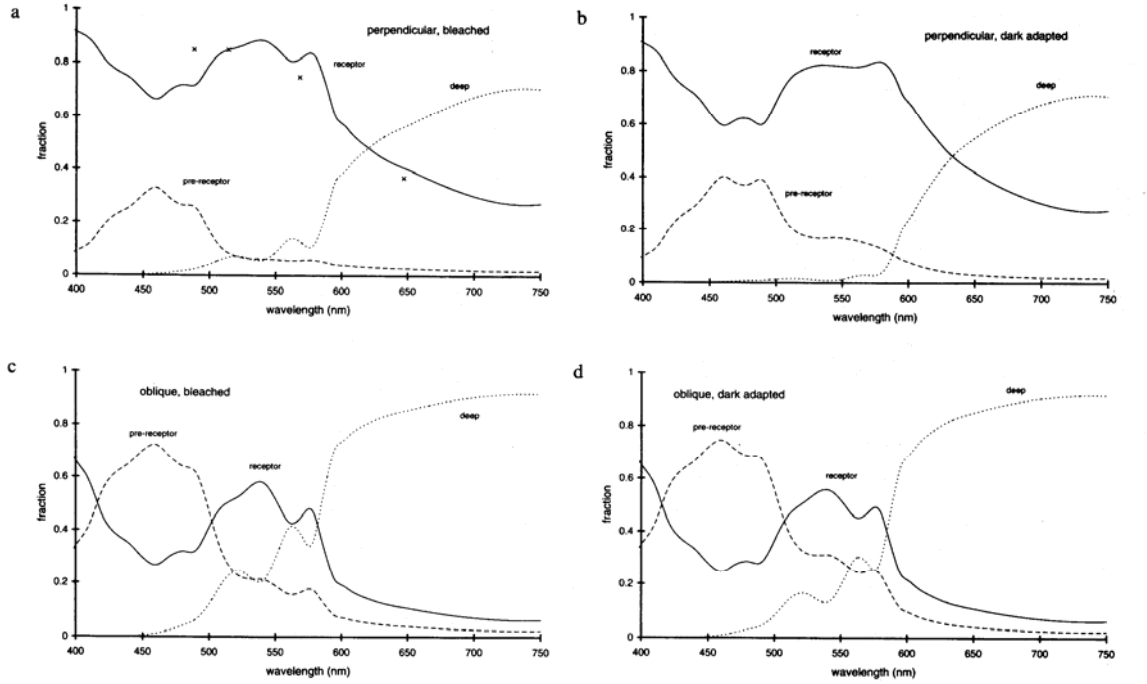

Fig. 6. Model predictions of the fractional components of the different pathways. These components describe the four conditions measured in subject JK. Panel a: bleached, perpendicular. Panel b: dark-adapted, perpendicular. Panel c: bleached, oblique. Panel d: dark-adapted, oblique. 'Pre-receptor' represents all light reflected in front of the photoreceptors (ILM). 'Receptor' represents the reflectance from the discs. 'Deep' represents reflectance from the sclera. Crosses in panel a are the fractions with maintained polarization replotted from van Blokland (1986).

The three major components of reflected light.

Once the total foveal reflectance has been put in a model, it is possible to show the underlying components. Plotted in Fig. 6 are the fractional contributions (as seen at the cornea) of the separate pathways; the ILM (pre-receptor), the discs (receptor), and the sclera (deeper layers). How the components behave as a function of wavelength in the four conditions is plotted in panels a, b, c and d. In Fig. 6a, in the mid-spectral range, the pre-receptor fraction (the superficial stray-light component from the ILM) and the deeper fraction (sclera) are small; the receptor outer segment disc fraction accounts for almost 90% of the light emerging from the eye. At long wavelengths, the 'deep' component dominates. Only this light has traveled the full layer of visual pigment twice (no leak in the perpendicular condition), as assumed in the simple model of the earliest densitometer

studies. Dark-adaptation of the visual pigments resulted in some loss of the receptor disc fraction around 550 nm, but also in an about a threefold increase of pre-receptor reflected light (Fig. 6b). This shows that 'stray-light' in densitometry has a more important role in dark-adapted conditions. However, 'stray-light' is even more important in the oblique conditions (Fig. 6c and 6d), and the receptor signal only accounts for about 60% of the total reflection from the eye at mid-spectral wavelengths. This illustrates the importance of using small entry and exit pupils in instruments designed for optimal detection of light from the cone photoreceptors.

General discussion

Our model is the first to incorporate a directional reflection from the stack of discs in the outer segments of the photoreceptor. This has a major influence on the estimate of the density of visual pigment. We found calculated densities ranging from 0.41 up to 0.80, in agreement with psychophysical data. These values were much higher than the densities obtained using the simple model with a double traversion of the visual pigment layer. Our measured densities ranged from 0.32 to 0.54, with a mean of 0.44. With the simple model, assuming no stray-light, the estimated density for visual pigment is only 0.22. The graded density in our model is an important determinant in these higher values; stray-light from the ILM has only a minor effect. It should be emphasized that the magnitude of the directional receptor component strongly depends on the measuring technique used. Fundus reflectometers with large exit pupils, as used in older studies, do not make optimal use of the directional properties of the foveal cones. This results in shorter pathways through the photopigments and a higher stray-light fraction, hence lower measured visual pigment densities.

Several origins of the retinal reflections have been proposed in previous studies. Polarization, spectral decomposition, image quality of reflected light and visual pigment bleaching have been used as tools to discriminate between different layers. Campbell and Gubisch (1966) used white illumination light and concluded that the retina had a nearly perfect non-directional character. This is not very surprising, given the dominating reddish nature of the spectral reflectance of the deeper layers. There is now consensus that the reflection from deeper layers is red, has poor (aerial) image quality and destroyed polarization. The discussion is now concentrated on additional reflectors. Van Blokland (1986) measured the degree of maintained polarization of light from the fovea. His data, replotted in Fig. 6a, show a striking resemblance to those for our receptor component. The decreasing polarization at longer wavelengths relates to the increasing fraction of deeper, unpolarized light. The reflection from the receptor discs seems to maintain polarization. As argued in the Introduction, we do not agree with his interpretation of the RPE as the main origin of reflected light, as we assumed that all light that travels beyond the receptor layer has no directional properties. Earlier, Weale (1966) used polarization as well as visual pigment bleaching and reported reflections from Bruch's membrane with maintained polarization. The polarization state did not change much after visual pigment bleaching. This conclusion is supported by the relatively high receptor fraction in the dark-adapted condition, as can be seen in Fig. 6b. Weale's experiments with different exit pupil sizes revealed that, consistent with our model, directional reflection occurred at mid-spectral wavelengths. Techniques that provide information supporting the receptor layer as an important reflector used the quality of the aerial image (Gorrand, 1985) and polarization (Rohler, Miller & Aberl, 1969) albeit without correction for retardation in the eye. In experiments in which adequate tools for discrimination are not used, the reflection from the receptors is easily confused with a reflection from the ILM (van Norren & Tiemeyer, 1986; Millodot, 1972; Charman, 1980) or RPE (van Blokland & van Norren,

1986).

Images of the fovea obtained with optical coherence techniques (Puliafito et.al., 1995) show a reflection from the region of the inner limiting membrane and relatively strong reflections in the region of the retinal pigment epithelium and choriocapillaris. Multiple scattering in the deeper layers is not detected with this technique. Similarly, distributed reflection along the depth of the outer segment may be underestimated. The use of IR wavelengths and entry and (large) exit pupils not aligned to the peak of the Stiles-Crawford maximum may further reduce the magnitude of the pronounced receptor component that we see with our instrument at wavelengths around 550 nm (Fig. 6). We suggest, in particular when looking at retinal detachment cases (for instance Puliafito et.al., 1995, case 9), that the double layer reflex near the RPE consists of a reflection from the outer segments and a reflection from for instance the choriocapillaris or Bruch's membrane. The comment made by the authors that the reflection at the receptors occurred due to 'the normal incidence of the probing beam' is in full support of our theory about the origin of the directional reflection. In our model we include the reflection from the choriocapillaris and RPE region to the total of the non directional reflectance from the deeper layers.

Using a laser slit lamp technique, Shahidi, Zeimer and Mori (1990) found a double peaked reflection profile in the retina of normal human subjects. In the fovea, the reflection (543 nm) assumed to originate from the ILM region is about 30% of the reflection assumed to originate from the RPE region. The depth resolution of this technique is too low, however, to detect a gradual disc reflection.

The stack of discs in the outer segment has a resemblance to an ordinary Yagi-type television antenna. We think that both the discs and the Yagi elements influence the electro-magnetic field in a similar way to achieve high forward sensitivity. The resulting increase in the average refraction index of the discs relative to the receptor interspaces forms the origin of the general wave guiding behavior (cf an optic fiber). We ignored the fact that the diameter of the outer segments of the receptor is small compared to the wavelength of light. Entering photons can be considered as Gaussian-shaped energy fields with, even when they enter perpendicular, some energy running in the interspace. On the other hand, interspace light may have some energy running in the outer segment. In the oblique condition, these factors cancel each other to a certain extent.

The advantages of receptor directionality include suppression of scattered light in the eye and efficient use of visual pigment in small cross-sectional outer segments, leaving an interspace for other purposes (supporting structures and transport). Our model does not require suppression of oblique light in an anatomically obscure absorber, shielding the visual pigment (Stiles & Crawford, 1933; van Blokland & van Norren, 1986). In addition, our model predicts that the light lost for vision is also lost for directional reflection. The directionality of the foveal reflectance is, however, more narrowly tuned than the one derived from psychophysical data. When fitted with a Gaussian curve, widths measured between the inflection points are found near 4.1 mm for the psychophysical data and 2.6 mm for reflection data (van Blokland, 1986). A possible explanation is that non-directional light reflected from deeper layers does not influence the width of the directional reflection data, while the part of the deeper reflected light traveling back through an outer segment broadens the width of the psychophysical data. Compare this with recapturing of light by neighbouring receptors (Chen & Makous, 1988). Psychophysical data (Smith & Pokorny, 1973; Burns & Elsner, 1993; Pokorny & Smith, 1976) suggest that the peak density of visual pigment in LWS cones is higher than the peak density in MWS cones. We tried to consider both densities as free parameters, but could not find satisfactory solutions of the fitting process because of a high

correlation between the LWS visual pigment density and the LWS coverage fraction. Perhaps the reddish nature of the deeper reflected light makes the LWS cones more efficient for visual perception.

At short wavelengths (< 510 nm) the reflection from the ILM becomes an important stray-light factor, since light originating from the receptor layer is attenuated by the macular pigment. This forms an extra handicap if one tries to make densitometric measurements of the already sparse SWS cones. We estimated, using an extended version of our model containing SWS cones (not shown), that a measured density at 440 nm of only 0.015 can be expected for the SWS cones outside the very center of the fovea.

In summary, our model describes the spectral magnitude of the three main reflecting components in the human fovea, for different bleach levels and retinal angles. Separate pathways for directional reflection from the foveal cone receptor discs and non-directional reflection from the pre- and post receptor layers were found. This may be relevant to other techniques based on reflected light from the retina (for an overview of other techniques cf. Knighton, 1995). The model yields estimates of the density of the visual pigments that are consistent with estimates based on psychophysical techniques. The model also yields estimates of the optical properties of other important absorbers. In spite of including the receptor layer with inherent refracting aspects, for the non directional reflection from the deeper layers in bleached conditions it can still be ignored. As we simplified the modeling of these deeper layers, more complex modeling would be needed to arrive at physiologically relevant estimates for the parameters in the choriodal space.

Appendix

The directional reflectance data from van Blokland (1986) shows how reflected light from the receptors is concentrated to a Gaussian spot in the pupil plane. The weighted area under the two-dimensional Gaussian spot, with inflection points separated by S = 2.6 mm, can be calculated as:

$$\pi \cdot S^2 / 2 = 10.6 \text{ mm}^2. \quad (16).$$

For the area of a hemisphere centered at the retina, with the distance retina-pupil plane (16.7 mm) as a radius (r), we find:

$$2 \cdot \pi \cdot r^2 = 1750 \text{ mm}^2. \quad (17).$$

The antenna gain is the ratio of the hemisphere area and Gaussian area, hence 165.

The diameter of the capture area is:

$$\text{Gain} \cdot \lambda^2 / (4 \cdot \pi) = 165 \cdot 0.55^2 / (4 \cdot \pi) = 4 \text{ µm}. \quad (18).$$

Thus, with inner segment diameters of foveal cones of about 2.5 mm (Polyak, 1941; Packer, Hendrickson & Curcio, 1989), the capture area of a single cone is indeed larger than the physical area of the inner segment. Cones are tightly packed in the fovea, we assume therefore that light does not enter the cone interspaces directly.

Acknowledgment
We thank Dr. J.J. Vos, Prof. V.C. Smith and Prof. J. Pokorny for their critical comments on the manuscript.

References

van Assendelft, O.W. (1970). Spectroscopy of hemoglobin derivatives (Springfield, IL: Thomas, C.C.).

van Blokland, G.J. & van Norren, D. (1986). Intensity and polarization of light scattered at small angles from the human fovea. *Vision Research, 26*, 485-494.

van Blokland, G.J. (1986). Directionality and alignment of the foveal receptors assessed with light scattered from the human fundus. *Vision Research, 26*, 495-500

Bone, R.A., Landrum, J.T. & Cains, A. (1992). Optical density spectra of the macular pigment in vivo and in vitro. *Vision Research, 32*, 105-110.

Burns, S.A. & Elsner, A.E. (1993). Color matching at high luminances: photopigment optical density and pupil entry. *Journal of the Optical Society of America, 10*, 221-230.

Campbell, F.W. & Gubisch, R.W. (1966). Optical quality of the human eye. *Journal of Physiology London, 186*, 558-578.

Charman, W.N. (1980). Reflection of plane-polarized light by the retina. *British Journal of Physiological Optics, 34*, 34-49.

Cicerone, C.M. & Nerger, N.L. (1989). The relative numbers of long-wavelength-sensitive to middle-wavelength-sensitive cones in the human fovea centralis. *Vision Research, 29*, 115-128.

Chen, B. & Makous, W. (1989). Light capture by human cones. *Journal of Physiology, 414*, 89-109.

Coble, J.R. & Rushton, W.A. (1971). Stiles-Crawford effect and the bleaching of cone pigments. *Journal of Physiology, 217*, 231-242.

Curcio, C.A., Allen, K.A., Sloan, K.R., Lerea, C.L., Hurley, J.B., Klock, I.B. & Milam, A.H. (1991). Distribution and morphology of human cone photoreceptors stained with anti-blue opsin. *Journal of Comparative Neurology, 312*, 610-624.

Delori, F.C. & Pflibsen, K.P. (1989). Spectral reflectance of the human ocular fundus. *Applied Optics, 28*, 1061-1077

DeMarco, P., Pokorny, J. & Smith, V.C. (1992). Full-spectrum cone sensitivity functions for X-chromosome-linked anomalous trichromats. *Journal of the Optical Society of America, 9*, 1465-1476.

Enoch, J.M., & Hope, G.M. (1973). Directional sensitivity of the foveal and parafoveal retina. *Investigative Ophthalmology and Visual Science, 12,* 497-503

Gabel, V.P., Birngruber, R. & Hillenkamp, F. (1978). Visible and near infrared light absorption in pigment epithelium and choroid. *XXIII Concilium Ophthalmologium*, Kyoto, Shimizu, Ed. Excerpta Medica, Amsterdam-Oxford: Elsevier.

Gorrand, J.M. (1985). Directional effects of the retina appearing in the aerial image. *Journal Optics (Paris), 16*, 279-287.

Gorrand, J.M. & Delori, F. (1995). A reflectometric technique for assessing photoreceptor alignment. *Vision Research, 35*, 999-1010.

Hee, M.R., Izatt, J.A., Swanson, E.A., Huang, D., Schuman, J.S., Lin, C.P., Puliafito, C.A. & Fujimoto, J.G. (1995). Optical Coherence Tomography of the human retina. *Archieves of Ophthalmology, 113,* 325-332.

Hitzenberger, C.K. (1991). Optical measurement of the axial eye length by laser doppler interferometry. *Investigative Ophthalmology and Visual Science, 32*, 616- 624.

Huang, D., Swanson, E.A., Lin, C.P., Schuman, J.S., Stinson, W.G., Chang, W., Hee, M.R., Flotte, T., Gregory, K., Puliafito, C.A., & Fujimoto, J.G. (1991). Optical coherence tomografy for micron-resolution imaging. *Science, 254*, 1178- 1181.

Jessop, G.R. (1971). VHF-UHF Manual. London: Radio Society of Great Britain.

King-Smith, P.E. (1973a). The optical density of erythrolable determined by retinal densitometry using the self-screening method. *Journal of Physiology, 230*, 535-549.

King-Smith, P.E. (1973b). The optical density of erythrolable determined by a new method. *Journal of Physiology, 230*, 551-560.

Knighton, R.W. (1995). Quantitative reflectometry of the ocular fundus. *IEEE Engineering in Medicine and Biology, 14*, 43-51.

Kraft, T.W., Makino, C.L., Mathies, R.A., Lugtenburg, J., Schnapf, J.L. & Baylor, D.A. (1990). Cone excitations and color vision. *Cold Spring Harbor Symposia on Quantitative Biology, Vol LV*.

Longhurst, R.S. (1973). Geometrical and physical optics. Hongkong: Commonwealth Printing Press Ltd.

Millodot, M. (1972). Reflection from the fundus of the eye and its relevance to retinoscopy. *Atti Fondatiore Georgi Ronchi, 27*, 31-50.

Miller, S.S. (1972). Psychophysical estimates of visual pigment densities in red-green dichromats. *Journal of Physiology London, 223*, 89-107.

van Norren, D. & van de Kraats, J. (1981). A continuously recording retinal densitometer. *Vision Research, 21*, 897-905.

van Norren, D. & van de Kraats, J. (1989). Retinal densitometer with the size of a funduscamera. *Vision Research, 29*, 369-374.

van Norren, D. & van de Kraats, J. (1989). Imaging retinal densitometer with a confocal scanning laser ophthalmoscope. *Vision Research, 29*, 1825-1830.

van Norren, D. & Tiemeyer, L.F. (1986). Spectral reflectance of the human eye. *Vision Research, 26*, 313-320.

van Norren, D & Vos, J.J. (1974). Spectral transmission of the human ocular media. *Vision Research, 14*, 1237-1243.

Packer, O., Hendrickson, A.E. & Curcio, C.A. (1989). Photoreceptor topography of the retina in the adult pigtail macaque. *The Journal of Comparative Neurology, 288*, 165-183.

Piket-May, M.J., Taflove, A. & Troy, J.B. (1993). Electrodynamics of visable-light interactions with the vertebrate retinal rod. *Optic Letters, 18*, 568-570.

Pokorny, J. & Smith, V.C. (1976). Effect of field size on red-green color mixture equations. *Journal of the Optical Society of America, 66*, 705-708.

Pokorny, J., Smith, V.C. & Lutze, M. (1987). Aging of the human lens. *Applied Optics, 26*, 1437-1440.

Polyak, S.L. (1941). The Retina (p 488). Chicago: University of Chicago Press.

Press, W.H., Flannery, B.P., Teukolsky, S.A. & Vettering, W.T. (1989). Numerical Recipes in Pascal, Cambridge:University Press.

Puliafito, C.A., Hee, M.R., Lin, C.P., Reichel, E., Schuman, J.S., Duker, J.S., Izatt, J.A., Swanson & E.A., Fujimoto J.G. (1995). Imaging of macular diseases with optical coherence tomography. *Ophthalmology, 102*, 217-229.

Ripps, H. & Weale, R.A. (1965). Analysis of foveal densitometry. *Nature London, 205*, 52-56.

Rohler, R., Miller, V., & Aberl, M. (1969). Zur messung der modulations- ubertragungs-funktion des lebenden menschlichen auges in reflektierten licht. *Vision Research, 9*, 407-428.

Rushton, W.A.H. (1965). Straylight and the measurement of mixed pigments in the retina. *Journal of Physiology, 176*, 46-55.

Rushton, W.A.H. & Henry G.H. (1968). Bleaching and regeneration of cone pigments in man. *Vision Research, 8*, 617-631.

Shahidi, M., Zeimer, R.C., Mori, M., (1990). Topography of the retinal thickness in normal subjects. *Ophthalmology, 97*, 1120-1124.

Smith, R.C. & Baker, K.S. (1981). Optical properties of the clearest natural waters. *Applied Optics, 20*, 177-184

Smith, V.C. & Pokorny, J. (1973). Psychophysical estimates of optical density in human cones. *Vision Research, 13*, 1199-1202.

Smith, V.C., Pokorny J. & van Norren, D. (1983). Densitometric measurement of human cone photopigment kinetics. *Vision Research, 23*, 517-524.

Snyder, A.W. & Pask, C. (1973). The Stiles-Crawford effect - explanation and consequences. *Vision Research, 13*, 1115-1137.

Stiles, W.S. & Crawford, B.H. (1933). The luminous efficiency of rays entering the eye pupil at different points. *Proceedings of the Royal Society B, 112*, 428-450.

Vos, J.J. & van Os, F.L. (1975). The effect of lens density on the Stiles-Crawford effect. *Vision Research, 15*, 749-751.

Vos, J.J. & Walraven, P.L. (1970). On the deriviation of foveal receptor primaries. *Vision Research, 11*, 799-818

Walraven, P.L. & Bouman, M.A. (1960). Relation between directional sensitivity and spectral response curves in human cone vision. *Journal of the Optical Society of America, 50*, 780-784.

Weale, R.A. (1966). Polarized light and the human fundus oculi. *Journal of Physiology, 186*, 175-186

Wyszecki, G. & Stiles, W.S., (1982). Color Science: concepts and methods, quantitative data and formulae. New-York: John Wiley and Sons inc.

Chapter 5

Optical density of the aging human ocular media in the visible and the UV

Jan van de Kraats and Dirk van Norren

Journal of the Optical Society of America A 24 1842-1857(2007)

Abstract

We analyzed the literature on the absorption in the young and aging human eye media. Five templates were derived to provide an adequate description of the spectra from 300 to 700 nm, for the lens, cornea, aqueous, and vitreous. Two templates were found in all media. They stand for Rayleigh scatter and the absorbance of tryptophan. Three additional templates for the lens represent absorbance in kynurenine derivatives like 3-hydroxykynurenine glucoside (3HKG), and absorbance in two substances found at older age. Except for Rayleigh scatter, all templates have a Gaussian shape. Aging trend functions were derived that show a linear slope on an age squared scale. The result can be used to correct for media losses in visual perception tasks, in fundus reflectometry, and in studies on light damage. © Optical Society of America.

*OCIS codes: 170.4470, 290.2200, 300.1030, 330.4060, 330.3350, 330.5370***.**

Introduction

The eye media consist of cornea, aqueous humor, lens, and vitreous. Their primary optical function is to focus light from the world around us to a sharp image on the retina. In addition, the cornea and lens filter optical radiation to prevent dangerous ultraviolet radiation from reaching the retina. The cornea strongly absorbs in the far UV, below 310 nm. The lens has major absorption (high density) in the near UV, and to a lesser extent in the visible. The aqueous humor and the vitreous have a low density in the visible and near UV part of the spectrum.[1-3] In the infrared region beyond 700 nm water becomes a major absorber.[4]

Knowledge of spectral transmission in the eye media is of importance in eye research. In vivo determinations of e.g. the visual pigment spectra, often rely on accurate data of the losses in the eye media.[5] With increasing age the media, in particular the lens, absorb more light, influencing the absolute sensitivity of the retina, as seen in e.g. visual field testing.[6] Autofluorescence measurements of lipofuscin[7] or Raman scattering measurements of macular pigment[8-11] also rely on accurate data on the transmission of the ocular media, particularly when older populations are tested. After cataract surgery the transmission at short wavelengths increases substantially. Generally, intraocular lenses have transmission properties that are a compromise between avoiding light damage to the retina and unnecessary loss of visual sensitivity and color perception.[12-15] Better characterization of the transmission properties of the natural lens as a function of age may optimize the design of these lenses. Finally, studies of light damage to the retina also benefit from an accurate characterization of the transmission of the media in particular at short wavelengths.[16,17]

Methods for estimating the absorption properties of the eye media all have their pros and cons. Transmission measurements on donor material can suffer from tissue deterioration. Intact lenses are difficult to measure at wavelengths below 400 nm because of the high densities involved; in addition they can be affected by autofluorescence. Psychophysical sensitivity comparisons of normal and aphakic subjects ignore absorption in other media than the lens. The Purkinje method suffers from the influence of scattered light from other reflecting layers.[18,19]

Existing spectral density data of the eye media[1,5,20-22] that have gained popularity all use the Wyszecki and Stiles data set[22] as a basic reference. The authors incorporated literature data from two different techniques: Transmission measurements of only six donor eyes above 436 nm (average age 58 years) and comparison of the spectral sensitivity of normal and aphakic subjects (average age 21 years) in the spectral region below 436 nm. They also considered measurements using the Purkinje images method, but the results were so deviant from other data, that they were finally not included in their compilation. They called their work “an attempt for a compromise curve”. This was a correct expression since spectral bandwidths, visual angles (important for scatter losses), and age-ranges for their two experimental data sets were different. The authors presented the data set as applicable for the young adult observer, recognizing that age effects should also be considered. Van Norren and Vos[20] proposed a minor adjustment below 435 nm, based on the difference of the CIE scotopic sensitivity data and the rhodopsin sensitivity using the Dartnall template.[1] In a review by Pokorny, Smith and Lutze,[21] the age aspect was specifically addressed. Based on age-dependent color matching data from Stiles and Burch,[23] they presented two spectral templates which, when added together, equaled the Wyszecki and Stiles[1] template. They also introduced a slightly modified version for the Van Norren and Vos[20] template. A formula for aging, based on work by Moreland,[24] was

given to calculate the media absorption from the two templates for a subject with a given age between 20 and 80 years. Stockman *et al.*[25] applied minor changes below 450 nm to the Van Norren and Vos[20] data set, to obtain an S-cone spectrum that better fitted with the L- and M-cone visual pigment templates. In a later paper Stockman *et al.* again provided similar changes.[5] Savage *et al.*[26] applied the method used by Van Norren and Vos[20] to peripheral vision. They came up with a simple formula for the average eye media density at different ages, completely independent of the data of Wyszecki and Stiles.[22]

A large amount of new data on ocular media absorption has appeared in the literature since Wyszecki and Stiles' initial work. The available data, together with the surprisingly narrow basis of the former spectral data, called for a reanalysis of the spectral absorption of the human media. We have addressed this issue by a critical examination of the available biological and experimental data. We developed new aging algorithms, based on five new spectral templates, to describe the absorption of all ocular media in the wavelength range from 300 to 700 nm.

2. General approach

We developed on the basis of biological and experimental literature data, a description of the optical density of the human ocular media $D_{media}(\lambda)$ as the sum of five components.

$$\begin{aligned} D_{media}(\lambda) = {} & d_{RL}(age) \times M_{RL}(\lambda) \\ & + d_{TP}(age) \times M_{TP}(\lambda) \\ & + d_{LY}(age) \times M_{LY}(\lambda) \\ & + d_{LOUV}(age) \times M_{LOUV}(\lambda) \\ & + d_{LO}(age) \times M_{LO}(\lambda) \\ & + d_{neutral} \end{aligned} \qquad (1)$$

M_i are templates (M for media) describing the spectral shape of each component, and d_i are age dependent scalar factors, the density coefficients. The subscripts RL, TP, LY, LOUV, and LO are explained in Subsection 2A. A component like $d_{RL} \times M_{RL}(\lambda)$ will be referred to in the text by using only the acronym, in this case RL. Water played no role, as we limited the spectral region of interest to below 700 nm. $d_{neutral}$ is to account for spectrally neutral absorbers, and does not need a template. We excluded material stated as cataractous. Chromophores in the retina, like macular pigment, were not supposed to be a part of the ocular media.

In this section, we will first define the shapes of the templates (Fig. 1). The characteristics of the templates are presented in Table 1. In subsequent sections on the separate eye media (i.e. lens, cornea, aqueous, and vitreous), we will provide a justification for the shape of the templates. The density coefficients of Eq. 1 were derived by fitting the components to the relevant data.

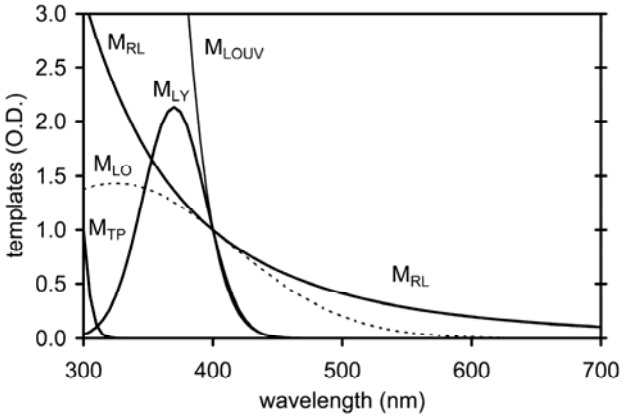

Fig. 1. Templates for the spectral density of the ocular media normalized to 1 at either 300 or 400 nm. The vertical scale is in optical density units (O.D.). M_{TP} (tryptophan), M_{LOUV} (old lens), M_{LO} (old lens), and M_{LY} (young lens) are Gaussians. M_{RL} describes scatter losses of the Rayleigh type. The peaks of M_{TP} and M_{LOUV} are off scale. The long-wavelength tails of M_{LY} and M_{LOUV} virtually overlap above 400 nm.

A. Templates

The spectral region of the templates was limited to 300-700 nm. One template is a function monotonically decreasing with wavelength, describing light losses due to Rayleigh scatter[27], the four others have a Gaussian shape.[28] As said, the first template is due to the light loss by Rayleigh scatter. It is to some degree present in all media layers, and is described by

$$M_{RL}(\lambda) = (400/\lambda)^4 \qquad (2)$$

A substance also present in all media layers is tryptophan, a building block of protein. It heavily absorbs below 310 nm. Detailed spectral density data on tryptophan are scarce. The first Gaussian M_{TP} was derived from a model fit to tryptophan data above 285 nm.[29] It is given by

$$M_{TP}(\lambda) = 10.68 \times \exp(-\{[0.057 \times (\lambda - 273)]^2\}) \qquad (3)$$

with 10.68 a constant to normalize the template to 1 at 300 nm, 0.057 the width of the Gaussian in nm^{-1}, and 273 the wavelength of the peak in nm.

The shapes of the last three templates, all normalized at 400 nm, describe absorbing substances in the lens based on experimental data. The major absorbing chromophore in the young lens is well described by

$$M_{LY}(\lambda) = 2.13 \times \exp(-\{[0.029 \times (\lambda - 370)]^2\}) \qquad (4)$$

The absorbing chromophore in the old lens with major influence in the UV is expressed as

$$M_{LOUV}(\lambda) = 11.95 \times \exp(-\{[0.021 \times (\lambda - 325)]^2\}) \qquad (5)$$

Another much broader Gaussian for the old lens, with its tail extending far into the visible region is described by

$$M_{LO}(\lambda) = 1.43 \times \exp(-\{[0.008 \times (\lambda - 325)]^2\}) \quad (6)$$

We will justify the adequacy of these templates by examination of the residues in the fitting of spectral data for the lens in Subsections 3B, 3C, and 3D.

Table 1. Templates describing the spectral density of the ocular media from 300 to 700 nm.

Name	Description	Peak wavelength (nm)	Width factor (nm^{-1})	normalization	location
M_{RL}	**R**ayleigh **L**oss			1 (400 nm)	all media
M_{TP}	**T**ry**P**tophan	273	0.057	10.68 (300 nm)	all media
M_{LY}	**L**ens **Y**oung	370	0.029	2.13 (400 nm)	lens
M_{LOUV}	**L**ens **O**ld **UV**	325	0.021	11.95 (400 nm)	lens
M_{LO}	**L**ens **O**ld	325	0.008	1.43 (400 nm)	lens

B. Age-related density coefficients

We will show that the age relationships for d_i were generally best described by a quadratic age-relationship rather than by a linear one.

$$d_i = d_{i,0} + \alpha_i \times age^2 \quad (7)$$

with $d_{i,0}$ the density at age 0, α_i the aging in $years^{-2}$, and *age* in years.

C. Curve fitting approach

We fitted all spectral data sets to Eq. 1. We used the Solver in Microsoft Excel 2003 to find the lowest chi-square when fitting the model curve to the data by adjusting the density coefficients d_{RL}, d_{TP}, d_{LY}, d_{LOUV}, d_{LO}, and an additional offset $d_{neutral}$. They are the densities at 400 nm at a given age because the templates were normalized to 1, except for d_{TP} because TP was normalized at 300 nm. The original noise in the data was unknown in most cases. In addition, the differences in spectral shapes of the data on specific media from different publications often depend more on the conditions and techniques, than on noise. Therefore the weighting used in the fit was set equal for all data sets at all wavelengths.

Spectrally neutral losses described by $d_{neutral}$, and generally caused by scattering of light by large particles (such as is the case for glare,[30]) could often not be derived from available data due to unknown absolute sensitivities. This was for instance the case when spectral density was derived by subtracting the log spectral sensitivity at the corneal level and the log spectrum of rhodopsin. Thus, only with the absolute data from donor material measured in a spectrometer, $d_{neutral}$ in the model had a meaning. Similarly, for data derived using only the aging of spectral sensitivity it was impossible to calculate the $d_{i,0}$ parameter. The resulting density coefficients from many literature sources were plotted as a function of age to calculate regression formulas yielding $d_{i,0}$ and α_i (Eq. 7). They are specified in summarizing tables.

3. Lens

The lens provides by far the dominant element in the spectral absorption of the eye media. We will show that all five templates were needed to model its density over the full range 300-700 nm. Only two templates sufficed to model the other media, the ones for tryptophan and Rayleigh scatter.

A. Light Scattering, RL

That losses caused by the scattering of light play a (minor) role becomes evident by plotting the density difference between small and large detection fields in transmission measurements of donor lenses. The losses are expected to increase with decreasing field size. We could trace only two publications with sufficiently detailed spectral information, one for the 4.5 year old lens,[2] and one for a lens curve with an average age of 72 year.[31] For the young lens transmission was given both for a 1 degree field (direct), and a 170 degree field (total). Because the absolute densities in the original data were about 1.0 at 400 nm, the density difference below 440 nm becomes very noisy (Fig. 2). RL provided a good fit through the data in the region from 450 nm even up to 1000 nm, with a density coefficient for d_{RL} of 0.14 at age 4.5 years. This is the same order of magnitude as will later be derived for the rest of the eye media together (Section 4). For the old lens the data was the difference of 1 degree, and 49 degree fields. The density coefficient for d_{RL} was 0.39 at age 72 years.

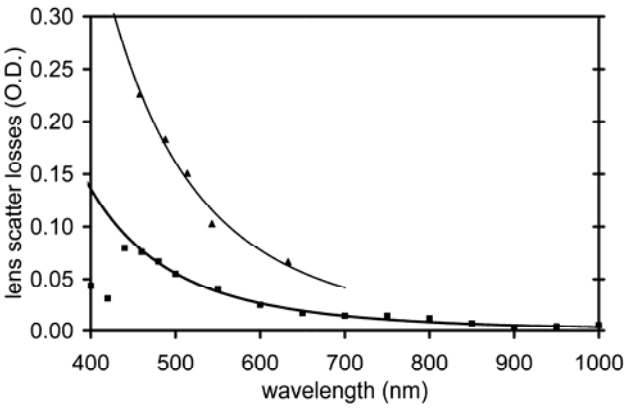

Fig. 2. Fit of RL with d_{RL} = 0.14 (thick model line), to the difference (solid squares) of the densities measured with small (1 deg) and large (170 deg) detectors from a young lens from Boettner.[2] Below 440 nm noise explodes because of the high densities in the original data (see Fig. 3). Similar data from the difference using small (1 deg) and large (49 deg) detectors from old lenses with mean age 72 from Thaung *et al.*[31] is also provided (solid triangles). d_{RL} for this older lens is 0.39 (thin model line).

B. Young lenses, LY and TP

It is generally agreed that the absorbing chromophores in the young lens in the 330 to 450 nm region are derivatives of kynurenine.[32-35] The dominant one is 3-hydroxykynurenine glucoside (3HKG), but kynurenine and 3-hydroxykynurenine (3HK) also contribute. The three data sets at the bottom of Fig. 3 on isolated 3HKG, and on 3HK[34,36,37] show that a fit with single Gaussians provides an excellent description. The spectra of these chromophores are only slightly different. For our purpose, describing young lens material, we therefore used a single Gaussian termed LY with a peak wavelength of 370 nm found by curve fitting in the pilot analyses. At wavelengths below 320 nm, tryptophan becomes the major absorber. The excellent

match of the model curves consisting of mainly LY and TP (plus an occasional trace of the old lens component LO; cf. next section) to published data sets on young lens material is demonstrated in Fig. 3. Only the Ambach data show a significant deviation from the model curve near the peak at 370 nm, probably due to the high densities reached in intact lenses. The data concern three intact lenses and two lens slices.[3,38-40]

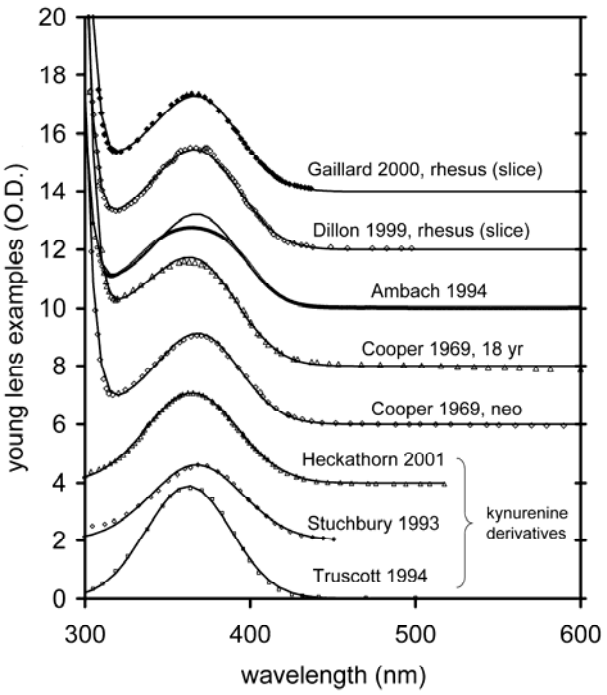

Fig. 3. Density spectra of young lens material from the literature (data points), fitted with a model curve (drawn lines) using the LY, TP and LOUV components. The curves containing a steep tryptophan edge near 300 nm are from slices of rhesus monkey lenses (Gaillard *et al.*,[40] Dillon *et al.,*[39]), or from intact human lenses (Ambach *et al.*,[3] and Cooper *et al.*[38]). All sets were normalized to the mean density of about a 10 year old of 1.35 at 400 nm for comparison. Successive curves were shifted by 2 density units, therefore the vertical axes was labeled relative density. The three data sets at the bottom demonstrate the fitting of isolated chromophores, applying single Gaussians with free parameters.

C. Old lenses, LOUV

When aging, the lens proteins undergo changes in structure, or in binding of kynurenine products. At the age of 50 the total amount of the young lens chromophore 3HKG is reduced to about 30 percent.[33,34,41] Gaillard *et al.*[40] recently showed that 3HKG resides mainly at the cortex (where new lens material is formed), but that another chromophore, with a very high density in the 300-340 nm range, is formed in deeper layers. They measured slices of a 48 year old lens, thereby overcoming the problem of low signal to noise ratio due to these high densities in the UV. They corrected their data for scattered light (Fig. 4). We found that, together with TP and LY, the template M_{LOUV} (first applied here) with a peak at 325 nm and a width factor of 0.021, described this kind of data well. For an explanation of the characters UV in LOUV, see Subsection 3D. The peak density of LOUV in a slice increased from 0.2 in the cortex to 0.8 in the nucleus (Fig. 4, A and D, respectively), whereas that of LY showed only a slight decrease. We will provide a more extensive justification of the LOUV template in Subsection 3H.

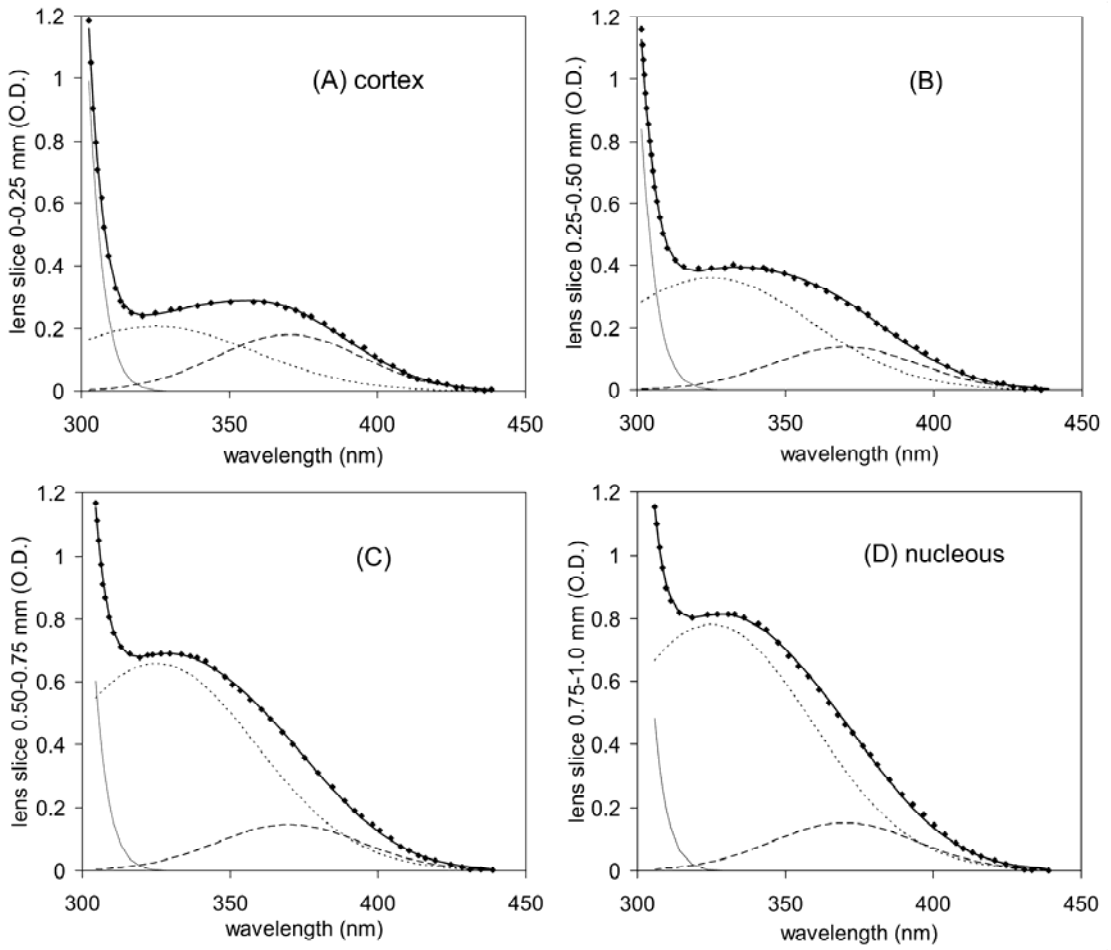

Fig. 4 Spectral lens density of slices of a 48 year old lens (Gaillard *et al.*[40]) from cortex towards the nucleus in 0.25 mm steps (panel A-D). Data were decomposed into three components: TP (thin line), LY (dashed line), and the new chromophore LOUV (dotted line). LOUV is seen to increase from the cortex to the nucleus, whereas LY slightly decreases.

D. Old lenses, LO

What Fig. 4 does not show well, is the data fit beyond 430 nm: the density of lens slices is very low here. We therefore investigated the extensive literature on the spectral density of intact donor lenses, generally only measured in the visible region (template M_{TP} is not relevant in that range). A further simplification is possible because the long-wavelength tails of M_{LY} and M_{LOUV} are nearly identical above 400 nm (Fig. 1). One of these could therefore be dropped; we chose M_{LOUV}. The drawback evidently was that it became impossible to determine the shift with increasing age, from the young lens template M_{LY}, to the old lens template M_{LOUV}. This problem is solved later (Subsection 3H). However, applying the residual templates M_{LY} and M_{RL} to data sets in the visible region resulted in unsatisfactory fits as is illustrated in Fig. 5A with a 77 year old intact donor lens from Ambach *et al.*[3] Apparently, M_{LY} is too steep and M_{RL} is too shallow beyond 440 nm. In Fig. 5B, we

therefore introduced the final template, M_{LO}, resulting in a model curve that almost coincided with the data points. Both old lens templates M_{LOUV} and M_{LO} have the same peak wavelength at 325 nm, but the width-factor of M_{LO} is 0.008 instead of 0.021 for M_{LOUV}. Therefore the shallower M_{LOUV} has the most impact in the UV (Fig. 1), hence it name. The scatter loss component RL now turned out to be zero. With all the older material from Ambach *et al.*,[3] (8 lenses from 4 subjects aged 71 to 80 year), similar high quality fits were found, again without any RL. This was most likely because of the large field used in the spectrometer.

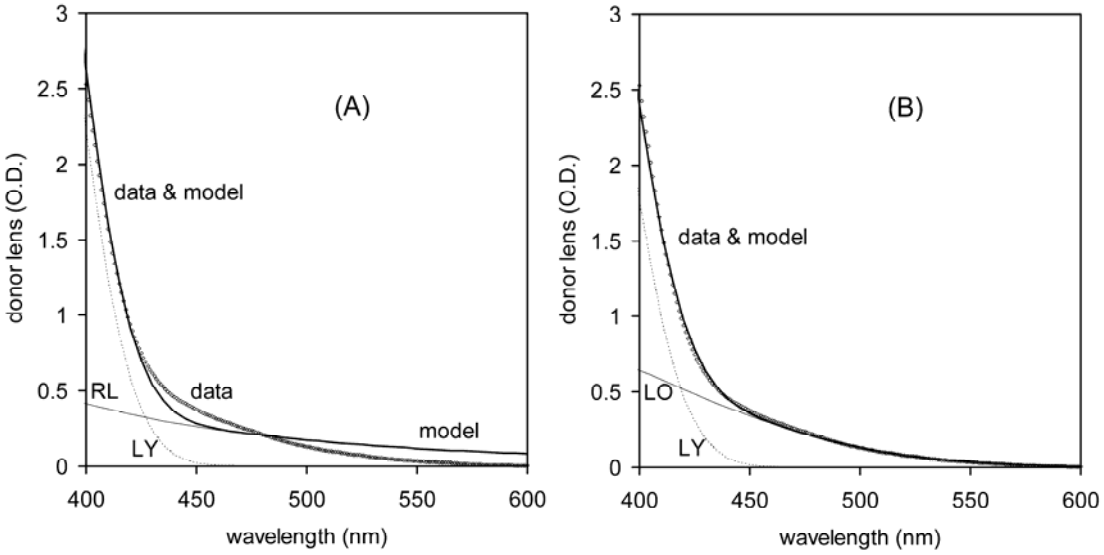

Fig. 5A. Unsatisfactory model fit (thick line) consisting only of the components LY (thin dotted line) and RL (thin line), to the spectral density of a 77 year old lens[3] (data points). The model fit deviates from the data around 450 nm and above 500 nm where it follows the RL component. Fig. 5B, a model fit (thick line) consisting of the components LY (thin dotted line), and LO (thin line). The data points and model now almost overlap.

In Fig. 6 examples from old donor material are given. Nearly all model curves, including those not shown, based on the decomposition in LY, LO, and RL show excellent fits to the data. The spectral shapes show a large variation; compare for instance Ambach and Terade. The different apertures, very large for Ambach and unknown, but likely small for Terade, offer an explanation for differences in d_{RL}. Yet, the cause for other differences remains obscure.

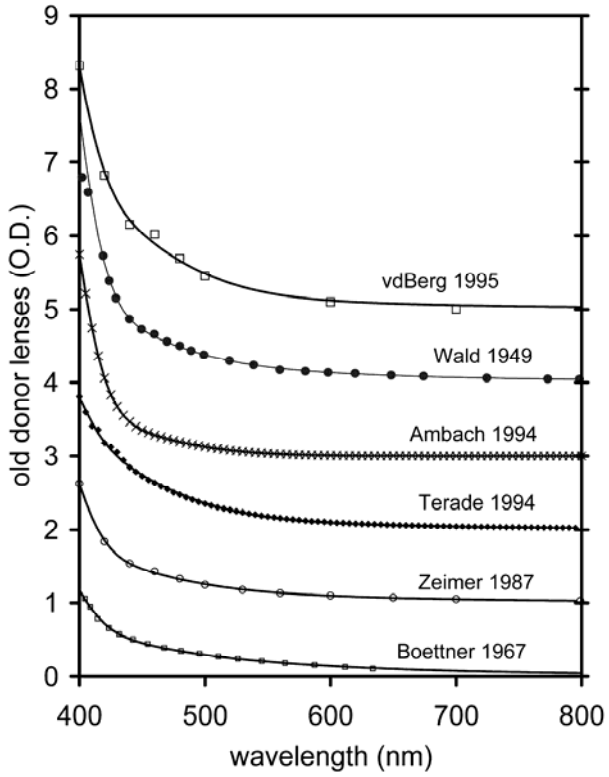

Fig. 6. Model fits (drawn curves) of literature data on examples of intact old donor material. The model curves are a combination of three components LY, LO, and RL. For clarity each curve was shifted by multiples of 1 density unit, and put in such an order to avoid overlap.

E. Aging in donor lenses (above 400 nm).

Having explained the origin of the templates, we analyzed spectra of 74 donor lenses from 20 different sources, covering the age range from 0 to 83 years (Table 2). Data from old donor lens material is more abundant than from young donors. We left out cataractous material.

Again, because of the limited spectral region, only the density coefficients d_{RL}, d_{LY}, and d_{LO} could be determined. In Fig 7 A-D the density coefficients are given as a function of age. It turned out that a linear plot against age squared yielded substantially lower chi-squares than versus linear age (e.g. 2.0 versus 2.9 in Fig 7A). See also the Discussion section. Coefficients of the aging trends are summarized in the upper part of Table 3. All trend lines in Fig 7 were highly significant. $d_{neutral}$ showed no significant aging, the mean was 0.111.

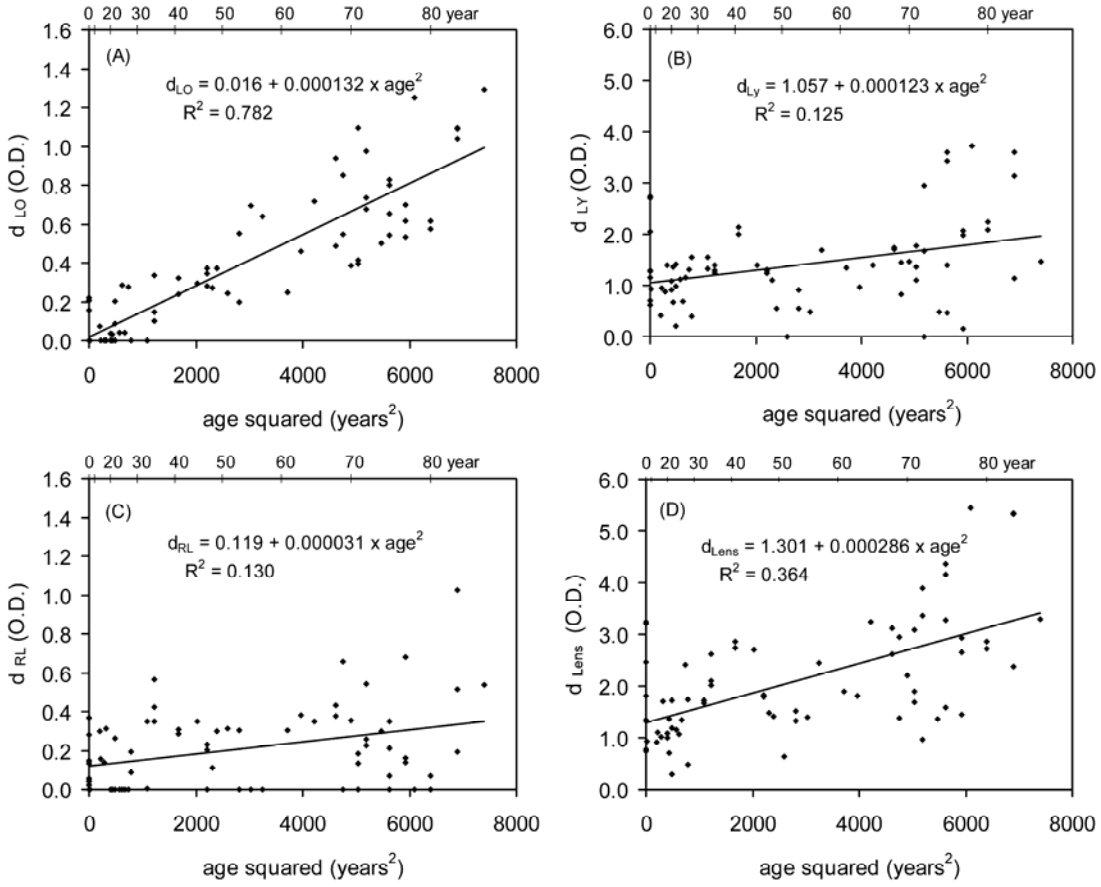

Fig. 7. The density coefficients (A, B, and C) from donor lenses as a function of age squared. All trend lines were highly significant. The LY density in panel B also includes LOUV. In panel D d_{lens} is shown, the sum of LO, LOUV, LY, RL, and $d_{neutral}$ at 400 nm. Note the difference in density scales.

F. Aging in psychophysical sensitivity (above 400 nm).

For an additional analysis of the aging effects we used data derived from the difference in psychophysical spectral sensitivity between young and aging subjects. Therefore these data include all media (Discussion). They were generally available down to 400 nm, thus only allowing the inclusion of LY, LO, and RL in the fit. With these differential data, the intercept has no meaning, and we will therefore fit these data with $d_{neutral}$ as a free offset. In total 17 curves were analyzed (Table 2). Kraft *et al.* [42] measured spectral sensitivity changes at various ages, using heterochromatic flicker photometry (HFP). They published at each wavelength the slope of the sensitivity over age (their Table 1) from which we calculated the difference from a mean 20 year to a mean 70 year old observer. Data from HFP with slope over age was also available from Sagawa *et al.*[43] We calculated the difference from a 21 year to a 71 year old observer. Savage *et al.*[26] estimated media densities from the spectral sensitivity at 15 degree eccentricity by subtracting the rhodopsin sensitivity. Again very satisfactory fits could be obtained (not shown). All age trends were significant (Fig. 8). Results are summarized in Table 3.

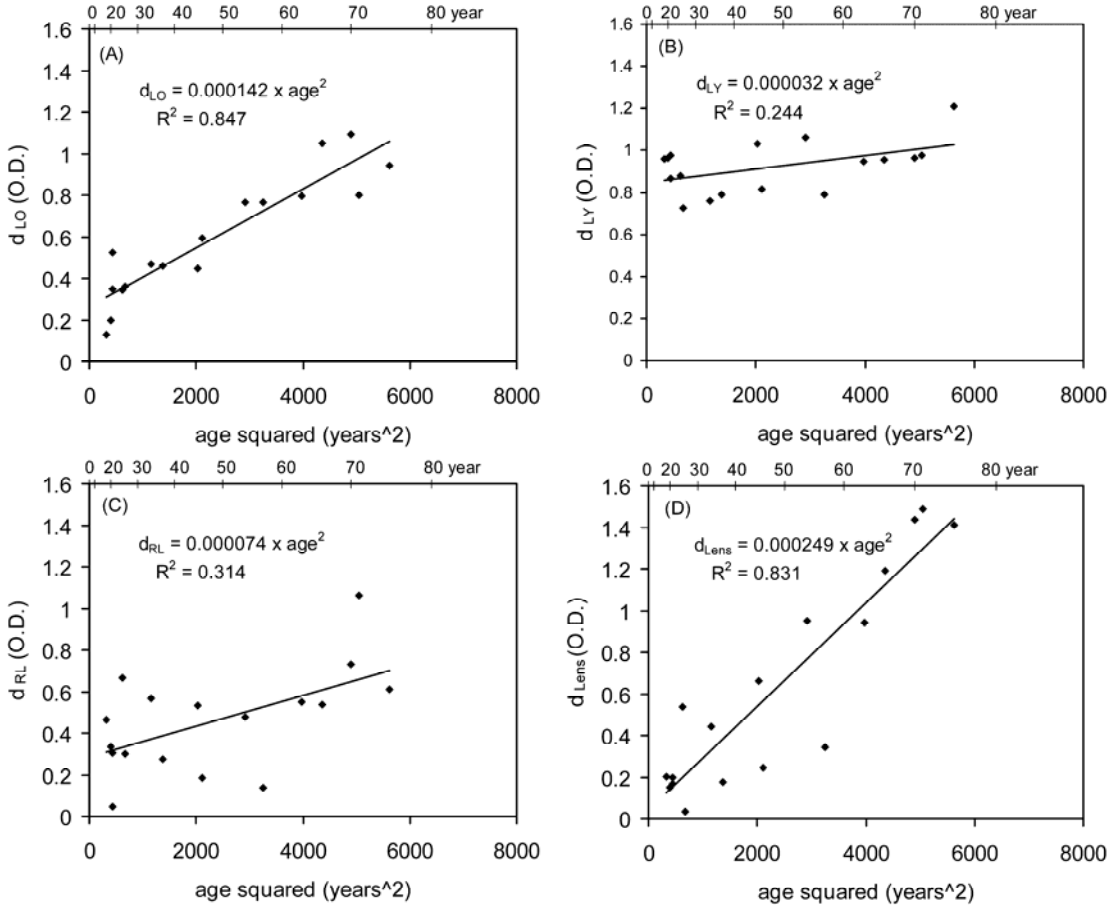

Fig. 8. The psychophysical aging of LO, LY, RL, and their sum at 400 nm. The LY density in Fig. 8B also includes LOUV.

Table 2. Origin of spectral data

source	method	N	ages (years)
Ambach *et al.*[3]	donor	12	0.6, 47, 71, 75, 77, 80 (OD and OS)
Terade *et al.*[71]	donor	12	0.25, 0.5, 1, 22, 35, 41, 72, 79, 83 (last 6 OD and OS)
Mellerio[72]	donor	6	26, 33, 47, 57, 71, 78
Cooper *et al.*[38]	donor	4	0, 18, 33, 63
Boettner[2]	donor	4	4.5, 20, 53, 75
Wald[73]	donor	1	20
Wright[74]	donor	1	27
Wald[75]	donor	2	21, 68
Mellerio[76]	donor	2	25, 55
Barker *et al.*[77]	donor	3	0, 1, 15
Zeimer *et al.*[78]	donor	1	53
Van den Berg[79]	donor	3	22, 28, 69
Van den Berg[80]	donor	6	21, 68, 86, 22, 28, 69
Van den Berg[81]	donor	4	24, 48, 70, 83
Van den Berg[82]	donor	1	61
Grover *et al.*[64]	donor	2	17, 77
Zigman *et al.*[83]	donor	4	35, 45, 65, 75
Weale[84]	donor	1	51
Weale[85]	donor	2	14, 49
Thaung *et al.*[31]	donor	1	mean 72
Crawford[86]	scotopic threshold	50	mean 18, 26, 37, 46, and 57
Ruddock[87]	color matching	50	mean 21, 63
Kraft *et al.* [42]	flicker photometry	50	mean 20, 70
Sagawa *et al.*[43]	flicker photometry	91	mean 21, 71
Savage *et al.*[26]	scotopic. threshold	82	mean 25, 34, 45, 54, 66 and 75
Xu[88]	optic disc reflex	26	mean 25, 32, 45, 55, 65, and 72
Delori *et al.*[7]	retina 7 deg. temp	218	mean 25, 32, 45, 55, 66, and 74
Liem *et al.*[44]	retina 16 deg. temp	16	mean 65
Johnson[19]	Purkinje reflex	40	mean 25, 35, 45, 55, 65, and 75
Savage[89]	Purkinje reflex	41	mean 24 and 50
Zagers *et al.*[28]	Foveal reflex	50	mean 20 and 56

G. Aging in spectral reflection (above 400 nm).

The third source for aging effects were reflectance spectra from young to old, and for phakic and aphakic subjects. In total 23 spectra (Table 2) were analyzed in the spectral region 430 – 700 nm. Spectra were averaged in age groups spanning a decade. Due to the double passage of the media, at lower wavelengths data reached the noise level of the instruments. The LY template, having influence below 430 nm, could therefore not be determined. In a pilot analysis it turned out that a contribution of RL was nearly never needed to achieve good fits; it was therefore kept at zero to prevent an occasional exchange with LO. Liem *et al.*[44] used reflection densitometry to study the density of the rod visual pigments at 16 degrees temporal; we used the difference of their log (reflectance) data for 8 phakic and 8 aphakic subjects (private communication). Data from complete media were mixed with data for the lens alone, because LO is only present in the lens; aging in the rest of the media was assumed zero (Section 4). The LO versus age squared is plotted in Fig. 9; results are summarized in Table 3.

Table 3. Density coefficients for the lens.

component	method	wavelength	$d_{i,0}$	α_i (year^{-2})	p
LO	donor [a]	400-700	0.016	0.000132	< 0.0001
LY	donor [a]	400-700	1.057	0.000123	0.002
RL	donor [a]	400-700	0.119	0.000031	0.002
sum	donor [a]	400-700	1.301	0.000286	< 0.0001
LO	psy [b]	400-700		0.000142	< 0.0001
LY	psy [b]	400-700		0.000032	0.044
RL (all media)	psy [b]	400-700		0.000074	0.019
sum	psy [b]	400-700		0.000249	< 0.0001
LO	reflec [c]	430-700		0.000143	< 0.0001
LOUV	donor [d]	300-700	0.059	0.000186	< 0.0001
LY	donor [d]	300-700	0.998	-0.000063	0.00023

a. from Subsection 3E; b. from Subsection 3F; c. from Subsection 3G; d. from Subsection 3H. The aging has to be applied as: $d_i = d_{i,0} + \alpha_i \times age^2$, with *age* in years.

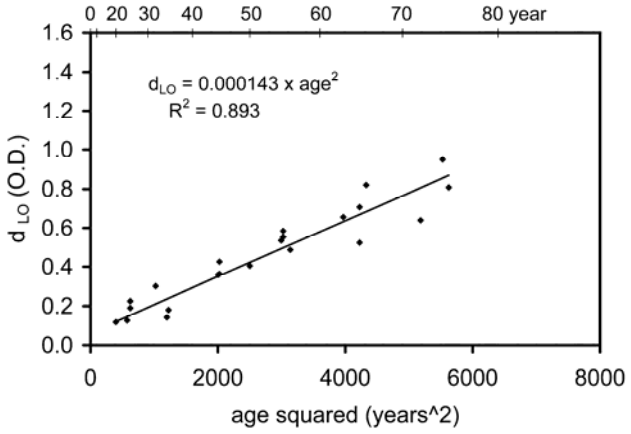

Fig. 9. The aging of the LO component derived from retinal reflection spectrometry, and from Purkinje reflection spectrometry from the lens.

H. Extrapolating lens data into the UV.

Finally, we analyzed data spanning the UV and visible region. Some data stem from intact lenses, other from lens slices and homogenized lens material (young; Fig. 3 and old; Fig. 10). To merge the results, we normalized each spectrum by its given age and kept the sum of LO, LY, and LOUV identical to the sum of the earlier donor lens aging results in the visible (see trend line in Fig. 7D). Aging trends in the density coefficients LOUV, LY, and LO were calculated. Results are displayed in Fig. 11, and summarized in Table 3). Not shown is the density coefficient $d_{LO} = 0.005 + 0.000282 \times age^2$. Although this was highly significant ($p < 0.0001$), we chose to ignore this trend, because the LO trend from the donor lens analysis with data covering the visible wavelengths ($d_{LO} = 0.016+0.000132 \times age^2$) is assumed to be much better determined in intact lenses with their higher total density of LO. The relatively large uncertainties in the tryptophan estimates, possibly due to different bandwidths combined with the extremely steep shape of the tryptophan curve, was an

argument for not deriving an age function for tryptophan. For d_{TP}, we therefore just used 12.36, the mean value over all ages.

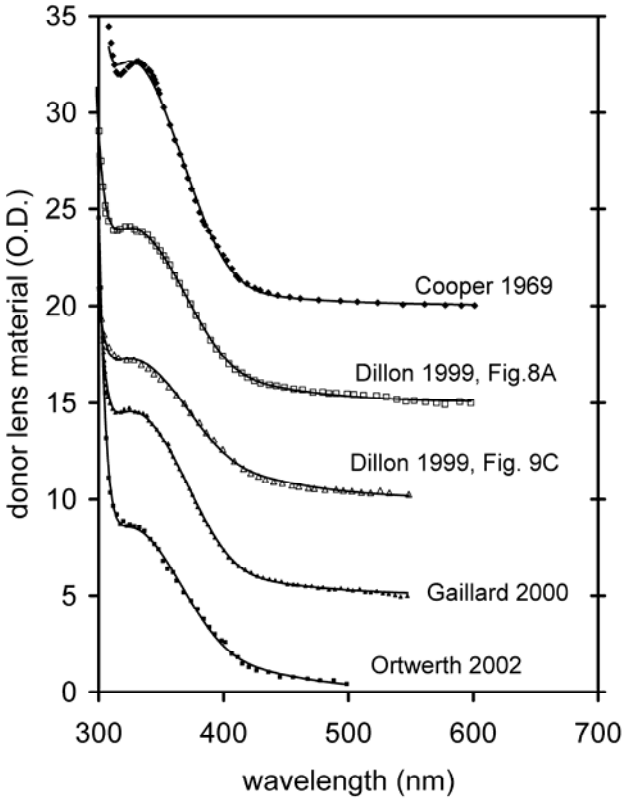

Fig 10. Model fit to data spanning the UV and visible region on lens slices (Cooper *et al.*,[38] Dillon *et al.*,[39] Gaillard *et al.*[40]), and homogenized lens material (Ortwerth *et al.*[90]) at older age. The model curves are a combination of four components LO, LY, LOUV, and TP. Each curve was scaled to a rather arbitrary density of 2.38 at 400 nm (our final density at age 55) for comparison. For clarity, successive curves were shifted by 5 density units, and put in such an order to limit overlap.

I. Well known lens data sets that were not included

The oldest spectral data set (400 - 800 nm) is from Ludvigh and McCarthy.[45] It was a synthesis of (mean) 21.5 year old lenses and the rest of the media from a 62 year old subject. In contrast to nearly all other literature data, their data had such peculiar shapes that, only when rejecting the data below 420 nm a good fit with the templates could be achieved, containing 1.15 d_{LY}, zero d_{LO}, and 0.47 d_{RL}. The data of Said en Weale[18] obtained with Purkinje reflection seemed to have suffered from substantial corneal reflections. For example, the oldest set (age 63) contains only the scattered light component (0.59 d_{RL}) and nothing else. Lerman[46] presented lens transmission data from 0.5 to 82 year. The density in the 300 to 400 nm region never exceeded 0.7, strongly suggesting that either a considerable amount of light leaked around the lenses, or fluorescence confounded their data. Griswold *et al.*[47] compared aphakic and phakic data from scotopic threshold measurements in the age range 26 - 60 years. No aging could be derived, because only one spectrum was presented for subjects with a mean age of 36 years. Their data resulted in 0.77 d_{LY}, 0.17 d_{LOUV}, and 0.03 d_{LO}, and 0.41 d_{RL}.

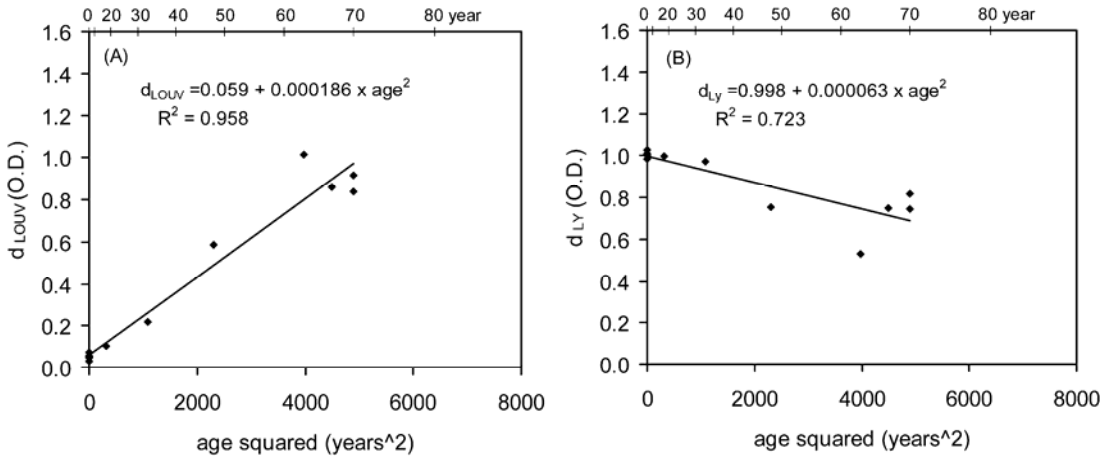

Fig 11. Discrimination of LOUV and LY by analyzing the spectral donor lens data extending into the UV.

4. Other eye media

A. The cornea, RL and TP

The cornea is nearly fully transparent in the visual region. Transmission measurements are available from Boettner[2] (two data sets: "total" for a large detector including most scattered light, and "direct" for a small detector of 1 degree angular field), Maher,[48] Van de Berg,[49] Beems and Van Best,[50] and Ambach *et al.*.[3] Data sets limited to the region below 400 nm are offered by Dillon *et al.*,[39] and Kolozsvari *et al.*[51] Although most data show similar spectral shapes, substantial deviations are also evident (Fig. 12). This may be attributed to the (not always specified) angular aperture of the detector, which can have a large effect on the losses due to the scattering of light. In fact, all spectral density shapes above 320 nm could be fitted with only the RL component. Rayleigh scatter is typically due to submicroscopic density fluctuations and thus can be found in all media. Below 320 nm, absorption by tryptophan residues in the proteins of the corneal stroma becomes substantial.[51] Except for Beems *et al.*, and Van den Berg *et al.*[49] there were sufficient data points to fit TP to the steep edge near 300 nm. Van den Berg presented their data as corneal, but in fact they include the humors as well. They took the scotopic spectral sensitivity of a group of aphakic subjects,[52] and subtracted the rhodopsin spectrum.[53] Their value of the scatter density coefficient d_{RL} was 0.34. This is about two times higher than found in most other sources. The low RL contribution from the aqueous and vitreous (Subsection 4B) cannot explain the difference. Perhaps there is an additional retinal scatter component when measuring the rods, for instance the (thick) nerve fiber layer overlying the stimulated retinal site. We chose to rely on direct measurements and therefore did not include their data in calculating the mean.

Density coefficients yielding the best fit, are presented in Table 4. As is evident from the Boettner[2] data, the density coefficient d_{RL} strongly depends on the scatter angle. This important detail was not always provided in publications. Similarly, the fit with TP depends on the often unspecified bandwidth of the filters, or that of the spectrometer. Aging of the optical density of the cornea is assumed to be absent.[2,49] A model curve for the mean data is shown as the thick line in Fig. 12, almost duplicating the Ambach model curve. Ignoring the differences in angular fields, the mean density coefficient for d_{RL} was 0.139 (400 nm); for d_{TP} it was 0.70 (300 nm).

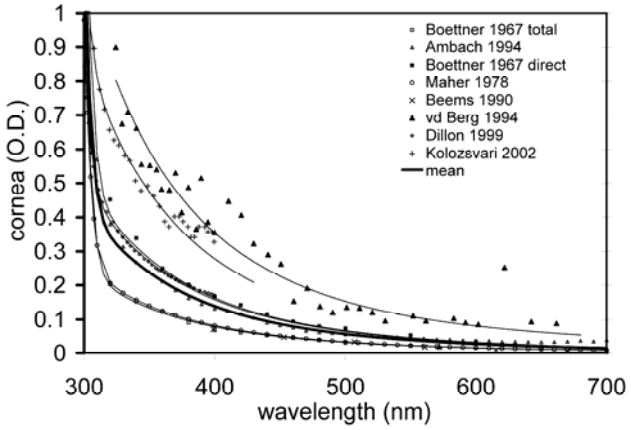

Fig. 12. RL and TP fitted to data sets on spectral absorption of the cornea. The data set from Van den Berg *et al.*[49] includes the humors. The thick line represents the mean model curve.

B. Aqueous humor and vitreous, RL and TP

Above 320 nm, the aqueous humor and the vitreous have very low densities compared to the cornea and lens. The data on the aqueous humor of Boettner,[2] Ambach *et al.*[3] and Maher,[48] (Fig. 13) again could be fitted well using only the scatter component RL. Similar to the corneal data, below 320 nm TP was also needed. For Boettner's[2] data on the vitreous we took those of the monkey, because the human data were probably contaminated with lens material as stated by the authors. This was probably also the case for the vitreous data from Maher, and the aqueous humor from Boettner's data.[2] According to Boettner,[2] the small and large field densities of the aqueous humor were identical; for the vitreous the data for small fields might be somewhat higher. Aging of the optical density of the humors is assumed to be absent.[2] We finally selected the Ambach *et al.*[3] aqueous and vitreous data for further use; they seemed to lack contamination and are spectrally detailed. The results are presented in Table 4.

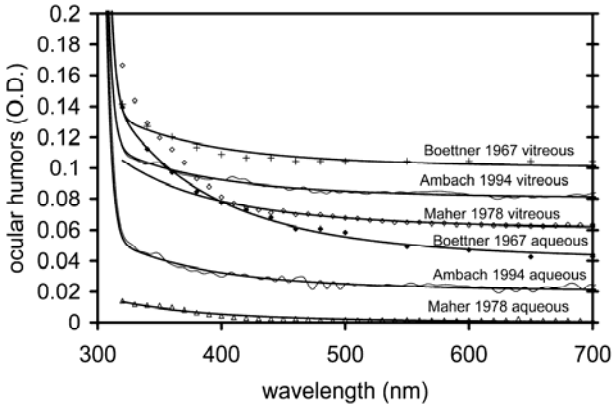

Fig. 13. Combined contributions of RL and TP (thick lines), fitted to data sets on spectral densities of aqueous humor and vitreous. For clarity, successive curves were shifted 0.02 density units. Two curves seem to be contaminated with lens extracts; vitreous data from Maher, and aqueous humor data from Boettner.

Table 4. Density coefficients for TP and RL for the cornea, the aqueous humor, and the vitreous (all ages).

media type	source	d_{TP}	d_{RL}
cornea	Ambach 1994[3]	0.87	0.140
	Beems 1990[50]		0.073
	Boettner 1967 total[2]	0.81	0.078
	Boettner 1967 direct[2]	1.07	0.163
	Maher 1978[48]	0.72	0.082
	Dillon 1999[39]	0.38	0.158
	Kolozsvari 2002[51]	0.33	0.278
mean cornea		0.70	0.139
aqueous	Ambach 1994[3]	0.59	0.012
vitreous	Ambach 1994[3]	0.54	0.012
rest of media	sum	1.83	0.164

C. Sum of the eye media excluding the lens.
In Table 4 the values of d_{TP} and d_{RL} for the cornea, the aqueous humor and the vitreous were summed to obtain the total values for the rest of the media (media excluding lens). For the cornea sufficient data are available to differentiate between fields (while still in good agreement with the mean corneal data in Table 2): Boettner's[2] 0.082 for a large field, and 0.163 for a small field (one degree). d_{RL} for total media without the lens then becomes 0.106 for large fields, and 0.187 for small fields.

5. Former compilations of media spectral density

With the new templates we analyzed former compilations for the total ocular media[1,5,20,21,25,26] , mentioned in the Introduction. Fig. 14 shows the plots, and Table 5 the resulting density coefficients. The offset $d_{neutral}$ is also provided to enable an exact replication. The offset depends mostly on the reference wavelength where the spectral density was assumed to be zero. The sum of all density coefficients gives the total density at 400 nm. A measure for the error between the data and the model is also provided (chi). Even despite the limited wavelength range the Savage[26] template (in fact not a compilation) showed a relatively poor fit, with the chi value an order of magnitude higher than the other sets. The shape was supposed to apply (with a scalar) to the whole age range. The Pokorny[21] data are based upon Wyszecki and Stiles[22] but split into a component which is constant for all ages (non-aging), and a component depending on age (aging). All former compilations are for young subjects, i.e. about 25 years, with exception of the Pokorny and Savage sets which are scalable with age. We added in the bottom row of Table 5 for comparison our proposal for a 25 year old subject (Section 6).

Table 5 Density coefficients for optimum model fits to former compilations.

source	d_{LOUV}	d_{LO}	d_{LY}	d_{RL}	$d_{neutral}$	sum	chi
WyszStiles 1967[1]	0.233	0.144	0.474	0.344	0.046	1.242	0.021
VanNorrenVos 1974[20]	0.000	0.000	1.061	0.449	0.062	1.572	0.010
Pokorny 1987 non-aging[21]	0.000	0.000	1.019	0.000	0.000	1.019	0.010
Pokorny 1987 aging[21]	0.000	0.000	0.078	0.605	0.082	0.765	0.004
Stockman 1993[25]	0.288	0.015	0.874	0.528	0.074	1.780	0.007
Stockman 1999[5]	0.010	0.000	1.284	0.550	0.075	1.920	0.008
Savage 1993[26]	0.000	0.644	0.902	0.000	0.023	1.568	0.162
our age 25	0.175	0.099	0.959	0.465	0.000	1.698	0.000

6. Final proposal for mean density and aging coefficients

Table 6 shows the density coefficients for the aging lens and the rest of the media obtained from Tables 3 and 4 (see table notes for specific origin). Together with the template shapes from Table 1, these coefficients allow, using Eq. 1, the estimation of the optical density at any wavelength and for any age.

For the density of the complete media of a newborn the density coefficients for the rest of the media in the second row and the values at age 0 for the donor lens in the third row have been added in the third row. To arrive at the density coefficients of the complete media at any age, the aging formula has to be applied: $d_i = d_{i,0} + \alpha_i \times age^2$, with *age* in years, $d_{i,0}$ from the third row, and α_i from the last row. The total density is obtained by multiplying these density coefficients with the corresponding template shapes and summing them as in Eq. 1. An expanded example for a 1 degree field yields:

$$\begin{aligned} D_{media}(\lambda) = {} & (0.446 + 0.000031 \times age^2) \times (400/\lambda)^4 \\ & + 14.19 \times 10.68 \times \exp\mathbf{(}-\{[0.057 \times (\lambda - 273)]^2\}\mathbf{)} \\ & + (0.998 - 0.000063 \times age^2) \times 2.13 \times \exp\mathbf{(}-\{[0.029 \times (\lambda - 370)]^2\}\mathbf{)} \\ & + (0.059 + 0.000186 \times age^2) \times 11.95 \times \exp\mathbf{(}-\{[0.021 \times (\lambda - 325)]^2\}\mathbf{)} \\ & + (0.016 + 0.000132 \times age^2) \times 1.43 \times \exp\mathbf{(}-\{[0.008 \times (\lambda - 325)]^2\}\mathbf{)} \\ & + 0.111 \end{aligned} \quad (8)$$

For large fields (> 3 degrees) the d_{RL} of 0.446 has to be replaced by 0.225. Fig. 15 shows the impact of aging over a lifetime. For comparison the Pokorny *et al*.'s aging spectra[21] are also shown.

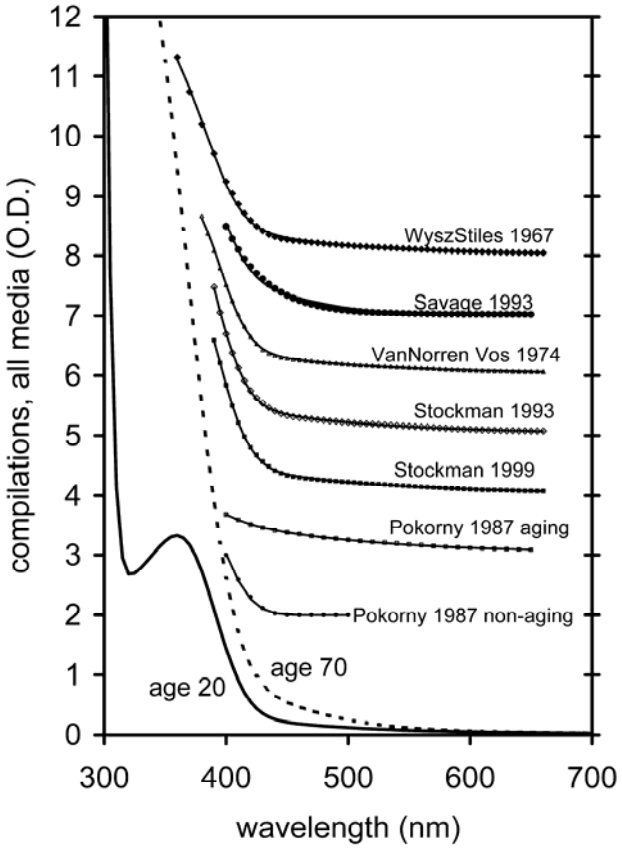

Fig 14. Model fit to the data of former compilations. The density coefficients are provided in Table 6. For clarity, successive curves were shifted by 1.0 density units, and put in such an order to limit overlap. Also shown are the proposed density spectra for the 20 and 70 year old media on an absolute density scale (Section 6).

Table 6. Mean density coefficients for the 5 spectral templates and their age-relationship.

	medium	d_{RL} 1 degree	d_{RL} >3 degree	d_{TP}	d_{LY}	d_{LOUV}	d_{LO}
all ages	cornea, aqueous, vitreous	0.187 [c]	0.106 [c]	1.83 [c]	0	0	0
$d_{i,0}$	lens	0.259 [d]	0.119 [a]	12.36 [b]	0.998 [b]	0.059 [b]	0.016 [a]
$d_{i,0}$	sum total media	0.446	0.225	14.19	0.998	0.059	0.016
α_i	lens	0.000031 [a]	0.000031 [a]	0 [b]	-0.000063 [b]	0.000186 [b]	0.000132 [a]

a. from Subsection 3E; b. from Subsection 3H; c. from Subsection 4C; d. for 1 degree, 0.14 from Subsection 3A is added to d_{RL} > 3 degree. $d_{i,0}$ are expressed in OD (optical density units), and α_i in OD x (Years)$^{-2}$. Some data was shown previously in Tables 3 and 4.

7. Comparison with single measurement condition aging studies

A check of the derived aging function was available from literature data on aging at a single wavelength. In case a technique was used where the lens density index was calculated referenced to a longer wavelength, such data was corrected with our aging result at that wavelength. Coren *et al.*[54] calculated aging from metameric color matching. Moreland[55] used anomaloscope settings. Sample *et al.*[56] measured the scotopic sensitivity at two wavelengths. Weale[57] used donor lenses; he also derived an aging function. Hammond *et al.*[58] measured the scotopic sensitivity at two wavelengths in subjects with light and dark irises; both types were included. Delori *et al.*[7] used reflection at the 7 degrees temporal retina. Results are summarized in Table 7. In Fig. 16 the spectral dependence is given, together with the aging functions of Pokorny *et al.*[21] and Savage *et al.*[26] The single wavelength data prove to nicely scatter around our derived aging trends (thick lines in Fig. 16) and Pokorny *et al*'s (thin line), rather than the Savage function.

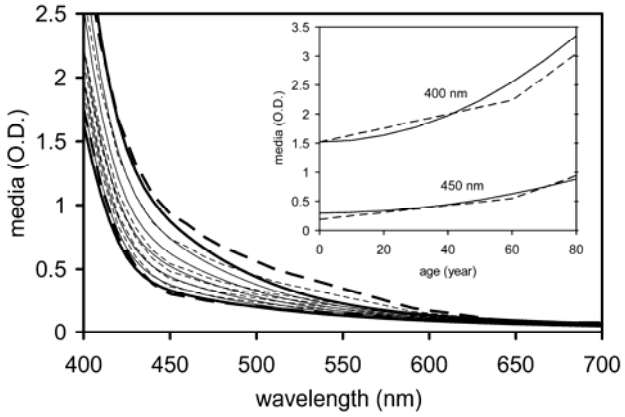

Fig 15. Density spectra of the complete media in the visible for each decade from 20 - 80 year (lines). The density coefficients are taken from donor lens, small field results in Table 6. Calculated density spectra from Pokorny *et al.*[21] (also for small fields) are shown for comparison (dashed lines). The 20 and 80 year lines of both sets are marked with thick lines. The 20 year data nearly match; the 80 year data are clearly distinct. The Pokorny spectra were shifted vertically by 0.077 for an optimal match with our results at 700 nm. The insert shows the optical density of the media at 400 and 450 nm versus age (lines), again with Pokorny *et al.*[21] (dashed lines) for comparison.

Table 7. Single measurement condition aging studies

source	n	method	primary wave (nm)	our α_i (year^{-2})	ref. wave (nm)	our α_i (year^{-2})	lit. α_i (year^{-2})
Coren *et al.*[54] 1972	256	psy	490	0.000047			0.000061
Grover *et al.*[64] 1972	37	donor	440	0.000107			0.000146
Moreland[55] 1978	167	psy	439	0.000107	499	0.000039	0.000106
Bettelheim[65] 1985	27	donor	546	0.000018			0.000021
Bettelheim[65] 1985	27	donor	436	0.000116			0.000016
Sample[56] 1988	84	psy	410	0.000204	560	0.000014	0.000221
Weale[57] 1988	24	donor	450	0.000091			0.000099
Hammond[58] 2000	90	psy	410	0.000204	550	0.000016	0.000140
Delori *et al.*[7] 2001	145	refl	510	0.000033			0.000059

8. Discussion

A. Templates

We derived five templates that adequately describe the literature on spectral density of the ocular media in the ultraviolet and visible part of the spectrum. Retinal chromophores like macular pigment were not included. Three templates will probably meet little discussion, those related to absorption in tryptophan and (derivatives of) kynurenine, and light loss caused by Rayleigh scatter. The two remaining templates are related to the aging lens. LOUV was derived from slices of donor lens material in the UV, and LO from analysis of intact donor lenses, psychophysics, and reflection measurements. For Mie scattering[27] on particles large in relation to wavelength, the resulting spectral shape is constant over wavelength and data could only be retrieved in donor lens measurements. For Rayleigh-Gans scattering[59] on intermediately sized particles, the resulting spectral shape is somewhere between constant over wavelength and the shape of the Rayleigh component. Linear combinations of the Rayleigh component and the LO component proved to approximate these intermediate Rayleigh-Gans shapes quite well, thus another template was not necessary. Despite biochemical indications to the contrary,[60] we found no evidence for optically relevant amounts of lutein or zeaxanthin in the lens. In principle, data are now available from 300-2500 nm, because beyond 700 nm water is the only absorber [61] and its absorption has been adequately tabulated up to 2500 nm.[4]

In a previous paper from our group, Zagers *et al.*[28] proposed a single template for the absorption of the aging eye, largely based on slices of donor lens material.[62] It was a little broader than our LOUV template. The analysis led to somewhat unlikely near zero density of the media above 500 nm.[11] In this study, which was in part motivated by this questionable prediction, we had to introduce two templates, a combination of a narrow (LOUV), and a broad one (LO) to explain the broader literature data. In Zagers *et al.,* the analysis was based on spectral reflection from the fovea with a model that also incorporated the density to the macular pigment.[63] From the perspective of our new templates, their single template for the aging lens can be understood by supposing that in their model analysis parameters for the lens density and macular pigment were to some degree exchanged.

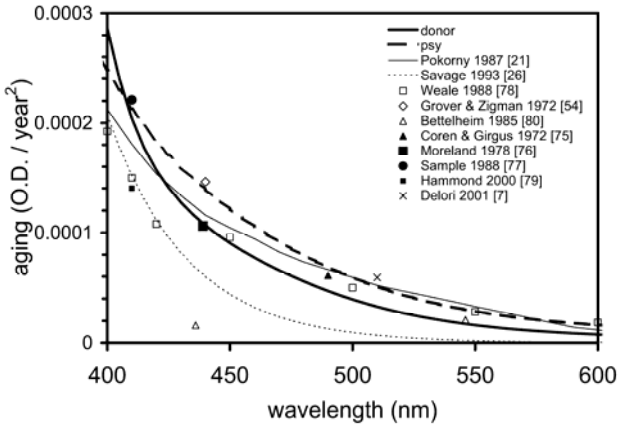

Fig 16. Aging at single wavelengths from literature (various types of data points, see legend in figure) compared with our aging from donor lenses (thick line), and psychophysics (dashed thick line). Aging functions with more complete spectra are also shown: the often used Pokorny *et al.*[21] aging (thin line), the aging function from Savage *et al.*[26] (thin, dotted line), and multiple points defined by Weale[57] (open squares). Open symbols were chosen for psychophysical, filled symbols for donor, and crosses for reflection techniques**.**

B. Aging

The new templates were used to derive aging trends. We have chosen a quadratic trend with age based on Coren *et al.*[54] who as early as 1972 applied a second degree polynomial. We ignored their linear term as it was almost zero. Fitting their model curve (not the data) at 490 nm resulted in D = 0.126 + 0.000061* age^2 (R^2=0.999). Weale's[57] aging model is also perfectly (R^2=0.997) described by D =0.877 + 0.000192 * age^2 (400nm). The well known Pokorny *et al.*[21] aging function was actually based on the Moreland data.[55] Fitting the latter data with an age squared trend gave R^2 = 0.975, higher than R^2 = 0.908 with a linear trend. Similar comparisons for Grover *et al.,*[64] Sample,[56] Delori *et al.,*[7] Hammond[58] and Bettelheim[65] all gave better fits with an age squared term than with a linear one. Only Werner's [66] data based on visual evoked potentials to assess the scotopic sensitivity, had a reversed preference. Savage *et al.*[26] concluded that a linear change with age is correct when cataractous lenses are excluded, but even their data showed a preference for an age squared trend. We have ignored all data which were called cataractous, but acknowledge that at advanced age there is only a soft border with normal old lenses. It is even likely that not all individuals in all studies were thoroughly screened for early cataract,[67] diabetes[68] or other medical conditions, leading to an unknown bias towards increased lens density at older age.

By having the same formula $d_i = d_{i,0} + \alpha_i$ x age^2 for all components, calculations involving addition of components are relatively simple. The aging of RL (α_{RL}) based on donor lenses was 0.000031. With psychophysics a much higher number (0.000074; Table 3) was found, be it including all media. However, the significance of this value was much lower. In addition, in Section 4 it was argued that no aging occurred in cornea, aqueous, and vitreous. If the difference is real, it can be explained by assuming an additional scatter source located at the retinal level, and/or scatter compensation in donor lens measurements that was occasionally applied but not accounted for. In contrast stands the absence of aging of RL (α_{RL}) in the reflection data. This is possibly caused by the relative large fields in this type of measurements. Estimates of losses of light scattered outside a retinal field of 1 degree from Vos *et al.*[69] result in a density of only 0.03 for the complete media, but this holds for the relatively young eye. Values of d_{RL} in Table 4 are much higher. A partial explanation may be deterioration in donor material, but the physical data from reflection measurements also yield a lower increase in d_{RL} than the psychophysical data. Increased scatter with age in the retinal plane itself again would offer an explanation.

No aging was assumed in tryptophan (TP); data on media density in the spectral region 300 nm were scarce and noisy. However with a d_{TP} for all media of about 14 some variation in this number would have little practical impact.

The aging of LO (α_{LO}), most prominent in the visible, was found (Table 3) comparable for all techniques, donor material (0.000132), psychophysics (0.000142), and reflection measurements (0.000143).

The aging coefficient of LY (α_{LY}) is 0.000032 for psychophysics, compared to 0.000123 for the sum of the aging of LY and LOUV for the donor lenses. Given the fact that the data from psychophysics hardly reached significance (p = 0.044), and that the 400 to 420 nm region not always contained data, we trust the donor material better. Additional spectral data from donor lenses would be needed to better discriminate between the aging trend in LY and LOUV. Biochemical analysis showed that at the age of 50 the total amount of the young lens chromophore 3HKG is reduced to about 30 percent.[33,34,41] Because it is unknown what part of the transformed products still have spectral properties similar to 3HKG, a judgment

about the aging trend for LY is difficult. Looking again at Table 3, it is attractive to assume a common substance for LOUV and LO, consisting of a broad (LO), and a shallow (LOUV) absorption curve. The density at age 0 is very close to zero for both. Comparing the aging values is not relevant, because they are a consequence of choosing the reference wavelengths at 400nm. We tried to find evidence in individual measurements, but this proved to be difficult. Depending on the method used, often when LO was well determined, LOUV was not, and vice versa. To resolve this issue additional data is needed with a large dynamic range in the UV and visible, and no scatter compensation applied.

Weale[57] also presented a model to calculate the density of the lens as a function of age for a limited number of wavelengths. The aging coefficients resulting from analysis with our model show a somewhat peculiar plateau around 440 nm (Fig. 16). In addition, the generated density spectra in the UV strongly deviate from the literature data presented in Fig.10.

C. Comparison with former compilations

None of the former compilations included absorption by tryptophan, because they lacked data at the very short wavelengths. It turned out that the Wyszecki and Stiles[22] compilation consisted of a mixture of all four templates (Table 3). It had the lowest wavelength limit (360 nm), and therefore could not do without LOUV. The Van Norren and Vos[20] compilation needed only LY and RL. It was based on the difference of the CIE scotopic sensitivity data and the rhodopsin sensitivity using the Dartnall template.[1] When we repeated the calculations with the CIE scotopic sensitivity data and the rhodopsin spectrum from Dartnall, or templates from Stavenga *et al.*,[70] the method revealed a great sensitivity for parameters like the peak wavelength and peak density of rhodopsin. This could show up as irregularities in the relatively flat region between 450 and 600 nm, but was not so easily noticed in the steep curve below 430 nm. In general, techniques based on subtraction of spectral data sets from sources with very likely different bandwidths of their filters, combined with steep spectral sensitivity curves, are prone to errors. Preferably, both measurements in the subtraction should be performed on the same instrument, using the same subjects.

The RL component in the compilations, first matching the data above 436 nm from donor eyes in the Wyszecki and Stiles[22] compilation, later appeared as the aging component in the often used Pokorny *et al.*[21] algorithm. We found that it almost purely consisted of the RL component. The Pokorny proposal was based on small field psychophysical data. From Fig 16 we learn that their aging is roughly comparable to our data. Apart from minor details, their non-aging component was identical to LY, as earlier pointed out by Zagers *et al.*[28] We can offer no explanation why LO is absent in their proposal, but needed in nearly all literature data on aging lenses.

Savage *et al's* .[26] proposal had the advantage of simplicity because it was supposed to hold over the whole age range with a single template, be it at a rather limited wavelength range. Given the large chi in Table 5 the solution is probably too simple. As stated before subtraction of the rhodopsin sensitivity from the scotopic sensitivity at the corneal level is prone to errors. From Fig. 16 we suspect an underestimation of densities at the longer wavelengths.

Stockman *et al.*'s[5] most recent proposal contains LY and RL, with a negligible amount of LOUV, and LO. Being applicable for the young eye, this seems reasonable. It shows a striking resemblance with our proposal for the 30 year old eye media (not shown).

D. Conclusions

We derived, taking nearly the complete literature with stated exceptions into account, a useful set of five templates to describe the spectral density of the human eye media, together with their aging functions. Data from material stated as cataractous were left out. Residue analyses did not point to the conclusion that an important template was overlooked. Combining data from many different sources leads to uncertainties. There is therefore room for improvement, in particular for the aging of the Rayleigh component in relation to field size, and in discriminating between the Lens Old UV and the Lens Young components.

Acknowledgments

We thank Dr. Mario Blumthaler for retrieving and making available the original data files of Ambach *et al.,*[3] and Dr Hans Vos and Prof. Dr François C. Delori for critical comments and suggestions on earlier versions of the manuscript. Address correspondence to Jan van de Kraats, UMC Utrecht, Dept of Ophthalmology AZU E03.136, P.O. Box 85500, NL-3508 GA, Utrecht, the Netherlands, or e-mail: jkraats@umcutrecht.nl.

References

1. G. Wyszecki and W. S. Stiles, "Color Science: Concepts and Methods, Quantitative Data and Formulae, 2nd edition," John Wiley & Sons, (1982).

2. Boettner, E. A. Spectral Transmission of the Eye. Report of the University of Michigan Ann Arbor Contract AF41-609-2966. (1967).

3. W. Ambach, M. Blumthaler, T. Schopf, E. Ambach, F. Katzgraber, F. Daxecker, and A. Daxer, "Spectral transmission of the optical media of the human eye with respect to keratitis and cataract formation," Doc. Ophthalmol 88, 165-173 (1994).

4. T. J. T. P. van den Berg and H. Spekreijse, "Near infrared light absorption in the human eye media," Vision Res. 37, 249-253 (1997).

5. A. Stockman, L. T. Sharpe, and C. Fach, "The spectral sensitivity of the human short-wavelength sensitive cones derived from thresholds and color matches," Vision Res. 39, 2901-2927 (1999).

6. C. A. Johnson, A. J. Adams, J. D. Twelker, and J. M. Quigg, "Age-related changes in the central visual field for short-wavelength-sensitive pathways," J. Opt. Soc. Am. A 5, 2131-2139 (1988).

7. F. C. Delori, D. G. Goger, and C. K. Dorey, "Age-related accumulation and spatial distribution of lipofuscin in RPE of normal subjects," Invest. Ophthalmol. Vis. Sci. 42, 1855-1866 (2001).

8. P. S. Bernstein, M. D. Yoshida, N. B. Katz, R. W. McClane, and W. Gellermann, "Raman detection of macular carotenoid pigments in intact human retina," Invest. Ophthalmol. Vis. Sci. 39, 2003-2011 (1998).

9. P. S. Bernstein, D. Y. Zhao, S. W. Wintch, I. V. Ermakov, R. W. McClane, and W. Gellermann, "Resonance Raman measurement of macular carotenoids in normal subjects and in age-related macular degeneration patients," Ophthalmology 109, 1780-1787 (2002).

10. W. Gellermann, I. V. Ermakov, M. R. Ermakova, R. W. McClane, D. Y. Zhao, and P. S. Bernstein, "In vivo resonant Raman measurement of macular carotenoid pigments in the young and the aging human retina," J Opt. Soc Am A Opt. Image Sci Vis 19, 1172-1186 (2002).

11. B. R. Hammond and B. R. Wooten, "Resonance Raman spectroscopic measurement of carotenoids in the skin and retina," J Biomed. Opt. 10, 054002 (2005).

12. M. A. Mainster, "Intraocular lenses should block UV radiation and violet but not blue light," Arch Ophthalmol 123, 550-555 (2005).

13. R. E. Braunstein and J. R. Sparrow, "A blue-blocking intraocular lens should be used in cataract surgery," Arch. Ophthalmol. 123, 547-549 (2005).

14. M. A. Mainster, "Violet and blue light blocking intraocular lenses: photoprotection versus photoreception," Br. J. Ophthalmol. 90, 784-792 (2006).

15. J. van de Kraats, and D. van Norren, "Sharp cutoff filters in intraocular lenses optimize the balance between light reception and light protection." J. Cataract Refract. Surg. in press. (2007).

16. W. T. Ham, Jr., H. A. Mueller, J. J. Ruffolo, Jr., D. Guerry, III, and R. K. Guerry, "Action spectrum for retinal injury from near-ultraviolet radiation in the aphakic monkey," Am. J. Ophthalmol. 93, 299-306 (1982).

17. W. T. Ham, Jr., H. A. Mueller, and D. H. Sliney, "Retinal sensitivity to damage from short wavelength light," Nature 260, 153-155 (1976).

18. F. S. Said and R. A. Weale, "The variation with age of the spectral transmissivity of the living human crystalline lens," Gerontologia 3, 231 (1959).

19. C. A. Johnson, D. L. Howard, D. Marshall, and H. Shu, "A noninvasive video-based method for measuring lens transmission properties of the human eye," Optom. Vis. Sci. 70, 944-955 (1993).

20. D. van Norren and J. J. Vos, "Spectral transmission of the human ocular media," Vision Res. 14, 1237-1244 (1974).

21. J. Pokorny, V. C. Smith, and M. Lutze, "Aging of the human lens," Appl. Opt. 26, 1437-1440 (1987).

22. G. Wyszecki and W. S. Stiles, "Color Science: Concepts and Methods, Quantitative Data and Formulae, 1st edition," John Wiley & Sons, (1967).

23. W. S. Stiles and J. M. Burch, "N.P.L. Colour-Matching Investigation: Final Report (1958)," Optica Acta 6, (1959).

24. J. D. Moreland, "The effect of inert ocular pigments on anomaloscope matches and its reduction," Mod. Probl. Ophthalmol. 11, 12-18 (1972).

25. A. Stockman, D. I. A. MacLeod, and N. E. Johnson, "Spectral sensitivities of the human cones," J. Opt. Soc. Am. A 10, 2491-2521 (1993).

26. G. L. Savage, G. Haegerstrom-Portnoy, A. J. Adams, and S. E. Hewlett, "Age-Changes in the Optical-Density of Human Ocular Media," Clinical Vision Sciences 8, 97-108 (1993).

27. H. C. van de Hulst, "Light Scattering by Small Particles," Dover Publications.Inc., New York, USA, (1957).

28. N. P. A. Zagers and D. van Norren, "Absorption of the eye lens and macular pigment derived from the reflectance of cone photoreceptors," J. Opt. Soc. Am. A 21, 2257-2268 (2004).

29. Fuh. "Spectral absorbance data of tryptophan." Avalaible at http://omlc.ogi.edu/spectra/PhotochemCAD/abs_html/tryptophan.html (1995).

30. J. J. Vos, "On the cause of disability glare and its dependence on glare angle, age and ocular pigmentation," Clin. Exp. Optom. 86, 363-370 (2003).

31. J. Thaung and J. Sjostrand, "Integrated light scattering as a function of wavelength in donor lenses," J. Opt. Soc. Am. A 19, 152-157 (2002).

32. R. van Heyningen, "Fluorescent glucoside in the human lens," Nature 230, 393-394 (1971).

33. M. Bando, A. Nakajima, and K. Satoh, "Spectrophotometric estimation of 3-OH L-kynurenine O-beta-glucoside in the human lens," J. Biochem. Tokyo 89, 103-109 (1981).

34. G. M. Stutchbury and R. J. W. Truscott, "The modificationof proteins by 3-hydroxykynurenine," Exp. Eye Res 57, 149-155 (1993).

35. L. A. Ervin, J. Dillon, and E. R. Gaillard, "Photochemically modified alpha-crystallin: A model system for aging in the primate lens," Photochem. Photobiol. 73, 685-691 (2001).

36. R. J. W. Truscott, A. M. Wood, J. A. Carver, M. M. Sheil, G. M. Stutchbury, J. L. Zhu, and G. W. Kilby, "A New Uv-Filter Compound in Human Lenses," Febs Letters 348, 173-176 (1994).

37. R. C. Heckathorn, J. Dillon, and E. R. Gaillard, "Synthesis and purification of 3-hydroxykynurenine-O-beta-glucoside, a primate lens ultraviolet filter, and its application in a two-step assay for beta-glucosidase activity," Analytical Biochemistry 299, 78-83 (2001).

38. G. F. Cooper and J. G. Robson, "The yellow colour of the lens of man and other primates," J. Physiol 203, 411-417 (1969).

39. J. Dillon, L. Zheng, J. C. Merriam, and E. R. Gaillard, "The optical properties of the anterior segment of the eye: implications for cortical cataract," Exp. Eye Res. 68, 785-795 (1999).

40. E. R. Gaillard, L. Zheng, J. C. Merriam, and J. Dillon, "Age-related changes in the absorption characteristics of the primate lens," Invest. Ophthalmol. Vis. Sci. 41, 1454-1459 (2000).

41. L. M. Bova, M. H. J. Sweeney, J. F. Jamie, and R. J. W. Truscott, "Major changes in human ocular UV protection with age," Invest. Ophthalmol. Vis. Sci. 42, 200-205 (2001).

42. J. M. Kraft and J. S. Werner, "Spectral Efficiency Across the Life-Span - Flicker Photometry and Brightness Matching," J. Opt. Soc. Am. A 11, 1213-1221 (1994).

43. K. Sagawa and Y. Takahashi, "Spectral luminous efficiency as a function of age," J. Opt. Soc. Am. A Opt. Image Sci. Vis. 18, 2659-2667 (2001).

44. A. T. Liem, J. E. Keunen, D. van Norren, and J. van de Kraats, "Rod densitometry in the aging human eye," Invest. Ophthalmol. Vis. Sci. 32, 2676-2682 (1991).

45. E. Ludvigh and E. F. McCarthy, "Absorption of the visible light by the refractive media of the human eye," Arch Ophthalmol 20, 37-51 (1938).

46. S. Lerman and R. Borkman, "Spectroscopic evaluation and classification of the normal, aging and cataracous lens," Ophthalmol Res 8, 335-353 (1976).

47. M. Scott Griswold and W. S. Stark, "Scotopic Spectral Sensitivity of Phakic and Aphakic Observers Extending into the Near Ultraviolet," Vision Res. 32, 1739-1743 (1992).

48. E. F. Maher, "Transmission and absorption coefficients for ocular media of the rhesus monkey." Brooks Air Force Base, TX: USAF School of Aerospace Medicine. Report SAM-TR-78-32 (1978).

49. T. J. T. P. van den Berg and K. E. Tan, "Light transmittance of the human cornea from 320 to 700 nm for different ages," Vision Res. 34, 1453-1456 (1994).

50. E. M. Beems and J. A. van Best, "Light transmission of the cornea in whole human eyes," Exp. Eye Res. 50, 393-395 (1990).

51. L. Kolozsvari, A. Nogradi, B. Hopp, and Z. Bor, "UV absorbance of the human cornea in the 240-to 400-nm range," Invest. Ophthalmol. Vis. Sci. 43, 2165-2168 (2002).

52. K. E. W. P. Tan, "Vision in the ultraviolet," PhD Thesis, Utrecht University, (1971).

53. F. D. Collins, R. Love, and R. Morton, "Studies in rhodopsin. 4. Preparation of rhodopsin," Biochem. J. 51, 292-298 (1952).

54. S. Coren and J. S. Girgus, "Density of human lens pigmentation: in vivo measures over an extended age range," Vision Res. 12, 343-346 (1972).

55. J. D. Moreland, "Temporal variations in anomaloscope equations," Mod. Probl. Ophthalmol 19, 167-172 (1978).

56. P. A. Sample, F. D. Esterson, R. N. Weinreb, and R. M. Boynton, "The aging lens: in vivo assessment of light absorption in 84 human eyes," Invest. Ophthalmol. Vis. Sci. 29, 1306-1311 (1988).

57. R. A. Weale, "Age and the transmittance of the human crystalline lens," J. Physiol. 395, 577-587 (1988).

58. B. R. Hammond, Jr., J. E. Nanez, C. Fair, and D. M. Snodderly, "Iris color and age-related changes in lens optical density," Ophthalmic Physiol Opt. 20, 381-386 (2000).

59. J. E. Coppens, L. Franssen, and T. J. T. P. van den Berg, "Wavelength dependence of intraocular straylight," Experimental Eye Research 82, 688-692 (2006).

60. P. S. Bernstein, F. Khachik, L. S. Carvalho, G. J. Muir, D. Y. Zhao, and N. B. Katz, "Identification and quantitation of carotenoids and their metabolites in the tissues of the human eye," Exp. Eye Res. 72, 215-223 (2001).

61. Vos, J. J., "The action spectrum of retinal burn." Report IZF 1974-23. Soesterberg the Netherlands, Instituut voor Zintuigfysiologie TNO. (1974).

62. J. Dillon, R. H. Wang, and S. J. Atherton, "Photochemical and photophysical studies on human lens constituents," Photochem Photobiol. 52, 849-854 (1990).

63. J. van de Kraats, T. T. J. M. Berendschot, and D. van Norren, "The pathways of light measured in fundus reflectometry," Vision Res. 36, 2229-2247 (1996).

64. D. Grover and S. Zigman, "Coloration of human lenses by near ultraviolet photo-oxidized tryptophan," Exp. Eye Res 13, 70-76 (1972).

65. F. A. Bettelheim and S. Ali, "Light scattering of normal human lens. III. Relationship between forward and back scatter of whole excised lenses," Exp. Eye Res. 41, 1-9 (1985).

66. J. S. Werner, "Development of scotopic sensitivity and the absorption spectrum of the human ocular media," J. Opt. Soc. Am. 72, 247-258 (1982).

67. J.D. Moreland, E. Torczynski and R. Tripathi, “Rayleigh and Moreland matches in the ageing eye” in Colour Vision Deficiencies X, B. Drum, J.D. Moreland & A. Serra (eds), Kluwer Academic Publishers, Dordrecht, 347-352 (1991)

68. M. Lutze and G. H. Bresnick, "Lenses of diabetic patients "yellow" at an accelerated rate similar to older normals," Invest Ophthalmol Vis. Sci. 32, 194-199 (1991).

69. J. J. Vos, J. Walraven, and A. van Meeteren, "Light profiles of the foveal image of a point source," Vision Res. 16, 215-219 (1976).

70. D. G. Stavenga, R. P. Smits, and B. J. Hoenders, "Simple exponential functions describing the absorbance bands of visual pigment spectra," Vision Res. 33, 1011-1017 (1993).

71. H. Terade, M. Sawa, J. Akiba, N. Ueno, and B. Chakrabarti, "Spectral transmittance of normal human crystalline lens," Nippon Ganka Gakkai Zasshi 98, 1101-1108 (1994).

72. J. Mellerio, "Yellowing of the human lens: nuclear and cortical contributions," Vision Res. 27, 1581-1587 (1987).

73. G. Wald, "Human vision and the spectrum," Science 101, 653-658 (1945).

74. W. D. Wright, "The visual sensitivity of normal and aphakic observers in the ultra-violet," Ann. Psychol. 50, 169-177 (1951).

75. G. Wald, "The photochemistry of vision," Documenta ophthalm. 3, 94-137 (1949).

76. J. Mellerio, "Light absorption and scatter in the human lens," Vision Res. 11, 129-141 (1971).

77. F. M. Barker, and G. C. Brainard, "The Direct Spectral Transmittance of. the Excised Human Lens as a Function of Age." DC, FDA 785345 0090 RA, US Food and Drug Adminstration, Washington DC. (1991).

78. R. C. Zeimer, H. K. Lim, and Y. Ogura, "Evaluation of an objective method for the in vivo measurement of changes in light transmittance of the human crystalline lens," Exp. Eye Res 45, 969-976 (1987).

79. T. J. T. P. van den Berg, "Quantal and visual efficiency of fluorescence in the lens of the human eye," Invest. Ophthalmol. Vis. Sci. 34, 3566-3573 (1993).

80. T. J. T. P. van den Berg and J. Felius, "Relationship between spectral transmittance and slit lamp color of human lenses," Invest. Ophthalmol. Vis. Sci. 36, 322-329 (1995).

81. T. J. T. P. van den Berg and J. K. IJspeert, "Light scattering in donor lenses," Vision Res. 35, 169-177 (1995).

82. T. J. T. P. van den Berg, "Depth-dependent forward light scattering by donor lenses," Invest. Ophthalmol. Vis. Sci. 37, 1157-1166 (1996).

83. S. Zigman, J. Groff, T. Yulo, and G. Griess, "Light extinction and protein in lens," Exp. Eye Res. 23, 555-567 (1976).

84. R. A. Weale, "Light absorption by the lens of the human eye," Optica Acta 1, 107-110 (1954).

85. R. A. Weale, "The post-mortem preservation of the transmissivity of the human crystalline lens," Exp. Eye Res. 41, 655-659 (1985).

86. B. H. Crawford, "The scotopic visibility function," Proc. phys. Soc. 62B, 321-334 (1949).

87. K. H. Ruddock, "The effect of age upon colour vision. II. Changes with age in light transmission of the ocular media," Vision Res 5, 47-58 (1965).

88. J. Xu, J. Pokorny, and V. C. Smith, "Optical density of the human lens," J. Opt. Soc. Am. A 14, 953-960 (1997).

89. G. L. Savage, C. A. Johnson, and D. L. Howard, "A comparison of noninvasive objective and subjective measurements of the optical density of human ocular media," Optom. Vis Sci 78, 386-395 (2001).

90. B. J. Ortwerth, V. Chemoganskiy, and P. R. Olesen, "Studies on singlet oxygen formation and UVA light-mediated photobleaching of the yellow chromophores in human lenses," Experimental Eye Research 74, 217-229 (2002).

Chapter 6

Sharp cutoff filters in intraocular lenses optimize the balance between light reception and light protection

Jan van de Kraats and Dirk van Norren

Journal of Cataract and Refractive Surgery 33, 879-887 (2007)

Abstract

Purpose: To facilitate the selection of the spectral filter in intraocular lenses.
Setting: Department of Ophthalmology, University Medical Center Utrecht
Methods: We measured the spectral transmission of commercially available intraocular lenses and gathered information from manufacturer datasheets and the literature. Illumination with sunlight filtered by the natural (age 20 and 70) and artificial eye media resulted in calculated values for the blue light damage and the signals from the sensory systems (rods, cones, melatonin suppression, and melanopsin). Results were presented as log differences with respect to the 20 year old human lens. A single rating value for each lens was calculated to facilitate the selection.
Results: The 70 year old lens offers a reduction in blue light damage of 0.45 log unit compared to the 20 year lens, although a similar reduction occurs in the signal from the short wave sensitive (SWS) cones. Intraocular lenses showed a range of nearly 1 log unit in blue light damage protection. A change in dioptric power in blue filtering lenses, with a corresponding change in thickness, strongly influenced behavior; dioptric power was less of a factor in lenses with sharp cuttoff filters.
Conclusions: Blue filtering lenses showed sometimes density spectra very different from the natural lens, but their filtering generally caused only mild sensory losses. Nearly none of these lenses offers an optimal trade-off between protection and signal reduction. Sharp cutoff filtering near 445 nm provide a better performance and also remove limitations in the optical design.

Introduction

The first implant lenses were made of clear polymethylmethacrylate (PMMA). This material transmits optical radiation up to 320 nm. Several years after the introduction of intraocular lenses it was realized that ultraviolet (UV) radiation is far more dangerous to the retina than visible light,[1,2] and that healthy human lenses do not transmit that part of the spectrum.[3] Therefore, filter material that strongly absorbed radiation below 400 nm was finally introduced in nearly all commercially available intraocular lenses. Later, lenses appeared on the market that not only cut off the UV, but also more strongly absorbed the violet (400-440 nm) part of the spectrum. The main argument for enhancing the absorption in the short wavelength part of the visible spectrum was fear for the so-called "blue light damage". Ham et al.[1,2] had clearly demonstrated that the action spectrum of photochemical damage extended well into the violet and even blue (440-500 nm) part of the spectrum. Yet, Ham's experiments only concerned acute damage, i.e. damage that appeared within 24 hours after exposure. Such damage is not often seen in natural conditions. In practice, conditions for acute damage are only met after prolonged (i.e. minutes) staring in the sun. From ancient times, this is relatively often the case with solar eclipses. With artificial light sources, acute photochemical damage is extremely rare. Arguments in favor of offering more protection from short wavelength light also derived from the fear that the cumulative dose of such light during a lifetime might be a factor in age-related macular degeneration (AMD).[4-6] In addition, the notion emerged that the elderly lens, through the natural yellowing process, in principle offers more protection that the young adult lens.[4,7,8] The extra protection, might be warranted given the accumulation of metabolic products like lipofuscin that possibly play a role in (acute) light damage.[9-11] Hence, lenses with enhanced absorption in the blue part of the spectrum, mimicking 50-60 years old natural lenses recently appeared on the market. However, attenuating the blue wavelengths has disadvantages too. Rods receive less light, color vision might be reduced, and the pigments that are involved in the day-night rhythm (melatonin suppression and melanopsin) might be hampered in their functioning.[12-15]

In the debate about advantages and disadvantages, it is helpful to quantify the effects of the different filters. We therefore gathered information on the spectral characteristics of a series of commercially available and hypothetical implant lens filters, and calculated the impact on the sensory systems mentioned above. We thereby took the mean young (about 20 years old) lens as a reference.

Methods

Eye media

We recently compiled from the nearly complete literature, optical transmission data for the young and aging eye.[16] The data was defined for all eye media separately over the spectral range 300-700 nm. In Fig. 1 data for human lenses aged 20 and 70 years, and for the rest of the eye media are expressed in density units (density = - log transmission), enabling the visualization over a large dynamic range. The absorption in the cornea, aqueous humor, and the vitreous, was assumed to be stable over lifetime. The young lens has a window of relatively low density around 325 nm. With increasing age to 70 years, the density in the UV increases enormously, up to a density of about 13.5 (off the scale in Fig. 1) at 325 nm.

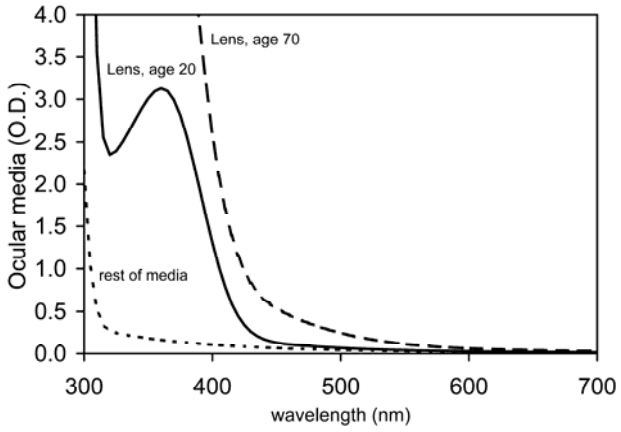

Fig. 1. The mean spectral density of the 20 year (solid line) and 70 year (dashed line) old human lens, together with the sum of the rest of the eye media (cornea, aqueous humor, vitreous; dotted line). The data are compiled from literature.[16] The 20 year lens data show a significant dip near 325 nm. The old lens reaches a density of 13.5 log units at 325 nm. To avoid compression of the data, the density scale was limited to 4 log units (0.01% transmission).

Blue light damage

For the blue light damage spectrum we went back to Ham's original data, because later compilations (e.g. INCIRP)[17] show peculiar humps and bumps. Ham measured retinal damage in monkey with laser illuminated spots for wavelengths ranging from 440-600 nm.[2] Later, wavelengths in the UV were added using a xenon arc lamp combined with interference filters with 10 nm bandwidth.[1] A complication arises as the laser spots on the retina had a Gaussian intensity distribution, whereas the spots in the UV had a flat distribution. Ham took the mean power between the $1/e^2$ points. It can be argued that the damage at the central peak of the Gaussian intensity distribution (being a factor 2.35 higher) is a more appropriate measure, as this is what triggers the formation of e.g. free radicals.[18] This correction leads to a smooth connection of the data points from both UV and the visual experiments (Fig. 2), similar to those for rats.[19] Log retinal sensitivity for photochemical damage can then be approximated with only two straight lines,

for $\lambda < 363$ nm $\log B(\lambda) = 0$,

and for $\lambda > 363$ nm $\log B(\lambda) = 5.366 - 0.0148 * \lambda$; (1)

with λ the wavelength in nm.

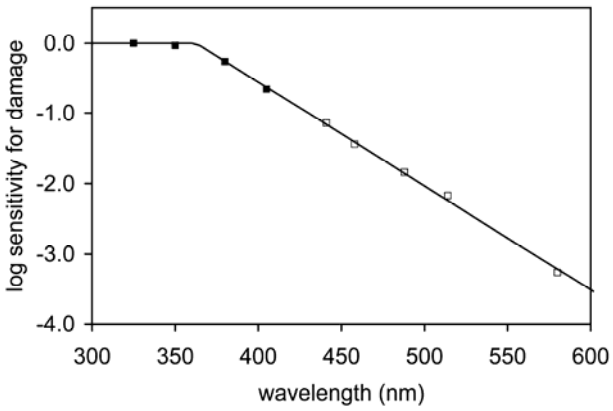

Fig. 2. Relative sensitivity of the retina for photochemical damage (squares),[1,2] and model fit (solid line). Data for the visual region[1] (open squares) were corrected for the Gaussian intensity distribution (see text).

Rods and Cones

For the rod spectral sensitivity at the retinal level we used human data from suction electrode recordings.[20] Such data do not have the uncertainty inherent to correction for prereceptor losses as in psychophysical data. For the SWS peripheral cones similar data were used, approximated by a polynomial template function.[21] MWS and LWS cones were not taken into account, because a calculation proved that these systems are only minimally affected by lens filtering. For the SWS foveal cones, the spectral sensitivity was reduced by absorption in macular pigment. Although there are no SWS cones in the very center of the fovea, they are present in large numbers in a field of a few degrees where macular pigment absorption is high. Macular pigment offers its protection only to this very small retinal area, which is however very important for high acuity color vision. We used a mathematical description by Walraven (personal communication). Density at the peak wavelength of 455 nm is 0.355.

$$\begin{aligned} \text{Density}_{\text{macpig}}(\lambda) = \; & (\; 0.32 * \exp[-0.0012 * (436-\lambda)^2] + \\ & 0.32 * \exp[-0.0012 * (480-\lambda)^2] - \\ & 0.123 * \exp[-0.0012 * (458-\lambda)^2] + \\ & 0.12042 * \exp[-0.006 * (457-\lambda)^2] \;) \end{aligned} \qquad (2)$$

Melatonin

The sensory system for melatonin suppression is important in controlling the circadian rhythm. The action spectrum was, a few years ago, determined by Thapan et al.[22] (Fig. 3) and Brainard et al.[23] Their original results do not match very well. Both groups unconvincingly compared their results with a visual pigment template. Brainard et al.[23] corrected, rather crudely, for media absorption of their (relative young) observers, by assuming a 45% transmission for the 420 nm data point, and 100% for all other wavelengths. By correcting their data with our transmission data for the young human eye media (Fig. 3), their data become surprisingly similar to Thapan et al.'s.[22] Both data sets now also match with the spectrum for photo-dependent oxygen uptake in RPE cells, approximated by an exponential function.[24] We used the latter function to describe (and extrapolate) the shape of the melatonin spectrum to 380 nm.

$$\text{melatonin suppression} = c * \exp(-0.02 * \lambda) \qquad (3)$$

with c a constant, and λ the wavelength in nm.

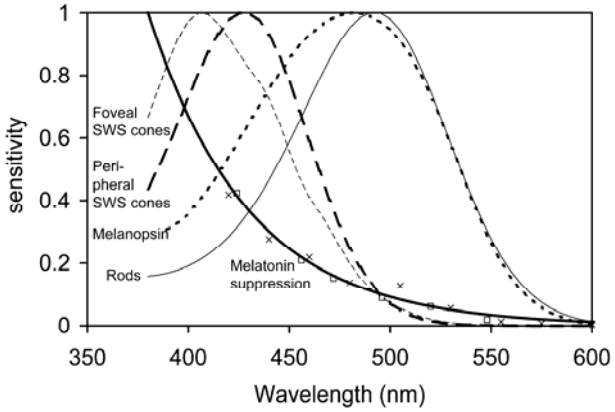

Fig. 3. Spectral sensitivities of the sensory systems at the retinal level. The SWS peripheral cone data (thick dashed line) are from Baylor et al.[21] using their template, the SWS foveal cone data (thin dashed line) are attenuated by macular pigment absorption. The rod data (thin solid line) are from Kraft et al.[20] also using Baylor et al.'s template. The action spectra for melatonin suppression in humans are from Thapan et al.[22] (boxes) and Brainard et al.[23] (crosses), the latter with our media correction for the young eye. The thick solid line is the spectrum for photo-dependent oxygen uptake in RPE cells from Rozanowska, approximated by a exponential function.[24] The spectral sensitivity of melanopsin (dotted line) is described with an A_1 type photo pigment with a peak at 482 nm.[27]

Melanopsin

Recently, a new visual pigment was discovered, having no image forming capabilities, but functioning as a sensory system for the circadian rhythm and other subconscious functions like driving the pupil.[25,26] It is present in ganglion cells with large dendritic connections. The spectral sensitivity can be described very well with a A_1 type photo pigment[27] having a peak of 482 nm (Fig. 3) as found by ERG and intracellular recordings.

Spectrum of sunlight

The importance of spectral filtering also depends on the mean optical radiation that reaches the eye. In theory, a weighted mean of spectral irradiances from natural and artificial sources should be taken. We approximated a worst case situation by taking the spectrum for diffuse solar radiation, because it is common, and contains a high fraction UV and blue light (Fig. 4).[28]

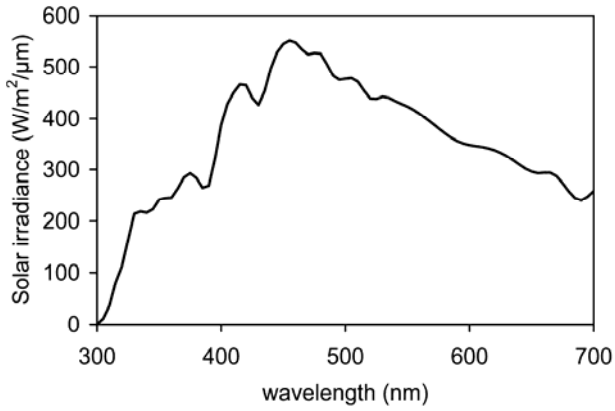

Fig. 4. The spectrum of diffuse sunlight from the blue sky, with added reflection from the ground.[28]

Obtaining the spectral density of intraocular lenses

Lenses of the Hoya-AF-1 UY type, the Acrysof Natural and the Ophtec Orange PC440Y type were measured using an Ocean optics spectrometer (SD2000; Ocean Optics, Dunedin, FL) with fiber optic input as the detector. The light source was a halogen lamp (HL 2000; Ocean Optics, Dunedin, FL) with fiber optic output. The lens under test was carefully placed on a horizontal platform containing a hole of 2 mm diameter, with the illuminating fiber from below, and the detector fiber above all lined up concentrically. The spectral range was from 350 to 880 nm. A reference spectrum of 100% was taken when no lens was inserted. Spectral characteristics of other commercially available and hypothetical implant lens filters were obtained from the literature and industry. Data for the PhysIOL YellowFlex were taken from the plot in the manufacturer's datasheet (PhysIOL Liege, Belgium). The Acrysof UV data was from Laube.[29] Dr. M. Mainster provided the tabulated data for the Eyeonics AT45, the AMO Clariflex, and the AMO OptiBlue intraocular lens (private communication).[14] Data for Schott filter material used for the hypothetical lenses were taken from the companies catalog (Schott AG, Mainz, Germany). To eliminate optical enlargement errors and deviations due to different media (air or saline) in which the lenses were measured,[30] the density spectra of all lenses were forced to zero above 700 nm, thus assuming equal reflection losses for all types, and no absorption of the chromophores at this wavelength..

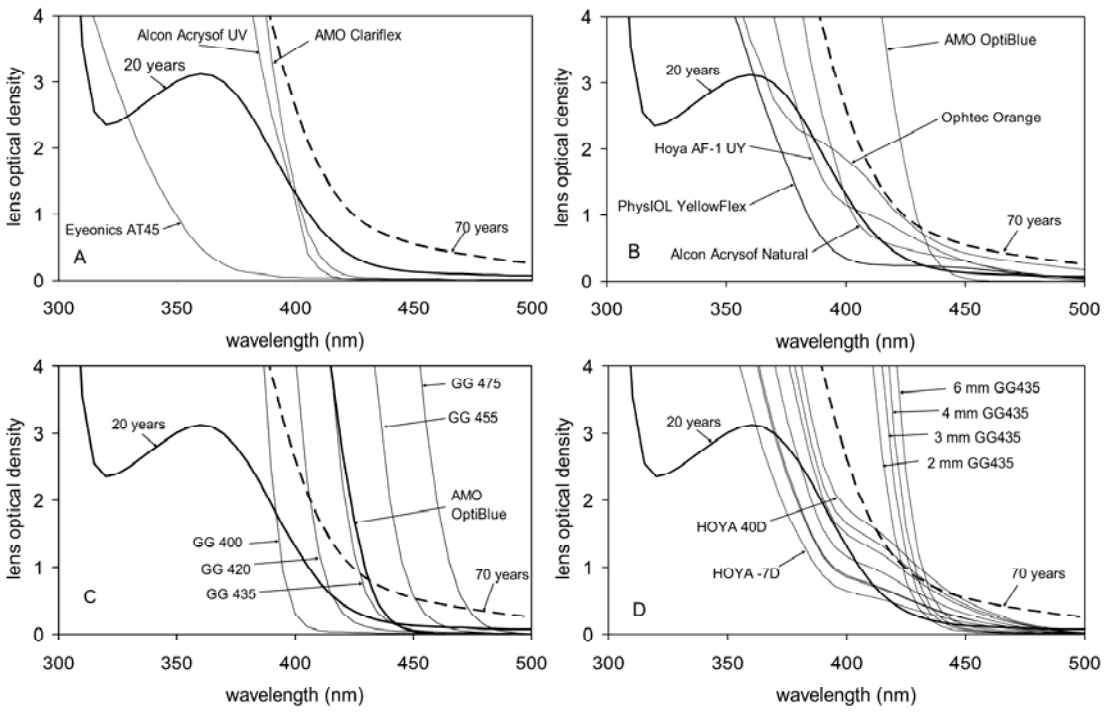

Fig. 5. Density spectra for intraocular lenses and sharp cutoff filters. For comparison, in each panel the density spectrum of the mean 20 year lens and the mean 70 year lens are given. A. Density spectra for typical 20D intraocular lenses with mainly UV filtering and one without UV filter. B. Density spectra for 20D intraocular lenses with violet and blue filtering. C. Density spectra of 3 mm Schott cutoff filters (GG400, GG420, GG435, GG455, and GG475). For comparison of the steepness, the AMO OptiBlue from panel B is also given here. D. Density spectra for Hoya AF-1 UY intraocular lenses with different refractive powers

(-7D, 6D, 10D, 20D, 30D, 34D, and 40D; in order from left to right). In addition, the density spectra of Schott GG435 cutoff filters (2 to 6 mm thickness) are given.

Calculation of damage and sensory signals

The blue light damage and the signals from the sensory systems (rods, foveal and peripheral SWS cones, melatonin suppression, and melanopsin) were calculated by multiplication of the pertinent spectra with the spectrum of diffuse solar light, filtered by the eye media, and integrated over the spectral range from 380 to 600 nm. For the blue light damage calculation, the range was extended to 300 nm, as damage below 380 nm is not negligible. Eye media consisted of the 20 year lens, the 70 year lens, a series of 20D intraocular lenses from different manufacturers, and a Hoya AF-1 UY intraocular lens with a series of refractive powers from –7D to +30D. In addition, hypothetical lenses were included consisting of 3 mm Schott filter material with various cutoff wavelengths (i.e. the wavelength at 50 % transmission), and a single Schott filter with thicknesses 2, 3, 4, and 6 mm. Where necessary, data were extrapolated to 4 density units by a polynomial fit. Reflection losses were assumed equal for all lens types; lens density spectra were moved vertically to set their mean value between 700 and 750 nm to zero.
The absorption in the rest of the eye media was always included. For the foveal SWS cone calculation macular pigment absorption was included. All results are presented as log differences referred to the results calculated for the 20 year old human lens.

Rating

Because selecting the filter in an intraocular lens is a trade off between suppressing blue light damage and low attenuation of the sensory system signals, a single rating number was defined as (log) SWS foveal cone signal subtracted by the (log) blue light damage. The outcome was multiplied by 100 for easy reading. The higher the number the better in terms of optimization.

Table 1. Log ratio of blue light damage and sensory system signals, referred to the 20 year old human lens.

	Blue light damage	SWS peri	SWS fovea	Rods	Melatonin suppression	Melanopsin	Rating
human lens age 20	0.00	0.00	0.00	0.00	0.00	0.00	0
human lens age 70	-0.45	-0.42	-0.42	-0.21	-0.33	-0.24	2*
Eyeonics AT45	0.67	0.26	0.32	0.09	0.41	0.12	-36
Alcon Acrysof UV only	0.25	0.20	0.22	0.09	0.19	0.11	-4
PhysIOL YellowFlex	0.23	0.04	0.08	-0.01	0.11	0.00	-15
AMO Clariflex	0.18	0.16	0.17	0.07	0.14	0.08	-2
Alcon Acrysof Natural	-0.08	-0.10	-0.10	-0.01	-0.06	-0.02	-2
Hoya AF-1 UY	-0.15	-0.16	-0.15	0.00	-0.09	-0.02	-1
AMO OptiBlue	-0.15	-0.06	-0.08	0.05	-0.05	0.04	6
Ophtec Orange PC440Y	-0.34	-0.32	-0.32	-0.13	-0.24	-0.15	1*
GG400 3 mm	0.32	0.22	0.25	0.09	0.22	0.11	-7
GG420 3 mm	0.06	0.09	0.08	0.06	0.06	0.07	2
GG435 3 mm	-0.13	-0.05	-0.07	0.05	-0.04	0.04	6
GG455 3 mm	-0.40	-0.34	-0.35	-0.01	-0.21	-0.04	5*
GG475 3 mm	-0.71	-0.78	-0.74	-0.11	-0.39	-0.16	-4*
Hoya -7D	0.08	0.00	0.02	0.03	0.04	0.03	-7
Hoya 6D	-0.03	-0.07	-0.06	0.02	-0.03	0.00	-4
Hoya 10D	-0.02	-0.07	-0.06	0.02	-0.02	0.01	-4
Hoya 20D	-0.15	-0.16	-0.15	0.00	-0.09	-0.02	-1
Hoya 30D	-0.26	-0.24	-0.25	-0.03	-0.16	-0.05	1*
Hoya 34D	-0.30	-0.28	-0.28	-0.03	-0.18	-0.06	1*
Hoya 40D	-0.36	-0.33	-0.33	-0.05	-0.21	-0.07	2*
GG435 2 mm	-0.09	-0.01	-0.03	0.05	-0.02	0.05	6
GG435 3 mm	-0.13	-0.05	-0.07	0.05	-0.04	0.04	6
GG435 4 mm	-0.17	-0.08	-0.10	0.04	-0.07	0.03	6
GG435 6 mm	-0.22	-0.13	-0.15	0.02	-0.10	0.01	6

All brand name intraocular lenses are 20D; Schott cutoff filters with different cutoff wavelengths and thicknesses are included for comparison. The range of dioptric powers refers to a Hoya AF-1 UY lens. For the Blue damage column, the most negative values are better, for all other columns the most positive values are better. Rating was defined in the Methods as the 100 times magnified difference between columns SWS fovea and Blue light damage; an asterix was added if one of the sensory signals dropped below the criterion of -0.2, yielding an unequal comparison.

Results

The measured density spectra of 20D Hoya AF-1 UY, Ophtec Orange and Alcon Acrysof Natural intraocular lenses together with the density spectra of other commercially available 20D intraocular lenses from manufactures datasheets and the literature are presented in Fig. 5A en B. For comparison, the spectra of the mean 20 and 70 year old lens are given in each panel. In Fig. 5C, the density spectra of Schott cutoff filters (GG400, GG420, GG435, GG455, and GG475) with a thickness of 3 mm are presented. The cutoff wavelength in the brand name (attenuation 50%) only holds for 3 mm thickness. With a different thickness, the actual cutoff wavelength changes. To demonstrate the very significant effect of lens power on the measured density spectrum, a range of -7D to plus 40D is presented for the Hoya AF-1 UY in Fig. 5D. Central thickness ranged from 0.42 to 1.3 mm (about a factor 3). We therefore also measured a steep cutoff filter (Schott GG435) with a thickness range of 3 (2-6 mm; Fig. 5D).

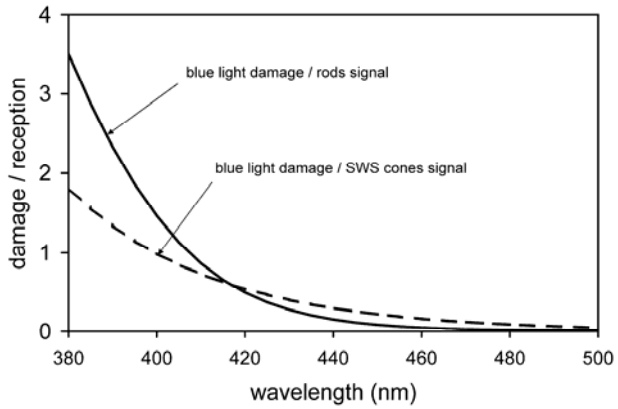

Fig. 6. Blue light damage divided by sensory signals versus wavelength shows that the shortest wavelengths contribute more to the damage than to the sensory signals in a continuously increasing way. This proves that a sharp cutoff filter within this wavelengths range is always optimal.

Log relative blue light damage and the signals from the sensory systems were calculated, referenced to a 20 year old lens (Table 1). For clarity the 20 year lens is included too (zeros). Intraocular lens entries were sorted with respect to the level of reduction of blue light damage. The 70 year old lens offers substantially more protection against light damage than the 20 year lens (0.45 log units, about a factor 3). However, a similar reduction in SWS cone signal occurs, and a somewhat lower but still substantial (-0.21 to –0.33) reduction in the other sensory systems. With regard to intraocular lenses the Eyeonics AT45 could yield substantially more (0.67 log units; almost a factor 5) blue light damage than the young human lens. At the other end of the scale, the Opthec Orange offered the highest (-0.34) protection against blue light damage. In contrast to the blue light damage column, in all other columns a more positive value should be judged as better, viz. less attenuation of sensory signals. The SWS cone data showed a similar data range as the blue light damage, except for the Eyonics and the PhysIOL Yellowflex lens that offered relatively little advantage for the SWS signal. Although the macular pigment attenuates the foveal SWS cone signal, after normalizing it with the young lens, most data hardly differed from those of the peripheral SWS cones. The absorption spectrum of the rods is more towards the long wavelengths and therefore showed, with all available intraocular lenses, at most a reduction of 0.13 log units. Melanopsin exhibited similar results. The range for melatonin suppression was somewhat less pronounced than that of the blue light damage and SWS cones. Blue light damage for refractive powers from -7D to +40D lied between those for the young and old human lens. The Schott cutoff filters showed an expected behavior when the cutoff wavelength moves towards longer wavelengths. A near equivalent of the 20 year old human lens was found between the GG420 and GG435 filter.

In Fig. 6 the ratio of the blue light damage to respectively, SWS peripheral cones, and rods is presented as a function of wavelength. The shorter wavelengths contribute more to the blue light damage than they add in a positive way to the receptor signals. For melatonin suppression and melanopsin similar curves were obtained (not shown). Because the ratios continuously decrease with increasing wavelength, attenuating shorter wavelengths by the intraocular lens filter is more advantageous than longer

wavelengths. Thus, a sharp cutoff filter with a cutoff wavelength between 380 and 500 nm as in Fig. 6 is always more effective (in terms of light protection versus light reception) than a shallow blue filtering lens. Note that the vertical scale in Fig. 6 is a relative one; no special meaning can be attributed to the value 1. The relation holds for the retinal, as well as for the corneal level.

We also calculated the attenuation of blue light damage and sensory signals as a function of cutoff wavelength (Fig. 7). Increasing the cutoff wavelength resulted in a rapid decrease of the blue light damage, and in general a somewhat slower drop in the signals from the sensory systems. The curves cross zero where the integrated signal equaled that from the 20 year lens because of the definition of the reference. A line was drawn at 0.2 log unit loss in signal. The wavelength where the curves fall below this line can be read from the cross point. For the most critical system, the SWS cones, it lies at 445 nm. In addition, at this wavelength the signal from the foveal and peripheral SWS cones is highest compared to the blue light damage. By coincidence, all curves crossed at about 0.1 near 420 nm, meaning that the combination of a simple 420 nm cutoff filter plus a neutral density filter of 0.1, has a similar effect under daylight illumination as the 20 year lens.

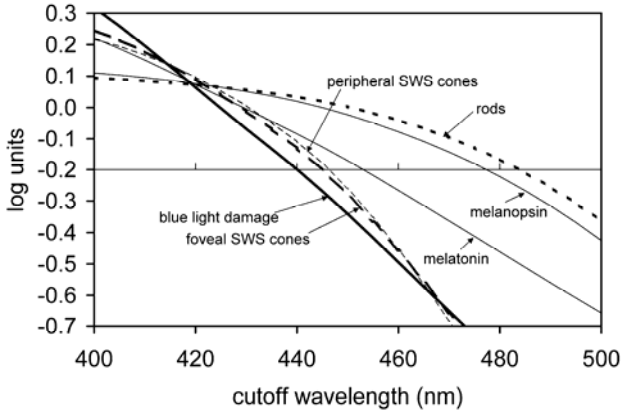

Fig. 7. Blue light damage and loss in sensory signals versus cutoff wavelength. A horizontal line was drawn at 0.2 log unit below the signals with the 20 year lens, to mark the limit of (the here chosen) acceptable loss.

Discussion.

With diffuse sunlight as a source we calculated the input to retinal systems through various pre-retinal filters with reference to the young adult eye. Thus, the trade-off between avoiding blue light damage and attenuating the useful signals from sensory systems could be quantified. Given what is commercially available, the cataract surgeon can freely select the virtual age of an intraocular lens; so to speak from a baby lens (with very high transmission at the low end of the visible range), to an elderly lens of about 60 years. There is consensus in the ophthalmologic community that UV radiation should be blocked, and nearly all intraocular lenses mentioned in this paper (with the notable exception of the Eyeonics AT 45 lens, and to some extend the PhysIOL YellowFlex) offer such protection. We are of the opinion that, to remain on the safe side, the density of the intraocular lens at the shortest visible wavelengths

(below 420 nm) should not drop below that of the young human lens, contrary to what was observed in several commercially available lenses. On the amount of filtering above 420 nm a debate is on-going.[12-15] Lenses with often curiously shaped filters have recently entered the market. The shape becomes more obvious in the (logarithmic) density plots presented in this paper, than in the usual (linear) transmission curves in commercial publications. However, what matters are not the details of the shape, but the overall impact on the various systems as we calculated here.

In our opinion, a loss of 0.2 log unit (37%) compared to the signals with the 20 year lens caused by the filter in the IOL, is of minor relevance in daily life. For color perception, daily variations in the spectrum of sunlight, let alone the shift from daylight to lamplight cause larger changes and have little consequences. Circadian rhythm is often disturbed at older age,[31] but a direct connection to reduced signals from the melatonin suppression or melanopsin systems through increased lens absorption seems difficult to make. The attenuation of these signals to below a certain level results perhaps in a shortening of the day by a few minutes, so the effect on circadian rhythm is probably very minor. It would be interesting to know whether elderly patients sleep better and maintain better circadian rhythm after their cataract operation.[32]

The rating, being the 100 times magnified difference between columns SWS fovea and Blue light damage, except rounding, (Table 1) provides a quick guide for making a selection, and enables comparison between spectrally very different lenses and cutoff filters. The more positive the rating, the better. The rating for the 70 year lens was 2, meaning that the gain in protection against blue light damage just was above the cost of attenuating the SWS cone signal. Rating for commercially available intraocular lenses ranged from -36 to 6, the selected sharp cutoff filters ranged from –7 to 6. The rating has the advantage of simplicity, but the disadvantage of simplification. Only the SWS signal was compared against damage, with loss in other sensory systems neglected. An argument for that simplification is that blue filtering IOLs generally hit the SWS system hardest. The SWS cone signal was given equal weight to the blue light damage. As an example, adding sunglasses with simple neutral density filtering at high illumination levels results in the same rating as without sunglasses. Lowering the light level a bit protects for blue light damage, but the loss in receptor signals are no problem at all; here a heavier weight of blue light damage in the rating seems better. At low illumination levels, blue light damage plays no role. Adding the sunglasses results in an unwanted loss in receptor signals. In that case, giving more weight to the SWS cone signal in the rating looks attractive. Yet, an argument against applying too much weight, is that contrast vision decreases far less than the signal itself.[15]

The gradual slope in spectral density that is often seen in recently introduced blue filtering lenses has a significant disadvantage. We demonstrated for such a lens (Hoya AF-1 UY) that the filtering properties strongly depend on refractive power, i.e. lens thickness (rating -7 to 2). This is quite a nuisance for the surgeon who opts for strong protection, because with low dioptric power filtering performance drops significantly, in an extreme case (-7D) even below that of the young adult lens. For a lens to have refractive power, thickness of course also varies from the center to the edge. A much better performance can be expected for filter materials with steep characteristics (Fig.

5D). Such filters have high densities at wavelengths below the cutoff and very low densities at higher wavelengths. We used Schott cutoff filters (Fig. 5) as an example to show what steepness is achievable with available chromophores. The rating showed no change with a similar variation in thickness as that for the Hoya lens. The higher thicknesses in absolute sense used for the Schott filters is not important because spectral characteristics are determined by the product of thickness and concentration of the chromophore.

That a sharp cutoff filter has better performance than a shallow one was shown in Fig. 6. A similar conclusion was reached on base of the ICNIRP aphakic damage function[17] (not shown). A commercial lens that has such a sharp cutoff filter is the AMO OptiBlue.[14] It comes close to the 4 mm Schott GG435 filter. The effects of the cutoff wavelength on the compromise between avoiding damage and undisturbed photoreception were quantified in Fig. 7. As soon as implant lenses with a series of cut off wavelengths would become available eye surgeons could set their own criterion of acceptable loss in signal.

Mainster recently also published a table with different types of commercially available and hypothetical lenses, comparing to a UV only blocking lens (AMO Clariflex).[14] Ratios were expressed as percentages. Log values seem more appropriate, because for the visual system the difference between e.g. 120 and 130 percent is not the same as between 20 and 30 percent. In addition, we believe comparison with the mean young human lens is more relevant. Mainster also provided an extensive discussion of the pros and cons of attenuating blue light.[12-14] We agree with his conclusions about the uncertainties in the relevance of the spectrum for acute light damage for development of AMD. As argued above, we feel somewhat less strongly, however, about his worries about the attenuation of the signals from the sensory systems caused by most blue filtering lenses.

The results of this paper apply only for illumination by sunlight. Incandescent lamps have far less blue light, thus less impact on the choice of intraocular filters. Other light sources, as for instance the recently developed white LED's with a strong 440 nm component (also used to excite the red-green phosphors), could lead to different conclusions.
Tinted lenses or filters attenuating blue light often give a subjective feeling of comfort, but scientific evidence for improvement of visual functions is hard to achieve.[33] Including sensory systems linked to photophobia and discomfort glare in the present study was not possible because action spectra at wavelengths below 440 nm are lacking. Possibly, the subjective feeling is based on the unconscious signals from the melatonin suppression, and melanopsin signals. Phototoxicity of rhodopsin was not included in our analysis,[34,35] because positive effects of filtering (less damage) are exactly compensated by negative effects of a lower sensory signal. We interpreted Ham's action spectra for blue light damage somewhat different, leading to a surprising simplification in mathematical description. The underlying mechanism for this spectrum is largely unknown. Margrain[5] stated that it resembles the spectra for photo-dependent oxygen uptake in RPE cells,[24] but on a log scale the difference is rather obvious. We demonstrated instead (Fig. 5), that there is a striking coincidence between the spectra for photo-dependent oxygen uptake in RPE cells[24] and the spectrum of melatonin suppression.

Conclusion.

At the age of seventy, the natural lens offers a factor three more protection against blue light damage than at twenty, at the cost of significant loss of signal for the sensory systems. Those losses are milder for most types of blue filtering intraocular lenses, thus hardly an argument against their use. Sharp cut-off filters in intraocular lenses would be the best compromise between providing safety and loosing information. In addition, such filters give more freedom in the geometrical design.

Acknowledgement.

We thank Dr. Martin Mainster for making available the tabulated data for the Eyeonics AT45, the AMO Clariflex, and the AMO OptiBlue intraocular lens.[14]

References

1. Ham WT, Jr., Mueller HA, Ruffolo JJ, Jr., Guerry D, III, Guerry RK. Action spectrum for retinal injury from near-ultraviolet radiation in the aphakic monkey. Am J Ophthalmol 1982;93:299-306.

2. Ham WT, Jr., Mueller HA, Sliney DH. Retinal sensitivity to damage from short wavelength light. Nature 1976;260:153-155.

3. Wyszecki G, Stiles WS. Color Science: Concepts and Methods, Quantitative Data and Formulae, 2nd edition. John Wiley & Sons, 1982.

4. Young RW. Solar radiation and age-related macular degeneration. Surv Ophthalmol 1988;32:252-269.

5. Margrain TH, Boulton M, Marshall J, Sliney DH. Do blue light filters confer protection against age-related macular degeneration? Prog Retin Eye Res 2004;23:523-531.

6. Van der Hoeve J. Eye lesions produced by light rich in ultraviolet rays. Senile cataract, senile degeneration of the macula. Am J Ophthalmol 1920;3:178-194.

7. Van der Hoeve J. Senile Maculadegeneration und senile Linsentrubung. Graefe's Arch Ophthalmol 1918;98:1-6.

8. Van der Hoeve J. Der Antagonismus zwischen seniler Katarakt und seniler Makuladegeneration (Haab); und die Frequenz der senilen Makuladegeneration unmittelbar nach Staroperation. Z Augenheilkd 1927;63:127-136.

9. Boulton M, Rozanowska M, Rozanowski B. Retinal photodamage. J Photochem Photobiol B 2001;64:144-161.

10. Feeney-Burns L, Berman ER, Rothman H. Lipofuscin of human retinal pigment epithelium. Am J Ophthalmol 1980;90:783-791.

11. Weiter JJ, Delori FC, Wing GL, Fitch KA. Retinal pigment epithelial lipofuscin and melanin and choroidal melanin in human eyes. Invest Ophthalmol Vis Sci 1986;27:145-152.

12. Mainster MA, Sparrow JR. How much blue light should an IOL transmit? Br J Ophthalmol 2003;87:1523-1528.

13. Mainster MA. Intraocular lenses should block UV radiation and violet but not blue light. Arch Ophthalmol 2005;123:550-555.

14. Mainster MA. Violet and blue light blocking intraocular lenses: photoprotection versus photoreception. Br J Ophthalmol 2006;90:784-792.

15. Werner JS. Night vision in the elderly: consequences for seeing through a "blue filtering" intraocular lens. Br J Ophthalmol 2005;89:1518-1521.

16. van de Kraats J. and van Norren D. Optical density of the aging human ocular media in the visible and the UV. J Opt Soc Amer (in press).

17. Guidelines on limits of exposure to broad-band incoherent optical radiation (0.38 to 3 microM). International Commission on Non-Ionizing Radiation Protection. Health Phys 1997;73:539-554.

18. Wu J, Seregard S, Algvere PV. Photochemical damage of the retina. Surv Ophthalmol 2006;51:461-481.

19. Gorgels TG, van Norren D. Ultraviolet and green light cause different types of damage in rat retina. Invest Ophthalmol Vis Sci 1995;36:851-863.

20. Kraft TW, Schneeweis DM, Schnapf JL. Visual transduction in human rod photoreceptors. J Physiol 1993;464:747-765.

21. Baylor DA, Nunn BJ, Schnapf JL. Spectral sensitivity of cones of the monkey Macaca fascicularis. J Physiol Lond 1987;390:145-160.

22. Thapan K, Arendt J, Skene DJ. An action spectrum for melatonin suppression: evidence for a novel non-rod, non-cone photoreceptor system in humans. J Physiol 2001;535:261-267.

23. Brainard GC, Hanifin JP, Greeson JM, Byrne B, Glickman G, Gerner E, Rollag MD. Action spectrum for melatonin regulation in humans: evidence for a novel circadian photoreceptor. J Neurosci 2001;21:6405-6412.

24. Rozanowska M, Jarvis-Evans J, Korytowski W, Boulton ME, Burke JM, Sarna T. Blue light-induced reactivity of retinal age pigment. In vitro generation of oxygen-reactive species. J Biol Chem 1995;270:18825-18830.

25. Dacey DM, Liao HW, Peterson BB, Robinson FR, Smith VC, Pokorny J, Yau KW, Gamlin PD. Melanopsin-expressing ganglion cells in primate retina signal colour and irradiance and project to the LGN. Nature 2005;433:749-754.

26. Hankins MW, Lucas RJ. The primary visual pathway in humans is regulated according to long-term light exposure through the action of a nonclassical photopigment. Curr Biol 2002;12:191-198.

27. Partridge JC, De Grip WJ. A new template for rhodopsin (vitamin A1 based) visual pigments. Vision Res 1991;31:619-630.

28. Bird RE, Riordan C. Simple Solar Spectral Model for Direct and Diffuse Irradiance on Horizontal and Tilted Planes at the Earth's Surface for Cloudless Atmospheres. Journal of Applied Meteorology 1986;25:87-97.

29. Laube T, Apel H, Koch HR. Ultraviolet radiation absorption of intraocular lenses. Ophthalmology 2004;111:880-885.

30. Schwiegerling J. Blue-light-absorbing lenses and their effect on scotopic vision. J Cataract Refract Surg 2006;32:141-144.

31. Foster RG. Keeping an eye on the time: the Cogan Lecture. Invest Ophthalmol Vis Sci 2002;43:1286-1298.

32. Charman WN. Age, lens transmittance, and the possible effects of light on melatonin suppression. Ophthalmic Physiol Opt 2003;23:181-187.

33. Eperjesi F, Fowler CW, Evans BJW. Do tinted lenses or filters improve visual performance in low vision? A review of the literature. Ophthalmic and Physiological Optics 2002;22:68-77.

34. Noell WK, Walker VS, Kang BS, Berman S. Retinal damage by light in rats. Invest Ophthalmol 1966;5:450-473.

35. Noell WK. Possible mechanisms of photoreceptor damage by light in mammalian eyes. Vision Res 1980;20:1163-1171.

Chapter 7

Spectral transmission of IOLs expressed as a virtual age

Dirk van Norren and Jan van de Kraats

British Journal of Ophthalmology, in press

Abstract

Aim: Available Intra Ocular Lenses (IOLs) have widely different spectral filters. It was our purpose to calculate the virtual age of IOLs with regard to photoprotection and photoreception, i.e. the age of the natural lens that has similar effects on these aspects.

Methods: With diffuse solar radiation as a light source the blue light damage was calculated for natural lenses at all ages, commercially available IOLs and Schott steep cut-off filters in the wavelength range 300 - 600 nm. Similarly, the input to the short wavelength cone system was calculated for the range 380 – 600 nm.

Results: The virtual age for photoprotection of IOLs and steep cut-off filters varied from <0 to 66 years. Most IOLs had similar ages for photoreception, and thus show a reasonable resemblance to the spectral properties of the natural lens. One IOL and all steep cut-off filters had a lower age for photoreception than for photoprotection, and thus outperformed the natural lens.

Conclusion: The virtual age of an IOL puts its spectral filtering properties in perspective of what happens in the healthy crystalline lens. Many older IOL types offer less protection than the lens of a newborn. Middle age seems a reasonable choice for an IOL.

Keywords: Intraocular lens, age, spectral transmission

Introduction

All intraocular lenses (IOLs) have a spectral filter for absorbing short wavelength radiation. When IOLs were first introduced they only mimicked the refractive properties of the crystalline lens. Later it was realized that unhampered transmission of ultraviolet radiation might harm the retina.[1] Only recently the thought emerged that visible short wavelength radiation might also cause acute or chronic damage. In the last few years new IOLs were therefore introduced with spectral filters extending far into the visible. Available IOLs now range in color from fully transparent, to light yellow up to orange.

The cataract surgeon faces the problem of how to choose the spectral filter. On this subject several papers have recently appeared[2-10] emphasizing the uncertainty in the effects of chronical damage through optical radiation, and thus in the wavelengths that should be cut, violet and/or blue.

It was the aim of the present paper to offer a practical help by introducing two numbers for an IOL, a measure for photoprotection, the virtual age Ap, and a measure for photoreception, the virtual age Ar. The idea is based on the fact that the spectral filter in the natural lens changes significantly with age. At birth the lens is perfectly transparent and nearly colourless; at old age a (healthy) lens is yellowish brown. In the (invisible) UV the changes are even greater. The optical density at 320 nm increases from about 2 at birth, to 18, i.e. virtually opaque at the age 80.[11] Thus, with increasing age more potentially dangerous short wavelength radiation is absorbed, be it at the cost of some reduction in photoreception. We calculated at what age of the natural lens a specific IOL has an identical effect for photoprotection. Similarly, we derived a virtual age for photoreception.

Methods

Mean spectral characteristics of the human media from were obtained from Van de Kraats and van Norren.[11] Spectral characteristics of IOLs, Schott cut-off filters, blue light damage, (peripheral) SWS cones, and diffuse sunlight were taken from another paper of these authors.[10] A number for photoprotection was derived by taking the integral from 300-600nm of (spectrum of blue light damage)* (spectrum of media transmission)*(spectrum of sunlight). A number for photoreception was obtained by integrating the products of the spectra for SWS cone sensitivity, media transmission and sunlight over the range 380 – 600 nm. Relating the numbers for an IOL to those of the natural lens led to the virtual ages Ap and As. An IOL has similar spectral characteristics as the natural lens when Ap = As.

Results

Calculated virtual ages for photoprotection and photoreception are summarized in Table 1. A high age for photoprotection should be interpreted as desirable, but for photoreception the reverse is true. Several IOLs had such high transmission that the virtual age was below that of a newborn (Ap, Ar < 0). In those cases the difference Ap-Ar could not be calculated. Other IOLs ranged from 34 to 60 years. To show what is in principle possible with commercial dyes, we also calculated the ages of hypothetical IOLs that have the dye of 3 mm Schott cut-off filters. These ages ranged from 5 to 66 years. The differences in age for photoprotection and photoreception were generally small. The AMO OptiBlue and all Schott steep cut-off filters had Ap-Ar > 0 .

Table 1 Virtual ages of IOLs for photoprotection (Ap) and photoreception (Ar).

IOLs	Ap	Ar	Ap-Ar
Eyeonics AT45	<0	< 0	
Alcon Acrysof UV only	<0	< 0	
PhysIOL YellowFlex	<0	< 0	
AMO Clariflex	<0	< 0	
Bausch & Lomb Sofport	14	<0	>14
Alcon Acrysof Natural	34	37	-3
Hoya AF-1 UY	42	44	-2
AMO OptiBlue	42	35	7
Ophtec Orange PC440Y	60	61	-1
Cut-off filters			
Schott GG420	5	< 0	> 5
Schott GG435	40	33	7
Schott GG455	66	64	2

Discussion

The virtual age of commercial IOLs differed enormously, from 'younger' than a newborn, to 60 years old. It was revealing to see that the older types of IOLs have such high transmission at the short wavelengths that they offer less protection than the lens of a newborn. Newer IOL types successfully imitate natural lenses in the range 34 – 60 year, with the notable exception of the recently introduced PhysIOL Yellowflex that falls in the group with age < 0. Most IOLs provide a reasonable imitation of the spectral characteristics of the natural lens, be it that the balance is a little less optimal than in the natural lens. The AMO OptiBlue (not commercially available) has an improved balance between photoprotection and photoreception compared to the natural lens. This is also the case for Schott cut-off filters that also illustrate the flexibility in virtual age that can in principle be achieved.[10]

The limits of the virtual age calculation become obvious in the IOLs with age < 0. Among these is the Eyeonics AT 45 with much higher transmission in the UV than the Alcon Acrysof UV only and the AMO Clariflex.[10] These details were lost in the virtual age calculation. On the other hand Ap < 0 clearly conveys the message that the IOL offers limited protection against short wavelength radiation.

What should the virtual age of an IOL preferably be? Are patients best off with a rejuvenation of their eyes after a cataract operation, or should the IOL mimic the older lens that it replaces? In fact at present the age choice is between either less than a newborn or, at least 30 years. For unhampered vision a very young IOL is fine, but to prevent chronic and acute light damage a safer course should be steered. To give an example, the time allowed for reaching damage threshold by staring into the sun with an unprotected eye is at the age of 80 more than 4 longer than for a newborn. The average middle aged subject has good vision in the blue range of the spectrum, no problems with night vision, does not suffer from sleep problems that might be related to problems with melatonin suppression or lesser stimulation of melanopsin,[8] yet at such age substantial protection against acute damage, and against possible chronic damage exists. Thus, we are of the opinion that the middle aged IOL offers a good compromise between photoprotection and photoreception.

For photoreception we only calculated the input to the SWS cone system. The spectral absorption curve of the SWS cones is closer to the blue light damage spectrum than

that of any other system that plays a role in human photoreception. The rod system, for instance, has an absorption spectrum that is shifted about 70 nm towards longer wavelengths and thus is far less influenced by IOL filters.
In conclusion, we propose a novel system to characterize the spectral properties of IOLs. The virtual age places the IOL in perspective of what happens in the healthy natural lens, and the difference in age for photoprotection and that for photoreception provides information about the degree of resemblance to natural lens. The filter in an IOL can, in principle, be designed such that it outperforms nature.

Reference List

1. Ham WT, Jr., Mueller HA, Ruffolo JJ, Jr. *et al*. Action spectrum for retinal injury from near-ultraviolet radiation in the aphakic monkey. *Am.J.Ophthalmol.* 1982;**93**:299-306.

2. Mainster MA, Sparrow JR. How much blue light should an IOL transmit? *Br J Ophthalmol* 2003;**87**:1523-8.

3. Laube T, Apel H, Koch HR. Ultraviolet radiation absorption of intraocular lenses. *Ophthalmology* 2004;**111**:880-5.

4. Margrain TH, Boulton M, Marshall J *et al*. Do blue light filters confer protection against age-related macular degeneration? *Prog.Retin.Eye Res.* 2004;**23**:523-31.

5. Braunstein RE, Sparrow JR. A blue-blocking intraocular lens should be used in cataract surgery. *Arch.Ophthalmol.* 2005;**123**:547-9.

6. Werner JS. Night vision in the elderly: consequences for seeing through a "blue filtering" intraocular lens. *Br.J.Ophthalmol.* 2005;**89**:1518-21.

7. Mainster MA. Intraocular lenses should block UV radiation and violet but not blue light. *Arch Ophthalmol* 2005;**123**:550-5.

8. Mainster MA. Violet and blue light blocking intraocular lenses: photoprotection versus photoreception. *Br.J.Ophthalmol.* 2006;**90**:784-92.

9. Schwiegerling J. Blue-light-absorbing lenses and their effect on scotopic vision. *J.Cataract Refract.Surg.* 2006;**32**:141-4.

10. van de Kraats J. and van Norren D. Sharp cutoff filters in intraocular lenses optimize the balance between light reception and light protection. *J Cataract Refract Surg.* 2007; (in press).

11. van de Kraats J. and van Norren D. Optical density of the aging human ocular media in the visible and the UV. *J Opt Soc Am A.* 2007 (in press).

Chapter 8

Fast assessment of the central macular pigment density with natural pupil using the Macular Pigment Reflectometer

Jan van de Kraats, Tos T. J. M. Berendschot, Suze Valen and Dirk van Norren

Journal of Biomedical Optics 11, 064031 (2006)

Abstract

We built a new Macular Pigment Reflectometer (MPR) for fast and objective measuring of the optical density of macular pigment in the human eye, using the undilated eye. The design is based on the spectral reflectance from a spot of white light at the fovea. To evaluate its performance, twenty healthy subjects, age 18-79 years, were measured in four conditions, (1) natural pupil in the dark, (2) natural pupil with dim room light, (3) dilated pupil in the dark, and for comparison with a different technique, (4) Heterochromatic Flicker Photometry (HFP) in dim room light with natural pupil. Condition (1) was repeated in a subset of 10 subjects after an interval of at least three days. Data analysis with a model of reflectors and absorbers in the eye provided the density of the macular pigment in conditions 1-3. Dim room light and pupil dilatation had no influence on measured density. Mean within subjects variation was typically 7 %. Mean difference between test and retest after at least three days was 1 %. Correlation between MPR and HFP was $r = 0.56$ ($p = 0.012$). Mean within subjects variation with HFP was 19 %. The new instrument holds promises for specific applications like epidemiological research.

Introduction

Macular pigments invoke increasing interest because of their putative role in preventing chronic adverse effects of light on the retina. In particular, there is an ongoing debate on the positive effects of the macular pigments lutein and zeaxanthin in preventing Age-related Macular Degeneration (AMD).[1-3] Several studies have shown that it is relatively easy to manipulate the amount of macular pigment by either food rich in lutein and zeaxanthin, or by taking supplements.[4-8] A pivotal element is assessing the amount of the macular pigments in the human retina. This is not a trivial task. Their overlapping spectral characteristics make individual assessments of lutein and zeaxanthin difficult, if not impossible in the living eye. Generally, overall macular pigment optical density (MPOD) is measured. There are two main approaches. The most widespread method makes use of psychophysical techniques. The subject adjusts color or luminosity, generally through a minimum flicker, or a minimum motion task.[9,10] The psychophysical approach has the advantage of requiring no special measures like pupil dilatation or head fixation, but a complete measurement is rather time consuming, and the task, in particular when making a match in the peripheral retina, is not trivial. The second approach is through analysis of light returning from the retina. It relies either on spectral analysis[11,12], autofluorescence[13], or on Raman spectroscopy.[14] It has the advantage of being objective and relatively fast, but it has the drawback of requiring sophisticated equipment that is only available in a few specialized laboratories.
In this study we aimed to build a specialized, but simple device for fast, reliable MPOD measurements, without the need for pupil dilatation. We compared the results of the new instrument with one based on heterochromatic flicker photometry.

Methods

Macular pigment reflectometer. The optical arrangement is shown in Fig. 1. Light from a 30 Watt halogen lamp, is delivered at the eye through three optical relay systems. The first relay (L1, L2) images the filament of the lamp on a mask. Between L1 and L2 filtering (GG395, Schott, Mainz, Germany) occurs to cutoff UV. This to reduce the level of dangerous light in subjects with their eye lens removed. The second relay (L3, L4) images the filament within the mask on a small mirror M at 45 degrees. The last relay (L5, L6) forms an image of the eye pupil at the plane of M, where the illumination beam coming from M, and detection beam, passing over M are separated ("pupil separator"). The relay (L5, L6) forms a Badal system, as L6 is movable to focus a stop (between L3 and L4) at the retina. Focussing range is from minus 15D to plus 15D. The resulting retinal spot has a diameter of one degree visual field, a retinal illuminance of 1.04×10^7 Troland, and a retinal irradiance of 4.6 mW/cm^2. The calculated maximum exposure time, based on the recommendations of the Health Council of the Netherlands (1993)[15] is 26 minutes; for aphakes it is 20 minutes. The detection channel has the Badal system (L5, L6) in common with the illumination system, with no overlap in the lenses itself to keep instrument stray-light to a minimum. The pupil separator contains masks to limit the illumination and detection configuration (separation 0.8 mm) in the pupil to a three mm circle (Fig. 1). For subjects with a pupil diameter smaller than three mm absolute calibration of percentage reflection no longer holds. This does however not immediately make accurate measurements of macular pigment impossible, as these are determined from the shape of the spectral reflection. A diameter of 2.3 mm is about the practical lower limit. Lenses L7 and L8 form an image of the retinal spot on the tip of an optical fiber.

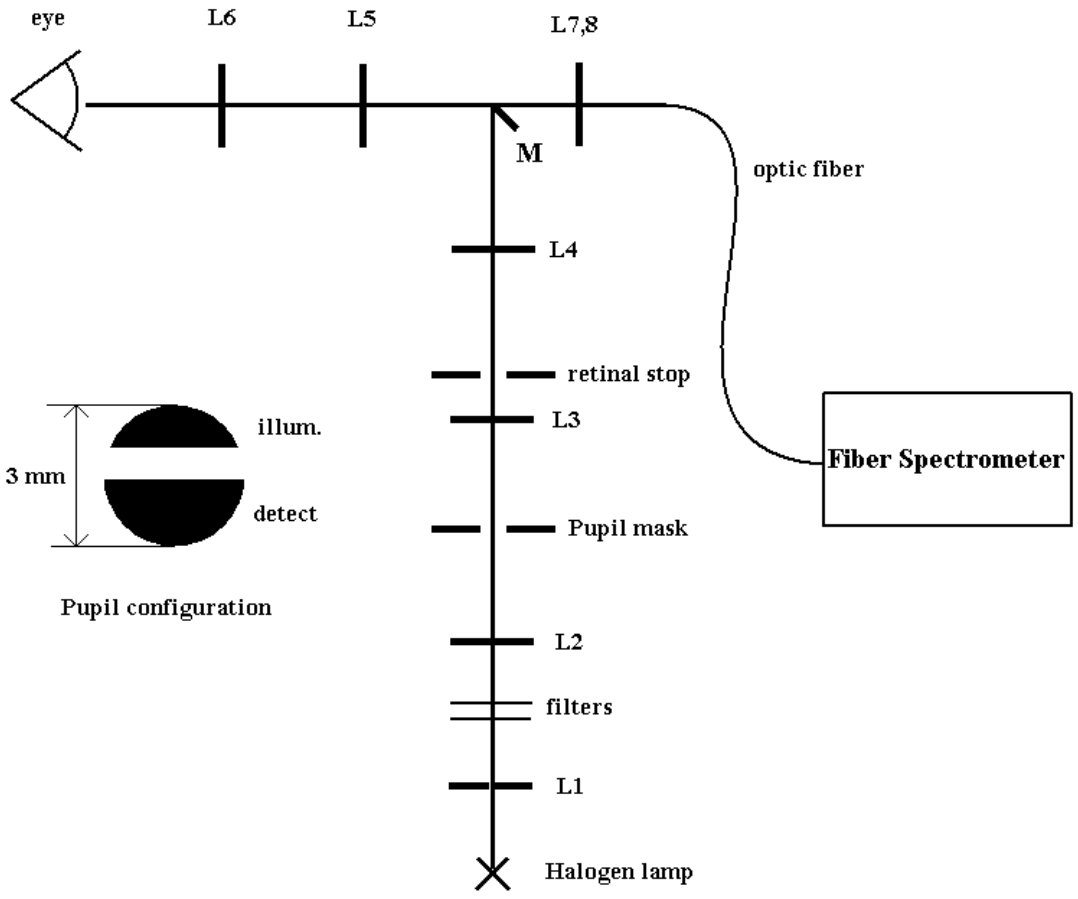

Fig. 1 Optical scheme of the Macular Pigment Reflectometer. An image of the filament of the halogen lamp is relayed by lenses L1-L4 to a mask and then to a mirror M. Filters (GG395, Schott) are inserted to reduce UV light. The Badal system L5-L6 has L6 as a movable lens to focus a retinal stop (between L3 and L5) on the retina. The detection channel has the Badal system in common with the illumination system, without overlap of the light paths in lenses. Lenses L7-L8 form an image of the retinal field on the tip of a fiber that connects to a commercial spectrometer. The insert shows the dimensions of the illumination and detection beams at the level of the pupil.

A mask at the tip of the fiber defines a diameter of one degree at the retinal plane. The fiber is the receiving part of a commercial fiber spectrometer (Ocean Optics SD2000, Ocean Optics Inc. Dunedin Florida, USA). Optical resolution is 5.8 nm (FWHM); the range 400-800 nm was used for analysis. The output of the spectrometer is sent to a personal computer. Integration time was set at one second. The displayed reflection spectrum is the mean and standard deviation of two succeeding one second periods. Reflectance was calibrated with a surface painted with Eastman 6080 white at a distance of 230 mm from the pupil plane position ("white calibration"). The surface was mounted at the end of a black anodized tube to eliminate room light. The Eastman 6080 white surface was compared with a BaSO4 surface. Differences were

accounted for in the software. During the calibration the spectrometer averaged 30 measurements of one second each. The first lens was set to a position such that the white surface was conjugate with the retinal planes of the instrument. Because the distance of 230 mm from the pupil plane is 10 times the focal distance of the eye, the measured spectrum equaled a one percent reflection from the eye. This reflection calibration accounts both for the spectral sensitivity of the detection system, as for the spectral content of the illumination. The “white calibration” was corrected for spurious reflections in the front lenses by averaging 30 measurements with a light trap at the position of the eye ("dark calibration"). The light trap consisted of two polished black plates at a tapering angle, positioned at the pupil plane of the instrument. The dark calibration was taken with the lens position optimized for each subject (cf protocol). Wavelength was calibrated with a lamp containing mercury and argon lines (Avalight-CAL, Avantes Eerbeek The Netherlands).

Heterochromatic flicker photometry (HFP). We used a portable instrument developed by Mellerio *et al*.[16] In summary, a test field flickers between a blue light that is highly absorbed by the MP and a green light that is not absorbed by the MP. A minimum flicker match is made by adjusting the intensity of the blue light when the retinal image of the one degree test field lies on the fovea. Another match is made away from the fovea, where the MPOD is assumed to be negligible. The test field was an annulus of 5 degrees inner radius and of one degree width, centered on the foveal fixation spot. The logarithm of the ratio of the blue luminosity for the foveal match to that for the extra-macular match gives the MPOD.
Protocol. The research followed the tenets of the Declaration of Helsinki and was approved by the local Medical Ethics Committee. All subjects (n=20, age 18-79 years) were Caucasian, not known to have an eye disease, and with a visual acuity of at least 0.8. The purpose was explained at the beginning of the experiment, and written informed consent was obtained. Chin rest and temple pads were used to help maintain head position. The instrument was aligned with the subject’s eye, using a joystick. The (clearly visible) illumination beam was set in the subject’s pupil a little above its center, allowing room for the invisible detection beam. The subject was asked to fixate the center of the 1 degree spot. Initial focusing was obtained with a diopter scale on the instrument using the spectacle prescription. Next the subject was asked whether the spot edges were sharply focused. If necessary, an adjustment was made. Correcting refraction resulted in concentric illumination and detection fields at the retina. Without focusing they are concentric posterior or anterior to the retina, and reflected light is lower in amplitude. Therefore, a final adjustment was made by optimizing the amplitude of the measured reflection spectrum. The experimenter viewed a reflectance curve, updated once per second, together with the highest curve (with maximum reflectance between 500-600 nm) obtained since the start of the measurement. This feature also facilitated optimizing the position of illumination and detection beam with regard to the subject's pupil. When the front lens was optimized, the subject leaned back, allowing the experimenter to perform the dark calibration. Thereafter, final alignment took place. Dark calibration changed very little over the course of hours, thus in fact it could have been taken less frequently. Reflections from the corneal surface and/or lens were minimized by adjusting the distance between eye and the instrument, and minor adjustments in the position of the illumination beam. Corneal reflections show up as a relatively high signal at the short wavelengths compared to the middle wavelengths. We estimated that alignment time was sufficient to bleach more than 95 % of the visual pigments. Subjects were asked to occasionally

blink but keep their eyes wide open during measurements. Five spectra were measured and stored on disc for further analysis in three conditions (1) natural pupil, dark room, for getting statistics on measurements with natural pupil in an optimal environment. (2) natural pupil dim room light, for getting statistics on measurements with natural pupil in a less optimal environment with a disturbing light, in this case from a dimmed incandescent lamp set at 3 lux at the eye, (3) dilated pupil, dark room, for having an optimal reference with no disturbing room light and no possible influence of interception of measurement light by the pupil edges. Ten subjects were re-measured in condition (1) after an interval of at least three days to check reproducibility.
With the HFP instrument, according to the prescribed protocol, also five measurements were taken.

Data analysis. A slightly modified model of pathways of light in the eye was used to analyze the spectral data.[17] Briefly, the model contains three reflectors, the inner limiting membrane (ILM), the cone receptor disks, and the choroidal space. Absorption anterior to the receptor layer takes place in the lens and in the macular pigment. Absorption posterior to the receptor layer is in melanin and blood. Absorption in visual pigment is neglected because of bleaching by the high light levels. The retinal area of 1 degree to be analyzed was considered homogeneous in macular pigment and melanin content, although we recognize that this is a simplification. A more detailed description of the model is in the Appendix.
The Levenberg-Marquardt routine[18] was used to fit the data with the model by minimizing chi-squares. The wavelength range used was from 400 to 800 nm. All parameters were allowed to vary simultaneously. For a single measurement the noise in the data points was assumed to originate mainly from photon noise, with a small addition from head or eye movements of the subject. The standard deviation in the spectral data points were therefore calculated from two succeeding one second periods, and were used to weight the data points in the fitting process. For a typical example of this noise, see the error bars in Fig 2 in the Result section. A single measurement containing relatively large eye movements was easily recognized by a large standard deviation at the long wavelength points, and was generally rejected and replaced immediately during the measurements.

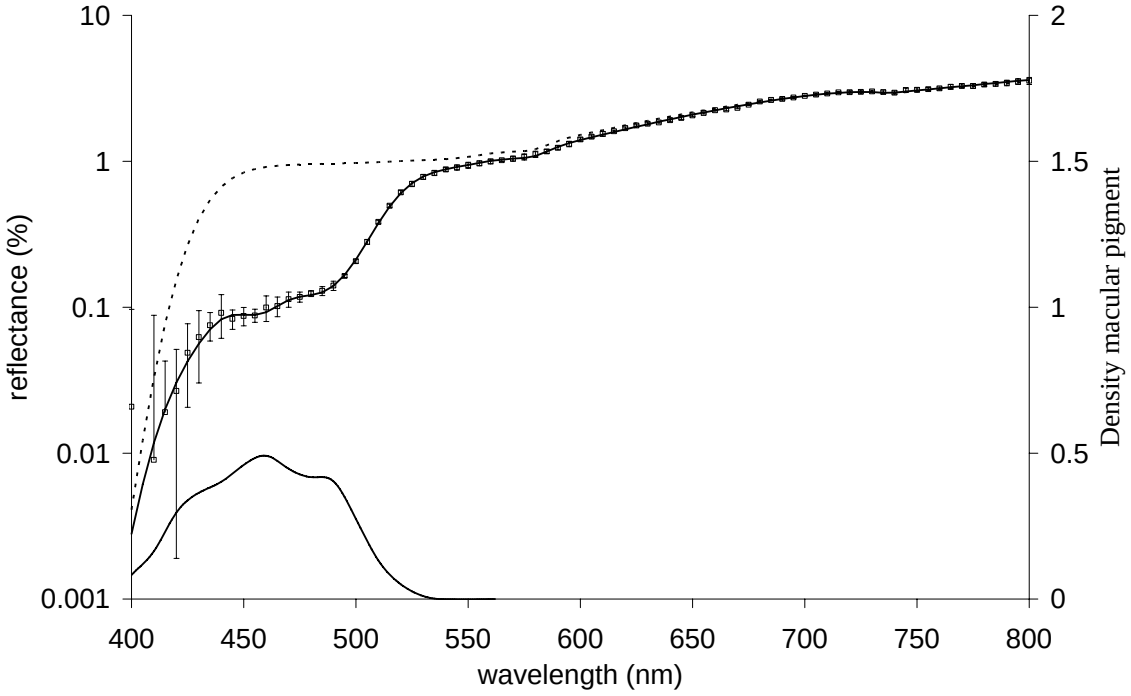

Fig. 2 Typical reflectance spectrum exhibiting high reflectance at long wavelengths, with a gradual decrease caused by absorption in melanin and blood. At about 550 nm the macular pigment causes a sharp decline, followed by a plateau between 500 and 450 nm. Thereafter, another sharp decrease is caused by absorption in the crystalline lens. A best fitting model curve is drawn through the data points. The error bars show the standard deviation in the data points. The same model curve, but with the absorption of MP set to zero, is shown as a dashed line. The absorption curve of macular pigment from literature,[31] as used in the model, is shown at the bottom (cf. the scale on the right).

Results

Measurements were successfully completed in all subjects. A typical reflectance spectrum is shown in Fig. 2. In the long wavelength region reflection is high because lens, macular pigment, blood and melanin have minimal absorption. At wavelengths below 600 nm the reflection declines because of increased absorption in blood and melanin. Around 560 nm a plateau is visible. Light is reflected by the spectrally neutral interfaces at the pigment epithelium/cone outer segment level. Below 510 nm macular pigment absorption sets in, and below 450 nm the lens increasingly absorbs nearly all incoming light. Consequently, in the blue region of the spectrum reflection is about a factor 100 below that of the red region.

Density of macular pigment (MPOD) was derived from the spectral reflection curves with the Van de Kraats model, as mentioned in the Methods.[17] MPOD with the natural pupil in a dark room was 0.55 ± 0.21 (condition 1), with dim room light 0.56 ± 0.23 (condition 2), and with dilated pupil 0.57 ± 0.22 (condition 3). No significant differences existed between conditions 1-3. With the heterochromatic flicker photometry (condition 3) a significantly lower MPOD of 0.35 ± 0.19 was found than in condition 1 (paired T-test; $p < 0.001$). Figure 3 shows MPOD as a function of age. No change with age was found (condition 1, $r = 0.15$, $p = 0.54$). Test-retest results after at least three days (Fig. 4a) showed a very high reproducibility ($r = 0.94$, $p <$

0.001). Correlation between the conditions natural pupil in dim light, and dark room were high ($r = 0.97$; $p<0.001$; Fig. 4 b), as was the correlation between dark room natural, and dilated pupil ($r = 0.90$; $p<0.001$; Fig. 4c). In Fig 4d the relation between the data obtained with reflectometry (condition natural pupil, dimly lit room) and HFP is given. Again a significant correlation was found ($r = 0.56$; $p = 0.012$). Five spectra were measured in each condition, which provided an estimate of the within subject variation. Mean within subjects variation for the MPR was typically 7 %. Mean within subjects variation with HFP was 19 %.

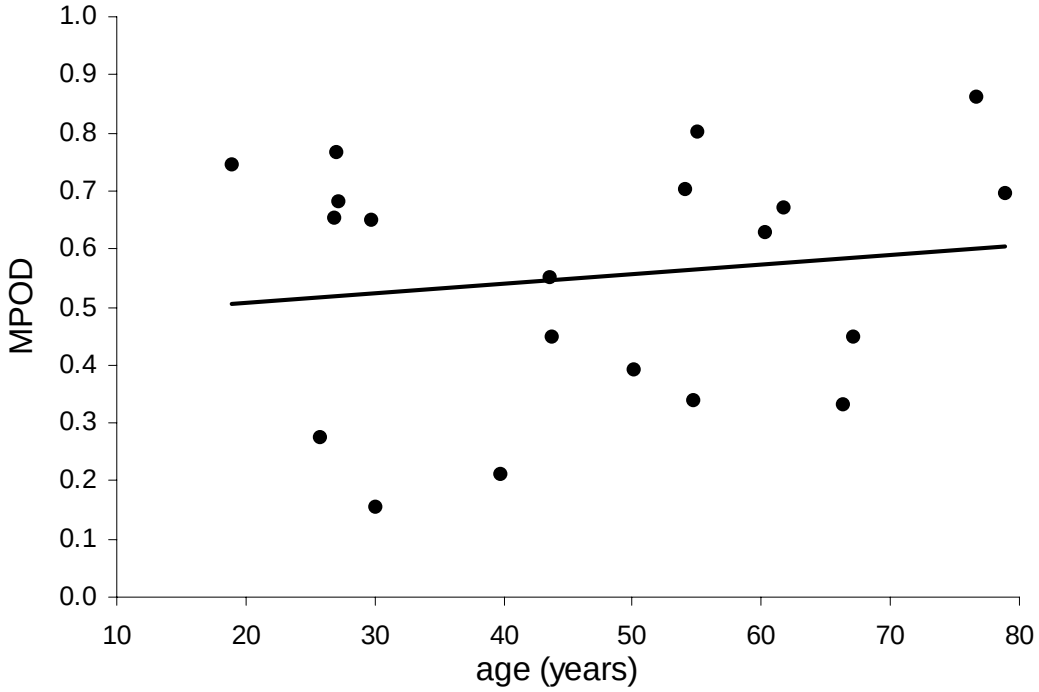

Fig. 3 MPOD showing no change with age. The solid line, provided as a guide to the eye, shows a positive, but not significant linear regression

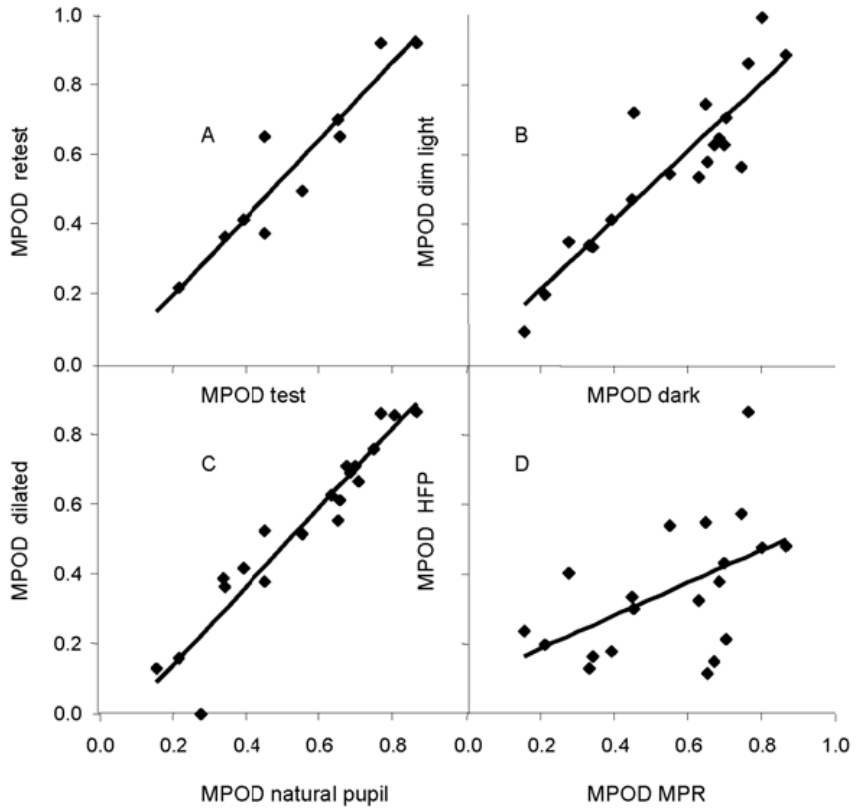

Fig. 4A Test-retest results for 10 subjects with a minimum interval of 3 days. Correlation was 0.94 ($p<0.01$). The solid line shows equality.
B. MPOD in a condition with dim room light and no room light. Correlation was 0.97 ($p < 0.001$). The solid line is the regression line
C. MPOD with natural pupil versus dilated pupil. Correlation was 0.98 ($p < 0.001$). The solid line is the regression line.
D. MPOD as measured with the Macular Pigment Reflectometer versus that with Heterochromatic Flicker Photometry. Correlation was 0.56 ($p = 0.012$). The solid line is the regression line.

Discussion

With the new Macular Pigment Reflectometer fast and reproducible estimates were obtained of the optical density of the macular pigment. An advantage inherent to the all techniques with physical detectors is that they require only minimal cooperation of the subject. After the preliminaries the subject is asked five times to fixate the stimulus for a few seconds. Such a task is far easier than the performance required with the widespread HFP technique. HFP asks for a substantial number of settings, which are not particularly easy to make with peripheral stimuli, in particularly for elderly subjects. Depending on the instrument used, this probably accounts for the much lower optical densities. The HFP apparatus used in this study for instance lacked an individual setting of flicker rates.[16] Related to this is the assumed similarity

in the receptor sensitivities between the foveal and peripheral sites, with perhaps different criteria attached. A second reason for lower densities with HFP may be the assumed zero macular pigment density at the peripheral site for the HFP technique, and other effects resulting from the spatial distribution of macular pigment. These differences between HFP and other techniques are not uncommon; see the more detailed discussion in papers by Delori and Berendschot *et al*.[19,20] With the new device the whole procedure takes, including calibration, less than 5 minutes, comparing favorably with the HFP that takes 10-15 minutes. As a benefit, it provides other parameters from the reflectance model, like lens density. Discussing these parameters is beyond the scope of this paper.

Hammond *et al*. stated that the validity of non invasive MP methods depends on that they must provide spectral absorption curves that match the extinction spectrum of xanthophylls.[21] With the new device a model uses the extinction spectrum of MP and finds, with the density as a free parameter, the best fit to the spectral reflection. Reflections at layers anterior to the MP are accounted for in the model thus an estimate of MP is obtained, undiluted by straylight. An indication for the validity of the technique comes from showing an increase in density of macular pigment with oral intake of lutein, similar to what was found with the HFP technique.[4] In addition, in a comparison of 5 different techniques Berendschot *et al*. found highly significant correlations of MPOD in a group of 53 subjects with methods based on the present technique (model analysis of spectral fundus reflectance) on the one hand, and SLO maps, SLO autofluorescence, and HFP on the other hand.[19] As mentioned before, just like with the present data, HFP showed the lowest correlation. The macular pigment density did not co-vary with other parameters in the model analysis, except with the ILM reflex. However, we found no correlation between macular pigment density and the ILM reflex in this dataset, indicating that the macular pigment estimates were not biased by incorrect ILM values.

Despite the fact that the present technique has no separate fixation target at the center of the one degree test field, test-retest reliability was very high ($r = 0.98$), even higher than in a HFP study with a very careful protocol (range 0.68-0.90 for different conditions).[22]

With no moveable fixation target available, the new device only allows central measurement of MP. This is a limitation in view of the increasing interest in the retinal distribution of MP.[23,24] HFP devices generally provide fixation targets at a number of locations, and hence data on the distribution of MP. The penalty is a very time consuming measurements (up to 45 min). In fact, two wavelength autofluorescence, measured with an SLO seems the ideal for providing detailed maps of MPOD. However such devices are costly, and often require pupil dilatation, rendering the method less suitable for larger scale investigations on MP.

MPOD showed no changes with age, a finding that is in line with most other studies[19], and even, despite strong indications to the contrary[25], with a recent study using Raman spectroscopy.[26]

In conclusion, we succeeded in building an instrument for fast, reliable measurement of macular pigment optical density. The instruments might be suitable for specific purposes in assessing MPOD. In particular it holds promises for epidemiological research and quick assessments for patients on supplements.

Acknowledgements

The authors thank John Mellerio for the use of his portable device for heterochromatic flickerphotometry.

Appendix

Reflectance Model

In the model first the light reflected in the choroidal space is described. The back scattering of light in the choroidal tissues is taken as a neutral reflection $R_{choroid}$. Light in the choroidal space is absorbed by blood and melanin. The density of a layer of blood with a thickness Th_{blood} in μm is:

$$D_{blood}(\lambda) = Th_{blood} * \alpha_{blood}(\lambda) \quad (1)$$

with $\alpha_{blood}(\lambda)$ the density of 1 μm 95% oxygenated blood.[27] To account for the variety of path lengths through the center and periphery of small and large blood vessels, we assumed a wedge shaped blood layer, with path lengths from zero to Th_{blood}. The transmission can be calculated as:

$$T_{blood}(\lambda) = (1.0 - 10.0 \,\hat{}\, (- D_{blood}(\lambda))) / (D_{blood}(\lambda) * \ln(10)) \quad (2)$$

For the transmission through a uniform layer of melanin we took the spectral data of Gabel,[28] approximated by:

$$\alpha_{melanin}(\lambda) = 2.45 * (0.007 + 0.165 * \exp(-\lambda * 0.0055) + 113 * \exp(-\lambda * 0.011) - 4300 * \exp(-\lambda * 0.022)) \quad (3)$$

The term 2.45 is to normalize the function to 1 at 500 nm, so that $D_{melanin}$ is the parameter for the density of melanin at 500 nm. The transmission of melanin becomes:

$$T_{melanin}(\lambda) = 10\hat{}\text{-}(D_{melanin} * \alpha_{melanin}(\lambda)) \quad (4)$$

Reflection at the level of the receptor layer is than described by:

$$R_{recep}(\lambda) = R_{rpe} + (T_{blood}(\lambda) * T_{melanin}(\lambda))^2 * R_{choroid} \quad (5)$$

with R_{rpe} the parameter for a neutral reflection at the retinal pigment epithelium (RPE), augmented with the reflection of the retinal cone receptors. We simplified the original model[17] by assuming the absence of visual pigments because of the high bleaching intensity level. Also, a single mean cone reflectance was taken, as the shape of the directional sensitivity cannot be discriminated with this simple instrument. Both the cone disc reflection and the RPE reflection are taken spectrally neutral. They can therefore not be distinguished from each other, and both are represented by the single RPE reflection value.
Transmission of the media is described by:

$$T_{media}(\lambda) = 10^{\wedge} -(D_{lensyoung} * \alpha_{Lensyoung}(\lambda) + D_{lensold} * \alpha_{Lensold}(\lambda) + 24 * \alpha_{water}(\lambda)) \quad (6)$$

Parameter $D_{lensyoung}$ is the density of the lens at 420 nm for the young age component having the spectral shape $\alpha_{Lensyoung}(\lambda)$ of the Pokorny aging template normalized at 420 nm.[29] Similarly, $D_{lensold}$ is the density at 420 nm for the old age component, with $\alpha_{Lensold}(\lambda)$ the corresponding Pokorny non-aging template normalized at 420 nm.[29] $\alpha_{water}(\lambda)$ is the density of 1 mm water.[30] The transmission of the macular pigment is described by:

$$T_{macpig}(\lambda) = 10^{\wedge} -(D_{macpig} * \alpha_{macpig}(\lambda)) \quad (8)$$

with $\alpha_{macpig}(\lambda)$ Walraven's description of the macular pigment data.[31] We normalized it to 1 at 460 nm, than parameter D_{macpig} is the density of macular pigment at 460 nm, and:

$$\begin{aligned}\alpha_{macpig}(\lambda) = (1/0.35) * \quad (\; & 0.32 * \exp[-0.0012(436-\lambda)^2] + \\ & 0.32 * \exp[-0.0012(480-\lambda)^2] - \\ & 0.123 * \exp[-0.0012(458-\lambda)^2] + \\ & 0.12042 * \exp[-0.006 \; (457-\lambda)^2] \;) \end{aligned} \quad (9)$$

At the level of the cornea, the reflection from the eye can now be described by:

$$R_{eye}(\lambda) = (T_{media}(\lambda))^2 * \quad (R_{ilm} + (T_{macpig}(\lambda))^2 * R_{recep}(\lambda)) \quad (10)$$

R_{ilm} represents a parameter for a neutral reflection at the back of the vitreous at the ILM.
Thus the model contains 7 free parameters: $R_{choroid}$, T_{blood}, $D_{melanin}$, R_{rpe} , $D_{lensyoung}$, $D_{lensold}$, and D_{macpig}.

Reference List

1. S.Beatty, I.J.Murray, D.B.Henson, D.Carden, H.Koh, M.E.Boulton, "Macular pigment and risk for age-related macular degeneration in subjects from a Northern European population", *Invest Ophthalmol Vis Sci*, 42, 439-446 (2001).

2. T.T.J.M.Berendschot, J.J.M.Willemse-Assink, M.Bastiaanse, P.T.V.M.de Jong, D.van Norren, "Macular pigment and melanin in age-related maculopathy in a general population", *Invest Ophthalmol Vis Sci*, 43, 1928-1932 (2002).

3. R.A.Bone, J.T.Landrum, S.T.Mayne, C.M.Gomez, S.E.Tibor, E.E.Twaroska, "Macular pigment in donor eyes with and without AMD: a case-control study", *Invest Ophthalmol Vis Sci*, 42, 235-240 (2001).

4. T.T.J.M.Berendschot, R.A.Goldbohm, W.A.Klöpping, J.van de Kraats, J.van Norel, D.van Norren, "Influence of lutein supplementation on macular pigment, assessed with two objective techniques", *Invest Ophthalmol Vis Sci*, 41, 3322-3326 (2000).

5. J.T.Landrum, R.A.Bone, H.Joa, M.D.Kilburn, L.L.Moore, K.E.Sprague, "A one year study of the macular pigment: the effect of 140 days of a lutein supplement", *Exp Eye Res*, 65, 57-62 (1997).

6. R.A.Bone, J.T.Landrum, L.H.Guerra, C.A.Ruiz, "Lutein and Zeaxanthin Dietary Supplements Raise Macular Pigment Density and Serum Concentrations of these Carotenoids in Humans", *J Nutr*, 133, 992-998 (2003).

7. B.R.Hammond, Jr., E.J.Johnson, R.M.Russell, N.I.Krinsky, K.J.Yeum, R.B.Edwards, D.M.Snodderly, "Dietary modification of human macular pigment density", *Invest Ophthalmol Vis Sci*, 38, 1795-1801 (1997).

8. S.Beatty, J.Nolan, H.Kavanagh, O.O'Donovan, "Macular pigment optical density and its relationship with serum and dietary levels of lutein and zeaxanthin", *Arch Biochem Biophys*, 430, 70-76 (2004).

9. J.D.Moreland, "Macular pigment assessment by motion photometry", *Arch Biochem Biophys*, 430, 143-148 (2004).

10. R.A.Bone, J.T.Landrum, "Heterochromatic flicker photometry", *Arch Biochem Biophys*, 430, 137-142 (2004).

11. T.T.J.M.Berendschot, P.J.DeLint, D.van Norren, "Fundus reflectance-historical and present ideas", *Prog Retin Eye Res*, 22, 171-200 (2003).

12. T.T.J.M.Berendschot, D.van Norren, "Objective determination of the macular pigment optical density using fundus reflectance spectroscopy", *Arch Biochem Biophys*, 430, 149-155 (2004).

13. F.C.Delori, "Autofluorescence method to measure macular pigment optical densities fluorometry and autofluorescence imaging", *Arch Biochem Biophys*, 430, 156-162 (2004).

14. P.S.Bernstein, D.Y.Zhao, M.Sharifzadeh, I.V.Ermakov, W.Gellermann, "Resonance Raman measurement of macular carotenoids in the living human eye", *Arch Biochem Biophys*, 430, 163-169 (2004).

15. Health council of the Netherlands, Committee on optical radiation, "Optical Radiation. Health based exposure limits for electromagnetic radiation in the wavelength region from 100 nanometer to 1 millimeter", *Health council of the Netherlands*, The Hague, (1993).

16. J.Mellerio, S.Ahmadi-Lari, F.van Kuijk, D.Pauleikhoff, A.Bird, J.Marshall, "A portable instrument for measuring macular pigment with central fixation", *Curr Eye Res*, 25, 37-47 (2002).

17. J.van de Kraats, T.T.J.M.Berendschot, D.van Norren, "The pathways of light measured in fundus reflectometry", *Vision Res*, 36, 2229-2247 (1996).

18. Press WH, Flannery BP, Teukolsky SA, Vetterling WT. Numerical recipes in pascal. The art of scientific computing. Cambridge: Cambridge University Press, 1989.

19. T.T.J.M.Berendschot, D.van Norren, "On the age dependency of the macular pigment optical density", *Exp Eye Res*, 81, 602-609 (2005).

20. F.C.Delori, D.G.Goger, B.R.Hammond, D.M.Snodderly, S.A.Burns, "Macular pigment density measured by autofluorescence spectrometry: comparison with reflectometry and heterochromatic flicker photometry", *J Opt Soc Am A Opt Image Sci Vis*, 18, 1212-1230 (2001).

21. B.R.Hammond, B.R.Wooten, B.Smollon, "Assessment of the validity of in vivo methods of measuring human macular pigment optical density", *Optom Vis Sci*, 82, 387-404 (2005).

22. D.M.Snodderly, J.A.Mares, B.R.Wooten, L.Oxton, M.Gruber, T.Ficek, "Macular Pigment Measurement by Heterochromatic Flicker Photometry in Older Subjects: The Carotenoids and Age-Related Eye Disease Study", *Investigative Ophthalmology Visual Science*, 45, 531-538 (2004).

23. T.T.J.M.Berendschot, D.van Norren, "Macular pigment shows ringlike structures", *Invest Ophthalmol Vis Sci*, 47, 709-714 (2006).

24. F.C.Delori, D.G.Goger, C.Keilhauer, P.Salvetti, G.Staurenghi, "Bimodal spatial distribution of macular pigment: evidence of a gender relationship", *J Opt Soc Am A Opt Image Sci Vis*, 23, 521-538 (2006).

25. P.S.Bernstein, "New insights into the role of the macular carotenoids in age-related macular degeneration. Resonance Raman studies", *Pure Appl Chem*, 74, 1419-1425 (2002).

26. K.Neelam, N.O'Gorman, J.Nolan, O.O'Donovan, H.B.Wong, K.G.A.Eong, S.Beatty, "Measurement of Macular Pigment: Raman Spectroscopy versus Heterochromatic Flicker Photometry", *Investigative Ophthalmology Visual Science*, 46, 1023-1032 (2005).

27. van Assendelft OW. Spectroscopy of hemoglobin derivatives. Springfield, IL: C.C. Thomas, 1970.

28. Gabel VP, Birngruber R, Hillenkamp F. Visible and near infrared light absorption in pigment epithelium and choroid. In: Shimizu K, Oosterhuis JA, eds. Excerpta Medica, International Congress Series. Amsterdam: Elsevier 1978:658-62.

29. J.Pokorny, V.C.Smith, M.Lutze, "Aging of the human lens", *Appl Opt*, 26, 1437-1440 (1987).

30. R.C.Smith, K.S.Baker, "Optical properties of the clearest natural waters", *Appl Opt*, 20, 177-184 (1981).

31. Walraven, P. L., "CIE report TC 1-36 Draft 7 Personal Communication", Soesterberg, (2003).

Chapter 9

Modeling the directional and non-directional spectral reflection from the human fovea

Jan van de Kraats and Dirk van Norren

Submitted for publication

Abstract

A model of the directional and non-directional reflection spectrum of the human fovea is developed, incorporating reflectors, absorbers and a wavelength dependent optical Stiles-Crawford effect (OSCE). Data from 53 healthy subjects between 19 - 75 years obtained with the Fundus Reflection Analyzer (FRA), an imaging spectrograph that measures directional reflection profile of the human fovea in the pupil plane from 400 to 950 nm were analyzed. Subgroups of young (<40 year) and old (> 50 year) observers were defined. Another group of 39 subjects (18 – 71) years was added for comparison.

Mean results of the young group defined a template for directionality versus wavelength. The model generated a nearly perfect fit to the mean spectral reflection of the young and old groups. For the whole group mean reflection from the cones was 1.9 %, from the retinal pigment epithelium 0.54 %, and from the choroid 7.84 %. Lens density, cone disc reflection and blood layer thickness showed a significant trend versus age. The second group showed similar parameter values.

The model for the first time simultaneously describes the spectra of the directional and non-directional reflection of the human fovea. Rayleigh scatter losses of the media only show up in the directional pathway. Mean density of macular pigment correlated significantly with independent data obtained with SLO (reflectance and autofluorescence) images and flicker photometry.

Keywords Optical Stiles-Crawford effect, cone receptor reflectance, macular pigment, melanin, spectroscopy, eye media optical density.

Introduction

Several attempts have been made to model the spectral reflection of the fundus of the eye by assuming reflection at different retinal layers interspaced with ocular absorbers. In 1986 Van Norren, and Tiemeijer[1] measured the reflectance of the fovea, a peripheral site, and the optic disc at 14 wavelengths. Measurements were rather cumbersome, as each wavelength needed a separate session. Their instrument optimized the directional reflection from the receptors (the optical Stiles-Crawford effect) by using entry and exit pupils that were small, and close together. Their model had two reflecting layers, one at the retinal pigment epithelium and one at the sclera. In addition, four absorbers were distinguished; lens, macular pigment, melanin and blood. In the same year Van Blokland and Van Norren[2] presented reflectance measurements with an instrument that enabled detailed information about the shape of the directional reflection, but only four laser wavelengths were available. In a descriptive model the authors suggested optical pathways in the receptor layer.

A few years later Delori and Pflibsen[3] build a reflectometer based on a grating spectrometer, allowing all wavelengths to be measured simultaneously. The optical design used the exit pupil of a Zeiss fundus camera and thus was not optimized for obtaining the directional reflection from the receptors. Their model added a graded reflection from the choroidal space to the model of Van Norren and Tiemeijer[1]. They achieved a better estimate of absorption in melanin and blood, but the receptor layer was ignored. Van Norren and Van de Kraats presented an instrument that could measure 15 wavelengths quasi-simultaneously.[4] It was again optimized for the directional reflection and it used low light levels to enable retinal reflection spectra with the nearly full complement of visual pigments. A new model was derived by Van de Kraats, Berendschot and Van Norren with detailed optical pathways in the receptor layer.[5] Spectral reflection was measured at two positions, one at the maximum of the directional reflection and one at a position with entry and exit pupil shifted horizontally for 2.5 mm. For the first time, a reflection from the stack of cone receptor discs was incorporated. Time consuming measurements with high and low levels of visual pigment, and with the high and low directional content, were used to refine the model. Although the measurements of the directional aspects were rather crude (only based on two points), it permitted the isolation of pre-receptor, receptor and post-receptor signals, thereby improving the accuracy of estimating the pre-receptor parameters, lens and macular pigment density.

A new instrument proposed by the first author and elaborated by Zagers et al.,[6] combined the directional resolution earlier presented by Van Blokland and Van Norren,[2] with the spectral resolution of Delori and Pflibsen.[3] It consisted of an imaging spectrometer with the entrance slit in the pupil plane, a prism and a sensitive CCD camera as a detector. In one second a 2D image could be measured from a foveal spot illuminated with intense white light, containing in one dimension the spectral aspects and in the other the directional aspects. In his data analysis Zagers,[6] as a first approach, used the directional component of the signal to estimate the pre-receptor absorbers, and parameters for the optical quality of the receptor layer.

The purpose of the present study was to propose and test a model that fully explains both the spectral and directional aspects of the reflection of the human fovea, i.e. the directional cone reflection and the non-directional background reflection. The model generates quantitative information about reflectors and absorbers. In addition, the dependence on age of these parameters was studied. A validation of the estimates of macular pigment density was obtained with three other methods in the same subjects.

Theory

Optical Stiles-Crawford effect in the pupil plane.

The angular reflection, $R_{(x)}$, from an illuminated spot at the fovea shows up in the pupil plane as a Gaussian shaped spatial intensity distribution (the directional component with amplitude A) on a pedestal of background light (the non-directional component B).[2,7,8]

$$R(x) = B + A \times 10^{-\rho(x-x_0)^2} \qquad (1)$$

with ρ the directionality, and x the horizontal location in millimeters in the pupil plane relative to the center of the pupil. The peak of the optical Stiles-Crawford effect is generally not exactly at the center of the pupil, the difference is x_0. Measured curves are cutoff by the edges of the (generally dilated) pupil (Fig.1).

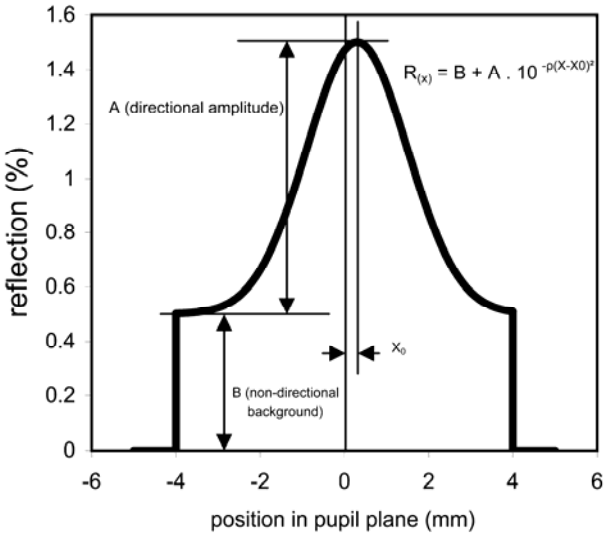

Fig. 1. Directional and non directional light measured across the (8 mm) pupil of the eye (artificial data). The directional part, the optical Stiles-Crawford effect, has a Gaussian shape. It sits on a pedestal of non-directional background light.

Spectral behavior of directionality ρ.

The directionality ρ of the Gaussian varies with wavelength.[9-11]

$$\rho(\lambda) = \rho_{wg} + \rho_{scatt} \times (550/\lambda)^2 \qquad (2)$$

with ρ_{wg} a waveguide component of the receptors itself, constant over wavelength, ρ_{scatt} a scalar preceding a scatter component which varies with wavelength due to interference effects originating in small differences in receptor length, and λ the wavelength in nm (Fig. 2; the data are described in the Results Section). The equation stems from Marcos et al.,[9] but it was slightly modified by the normalization at 550 nm, to enable easy comparison of the contributions of ρ_{wg} and ρ_{scatt}.

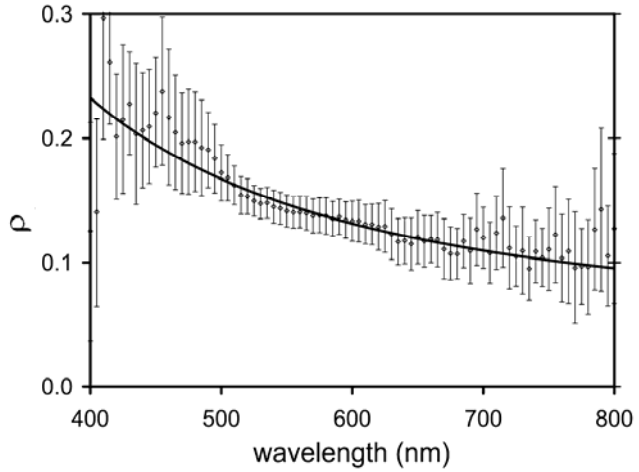

Fig. 2. The directionality ρ as a function of wavelength. Data points are the mean of the young group (cf Methods Section); error bars are the mean standard errors per subject.

Origin of the directional component.

The origin of the directional reflection lies either in the discs of the cone-receptors[5] or in a single layer at the end of the outer segments.[12] Experiments with the visual pigments in a bleached condition cannot discriminate between these two options. In line with an earlier interpretation[5] we consider the discs as the source of the directional reflection. The reflection from the layers posterior to the receptor layer is non-directional. This also holds for the light from posterior layers returning through the photoreceptors. We elaborate on this, because this is an important aspect. The principle is illustrated in Fig. 3. First assume at the bottom a perfectly white and diffuse scattering Lambertian reflector. A device measuring reflection, with illumination along the path of the detector, gives identical readings at all angles. A refracting element in the form of a lens or a photoreceptor positioned between the detector and the reflecting surface yields the same readings. It bends the incoming light rays to a smaller or wider distribution, but it finally hits the same Lambertian surface. Reciprocity theory states that the reflected rays take the same paths on their way back.

Similar results will be obtained replacing the white surface with a milky tissue with diffuse multiple scattering. All incoming light eventually enters the milky tissue, leading to a three dimensional cloud of light. This cloud of light forms a new source of illumination, as if the tissue was illuminated from the back. Any effort to concentrate this light at the far distance into a spot, with a lens or a photoreceptor will not work. This is nicely illustrated when looking at a white computer screen through a lens: The lens surface shows the same brightness as the screen just outside the lens.

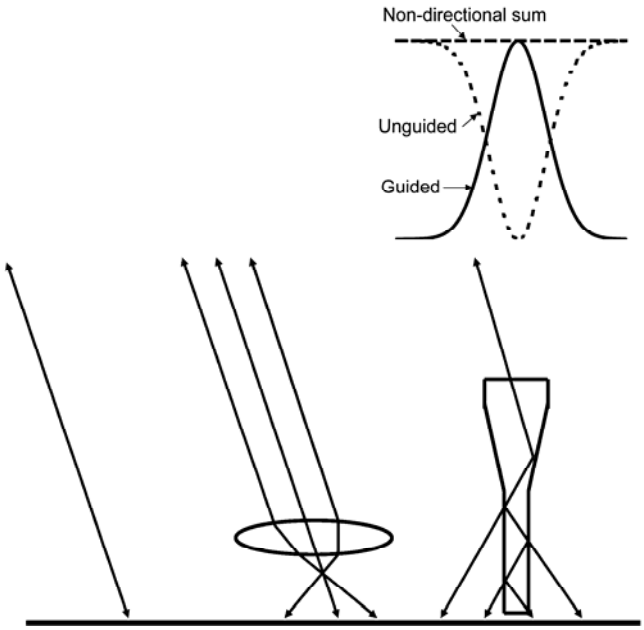

Fig. 3 Different refractive elements in front of a diffusely scattering Lambertian surface, all leading to non-directional behavior. At the left, a measuring device is looking directly at the surface (only one angle shown). At the center, light is bended through a lens. At the right, light is guided through, and escaping from a bleached cone receptor. The pathways to the surface are similar on the way back. Above the cone receptor the intensity distribution at the some distance (pupil plane in the eye) is shown, with the fraction guided through the receptor, the unguided fraction escaping the receptor, and the sum of both; forming again a non-directional background.

Apart from embedded absorbers like blood and melanin, the similarity between the choroid and the milky tissue is evident. Van de Kraats *et al.*[5] described an experiment with an illuminated annulus around the measuring area to feed a cloud of light in the choroid. The reflected light from the central, non illuminated part, showed heavy absorption because of blood and melanin, but no directionality. Similarly, using the fluorescence of lipofuscin in the pigment epithelium as a new source of light located behind the receptors, no directional light was found.[12-15] This does not mean that light is not taking the path through the (in this case bleached) photoreceptors on its way back (recaptured light).[12] It only means that directional reflected light guided through the photo receptors outer segments, is perfectly complemented with light through the same pathways as the light escaping the outer segments on entering the cones from the direction of the pupil (Fig. 3). In conclusion, any directional light must originate from reflections in the cones itself, and not from light that had also reached the layers behind it.

Cone capture area.

From (optical) antenna theory[16] it follows that the capture area of a cone, A_R, is not purely determined by its physical dimensions.

$$A_R \approx \lambda^2 / \Omega_R \qquad (3)$$

with λ the wavelength, and Ω_R the aperture of the directional beam in radians. A realistic directionality of the optical SCE of $\rho = 0.15$ at 550 nm as used in Fig. 1 shows a width at half maximum in the pupil plane w_p of 2.8 mm. With the focal length of the eye F_{eye} of 16.68 mm, Ω_R is calculated as

$$\Omega_R = \pi/4 \times (w_p / F_{eye})^2 = 0.00221 sr \qquad (4)$$

For 550 nm this gives an A_R of 13.7 μm^2. This converts to the diameter of a circular capture area of 4.2 μm, much larger than the cone diameters of about 2 to 3 μm in the central retina.[17] Estimations using waveguide theory also give a significantly higher effective capture area compared to the physical frontal area of a cone.[18] We therefore assumed that for light entering the cones perpendicularly, no light enters the cone interspaces. For oblique angles, light escapes from the cone outer segment into the interspaces, according to the generally accepted explanation of the Stiles-Crawford effect.[19] Energy distributions calculated in rods showed almost identical behavior for wavelengths of 475, 505 and 714 nm.[20] On this basis we also assumed that, again for the perpendicular case, the light captured by the foveal cones is constant over wavelength. In the bleached condition it passes the cones outer segments into the deeper layers. Due to the reciprocity principle a large part of the light reflected from the deeper layers must be recaptured by the cones.

Model

Overview.

An earlier version of the model with an extensive discussion was published by van de Kraats et al.[5] The main deviations concern different templates for the eye media, the regaining of scattered light in the non-directional condition, a wavelength dependent reflection from the cones, and the use of a tapered blood layer thickness. A schematic view of the model is given in Fig. 4. With the directional reflection originating from the cone receptors, only absorbers in front of the cones, i.e. lens and macular pigment, can leave their spectral fingerprint on it.[5,21] The non-directional amplitude is more complex, as it is in addition influenced by absorption in blood and melanin.[3] The different nature of directional and non-directional light provides a key to separate the components, and to improve the quantitative estimates of the different absorbers. In the anterior eye light is absorbed by the media. The first (non-directional) reflection occurs in front of the receptor layer, at the Internal Limiting Membrane (ILM). Reflections at the cornea, and at the anterior and posterior lens surfaces were ignored because of the separation of illumination- and detection beams by the instrument. Next, the important directional reflection takes place at the stack of discs in the cone outer segments, with in front absorption in the macular pigment. A further non-directional reflection occurs at the retinal pigment epithelium. Finally, light is reflected at the choroid, with absorption in blood and melanin. Probably, only a small fraction of the light ever reaches the sclera. To avoid complex formulas, losses at reflecting layers of a few percent were ignored in the calculation of posterior layers. Visual pigments were supposed to be fully bleached.

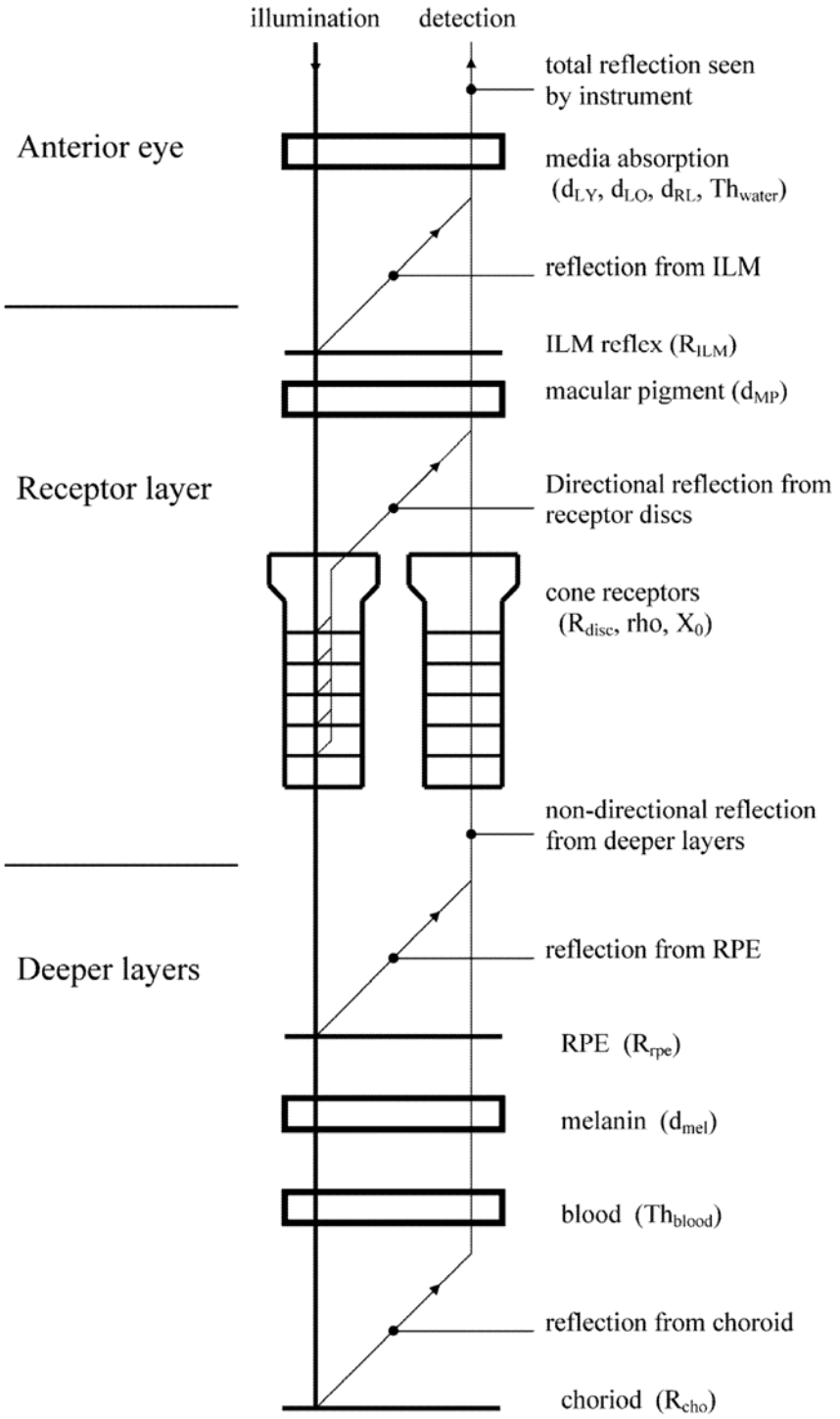

Fig. 4 Model of the reflection of the fovea. For didactical reasons, separate pathways were drawn for light entering the eye and for reflected light. Light enters the eye at the left (thick line, illumination) and meets several layers of tissues in the anterior eye, the receptor layer, and the deeper layers posterior to the retina. Absorbing layers are shown as boxes, reflecting layers as horizontal lines. Reflection takes places at four layers, and is symbolized by lines angled at 45 degrees, continuing as the thin line at the right going upwards to the detector. The only source of directional reflection seen by the instrument is from the cone discs, all others are non-directional. Abbreviations are explained in the remainder of this Section.

Absorbers in both directional and non-directional component.

The transmission of the various absorbing layers was described by their optical density (Fig. 5). In general

$$T = 10^{-dens} \tag{5}$$

The density of the media is given in our recent model.[22]

$$D_{meddir}(\lambda) = d_{RL} \times M_{RL}(\lambda) + d_{LY} \times M_{LY}(\lambda) + d_{LO} \times M_{LO}(\lambda) + 24 \times M_{water}(\lambda) \tag{6}$$

Briefly, $M_{RL}(\lambda)$ is a spectral template for losses in Rayleigh scatter in the cornea, humors, and lens, $M_{LY}(\lambda)$ a template for losses in the young lens, and $M_{LO}(\lambda)$ for losses in the aging lens. The parameters d_{RL}, d_{LY}, and d_{LO} derived from fitting the measured data to the model, were the age dependent densities at 400 nm. A term $d_{neutral}$ for a neutral density of the media to provide for some losses due to scatter by relative large scattering particles was ignored. $M_{water}(\lambda)$ is the density of 1 mm water; we used a fixed total thickness of water of 24 mm.[23]

For the case of non-directional reflected light we defined $D_{medNdir}(\lambda)$, almost similar to the one above, but with d_{RL} set to zero. The rationale is that although the light that is scattered in the media outside the measuring area on the retina is lost for the local directional reflection, it still contributes to the "cloud of light" in the choroidal space (see Theory Section). This, rather unexpected assumption of regaining scattered light was tested with nearly noiseless mean data from a young and old group (Result Section).

The transmission of the macular pigment was described by

$$D_{MP}(\lambda) = d_{MP} \times M_{MP}(\lambda) \tag{7}$$

We used an empirical description by Walraven (private communication), normalized to 1 at 460 nm. Thus parameter d_{mp} is the density of macular pigment at 460 nm, with

$$\begin{aligned} M_{MP}(\lambda) = (1/0.35) \times (&0.32 \times \exp\left[-0.0012(436-\lambda)^2\right] + \\ &0.32 \times \exp\left[-0.0012(480-\lambda)^2\right] - \\ &0.123 \times \exp\left[-0.0012(458-\lambda)^2\right] + \\ &0.12042 \times \exp\left[-0.006(457-\lambda)^2\right]) \end{aligned} \tag{8}$$

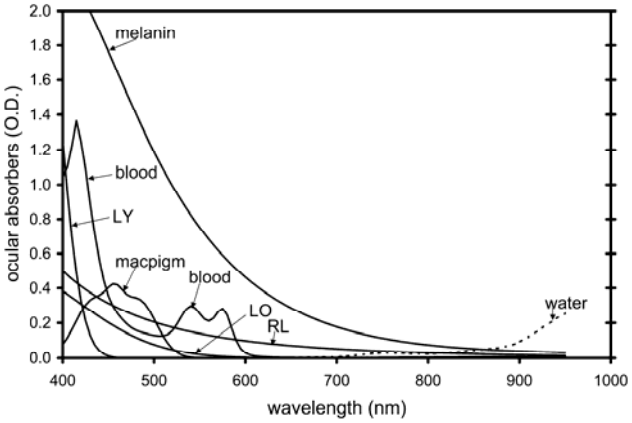

Fig. 5 Absorbers as appearing in the eye, displayed with the mean densities for our group of subjects. The absorbers in the eye media are LY (lens young), LO (lens old), RL (Rayleigh scatter losses), and above 800 nm water. In the retina, macular pigment absorbs from 400 to 520 nm. In the deeper layers, posterior to the retina light is absorbed by melanin and blood.

Directional component.

The optical Stiles-Crawford effect was described by a Gaussian shape in the pupil plane

$$SCE(x) = 10^{-\rho(x-x_0)^2} \qquad (9)$$

with ρ the directionality, and x the horizontal position relative to the entrance beam in the pupil plane of the instrument. Due to the alignment procedure (cf. Methods), the maximum of the OSCE at x_0 was always close to zero. Note first, that we did not use a reference position relative to the center of the pupil as in the general form in Eq. 1. Note too, that Eq. (1) also describes the non-directional component.
$R_{disc}(\lambda)$, the directionally reflected light originating from the cone discs, was assumed to decrease with wavelength as

$$R_{disc}(\lambda) = R_{disc} \times (550/\lambda)^2 \qquad (10)$$

with R_{disc} the summed reflectivity of the stack of outer segment discs. This assumption deviates from an earlier description[5] for reasons addressed in the Discussion.

At the level of the receptor layer, the directional reflection becomes

$$R_{recep}(\lambda, x) = SCE(x) \times R_{disc}(\lambda) \qquad (11)$$

At the level of the cornea, the directional component in both the spectral plane and in the pupil plane can be described by

$$R_{dir}(\lambda, x) = (10^{-2(D_{meddir}(\lambda)+D_{mp}(\lambda))}) \times R_{recep}(\lambda, x) \qquad (12)$$

Non-directional component.

The non-directional component is easiest considered from the choroidal space. The back scattering of light in the choroidal tissues was taken as a neutral reflection $R_{choroid}$. Light in the choroidal space is absorbed by blood and melanin.
We defined the density of a layer of 95% oxygenated blood with a thickness of 100 μm as $D_{blood\_100\mu m}(\lambda)$.[24] To account for the variety of path lengths through the center and periphery of small and large blood vessels, we assumed a wedge shaped blood layer, with path lengths from zero to 100 μm. The template for a wedge shaped layer of blood of 1μm can be calculated as

$$M_{blood}(\lambda) = -0.01 \times \log\{[1 - 10^{-D_{blood\text{-}100um}(\lambda)}]/[D_{blood\text{-}100um}(\lambda) \times \ln(10)]\} \quad (13)$$

The density of a layer of blood with a thickness Th_{blood} in μm is

$$D_{blood}(\lambda) = Th_{blood} \times M_{blood}(\lambda) \quad (14)$$

For the transmission through a uniform layer of melanin we took the spectral data of Gabel,[25] approximated by

$$M_{mel}(\lambda) = 2.45 \times (0.007 + 0.165 \times \exp(-\lambda \times 0.0055) + 113 \times \exp(-\lambda \times 0.011) - 4300 \times \exp(-\lambda \times 0.022)) \quad (15)$$

The term 2.45 served to normalize the function to 1 at 500 nm, so that D_{mel} is the parameter for the density of melanin at 500 nm. The density of melanin becomes

$$D_{mel}(\lambda) = d_{mel} \times M_{mel}(\lambda) \quad (16)$$

Reflection from the deeper layers at the level of the receptor layer is than described by

$$R_{deep}(\lambda) = R_{rpe} + R_{choroid} \times 10^{-2 \times (D_{blood}(\lambda) + D_{mel}(\lambda))} \quad (17)$$

with R_{rpe} the parameter for a neutral reflection at the RPE.

The complete description of the non-directional reflection is

$$R_{nondir}(\lambda) = 10^{-2 \times D_{medNdir}(\lambda)} \times (R_{ILM} + 10^{-2 \times D_{mp}(\lambda)} \times R_{deep}(\lambda)) \quad (18)$$

where R_{ilm} represents a parameter for a neutral reflection at the ILM, and $D_{medNdir}(\lambda)$ is the special case for the density of the media without Rayleigh scatter losses, as explained earlier in the Absorbers paragraph of this Model Section.

Complete model.

At the level of the cornea the total reflection is the addition of the directional component (Eq. 12) and the above calculated non directional component (Eq. 18).

$$R_{total}(\lambda, x) = R_{dir}(\lambda, x) + R_{nondir}(\lambda) \quad (19)$$

The total number of parameters in the model is 13. In a single measurement there are about 4500 free parameters (90 at 5 nm intervals in the spectral range from 400 - 950nm × 50 at 0.1 mm interval in the pupil range; cf Methods Section), but these are of course not completely independent.

Methods

Instrument

The instrument described by Zagers et al.[6] was redesigned into a desktop version that could be aligned with a joystick. In addition, the spectral range was extended to 400-950 nm and the switching mirrors were replaced by beamsplitters, enabling observation of both pupil and retina during measurements. A halogen lamp L (12V 30 W, Wotan 64260, Osram, München, Germany) illuminated a spot of 1.8 degree diameter on the fovea (Fig. 6). The light was spectrally filtered by F (6mm BG26 Schott AG, Mainz, Germany; 1 mm Schott UG3; Unaxis TL60, Linos Goettingen, Germany) for the comfort of the subject and to prevent overloading the sensitive CCD camera (KX85 Apogee Instruments, Inc. Auburn USA) that served as the detector. The intensity of the spot was 6.42 log Td; calculations showed that it could be viewed safely for 15 minutes.[26] The filament of the halogen lamp was imaged in the pupil plane of the eye where it defined the 2.6 × 1.3 mm entrance pupil. With a separation of 0.7 mm below this entrance pupil, a slit shaped exit pupil S of 15 × 1 mm formed the input for a prism based imaging spectrometer. The 2D image on the CCD detector had in one dimension the directional information, from the intensity distribution over the slit shaped exit pupil. In the other dimension, it contained the spectral information, as light from each point of the slit was decomposed by the prism. Only light from the central 1.5 degree foveal spot was used for detection. Because of the prism, the image at the CCD with 1300 × 1030 pixels had an a-linear spectral axis. It was transformed by software, using the dispersion calculation, to an intensity normalized and linear reflection image of 250 pixels at 0.1 mm intervals at the pupil axis, and 90 pixels at 5 nm intervals at the spectral axis (400 to 950 nm). Refraction errors were compensated by adjusting a Badal type front lens system (L1 and L2).

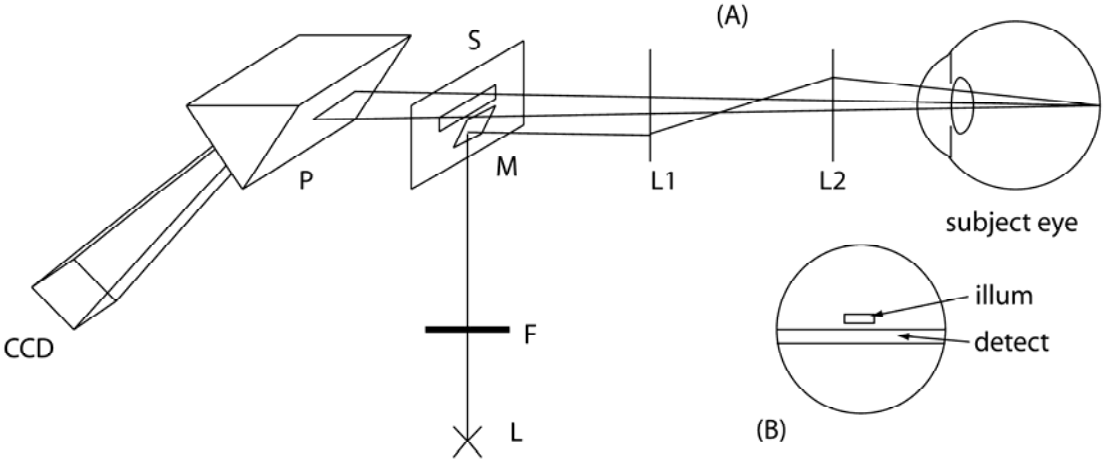

Fig. 6. (A) Simplified view of the instrument. L is a 30 watt halogen lamp. F are filters to attenuate the red part of the spectrum. The lamp illuminates a spot at the fovea of 1.8 degree via the small mirror M, and the front lenses L1 and L2 forming a Badal system. L2 can be moved for focusing the retina. The reflected light from the retina (central 1.5 deg) fills the entire pupil, but only the part remaining after the slit S conjugated to the pupil is drawn. This light is spectrally decomposed by the dispersion prism P and forms a two-dimensional image at the CCD camera. (B) The area in the subject's pupil used for illumination of the fovea, and the slit shaped area used for detection of reflected light from the fovea.

Calibration.

A mercury lamp (90W, type 93136, Philips, Eindhoven, The Netherlands) was used for spectral calibration. The lamp illuminated a white diffuse target at about 3 meter from the instrument, the size corresponding to the 1.5 degree retinal detecting area. A shifting offset applied to the image from the CCD detector in the dispersion calculation could get the mercury lines at their theoretical value with about 1 nm accuracy. Before each measurement session the instrument was calibrated for sensitivity by mounting two different calibration tubes on the front lens. The white reference tube contained at the end a surface painted with white paint (Kodak 6080 White Reflectance Coating, Eastman Kodak Company, Rochester, NY). The Badal front lens system was adjusted for a sharp image. Because the distance of the white surface was at 230 mm from the instruments pupil plane (10 times the focal distance of the eye), the measured white reference image represented a 1 percent reflection from the eye. The instrument stray-light was assessed with a dark reference tube, containing a light trap. The dark reference image was subtracted from the white reference image. As instrument stray-light mainly originates from ghost images in the Badal front lens system, it slightly depends on the refraction adjustment. Therefore, all measured images from the eye were corrected by subtracting the dark image taken at the corresponding refraction adjustment.

Protocol

Group 1. A group of 53 subjects, mean age 51, (range 19 - 75) year, took part in the measurements. In fact, the data were a re-analysis of measurements in our laboratory published elsewhere.[27] The tenets of the Declaration of Helsinki were followed and the local Medical Ethics Committee approved the protocol. Before the experiment started, the nature of the experiment was explained to the subjects and written informed consent was obtained. The pupil of one eye was dilated with one or two drops of tropicamide 0.5%. Subjects were aligned to the instrument, with the entrance beam clearly visible in the anterior eye. Initially, the entrance beam was placed somewhere above the center of the pupil, to allow space for the invisible detecting slit below the entrance beam. A chin rest and temple pads helped maintain the position of the head. The subjects were instructed to fixate the center of the illuminated spot. The front lens was adjusted for a sharp image of the retina at the monitor. Next, the patient leaned back and the dark reference image was taken. Measurements at a rate of about 2 per second were displayed at the computer screen in the form of two cross-sections of the 2D image, the spectral shape at pupil profile position zero, and the pupil profile at 540 nm. The alignment was optimized by searching in the pupil plane for the peak of the optical Stiles-Crawford effect. This process was facilitated by simultaneously displaying (in a different color) the highest profile from the start of the measurements. The optimal horizontal position in the pupil plane was easily found by moving the instrument until the peak position of the Gauss-shaped directional profile fell symmetrically around profile position zero. Profile position zero corresponds to the horizontal center of the entry beam. The optimal vertical position in the pupil plane was found by trial and error using the highest profile trace. During optimizing, the spectral view was watched to keep unwanted reflections from the anterior eye low. These reflections were recognized by their relatively high reflectances near 400 nm.

The optimization procedure took about 2 minutes, enough to bleach the visual pigments to almost 100%. At the optimal position, 5 measurements with an integration time of 1 second each were obtained. If necessary, subjects were readjusted when they drifted away from their optimal position, recognized by a drop in amplitude.
Group 2. We were allowed to analyze data (obtained for other purposes) of a second group of 39 subjects, mean age 47 (range 19 - 71). They were measured with the same instrument and protocol three years after the first group, by a different experimenter.

Pupil limits.

The reflection profile, as seen in the entrance slit of the instrument, is cut off by the pupil of the eye. Left and right limits in these pupil plane positions were determined as follows. First, the data in the spectral range from 500 to 600 nm (where the signal has low noise) were binned to 5 nm yielding 20 profiles. Next, left and right from the central pupil position those data points where the signal dropped to 20% of the central value were taken. From those 20 left and right limits we took the lowest. In the final step, the left and right limits were moved 1 mm to the center and applied to the complete measurement to avoid any interference from the pupil edge

Sub-selection young and old group.

To develop and evaluate the model, two sub selections were made from the group of subjects; a group < 40 years (mean 24), and a group > 50 years (mean 58). From the 5 measurements per subject (see Protocol Section), a further selection was made by only allowing measurements over at least 4 mm, with pupil limits outside the range -2.5, +1.5mm (nasal to temporal), and a minimum of 3 measurements per subject. This gave 45 measurements from 10 subjects for the young group, and 81 measurements from 18 subjects for the old group. To find a template for ρ as a function of wavelength, the pupil profiles at every wavelength (binned to 5 nm) for the young group were analyzed for ρ with the Gaussian model from Eq. 1. The means of the standard deviations within a subject were calculated to provide an indication for the error in the data points. Next, a ‘young measurement’ was calculated by averaging the data points in the young group within the pupil range they had in common in their original measurements; similarly an ‘old measurement’ was calculated.

Fitting the data.

For the pilot explorations with the young and old group data, the Solver in Excel2003 was used to fit the data with the model by minimizing chi-squares. All spectral templates were convoluted with the bandwidth of the spectrometer. For the final analysis of individual measurements with the 2D model, the Levenberg-Marquardt routine[28] was applied. The noise in the data points, used for weighting, was calculated from the square root of the photons counted.
The lower limit of ρ was set to 0.050. This avoided in cases with an almost flat pupil profile, fit results with a large amplitude, very broad Gaussian, instead of a large background and a small amplitude Gaussian of normal width.

Results

Single subject.

To illustrate the spatial profile and the spectral behavior of the directional and the non-directional components, the data from a single measurement of a 20 year old subject are presented in Fig. 7. The amplitudes of the directional component and the non-directional component were estimated by fitting the elevated Gaussian curve from Eq. 1, at each wavelength to the pupil profile. The result at 540 nm is presented in Fig. 7a. The amplitudes versus wavelength are presented in Fig. 7b. The total reflection at the peak of the profile was found by adding the amplitudes of directional component and the non-directional component. Going from left to right both curves show a sharp increase beyond 420 nm where the lens absorption ends (young eye), and a further increases near 500 nm where the absorption from the macular pigment (MP) ends. This effect is stronger in the directional curve than in the non-directional one. The non-directional curve displays an increase near 600 nm where blood no longer absorbs, together with a gradual increase due to increasingly less absorption in melanin. The directional curve lacks these features. Beyond 700 nm the curves show the influence of absorption by water, leading to a strong decline at 900 nm.
The more complex shape of the non-directional component due to the addition of light from the choroid, visible above 580 nm is evident. The dilution of the macular pigment fingerprint near 500 nm, due to pre-retinal reflectors, is also clearly visible. When the directional component becomes low in absolute sense, or low relative to the non-directional component, the estimation of ρ becomes increasingly noisy, visible below 500 and above 600 nm. The noise in ρ also causes noise in the directional and non-directional amplitude. To resolve this, a smooth template for ρ as function of wavelength was derived (see Result Section, ρ template).

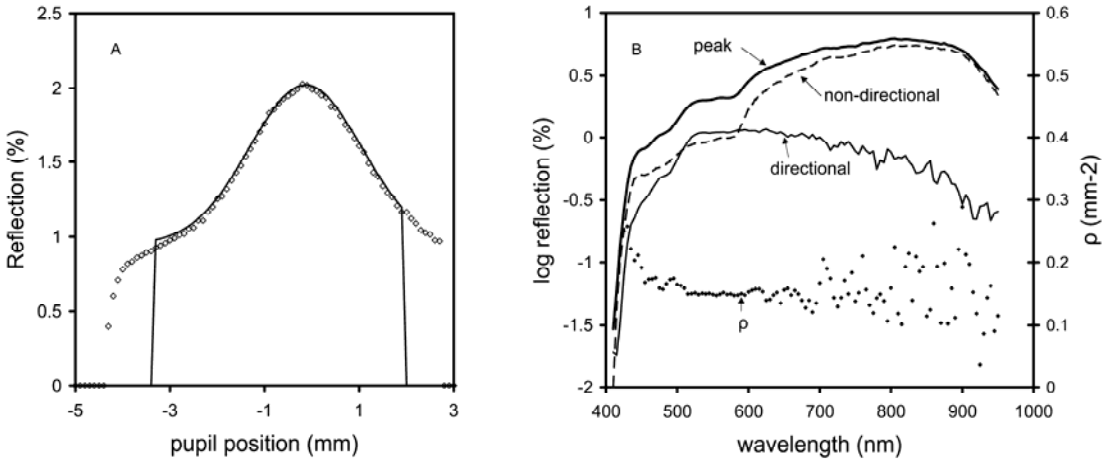

Fig. 7 Analysis of a single measurement using the Gaussian fit from Eq. 1. (a) Data points of the pupil profile at 540 nm (error bars smaller than the symbols), and model curve (solid line). (b) Spectral behavior of the directional reflection from the foveal cones (thin solid curve), the non-directional reflection (dashed curve) from the background, originating from pre- and post-receptor layers, and the sum of both (thick solid line). Continuous curves connecting the data points are presented for clarity. The data points in the lower half of the figure represent ρ (scale on the right). Because of the noisy appearance and to avoid overlap with the amplitude curves, ρ is not plotted below 420 nm. In such a single measurement the decline of ρ with wavelength is not clear, and can deviate from the mean result presented in Fig. 2.

ρ template.

Mean ρ in the young group as a function of wavelength (Fig. 2) was used to find the parameters ρ_{wg} and ρ_{scatt} in equation (2), resulting in.

$$\rho(\lambda) = 0.050 + 0.097 \times (550/\lambda)^2 \qquad (20)$$

A similar analysis of the old group yielded similar results in the spectral range from 500 to 600 nm, but outside this region the result was very noisy due to high density of the aged lens, and the more irregular non-directional component at the longer wavelengths. The error bars in Fig.2 are the means of the standard deviations within a subject. These values were used for weighing the data in the fitting process.
The template from Eq. 20 multiplied with a scalar ρ / (0.050+0.097) forced a smoother behavior of the directional and non-directional amplitude in the analysis of the rest of the paper. If the scalar was one, ρ equaled the mean value of 0.050+0.097 = 0.147, and reflects the value of the directionality at 550 nm.

Test of d_{RL} on mean directional and non-directional spectra for the young and old group.

The almost noiseless mean data from the young and mean old group was used to test the general concept of the spectral model from the Model Section, and in particular the assumption of $d_{RL} = 0$ for the non-directional spectra. With the fixed template for the spectrum of ρ (Eq. 20), data were fit using Eq. 1 to derive the directional and non-directional amplitudes. Results of these analyses are shown as the data points in Fig. 8. Model curves were drawn using the equations from the Model Section. The directional spectra were fitted first, resulting in parameter values for the densities of media, macular pigment and for the reflection of the cone discs. These were used next for the non-directional spectra. As an exception to the Model Section, a very small neutral reflex (fixed at 0.003 % = -2.4 log) at the corneal level was allowed for the directional spectra, to better fit the data near the noise level of the measurements. The media parameters d_{RL} and d_{LY} were fixed to the calculated values according to the mean ages of the groups.[22] Fitting the non-directional background spectra yielded the parameters for the ILM and post-receptor layers. The number of free parameters for the directional data was thus only 3 (d_{LO}, d_{MP}, R_{disc}), and 5 for the non-directional spectral data (d_{mel}, Th_{blood}, R_{ilm}, R_{rpe}, $R_{choroid}$). An almost perfect fit to the data could be obtained (chi^2 young = 17, chi^2 old = 17). With d_{RL} taken from the directional fit, used as fixed parameters for the fitting of the non-directional spectra, yielded chi^2 values that were more than an order of magnitude higher (chi^2 young = 244, chi^2 old = 257). The two step fit strategy of first fitting the media and macular pigment parameters with the directional component, and next fitting the parameters for the deeper layers, was only applied in this section for didactical reasons. In the rest of the paper all free parameters were fitted simultaneously.

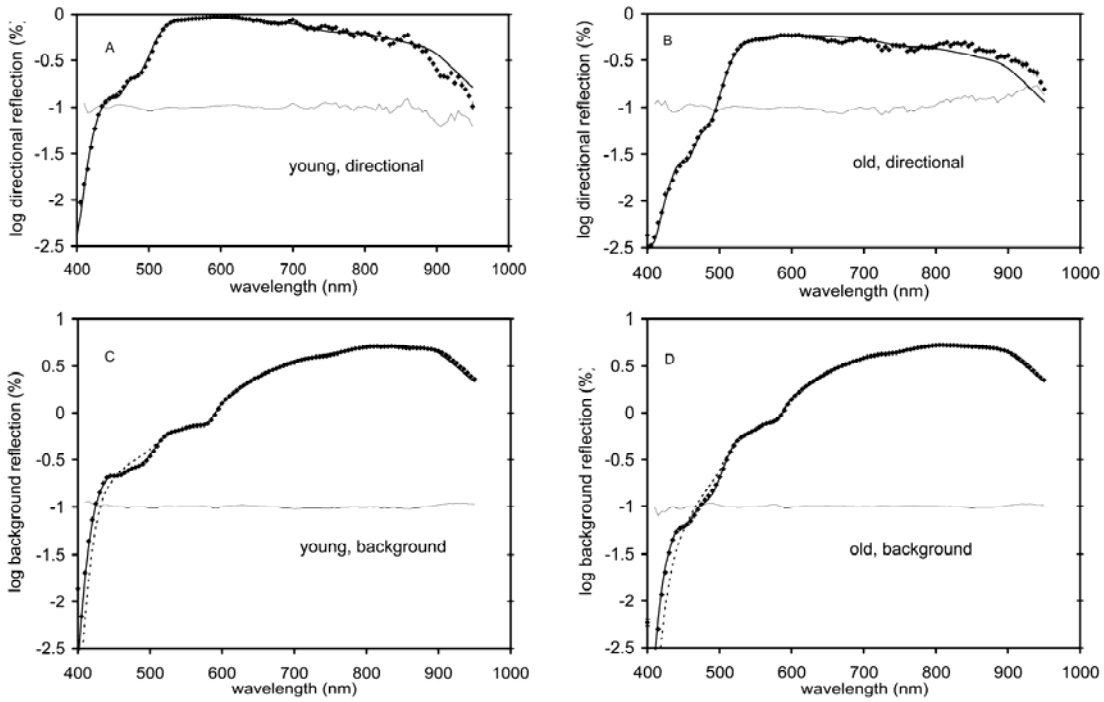

Fig. 8 Mean (log) reflection as a function of wavelength for the young (left) and old (right) group. The upper panels show the directional reflection from the cones, the lower panels the non-directional background reflection from layers anterior and posterior to the receptor layer. The data points have error bars with the mean standard deviation, but most are smaller than the symbols. The model curve (thick line) almost exactly replicates the data points. The residue, the difference between the data points and the model is shown as a thin line. It was shifted downwards 1 log unit for easy viewing. In the lower panels, the fit with the RL media component set to the same value as found in the directional fitting is shown for comparison (dotted line, no residue shown).

Age effects.

Next, the model was applied to the individual measurements allowing the study of age effects in the parameters. In total 265 measurements from 53 subjects were analyzed. At first all 13 parameters were allowed to vary, except water (fixed to 24 mm). The media parameters d_{LY} and d_{RL} showed no correlation with age, and were therefore set to the calculated values for a mean age of 40.[22] The directionality ρ also showing no correlation with age was set to the mean ρ of 0.147 found earlier (see Result Section, ρ template). This left 9 free parameters to fit at once. The mean results are summarized in Table 1. Parameters with a significant age trend ($p < 0.05$) were plotted versus age squared in Fig. 9. Age squared was used because it consistently yielded smaller chi^2 than a linear fit.[22] Reproducibility (Repro in the last column of Table 1) was defined as the average coefficient of variation (100 × standard deviation in the five measurements per subject / mean parameter value).

As check on the consistency of the mean parameters a second group of subjects (cf. Methods) was similarly analyzed. Their results are also presented in Table 1. None of the mean parameters were significantly different from those of group 1, except the age dependent parameters dLO and Rdisc. The latter differences are easily explained by the difference in the mean ages of the groups.

Tabel 1 Mean parameters for group 1 and group 2.

	group 1 (mean age 51)			group 2 (mean age 47)		
parameter	value	p-value for age effect	Repro (%) [b]	value	p-value for age effect	Repro (%) [b]
Th_{water} (mm)	24	fixed		24	fixed	
d_{LY}	1.260	fixed		1.260	fixed	
d_{LO}	0.383	**<0.001** [a]	4	0.295	**<0.001** [a]	8
d_{RL}	0.500	fixed		0.500	fixed	
R_{ilm} (%)	0.093	**0.0023** [a]	24	0.100	0.3319	26
d_{mp}	0.425	0.1691	6	0.477	0.0702	7
R_{disc} (%)	1.896	**<0.001** [a]	6	2.175	**<0.001** [a]	9
ρ (mm^{-2})	0.147	fixed		0.147	fixed	
d_{mel}	1.194	0.4781	1	1.213	0.1360	1
Th_{blood} (μm)	54.502	**<0.001** [a]	5	58.801	**0.0063**	6
R_{rpe} (%)	0.536	0.2419	5	0.534	0.5383	6
$R_{choroid}$ (%)	7.843	0.0662	2	8.089	0.3975	3
X_0 (mm)	-0.052		-200	-0.060		-246

[a] Significant p-values ($p < 0.05$) are printed in bold.
[b] The 5 measurements for each subject were used to calculate the standard deviation in the parameters as a measure for reproducibility. The mean of the reproducibility for the whole group as a percentage of the parameter value is given in the column Repro.

The mean covariances between parameters of all the individual measurements were calculated from the covariances provided by the fit routine. The three highest for group 1 were also the three highest for group 2 and showed almost similar. In the following results, group 2 results are in parenthesis. The mean covariance between choroidal reflection and melanin was: 0.67 (0.68), between ILM reflection and lens old: 0.59 (0.61), and between the ILM reflection and macular pigment density: 0.51 (0.53). Thus, in general all covariances stayed at acceptably low values.

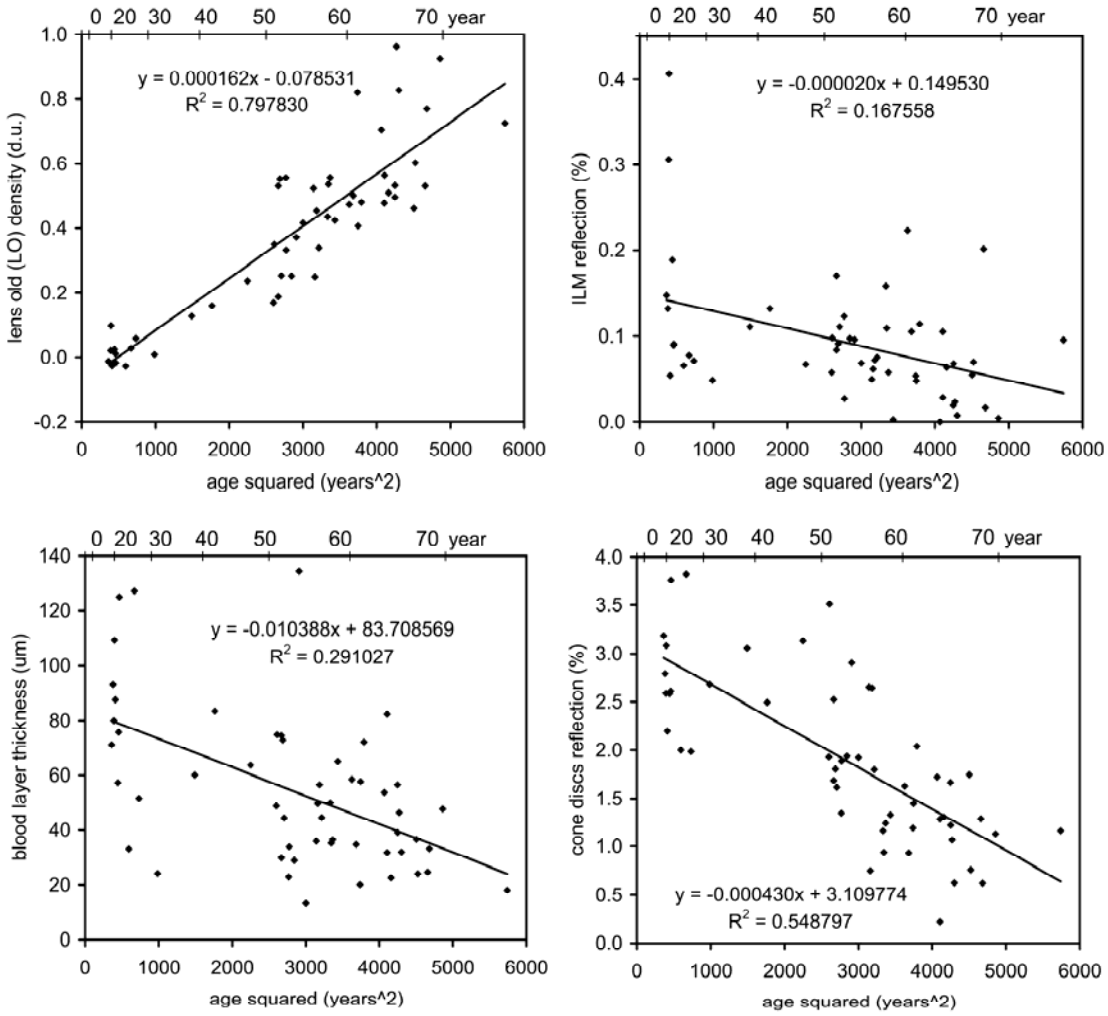

Fig. 9. Age trends for the parameters lens old, ILM reflection, blood layer thickness, and cone discs reflection.

Discussion

General

We developed a model for fundus reflection that for the first time simultaneously describes the spectra of the directional and non-directional reflection of the human fovea. The excellent fits support the assumption that the deeper layers generate no directional component. Van de Kraats et al.[5] already gave experimental and theoretical evidence, and it was also confirmed by Burns *et al*.[14] using the autofluorescence of lipofuscin. As the fluorescence is by nature omnidirectional, it formed a new source of light behind the receptor layer, undisturbed by preretinal reflections. We found that a large part of the light from deeper layers must be recaptured by the cones due to the reciprocity principle (Section Theory, cone capture area). An, at first glance, surprising aspect of the model is that Rayleigh scatter losses in the eye media only show up in the directional pathway. This will be discussed in the next paragraph.

Absorbers

Media

In the initial analysis of the complete group of subjects the lens young component d_{LY} and the Rayleigh scatter component d_{RL} were free parameters. In a pilot analysis they showed no significant age dependency and were therefore, in a second analysis, fixed to an age of 40 years.[22] This prevented exchange with other parameters. Especially at older age when d_{LO} increases substantially, the reflection near 400 nm is so low that it reaches the noise level of the instrument, causing the estimation of d_{LY} to become questionable. An error in d_{LY} may also convey to other parameters. The decrease with age of the lens young component as shown by Zagers probably was contaminated by this effect.[21] Going from 20 to 60 years the density for the total media at 420 nm in the Zagers study increased by 0.12 log units. Our data show a change of 0.43 at 420 nm. This suggests that Zagers increase in age of the lens old component was compensated by a too large decrease of the lens young component.
The mean value of 0.5 at the age of 40 for the Rayleigh scatter component d_{RL} we used stem from a literature study.[22] The significant improvement of the fits by using this d_{RL} of 0.5 in the directional reflection, but setting it to zero in the non-directional one, was surprising. A possible explanation is that the light scattered outside the directly illuminated spot, is regained in the deeper layers. Van den Berg *et al*.[29] presented optical scatter losses in the cornea, but in fact they included the humors as well. Their magnitude of the Rayleigh scatter losses for a 1 degree field can be calculated as 0.34. Estimates of losses of light scattered outside a retinal field of 1 degree for the relatively young eye from Vos et al.[30] result in a density of only 0.03 for the complete media. Perhaps a part of our Rayleigh scatter value of 0.5 originates from additional scatter losses in the retina itself. Such a scatter source in front of the receptors would partly destroy the directional component from the cones and convert it to a non-directional one.

Macular pigment

The macular pigment optical density in our group of subjects was analyzed before with two previous models, and compared with densities obtained with heterochromatic flickerphotometry (HFP), scanning laser ophthalmoscope (SLO)

reflectance difference at 488 and 514 nm, and SLO autofluorescence.[27] Analysis of the data with the 1996 version of the fundus reflection model[5] resulted in 0.42, comparing very well with the current 0.43. A simple model containing only the directional component[21] yielded 0.52, being too high because of the earlier mentioned interaction with the Zagers lens templates.[21] Comparing the absolute numbers with results from other instruments (Table 2) is more difficult because of the strong effect of the retinal area under test (here 1.5 degree). Surprisingly, the present and 1996 models yield the highest densities despite the use of a larger field. This is probably because the models compensate for all disturbing factors, like the diluting effect from light reflected at the ILM. The necessity for a good model is seen in Fig. 7b were the macular pigment fingerprint is unmistakably higher in the directional component compared to that of the non-directional component. The latter clearly shows the diluting influence of the ILM reflection. The SLO reflection method was lacking such a compensation. More difficult to understand is the low value for the SLO autofluorescence technique, because here dilution by preretinal reflections are not expected.
The covariance of 0.51 between the ILM reflection and macular pigment density and the well founded value of the latter probably just means a low exchange.

Tabel 2 Macular pigment density using different methods.

method	field size (degree)	d_{MP}	Correlation with current
current	1.5	0.43	1
Kraats 1996	1.5	0.42	0.97
Zagers 2004	1.5	0.52	0.88
SLO reflectance	0.5	0.32	0.68
SLO auto fluor.	0.5	0.32	0.60
HFP	1	0.30	0.55

We repeated the calculation of the Pearson bivariate correlations between the current model results, previous models, and the other techniques (Table 2). All correlations were highly significant ($p<0.001$). The d_{MP} parameter showed no significant change with age, like in most other studies.[27,31,32], with the notable exception of a recent study including over 800 subjects reported by Nolan et al. using HFP that showed a surprising decrease of 0.17 from 20 to 60 years.[33]

Blood

For the absorption in blood we used a template calculated for a wedge-shaped layer of blood. This is a more realistic model of the blood layer, because it contains a large range of path lengths through the blood layer instead of always the same length as with a homogeneous layer thickness. The result is that the large dynamic range in the transmissions over the whole spectrum in the case of a homogeneous layer thickness is compressed, yet without adding more parameters to the model.[3,34] Th_{blood} declines significantly with age, probably due to the accumulation of basal laminar deposits on the choriocapillaries and Bruchs membrane,[35-37] screening the choriocapillaris. Measurements of choroidal blood volume with a laser Doppler flow technique also shows a decrease of about 45% from 20 to 70 years.[38] Another study using

morphometric analysis showed a 45% decrease in the density and a 34% decrease in the diameter of the lumen of the choriocapillaris from the first to the 10th decade.[39]

Melanin

Melanin was not found to be age dependent. This is a minor contradiction with determinations from young and old donor material based on only the retinal pigment epithelium, decreasing about 37% in the macular area.[40] In analyzing the results of the macular area of only 16 subjects in another study an age relation could not be found.[41] Measured in optical density units, the fraction of the melanin in the RPE is about one-third of the total melanin.[25,42] If two-thirds of the melanin fraction in the choroidal space is constant with age, age dependency is expected to be much lower. While pure melanin is deceasing with age, more complex granules of the type melanolipofuscin and melanolysosomes are increasing by 72%.[40] With their absorption spectrum not very different from pure melanin,[43] discrimination with our reflection technique is not possible, another argument for an almost zero age dependency of melanin. More important is that in the case of using reflection techniques to derive the total melanin content, it better reflects the functionality of melanin for the stray light reduction in the retina. Other techniques based on pure melanin only, are perhaps less important in this respect.

Non directional reflectors

The first, small reflection (approximately 0.1 %) occurs at the ILM. A reflection at the OLM was not incorporated because it cannot be discriminated from the reflection R_{rpe} (0.54 %) located at the receptor layer / retinal pigment layer interface. Although a reflection at Bruchs membrane seems physiologically probable, it would add at least two parameters (R_{bruch} and $D_{RPEmelanin}$) to the deeper layers, like in Delori et al.[3] Without these extra parameters we obtained very good fits. The price to be paid is that the absolute values of d_{mel} and Th_{blood} have limited physiological meaning; trends are relevant however. Reflection of the ILM decreases with age (Fig. 9). This is a well known observation in funduscopy.

Directional reflection

In previous papers we assumed that the origin of the cone directional reflection lied in spectrally neutral Fresnell reflections by small differences in refractive index of the discs and the interstitional fluids.[5,21,44] Although this was supported by measurements of Zagers et al. on pseudophakic subjects,[21] Choi et al.[45] argued that the wavelength range used was too limited to support the conclusion. Other authors[46,47] assumed the integral volume of the Gaussian shape to show spectrally neutral behavior, as is commonly found in diffraction limited processes.[16] Consequently, the peak amplitude should drop with lambda^{-2}. With the current, much extended wavelength range, the peak amplitude was clearly seen to decrease at the longer wavelengths where other absorbers play no role (Figs. 7b and 8). We therefore also opted for lambda^{-2} behavior in the new model. Following Marcos et al.[9,10] the ρ of the wave guiding part of the optical SCE is constant with wavelength. Another scatter component from interference of light from neighboring cones introduces lambda^{-2} behavior, seen in Fig. 2. Summarizing, we have shown that the light intake by the cones on perpendicular entrance is neutral because of the large capture area (Section Theory, cone capture area). The summated reflection from the discs itself still remains a neutral Fresnell reflection. The light escaping the receptor in the backward direction

forms a Gaussian intensity distribution at the pupil plane, with the properties shown in Figs. 1 and 2. The volume however is taken as neutral. Choi et al.[45] stated, on base of three wavelengths (550, 650, and 750 nm), that the guided fraction under the two dimensional optical SCE is neutral with wavelength.[45] Our extensive wavelength data (Fig.10) follow the model curve and clearly show a strong wavelength dependency (note that absorption in the media is cancelled in the calculation), a maximum is at around 525 nm. Such wavelength dependence is obvious because below 525 nm the directional cone signal is reduced by macular pigment, while the ILM part of the non-directional reflection is not. At wavelengths above 580 nm the non-directional reflection from the deeper layers increases because blood and melanin become more and more transparent.

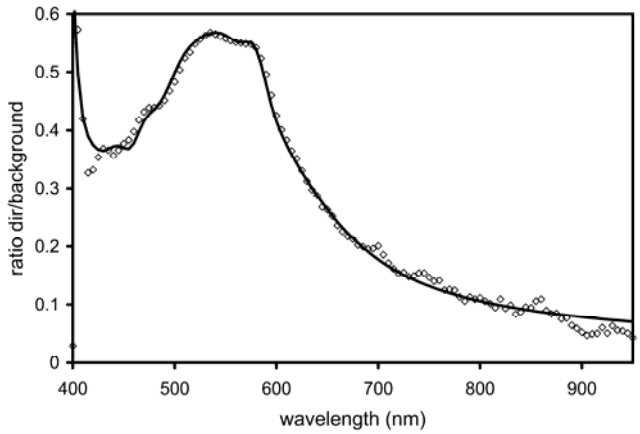

Fig. 10. The directional fraction of the total light reflected from the fovea versus wavelength for the young group. Maximum directionality is around 525 nm. At lower wavelengths the directional cone signal is reduced by macular pigment, while the ILM part of the non-directional reflection is not reduced. At longer wavelengths there is a growing influence from the non-directional reflection from the deeper layers because blood and melanin become more and more transparent.

For the present purpose with bleached visual pigments, R_{disc} might as well be taken as the outer-segment end reflection. That the discs are the origin could only be made plausible by experiments with dark adapting and bleaching of the visual pigments.[5] Fig. 9 shows a large decrease in the disc reflection as a function of age. That the large reflection from the choroid (8 %), and that from the retinal pigment epithelium (0.5 %) have no such a decrease, is a strong argument for the receptors as origin. Because the width of the Gaussian as given by ρ has no age dependency, and there is neither evidence for a large decrease in the number of cones, nor for a large decrease in length of the outer segments,[17,48] we might speculate that the indexes of refraction of the discs, and the interspaces between them, slowly drift towards each other at older age. In diseases like age-related macular degeneration (AMD) R_{disc} might decrease at a faster rate because here the number of cones or the lengths of the outer segments are possibly affected.

Conclusion

A new model gives fundamental insight in how the directional and non-directional spectral reflection from the fovea are related to each other. Previous attempts were less successful because the transmission in the eye media was taken equal in both components. Setting the Rayleigh scatter to zero in the non-directional reflection case caused a dramatic improvement of the model fit.
The model generates quantitative estimates of several important optical absorbers in the eye as macular pigment, lens density, blood and melanin, as well as parameters related to the optical quality of the cones, the cone disc reflection and ρ. In addition, it estimates the reflection from the retinal pigment epithelium, and the choroid. A validation of the macular pigment optical density was obtained by the significant correlations obtained with independent estimates. Parameter values in a second group measured 3 years later by another experimenter agreed very well with values found in the first group.

Acknowledgement.

The authors are indebted to dr Tos Berendschot, Martijn Kanis, and Robert Wisse for allowance to use their data.

References

1. D. van Norren and L. F. Tiemeijer, "Spectral reflectance of the human eye," Vision Res. **26**, 313-320 (1986).

2. G. J. van Blokland and D. van Norren, "Intensity and polarization of light scattered at small angles from the human fovea," Vision Res. **26**, 485-494 (1986).

3. F. C. Delori and K. P. Pflibsen, "Spectral reflectance of the human ocular fundus," Appl. Opt. **28**, 1061-1077 (1989).

4. D. van Norren and J. van de Kraats, "Retinal densitometer with the size of a fundus camera," Vision Res. **29**, 369-374 (1989).

5. J. van de Kraats, T. T. J. M. Berendschot, and D. van Norren, "The pathways of light measured in fundus reflectometry," Vision Res. **36**, 2229-2247 (1996).

6. N. P. A. Zagers, J. van de Kraats, T. T. J. M. Berendschot, and D. van Norren, "Simultaneous measurement of foveal spectral reflectance and cone-photoreceptor directionality," Appl. Opt. **41**, 4686-4696 (2002).

7. J. Krauskopf, "Some experiments with a photoelectric ophthalmoscope," in *Excerpta Medica, International Congress Series,* M. A. Bouman and J. J. Vos, eds., (Excerpta Medica, Amsterdam, 1965), pp. 171-181.

8. R. A. Applegate and V. Lakshminarayanan, "Parametric representation of Stiles-Crawford functions: normal variation of peak location and directionality," J Opt. Soc Am A **10**, 1611-1623 (1993).

9. S. Marcos, S. A. Burns, and J. C. He, "Model for cone directionality reflectometric measurements based on scattering," J. Opt. Soc. Am. A **15**, 2012-2022 (1998).

10. S. Marcos and S. A. Burns, "Cone spacing and waveguide properties from cone directionality measurements," J. Opt. Soc. Am. A **16**, 995-1004 (1999).

11. N. P. A. Zagers, T. T. J. M. Berendschot, and D. van Norren, "Wavelength dependence of reflectometric cone photoreceptor directionality," J. Opt. Soc. Am. A Opt. Image Sci. Vis. **20**, 18-23 (2003).

12. S. A. Burns, J. C. He, and F. C. Delori, "Do the cones see light scattered from the deep retinal layers," in *Vision Science and Its Applications, OSA Technical Digest Series,* (Optical Society of America, Washington D.C., 1997), pp. 94-97.

13. P. M. Prieto, J. S. McLellan, and S. A. Burns, "Investigating the light absorption in a single pass through the photoreceptor layer by means of the lipofuscin fluorescence," Vision Res. **45**, 1957-1965 (2005).

14. S. A. Burns, F. C. Delori, and J. C. He, "Back-illuminating the cones: Is the light from the RPE guided?," Invest. Ophthalmol. Vis. Sci. **38**, 57 (1997).

15. F. C. Delori, D. G. Goger, B. R. Hammond, D. M. Snodderly, and S. A. Burns, "Foveal lipofuscin and macular pigment," Invest. Ophthalmol. Vis. Sci. **38**, 1657 (1997).

16. A. E. Siegman, "The antenna properties of optical heterodyne receivers," Applied Optics **5**, 1588-1594 (1966).

17. C. A. Curcio, K. R. Sloan, R. E. Kalina, and A. E. Hendrickson, "Human photoreceptor topography," J. Comp. Neurol. **292**, 497-523 (1990).

18. A. W. Snyder and M. Hamer, "The light-capture area of a photoreceptor," Vision Res. **12**, 1749-1753 (1972).

19. W. S. Stiles and B. H. Crawford, "The luminous efficiency of rays entering the eye pupil at different points," Proc. R. Soc. Lond. [Biol]. **112**, 428-450 (1933).

20. M. J. Piket-May, A. Taflove, and J. B. Troy, "Electrodynamics of visible-light interactions with the vertebrate retinal rod," Optic Lett. **18**, 568-570 (1993).

21. N. P. A. Zagers and D. van Norren, "Absorption of the eye lens and macular pigment derived from the reflectance of cone photoreceptors," J. Opt. Soc. Am. A **21**, 2257-2268 (2004).

22. J. van de Kraats and van Norren D., "Optical density of the aging human ocular media in the visible and the UV (in press)," J Opt. Soc Am A (2007).

23. R. C. Smith and K. S. Baker, "Optical properties of the clearest natural waters," Appl. Opt. **20**, 177-184 (1981).

24. O. W. van Assendelft, *Spectroscopy of hemoglobin derivatives*, C. C. Thomas, ed., (C.C. Thomas, Springfield, IL, 1970).

25. V. P. Gabel, R. Birngruber, and F. Hillenkamp, "Visible and near infrared light absorption in pigment epithelium and choroid," in *Excerpta Medica, International Congress Series,* K. Shimizu and J. A. Oosterhuis, eds., (Elsevier, Amsterdam, 1978), pp. 658-662.

26. "Guidelines on limits of exposure to broad-band incoherent optical radiation (0.38 to 3 microM). International Commission on Non-Ionizing Radiation Protection," Health Phys. **73**, 539-554 (1997).

27. T. T. J. M. Berendschot and D. van Norren, "On the age dependency of the macular pigment optical density," Exp. Eye Res. **81**, 602-609 (2005).

28. W. H. Press, B. P. Flannery, S. A. Teukolsky, and W. T. Vetterling, *Numerical Recipes in Pascal*, (Cambridge University Press, 1989).

29. T. J. T. P. van den Berg and K. E. Tan, "Light transmittance of the human cornea from 320 to 700 nm for different ages," Vision Res. **34**, 1453-1456 (1994).

30. J. J. Vos, J. Walraven, and A. van Meeteren, "Light profiles of the foveal image of a point source," Vision Res. **16**, 215-219 (1976).

31. R. A. Bone, J. T. Landrum, L. Fernandez, and S. L. Tarsis, "Analysis of the macular pigment by HPLC: retinal distribution and age study," Invest. Ophthalmol. Vis. Sci. **29**, 843-849 (1988).

32. W. M. R. Broekmans, T. T. J. M. Berendschot, W. A. Klöpping, A. J. de Vries, R. A. Goldbohm, C. C. Tijssen, M. Karplus, and G. van Poppel, "Macular pigment density in relation to serum and adipose tissue concentrations of lutein and serum concentrations of zeaxanthin," Am. J. Clin. Nutr. **76**, 595-603 (2002).

33. J. M. Nolan, J. Stack, D. O. O', E. Loane, and S. Beatty, "Risk factors for age-related maculopathy are associated with a relative lack of macular pigment," Exp. Eye Res. **84**, 61-74 (2007).

34. J. van de Kraats, T. T. Berendschot, S. Valen, and D. van Norren, "Fast assessment of the central macular pigment density with natural pupil using the macular pigment reflectometer," J. Biomed. Opt. **11**, 064031 (2006).

35. I. Lengyel, A. Tufail, H. A. Hosaini, P. Luthert, A. C. Bird, and G. Jeffery, "Association of drusen deposition with choroidal intercapillary pillars in the aging human eye," Invest Ophthalmol. Vis. Sci. **45**, 2886-2892 (2004).

36. K. U. Loffler and W. R. Lee, "Basal linear deposit in the human macula," Graefes Arch. Clin. Exp. Ophthalmol. **224**, 493-501 (1986).

37. L. Feeney-Burns and M. R. Ellersieck, "Age-related changes in the ultrastructure of Bruch's membrane," Am. J. Ophthalmol. **100**, 686-697 (1985).

38. J. E. Grunwald, S. M. Hariprasad, and J. DuPont, "Effect of aging on foveolar choroidal circulation," Arch Ophthalmol **116**, 150-154 (1998).

39. R. S. Ramrattan, T. L. Vanderschaft, C. M. Mooy, W. C. Debruijn, P. G. H. Mulder, and P. T. V. M. Dejong, "Morphometric Analysis of Bruchs Membrane, the Choriocapillaris, and the Choroid in Aging," Invest. Ophthalmol. Vis. Sci. **35**, 2857-2864 (1994).

40. L. Feeney-Burns, E. S. Hilderbrand, and S. Eldridge, "Aging human RPE: morphometric analysis of macular, equatorial, and peripheral cells," Invest Ophthalmol Vis. Sci. **25**, 195-200 (1984).

41. T. Sarna, J. M. Burke, W. Korytowski, M. Rozanowska, C. M. Skumatz, A. Zareba, and M. Zareba, "Loss of melanin from human RPE with aging: possible role of melanin photooxidation," Exp. Eye Res. **76**, 89-98 (2003).

42. J. J. Weiter, F. C. Delori, G. L. Wing, and K. A. Fitch, "Retinal pigment epithelial lipofuscin and melanin and choroidal melanin in human eyes," Invest. Ophthalmol. Vis. Sci. **27**, 145-152 (1986).

43. M. Boulton, F. Docchio, P. Dayhaw-Barker, R. Ramponi, and R. Cubeddu, "Age-related changes in the morphology, absorption and fluorescence of

melanosomes and lipofuscin granules of the retinal pigment epithelium," Vision Res. **30**, 1291-1303 (1990).

44. N. P. Zagers and D. van Norren, "Photoreceptors Act as Spectrally Flat Reflectors," Invest. Ophthalmol. Vis. Sci. **44**, 2873 (2003).

45. S. S. Choi, N. Doble, J. Lin, J. Christou, and D. R. Williams, "Effect of wavelength on in vivo images of the human cone mosaic," J. Opt. Soc. Am. A **22**, 2598-2605 (2005).

46. S. A. Burns, S. Wu, J. C. He, and A. E. Elsner, "Variations in photoreceptor directionally across the central retina," J. Opt. Soc. Am. A **14**, 2033-2040 (1997).

47. B. Vohnsen, I. Iglesias, and P. Artal, "Guided light and diffraction model of human-eye photoreceptors," J. Opt. Soc. Am. A **22**, 2318-2328 (2005).

48. C. A. Curcio, C. L. Millican, K. A. Allen, and R. E. Kalina, "Aging of the human photoreceptor mosaic: evidence for selective vulnerability of rods in central retina," Investigative Ophthalmology Visual Science **34**, 3278 (1993).

Chapter 10

Summary
Samenvatting
About the author
Curriculum Vitae
Dankwoord
List of publications

Summary and conclusion

The main theme of this thesis is on the modeling of the optical reflection of the human fovea, and on the instruments build for retrieving the data.

Chapter 1
Here the outline of the thesis is provided, together with a simple anatomy of the eye with respect to the optical pathways.

Chapter 2
A historic overview is given of the electronics, computers, and instruments (co-)developed by the author in the past 40 years.

Chapter 3
In this chapter the instruments are described that were used to retrieve the data for this thesis. The data for the 1996 model paper (Chapter 4) were measured with densitometer version 4. A reflected spectrum from an illuminated spot on the human fovea of 14 discrete wavelengths could be measured not only in a state with the visual pigments bleached, but even in the dark adapted state of the retina. To achieve this, the light level for the measurement was just over 3 log Troland. To reach an acceptable signal to noise ratio in measuring a single reflection spectrum, about two minutes accumulation time were needed. For modeling the directional aspects, measurements were taken at the pupil position corresponding with the peak of the Stiles-Crawford effect (SCE), and at a position 2.5 mm from the peak. Allowing for visual pigment bleaching and regeneration at the four conditions took more than one hour.

De Lint showed a high correlation between the measured visual pigment density and the SCE. Thus, in most cases the SCE is probably sufficient for probing the optical condition of the fovea. The SCE is a steady state condition with no need for dark adapted measurements. For speeding up the measurement time, important in working with patients, a new instrument was developed; the Profile Spectrometer (ProfSpec). It needed much more light to achieve a good signal to noise ratio for a measurement in about one second. The possibility to measure a dark adapted retina was dropped. The first prototype of the ProfSpec, was build by Niels Zagers as part of his thesis work. He called it the Foveal Reflection Analyzer (FRA). The optical setup was on a large (and very heavy) optical bench that could be easily modified. A subjects' head had to be moved in all directions to align with the instrument. Later, much more compact instruments were developed for the thesis work of Martijn Kanis, the ProfSpec 2 and ProfSpec 3. These instruments could be aligned with a joystick, just like other ophthalmic instruments. In the measure time of about one second a complete dataset containing detailed spectral and directional information could be gathered. A spot of white light illuminated the retina. Reflected light from the retina fills the whole pupil of the eye. Using only the light passing through a slit from an imaging spectrometer positioned in the pupil plane, a two dimensional image from a CCD detector resulted, incorporating both the spectral, and the directional aspects. The challenge was to also model the data of this image.

To facilitate the measurement of macular pigment, the Macular Pigment spectrometer was build. It did not contain the extra CCDs for viewing the subjects' pupil and retina. It did not even contain the imaging spectrometer with the slit and the prism. Instead,

an external fiber optic spectrometer was applied, with the input mask of the fiber functioning as the limit of the retinal detection field. A Badal system, for focusing the retina and simultaneously acting as a pupil plane relay, was used with offset illumination and detection beams. These beams never hit the center of the lenses, and never overlapped in the lenses themselves to avoid ghost images and stray light from this stage of the instrument. In the pupil plane both the illumination and detection pupils fitted in a circle with 3 mm diameter. This made measurements in eyes with undilated pupil possible.
The intellectual property (IP) was sold by the UMC Utrecht to the US company Zeavision. A patent was applied for. Development of a commercial instrument is slowly moving on. Zeavision sells supplements to increase macular pigment, and intends to sell the apparatus to optometrists and ophthalmologists to advice their patients.

Chapter 4
The first model of the foveal reflection was presented in 1996. It was based on the Van Norren Tiemeijer 1986 model, and extended with cone receptors containing visual pigment. A new concept was the inherent non-directionality of layers posterior to the receptors. This pointed to the cone receptors as the source of the directional component in the foveal reflection (eureka moment 1). A second important message was that the origin of the directional reflection was at the cone discs (eureka moment 2). This concept was needed to bring the density of the visual pigment in line with values from the literature, based on other techniques. Supporting evidence has not appeared since. In the case of bleached visual pigment outcomes do not change much if instead of the discs, the end of the receptor outer segment is taken as the reflector. Further development of ultra high resolution Optical Coherence Tomography (OCT) will probably give a final answer in the coming years.

Chapter 5
In modeling the reflection from the retina, compensating for the transmission in the eye media is mandatory. In the 1996 model we used the Pokorny et al. templates. This was not completely satisfactory. Zagers presented two templates for the transmission of the lens (JOSA, dec. 2004). One for the young eye based on the spectral density of the biochemical substance 3HKG, and an additional one for the aging eye based on measurements from lens slices from Heckathorn et al. Zagers' proposal received criticism in a paper by Hammond and Wooten (JBO, sept. 2005) as the density was zero near 500 nm, contradicting psychophysical data. Personal comments came from Francois Delori and Joel Pokorny.
Therefore, a large literature investigation was started to find basic spectral shapes for the eye media. The literature data involved donor material, and from living human eyes, psychophysical and reflection data. Because aging has a profound effect on lens density, age was an important parameter. Finally, five templates proved sufficient and necessary to describe all literature data in great detail. For wavelengths shorter than 320 nm tryptophan absorption was present in all parts of the eye media (cornea, aqueous humor, lens, and vitreous). Losses due to Rayleigh scatter also appeared in all media. For the young lens the 3HKG template from Zagers was taken in a slightly modified form. For the old lens two templates were needed, one mainly functional in the UV, and one extending from the UV into the visual region. One (complex) formula was given to calculate the density of the human media for every wavelength, at any age.

Chapter 6
A spin-off from the work on the transmission of the eye media was a paper on optimal spectral shapes of the filters in intraocular lenses. These lenses are implanted after cataract surgery (removing the clouded lens at old age). The new implanted artificial lens should provide spectral filtering to prevent dangerous UV radiation, and violet light from reaching the retina. At the same time, the perception of violet and blue asks for minimal attenuation of short wavelengths. First, we retrieved from the literature all the spectra involved in this discussion. For the so called 'blue light damage' a very simple approximation of the spectrum based on the original data from Ham was proposed. For the light source, the spectrum of diffuse sunlight was used. Two literature sources of the suppression of melatonin with different spectra were brought in line by using our correction for the eye media. We measured several types of modern lenses which claimed to have sufficient filtering ('blue blockers'). Also data from the literature and datasheets from companies were used. The question is, what is the optimal trade-off between to be on the safe side for damaging the retina, and the loss of light for perception. We calculated these values for all lenses. It appeared that most older types of lenses, and even one claimed as a modern type, transmitted more dangerous UV radiation than the human lens at the age of 20. The lenses were labeled with a rating number based on the balance between damage and perception. This makes selection of lenses much easier.

Chapter 7
A paper strongly related to the one described in the previous Chapter concerns the concept of 'Virtual Age' of an IOL. The blue light damage and the loss of light for perception by the blue cones, was calculated as the virtual age; that is, the age of human lenses that have a comparable effect. Commercially available IOLs proved to have virtual ages ranging from < 0 to 61. With such data available the patient and/or the surgeon can make a selection based on a concept they are familiar with. The decision between a lens of the age of 40 or 60 years can be better understood than abstract scientific data. We advise the use of middle aged lenses.

Chapter 8
The macular pigment is a topic of research because of its assumed positive contribution in keeping a healthy retina at older age. The conventional way to measure the amount of macular pigment in the living human eye is by using heterochromatic flicker photometry (HFP). This psychophysical procedure requires active involvement of the subject. The technique is lengthy, and difficult to perform, especially for children and older subjects. Therefore the macular pigment instrument was developed (Chapter 3) to allow a measurement to be performed in a matter of seconds, and without active help of the subject.
The instrument measures the spectral reflection of the fovea through an undilated pupil. To keep the instrument cheap, it lacks the CCD cameras for viewing the pupil and the retina as present in the Profile Spectrometer (Chapter 3). The spectrum is analyzed with an optical model containing parameters for absorption in the lens, the macular pigment, and in blood and melanin. In addition there are parameters for reflection at the inner limiting membrane, the pigment epithelium, and the choroid. As the instrument because of the small pupil, also lacks the directional reflection information obtained with the Profile Spectrometer, some parameters are less precisely determined. In the paper in Chapter 8, the instrument is validated in terms of reproducibility and compared with results from other instruments. Macular pigment,

with its clearly distinct absorption spectrum, is determined very well with this instrument.

Chapter 9
A model explaining both the directional and the non-directional part of the foveal reflection is presented. It can be viewed as a next step in the evolution of the 1996 model, with elements from Zagers' publications, and newly included concepts. Zagers' description of the directional reflection with a neutral reflection from the cones, and absorption in the media and in macular pigment was complicated by the interaction of the spectra involved. The thesis work of Niels Zagers concentrated on modeling only the spectral reflection from the directional component in the pupil profile. Simultaneously modeling the non-directional background could not be achieved in his limited time frame. With the templates for the eye media found in Chapter 5, some uncertainties evaporated. With the much expanded spectrum measured by ProfSpec 2 and ProfSpec 3 compared to the Zagers instrument, a simple neutral reflector for the reflection from the cones did not satisfy, it now clearly dropped towards the longer wavelengths. The so-called Marcos effect for describing a wavelength dependent directionality for the cones was embraced by Zagers in its first order. Second order effects on the spectrum of the light reflected by the cones were neglected. In the new model the reflection from the cones is the combined effect of (1) spectrally flat reception by the cones (at perpendicular angle all light is captured by the cones and not lost in the cone interspaces), (2) the neutral Fresnel reflection at the cone discs, and (3) the one over wavelength squared behavior of the amplitude at perpendicular angle of the emitted light (the volume under the lobe is neutral). Simultaneously modeling the directional and of the non-directional reflection remained problematic. Using the same losses for the eye media in both, asked for strange absorbers in the non-directional reflection. A new insight, that light losses by scattering were not lost for the reflection from the layers posterior to the receptors solved it all (eureka moment 3). Very different looking measurements from young and old subjects could all be fitted very well. Aging of the lens, and the decrease of the reflection of the cones at older age, was found as expected in a group of normal subjects. Measurements in patients without any directional reflection are calling for special measures like setting certain parameters fixed in the model. These problems are presently tackled in the thesis work of Martijn Kanis.

In conclusion, instruments and optical models have been developed to measure and explain the light reflected from the human fovea. Age trends for media absorption in normal subjects were established. The results of this work are presently applied in an evaluation of the usefulness of the FRA in different groups of patients.

Samenvatting

Dit proefschrift beschrijft onderzoek aan het menselijke oog met behulp van licht. Voor het begrijpen van de metingen van de voor dit doel gebouwde instrumenten, is een optisch model ontwikkeld dat in de loop der jaren steeds meer verfijnd werd. Het oog is vaak vergeleken met een fotocamera. Er is een lens om een afbeelding te maken; in het oog wordt die lens gevormd door de kromming van het hoornvlies en de ooglens zelf. Deze laatste kan in sterkte variëren om dichtbij en veraf gelegen voorwerpen scherp te zien. Dit wordt op oudere leeftijd steeds lastiger omdat de lens verhard. We hebben dan een leesbril nodig. Verder is er in de fotocamera een irisdiafragma, dat de hoeveelheid binnengelaten licht regelt. In het oog is dit te vergelijken met de pupil. Bij veel licht wordt de pupil klein. Er moet wel opgemerkt worden dat de lichtvermindering d.m.v. een iris niet erg groot is, ongeveer een factor 10. Er is wel een bijbehorende verandering van de scherptediepte, die misschien wel belangrijker is. Dan is er in een camera de belangrijke fotografische plaat met de foto-emulsie. In het oog vervult het netvlies met de visuele pigmenten in de staafjes en kegeltjes die functie. Het visuele pigment is donker en absorbeert daarom licht. Die absorptie heeft een elektrische prikkel tot gevolg, die uiteindelijk leidt tot de waarneming. Absorptie leidt ook tot het transparant worden van het pigment. Dit donker en licht worden van het netvlies is met één van onze instrumenten te meten. In dit proefschrift beperken we ons tot het centrale stukje netvlies, de fovea. Hier kunnen we het scherpst mee zien. Er zijn voornamelijk kegeltjes aanwezig in een zeer dichte pakking. Er zijn drie soorten kegeltjes, elk gevuld met een verschillend pigment, in lekentaal de rode, groene, en blauwe kegels. Hiermee is kleurenzien mogelijk. De enorme gevoeligheidsvariaties die wij kunnen overbruggen worden grotendeels door mechanismen in de kegels zelf bepaald. Dit is nog het best vergelijkbaar met de sluitertijdregeling in een fotocamera.

De kegeltjes hebben optisch gezien speciale eigenschappen, want zij lijken op de ouderwetse televisie harkantennes. Recht vooruit zijn ze gevoelig, maar iets opzij daalt de gevoeligheid snel. Bij een televisieantenne onderdrukt dit storende zenders uit een andere richting, en verhoogd het de gevoeligheid aanmerkelijk. In het oog spelen vergelijkbare zaken een rol. Vanaf het netvlies gezien staan de kegels met maximale gevoeligheid op het midden van de pupil gericht. Licht door de randen van de ooglens (dat een minder scherp beeld zou geven) wordt zodoende verzwakt. Ook strooilicht afkomstig van andere delen van het oog wordt verzwakt. Het verschijnsel van de richtingsgevoeligheid van de kegeltjes werd al voor de tweede wereldoorlog door de onderzoekers Stiles en Crawford gevonden. Waar men eigenlijk nooit bij stilstaat, is dat een klein gedeelte van het licht dat op de kegels valt teruggekaatst wordt, en wel met dezelfde bundelingeigenschappen. Dit is een belangrijk element in het onderzoek binnen onze groep, want een normale bundeling betekent gezonde kegels, een verslechterde bundeling aangetaste kegels. Behalve de visuele pigmenten die nodig zijn voor de waarneming van licht, zijn er ook pigmenten in het oog die als een kleurfilter werken. Sommige filters zijn nodig voor de veiligheid van het oog. Ultraviolet (UV) licht kan namelijk het netvlies beschadigen. Het hoornvlies houdt al een belangrijk gedeelte van de optische straling tegen (beneden 320 nm). Het kamerwater tussen het hoornvlies en de ooglens is vrij transparant. De ooglens bevat een ander belangrijk filter voor UV licht, nl. dat beneden 400 nm. Bij het ouder worden vergeelt de lens en word er steeds meer kortgolvig licht tegengehouden. Ook wordt de lichtverstrooiing ongunstiger. Uiteindelijk kan de lens helemaal troebel worden, de zogenaamde staar. Tegenwoordig word de ooglens dan vervangen door een kunstlens. Het glasvocht is weer vrij transparant. Vlak voor het netvlies, en dan

voornamelijk geconcentreerd in de fovea, vinden we ook nog het macula pigment. Het is een (geel gekleurd) filter dat blauw licht sterk onderdrukt. Over de precieze functie van het maculapigment zijn de geleerden het niet eens. Het is mogelijk voornamelijk aanwezig om gevaarlijke zuurstofmoleculen weg te vangen en daarmee belangrijk voor het gezond houden van het netvlies. Het maculapigment bestaat uit de stoffen luteine en zeaxantine, die het lichaam niet zelf kan aanmaken. Ze komen via de voeding binnen. Vooral eigeel, spinazie, broccoli en maïs zijn belangrijk in dit verband.
Tenslotte moeten we nog twee andere filters noemen, bloed en melanine. Deze bevinden zich achter het netvlies. Bloed is er voor aanvoer van de noodzakelijke voedingsstoffen. Het is ook van groot belang voor de koeling van het netvlies als dat blootgesteld wordt aan veel licht. Melanine is het bruine pigment dat ook de huid donker kleurt. Achter het netvlies vangt het licht weg dat aan onze waarneming ontsnapt is. Het voorkomt zo hinderlijk strooilicht. Bij onze metingen zijn al deze filters belangrijke elementen waar we rekening mee moeten houden.

Hoofdstuk 2
Hierin word een kort overzicht gegeven van de apparatuur die voor het oogonderzoek ontwikkeld is binnen de afdeling Oogheelkundige Fysica.

Hoofdstuk 3
Alle in dit proefschrift besproken instrumenten werpen een klein rond lichtvlekje op de fovea en meten het licht dat terugkomt uit het oog. Dat is maar een zeer kleine fractie, in de orde van 1 op de 100.000. De meetapparatuur moet daarom zeer gevoelig zijn. Het eerste instrument dat we noemen is de Densitometer. De naam is afgeleid van densiteit, in ons geval de dichtheid van de visuele pigmenten. Er zijn verschillende versies gebouwd in de loop der jaren; we bespreken hier Densitometer 4. Die is opgebouwd rond een groot wiel met allerlei kleurfilters, gaten en spiegels. Het wiel draait 14 keer per seconde rond, en in elke omwenteling worden achtereenvolgens 16 verschillende kleuren doorgelaten. Het gereflecteerde licht wordt opgevangen door een zogenaamde photomultiplierbuis, een zeer gevoelige detector, die afzonderlijke lichtdeeltjes (fotonen) kan tellen.. Dit gebeurt door een kleine computer die ook bijhoudt van welke kleur licht ze afkomstig waren. Eén keer per seconde wordt dan als resultaat een gemeten spectrum verstuurd naar een gewone PC. Het licht nodig om te meten is zo zwak gehouden, dat de visuele pigmenten er nauwelijks door gebleekt (lees transparant) worden. Daarom is ook een tweede, maar dan heel felle lichtbundel beschikbaar om de pigmenten wel te bleken. Als deze lichtbron aan staat kan het netvlies bekeken worden door de proefleider om te zien of alles goed ingesteld staat. Na het uitschakelen van de lichtbron heeft het oog ongeveer 8 minuten nodig om weer de normale hoeveelheid visueel pigment voor de kegeltjes aan te maken. Ondertussen kan steeds gemeten worden. Er ontstaat zo een karakteristieke regeneratiekromme.
Een volledige meting van de reflectie in de condities donkergeadapteerd, en lichtgeadapteerd op het maximum van de kegelgevoeligheid en ernaast kostte ongeveer één uur.
Voor het meten aan patiënten is dit erg lang. Daarom werd een nieuw instrument bedacht, de Profiel Spectrometer (ProfSpec). Hierin werd ten eerste veel meer meetlicht gebruikt waardoor de meettijd teruggebracht kon worden tot ongeveer één seconde. Daarbij kwam nog dat niet alleen op het maximum van de kegelgevoeligheid werd gemeten, maar binnen diezelfde seconde ook een totale dwarsdoorsnede van de

gevoeligheid over de pupil kon worden bepaald. Dat leverde een klokvormige kromme op, meteen uiteen gesplitst in alle kleuren van het licht (spectrale analyse). Er moest hiervoor wel iets ingeleverd worden, namelijk het meten aan een donkergeadapteerd netvlies. De eerste praktische uitvoering van dit instrument werd gedaan door Niels Zagers als onderdeel van zijn promotieonderzoek. In zijn publicaties werd het apparaat bekend als de Foveale Reflectie Analysator (FRA). Om gemakkelijk wijzigingen in de optiek te kunnen doorvoeren, was alles op een grote (en loodzware) optische tafel gemonteerd. De proefpersonen moesten dan door het verplaatsen van hun hoofd, met hun oog op de juiste plaats achter het apparaat gemanoeuvreerd worden. Latere, veel compactere versies die ontwikkeld werden (ProfSpec 2, en ProfSpec 3) hadden dit bezwaar niet. Zij konden eenvoudig met een stuurknuppeltje op de juiste plaats voor het oog geplaatst worden. Momenteel worden deze beide apparaten gebruikt in het promotieonderzoek van Martijn Kanis. De uitdaging was allereerst het volledig begrijpen van de gegevens die uit het apparaat komen bij gezonde personen.
Maculapigment is een stofje in het netvlies waaraan beschermde eigenschappen worden toegeschreven. Gebruikelijke methoden voor het meten van maculapigment zijn gebaseerd op flikkerende lichtjes die door de patiënt moeten worden ingesteld op minimale flikker. Dit is voor kinderen en ouderen een soms moeilijk. Met onze ProfSpec kunnen we ook heel goed maculapigment meten. Het is echter een complex en daarom duur apparaat. We zochten daarom naar een goedkopere oplossing. Het resultaat was de Macula Pigment Reflectometer. Het moet het zonder de observatiecamera's van de pupil en van het netvlies doen. Ook is afgezien van het meten van de klokvormige gevoeligheidskromme van de kegels. Maar het apparaat heeft als groot voordeel dat met de natuurlijke pupil gemeten kan worden. Het instrument werpt weer een lichtvlekje op de fovea, en dit zelfde gebiedje word weer afgebeeld op de optische fiber van een commercieel verkrijgbare en redelijk betaalbare spectrometer.
Het instrument bleek heel goed te voldoen en het ontwerp is uiteindelijk verkocht aan een Amerikaanse firma die pillen verkoopt om de hoeveelheid macula pigment in het oog te verhogen. De firma wil het apparaat verkopen aan opticiens en oogartsen die dan hun patiënten kunnen adviseren. Een patent is geschreven en aangevraagd.

Hoofdstuk 4
Het eerste artikel in dit proefschrift uit 1996 beschrijft een computermodel over hoe het licht het oog binnenkomt, en vervolgens reflecteert aan verschillende lagen zoals de voorkant van het netvlies, de kegeltjes zelf, en de lagen achter het netvlies. Ondertussen worden ook de hiervoor genoemde absorberende stoffen gepasseerd, zoals die in de lens, in het macula pigment, in bloed, en in melanine. Door de computer aan (denkbeeldige) knopjes te laten draaien overeenkomend met de sterkte van reflecterende en de absorberende lagen, kan een spectrum gemaakt worden dat heel erg lijkt op de metingen. We mogen dan aannemen dat de stand van de knoppen erg lijkt op de overeenkomende lagen in het oog zelf. Het model had enkele bijzondere eigenschappen. Zo werd aangenomen dat het licht met gebundelde eigenschappen alleen maar van de kegels afkomstig kon zijn. Het niet gebundelde licht kwam dan van lagen vóór, of achter de kegels. Dit was een belangrijke ontdekking voor het algehele begrip van de reflectie van licht aan het netvlies. Een tweede veronderstelling was dat het licht in de kegels gereflecteerd werd aan de honderden gestapelde schijfjes waar ook het visuele pigment zit. Deze

veronderstelling maakte onze bepaling van de hoeveelheid visueel pigment vergelijkbaar met andersoortige bepalingen uit de literatuur.

Hoofdstuk 5
Om de reflectie van het licht aan het netvlies te begrijpen moet er gecompenseerd worden voor de spectrale verliezen in de oogmedia (voornamelijk hoornvlies en ooglens). Niels Zagers concentreerde zich op het begrijpen van de metingen van alleen de klokvormige component, afkomstig van de kegels zelf. De analyse van het gelijktijdig gemeten voetstuk onder de klok, afkomstig van lagen voor en achter de kegels werd (binnen de beperkte duur van zijn promotie) maar even gelaten voor wat het was. Eén van de uitkomsten van Zagers was de elementaire vorm van het absorptiespectrum van de jonge en van de ouder wordende ooglens. De laatste suggestie ondervond wel enige kritiek.
Om de juiste vorm hiervan te bepalen, en niet alleen uit te gaan van de bekritiseerde uitkomsten van Zagers, werd een zorgvuldig onderzoek gedaan naar wat er in de loop van de tijd in de literatuur voor informatie beschikbaar was. Er was materiaal van donor ogen, van waarnemingsproeven, en van allerlei types van reflectiemetingen. Omdat de lens bij het ouder worden steeds geler word, was leeftijd een belangrijke factor. Uiteindelijk lukte het met vijf basisvormen alle literatuurgegevens heel goed te beschrijven. De eerste basisvorm werd gekoppeld aan tryptofaan, een eiwit. Dit heeft alleen een absorptie in het verre UV beneden 320 nm. Het komt overal voor in de oogmedia. Als tweede basisvorm waren er de zogenaamde Rayleigh verliezen. Dit is een gevolg van lichtverstrooiing, vooral bij kortere golflengten. Dezelfde verstrooiing vindt ook in de atmosfeer plaats en maakt dat de hemel blauw ziet. De derde basisvorm is gekoppeld aan een pigment in de jonge ooglens; Zagers had dat ook al geconstateerd. Tenslotte vonden we twee absorptiespectra in de oudere ooglens, beide vooral actief in het UV, maar één ervan met zijn ‘staart’ tot in het zichtbare gebied. Voor alle basisvormen beschreven we de afhankelijkheid van de leeftijd. Zo werd uiteindelijk één grote formule gevonden om de verzwakking van het licht in de oogmedia te beschrijven, voor alle golflengten, en voor alle leeftijden. Met een PC is het dan een fluitje van een cent om zoiets uit te rekenen. We hebben goede hoop dat deze formule brede toepassing zal vinden.

Hoofdstuk 6
Een zijsprong van het onderzoek naar de spectrale verliezen in de oogmedia, was het vinden van het juiste kleurfilter in implantlenzen. Dat zijn de lenzen die na een staaroperatie in het oog worden geplaatst. UV licht, en in mindere mate violet en blauw licht, kan namelijk erg schadelijk voor het netvlies zijn. Dus dat willen we zoveel mogelijk tegenhouden. Aan de andere kant is teveel kortgolvig licht tegenhouden ongunstig voor de waarneming. Ook pas ontdekte vormen van onbewuste waarneming voor het aansturen van de oogpupil, en voor het in de pas houden van het dag-nacht ritme werden bekeken, Als eerste werd opnieuw gekeken naar de vorm van de zogenaamde blauwlicht schade aan het netvlies. Op basis van een nieuwe interpretatie van de literatuur werd hiervoor een heel eenvoudige formule gevonden. Als lichtbron namen we diffuus daglicht.
Oudere typen implantlenzen lieten vaak veel te veel UV en/of blauw licht door. We hebben van een aantal moderne lenzen, die claimen dat ze erg veilig zijn, het absorptiespectrum gemeten. We gebruikten ook gegevens uit de literatuur en van fabrikanten. Nu al deze spectra bekend waren, konden we de werkelijke (potentiële) lichtschade aan het netvlies en de invloed op de waarneming uitrekenen. Vervolgens

hebben we dat afgezet tegen de uitkomsten van een lens van een 20 jarige. Nu is het relatief inzichtelijk een keuze van de gewenste implantlens te maken.

Hoofdstuk 7
In een hiervan afgeleid verhaal probeerden we het nog inzichtelijker te maken door de getallen te presenteren als de vergelijkbare leeftijd van een menselijke lens. Een 60 jarige lens bijvoorbeeld is erg veilig wat betreft blauwlichtschade, maar minder gunstig voor waarneming van blauw licht. Een 20 jarige lens is veel transparanter. Dat is gunstig voor de waarneming, maar met wat meer kans op netvliesschade. Die zg. virtuele leeftijd van implantlenzen maakt het zowel voor de chirurg en als voor de patiënt gemakkelijker een keuze te maken uit bijvoorbeeld een type van een 40 of 60 jarige. Het bleek overigens dat een aantal moderne lenzen op een leeftijd beneden 0 jaar uitkwam. De fabrikanten hiervan moeten dus diep gaan nadenken over de eigenschappen van hun product.

Hoofstuk 8
Maculapigment is erg in de belangstelling vanwege zijn veronderstelde belang voor het gezond houden van het netvlies op oudere leeftijd. Meer lijkt dan beter. Eten van bijvoorbeeld eieren, broccoli, spinazie en maïs, maar ook het slikken van speciaal hiervoor op de markt gebrachte pillen, zijn een manier om dit pigment op peil te houden of zelfs in dichtheid te verhogen. De gebruikelijke manier om de hoeveelheid macula pigment te meten is een ingewikkelde en langdurige waarnemingsproef met flikkerende lichtjes. Vooral voor ouderen is dit een lastige taak. We ontwikkelden daarom een speciaal instrument voor het meten van maculapigment, de Macular Pigment spectrometer (hoofdstuk 3). Dit is een vereenvoudigde versie van de Profiel Spectrometer. Het apparaat meet, bij een onverwijde pupil, de spectrale reflectie; daarna volgt een modelanalyse waaruit als parameter de dichtheid van het maculapigment komt. De metingen bleken betrouwbaar.

Hoofdstuk 9
Het laatste artikel, dat nog onderweg is voor publicatie in een tijdschrift, gaat over een nieuw model van de reflectie van het netvlies. Het model kan gelijktijdig de eigenschappen van het gerichte licht van de kegels, en het niet gerichte licht van lagen vóór, en achter de kegels verklaren. Het is eigenlijk een verfijning van het model uit 1996, met resultaten van Zagers, en een aantal nieuwe inzichten. Zagers had aangenomen, uitgaande van het 1996 model, dat de reflectie van de kegels voor alle golflengten gelijk was. Hiermee kon hij de vorm van de lichtabsorptie in macula pigment en de oogmedia bepalen. Zijn golflengte gebied was echter beperkt tot 420 - 700 nm. Achteraf kan gezegd worden dat dit te beperkt was om juiste uitspraken te doen. Met de nieuwere ProfSpec 2 en ProfSpec 3 loopt het golflengte gebied van 400 tot 950 nm. Met de nieuw gevonden basisvormen voor de oogmedia kon een veel betere uitspraak gedaan worden over het neutraal zijn van de kegelreflectie. Ten eerste werd op theoretische gronden uit de (antenne theorie) geconcludeerd dat bij loodrechte inval er geen licht tussen de kegels doorlekt. Alle golflengten worden dus even goed opgenomen door de kegels. Ten tweede wordt nog steeds zoals in het model uit 1996 de reflectie aan de schijfjes in de kegels neutraal verondersteld (Fresnell reflectie). Ten derde, en dat is nieuw, de bundelingeigenschappen zijn nu golflengte afhankelijk. Dit is in de literatuur door Marcos in 1998 voor het eerst beschreven, en door Zagers experimenteel bevestigd. Met een scherpere bundeling bij

kortere golflengten, en het neutrale aspect van punt 1 en punt 2, moet de amplitude op de piek wel groter worden.
Met het begrip van de gebundelde kegelreflectie was de niet gebundelde diffuse reflectie van de lagen voor en achter de kegels alleen met erg vreemd-vormige absorptiespectra kloppend te krijgen. Pas nadat het kwartje gevallen was, dat het verstrooide licht in de oogmedia in de lagen achter de kegeltjes door hernieuwde verstrooiing weer in het meetveld terecht kwam, lukte de aanpassing opeens uitstekend. Zowel metingen van jonge als van oude ogen, met weinig of met veel maculapigment werden door het nieuwe model verklaard. In normale proefpersonen kwamen het verouderen van de ooglens, en de verminderde reflectie van de kegels op oudere leeftijd, zoals gevonden door Zagers, duidelijk naar voren. Metingen aan patiënten waarbij de bundeling van de kegels soms helemaal ontbreekt, heeft weer zijn eigen uitdagingen. Dit is een van de zaken waar Martijn Kanis zich in zijn promotieonderzoek mee bezig houdt.

Concluderend, we ontwikkelden computermodellen over hoe het licht door het centrale deel van het netvlies wordt gereflecteerd. Daarmee kunnen we de meetgegevens begrijpen van de door ons ontwikkelde instrumenten. Voor normale proefpersonen werd het leeftijdsaspect onderzocht. Voor patiënten is het onderzoek nog in volle gang.

About the Author

The author of this thesis was born on October 17, 1949 in Putten, The Netherlands. On advice of his father he followed an education in electro-engineering at the Technical School in Harderwijk. This was, at that time, somewhat unusual for a farmers' son. A next higher level in electro-engineering was followed in Utrecht. By lack of financial means for further education he looked for a job. It became the RIHA company in Harderwijk, where electronic organs were build. His job was to test and solve problems in the end product. Shortly thereafter (in 1968) he was asked by the University Utrecht to apply for a job of electronic designer at the Ooglijdersgasthuis hospital in Utrecht. They knew him from a period of practical education there. In 1989 the Ooglijdersgasthuis was integrated in the new University Hospital in Utrecht, were he is currently employed.
The thesis work was done at this site under the responsibility of professor Dirk van Norren, PhD.

Curriculum Vitae

De auteur van dit proefschrift werd geboren op 17 oktober 1949 te Putten. Mede op advies van zijn vader volgde hij, in die tijd enigszins bijzonder als boerenzoon, een elektrotechniekopleiding aan de Ambachtschool te Harderwijk. Na de Ambachtschool volgde hij een vervolgopleiding op de Uitgebreid Technische School (UTS) Scutos te Utrecht. Wegens ontbrekende financiële middelen was er geen verdere dagopleiding weggelegd. Een latere Hogere Technische School opleiding in de avonduren werd halverwege afgebroken wegens andere bezigheden. Er volgde een baan van 3 maanden bij de elektronische orgelfabriek RIHA te Harderwijk, als tester en probleemoplosser van het eindproduct (1968). Kort daarop werd hij wegens een positief verlopen stage vanuit de UTS (1967), gevraagd om bij de afdeling Medische en Fysiologische Fysica van de Universiteit van Utrecht te komen werken. Van daaruit werd hij gedetacheerd bij het Koninklijk Nederlands Gasthuis voor Ooglijders te Utrecht in de functie van elektronicus (1968-1981). Dezelfde functie, inmiddels onder de vlag Research Medewerker bij de groep Oogheelkundige Fysica, werd voortgezet in dienst van het Ooglijdersgasthuis (1981-1989) en na de integratie bij het UMC Utrecht (1989-heden).
Het promotieonderzoek werd uitgevoerd bij deze groep onder leiding van prof. Dr. D. van Norren.

Dankwoord

Op deze plaats wil ik iedereen bedanken die mij als collega, als familielid of als vriend of vriendin heeft ondersteund, in welke vorm dan ook, bij de totstandkoming van dit proefschrift. Hieronder moet ook worden verstaan de prettige samenwerking en de morele ondersteuning. Een aantal mensen wil ik graag persoonlijk noemen,

Dick van Norren, jou komt alle eer toe als de drijvende kracht om dit proefschrift te schrijven. Wij kennen elkaar al heel lang, nog van tijdens je eigen promotieonderzoek bij TNO Soesterberg. Later werd je, voor één dag in de week, hoofd van onze afdeling Oogheelkundige Fysica in het Ooglijdersgasthuis. Dit is een gelegenheid om op te merken dat onze samenwerking altijd bijzonder prettig is geweest. Je hebt me altijd alle vrijheid en ondersteuning gegeven om mijzelf in mijn functie verder te ontwikkelen. Toen ik later zelf wetenschappelijke artikelen begon te produceren was jij de niet aflatende meedenker en corrector van mijn, vooral in het begin, matige kennis om een goed stuk te produceren. In de huidige fase ben je een ware evangelist van mijn gedachtegoed, door het op congressen en symposia wereldkundig te maken. Behalve een baas ben je ook een goede vriend gebleken, zoals ik ondervonden heb in persoonlijk moeilijke tijden. Als laatste moet genoemd worden dat je ondanks je emeritaat nog steeds heel veel tijd in ons en onze afdeling investeert.

Pien van Norren, uit de voorgaande zin blijkt al dat Dick ondanks zijn pensioen veel tijd besteed aan onze afdeling en daarom niet aan gezellige dingen met jou. We kunnen ons voorstellen dat de vele telefoontjes van onze kant je weleens in een minder prettige stemming gebracht zullen hebben. Toch was je altijd buitengewoon aardig en meelevend; heel veel dank hiervoor.

Tos Berendschot, ook met jou heb ik vele jaren samen gewerkt op een hele prettige manier. In de privésfeer zal ik altijd terugdenken aan de doedelzakserenade op mijn boerderij en het abseilen vanaf mijn windmolen. Helaas is de afstand nu je in Maastricht werkt een belemmering om even langs te gaan. Gelukkig zijn de telefoon en email vaak goede vervangers. Behalve het nog lopende gemeenschappelijke onderzoek is ook de uitgeleende apparatuur een reden elkaar weer te zien.

Gerjan van der Wildt, jij was aan het begin van mijn loopbaan degene die mij altijd bij het onderzoek betrok en mijn fantasie prikkelde. Je stimuleerde mij om in de avonduren HTS elektrotechniek te gaan studeren; dat heb ik niet afgemaakt, mede omdat ik al zo'n interessante baan had waar ik alles in kwijt kon. Daarbij was de elektrotechniek toen voornamelijk gericht op installaties en motoren. Dat was wellicht goed van pas gekomen in onze vroegere activiteiten op privé gebied, namelijk het opwekken van windenergie. Ik vergeet niet gauw het moment dat ik tijdens je vakantie de gelegenheid gebruikte om je meetopstelling grotendeels om te gooien. Helaas was het bij je terugkeer nog niet af. Het is goed afgelopen; nog steeds zoeken we elkaar enkele keren per jaar op.

Aart Kooijman, jij was tijdens mijn stageperiode in 1967 nog student op het Ooglijdersgasthuis, en met jou heb ik de eerste stappen gezet op het gebied van de wetenschap door mee te doen aan het onderzoek van de pupilbewegingen. De pupillograaf die hiervoor nodig was werkte met een Nipkov schijf die als een stofzuiger in het rond gierde. Ik denk ook nog met een glimlach terug aan de aanschaf van een statiegeldfles Bokma, die diende als een met water gevuld cuvet voor de onderdrukking van infrarood licht.

Maarten Bouman, als hoofd van de afdeling Medische en Fysiologische Fysica van de Universiteit van Utrecht heb je er voor gezorgd dat mijn functie gecreëerd werd. Later heb je er voor gezorgd dat Dick van Norren hoofd van onze groep werd.

Daarvoor heb ik een tijd alleen geprobeerd het onderzoek gaande te houden; je kwam elke week langs voor nuttige discussies.

Annette Ossewaarde-van Norel, ik dank je voor de warme vriendschapsband die wij mogen hebben. Je hebt als een van de weinigen lange tijd een kamer met mij gedeeld, en je hebt tijdens moeilijke privé omstandigheden mij hernieuwde moed gegeven het leven weer op te pakken. Promoveren valt hierbij in het niet.

Mary van Schooneveld, Pieter van den Biesen, en Peter Schellekens, ook al zijn onze huidige ontmoetingen vaak niet meer dan van het vluchtige soort op de gang, toch wil ik jullie als voormalige leden van onze werkgroep hier speciaal noemen.

Hans Vos, pas de laatste jaren heb ik je beter leren kennen. Bedankt voor je wetenschappelijke adviezen, voor het corrigeren van enkele van mijn artikelen, en bovenal voor al je niet aflatende bereidwilligheid hierin. Ik ben jaloers op jouw wetenschappelijke en didactische kennis en niet te vergeten je goede geheugen.

Voormalige promovendi en collega's, Daan van Hoek, Ton Scholtes, Jan Slooter, Gerard van Meel, Jan Keunen, Theo Gorgels, Eelco Busch, Albert Liem, Peter Jaap de Lint, Niels Zagers, en als laatste nog onderweg Martijn Kanis, bij een ieder van jullie zou ik een heel (positief) verhaal kunnen vertellen, te lang voor deze plaats. Een uitzondering wil ik maken voor mijn huidige collega promovendus Martijn voor het gebruik mogen maken in dit proefschrift van zijn metingen en niet te vergeten de aangename discussies over auto's repareren, computer problemen en huizen verbouwen.

Collega's van de functie afdeling, jullie zullen wel vaak gedacht hebben wat doen ze daar eigenlijk. De contacten met jullie, vaak ook bij de koffieautomaat en met het vieren van verjaardagen waren altijd zeer plezierig. Met name Celia wil ik bedanken voor het in de gaten houden van mijn kleding.

Birgit Wilms, Op mijn dagelijkse rondje langs de post was er altijd een opgestoken hand van jou.

Collega's van de instrumentele dienst, met name de vroegere collega's nog van het Ooglijdersgasthuis Jan Scheerder en Cees van der Linden, voor het vervaardigen van de vele apparaten vanaf mijn werktekeningen op papier waren jullie onmisbaar.

Lieve Roel en Jasper, als mijn zonen zijn jullie mij zeer dierbaar. Nu treden jullie gezamenlijk op als paranimf op mijn promotie; wie had dat ooit kunnen bedenken. Toen jullie jong waren kon ik dagelijks mijn kennis op jullie botvieren. Ik weet dat ik met mijn enthousiasme voor de meccanodoos hierin te ver gegaan ben; die verdween onder het bed. Door in het vervolg de zaken wat meer te doseren, ging het beter en hadden we vaak fantasievolle discussies zoals over een robot die onkruid zou kunnen wieden in de mais. Nu hebben jullie beiden een eigen gezin en zien we elkaar minder vaak dan toen jullie nog thuis woonden. Het is in ieder geval een groot genoegen veel dingen van mezelf weer in jullie terug te zien.

Lieve Corrie en Diny, met jullie heb ik vele jaren het leven gedeeld. Ik ben jullie nog steeds dankbaar voor al het goede dat jullie mij gegeven hebben. Intussen ben ik ouder en wellicht milder geworden. Nu, gedurende het samenstellen en afronden van mijn proefschrift voel ik mij ondersteund door de liefde gevonden met Joanke.

Publications by Jan van de Kraats.

First author

1. J. van de Kraats and J. H. Slooter, "Objective measuring techniques with the aid of pupillography," Ophthalmologica **175**, 51-52 (1977).

2. J. van de Kraats, T. T. J. M. Berendschot, and D. van Norren, "The pathways of light measured in fundus reflectometry," Vision Res. **36**, 2229-2247 (1996).

3. J. van de Kraats, T. T. J. M. Berendschot. and N. P. A. Zagers. “Apparatus and method for measurement of specific characteristics of eyes.” Patent WO2002NL00290 20020502[WO02087427]. Universiteit Utrecht. 11-7-2002.

4. J. van de Kraats, T. T. J. M. Berendschot, D. van Norren, “Reflectometry instrument and method for measuring macular pigment” [52871-00009USPT]. Applied for patent 2006.

5. J. van de Kraats, T. T. J. M. Berendschot, S. Valen, and D. van Norren, "Fast assessment of the central macular pigment density with natural pupil using the macular pigment reflectometer," J. Biomed. Opt. **11**, 064031 (2006).

6. J. van de Kraats and D. van Norren. “Optical density of the young and aging human ocular media in the visible and the UV,” J. Opt. Soc. Am. A, July (2007).

7. J. van de Kraats and D. van Norren. “Sharp cutoff filters in intraocular lenses provide optimal protection,” J. Cataract Refr. Surgery 33, 879-887 (2007).

8. J. van de Kraats and D. van Norren. “Modeling the directional and non-directional spectral reflection from the human fovea,” submitted.

Co-author

1. T. T. J. M. Berendschot, J. van de Kraats, and D. van Norren, "Foveal cone mosaic and visual pigment density in dichromats," J. Physiol. **492**, 307-314 (1996).

2. T. T. J. M. Berendschot, R. A. Goldbohm, W. A. Klöpping, J. van de Kraats, J. van Norel, and D. van Norren, "Influence of lutein supplementation on macular pigment, assessed with two objective techniques," Invest. Ophth. Vis. Sci. **41**, 3322-3326 (2000).

3. T. T. J. M. Berendschot, J. van de Kraats, and D. van Norren, "Wavelength dependence of the Stiles-Crawford effect explained by perception of backscattered light from the choroid," J. Opt. Soc. Am. A **18**, 1445-1451 (2001).

4. P. J. DeLint, T. T. J. M. Berendschot, J. van de Kraats, and D. van Norren, "Slow optical changes in human photoreceptors induced by light," Invest. Ophth.. Vis. Sci. **41**, 282-289 (2000).

5. A.T. Liem, J.E. Keunen, D. van Norren, and J. van de Kraats, "Rod densitometry in the aging human eye," Invest. Ophth.. Vis. Sci. **32**, 2676-2682 (1991).

6. G.J. van der Wildt, M.A. Bouman, and J. van de Kraats, "The effect of Anticipation on the Transfer Function of the Human Lens System," Optica Acta **21**, 843-860 (1974).

7. G. J. Van Meel, D. van Norren, and J. van de Kraats, "Scanning Laser Densitometry in 2 Patients with Retinitis-Pigmentosa," Clin. Vis. Sci. **7**, 501-509 (1992).

8. G. J. van Meel, J. E. Keunen, D. van Norren, and J. van de Kraats, "Scanning laser densitometry in multiple evanescent white dot syndrome," Retina **13**, 29-35 (1993).

9. J. Ossewaarde-Van Norel, P. R. van den Biesen, J. van de Kraats, T. T. J. M. Berendschot, and D. van Norren, "Comparison of fluorescence of sodium fluorescein in retinal angiography with measurements in vitro," J. Biomed. Opt. **7**, 190-198 (2002).

10. D. van Norren and J. van de Kraats, "A continuously recording retinal densitometer," Vision Res. **21**, 897-905 (1981).

11. D. van Norren and J. van de Kraats, "Interactive computer program for clinical electrophysiology," Doc. Ophthal. Proc. Ser. **37**, 193-197 (1983).

12. D. van Norren and J. van de Kraats, "User friendly system for electrodiagnosis," Doc. Ophth. **58**, 251-256 (1984).

13. D. van Norren and J. van de Kraats, "Retinal densitometer with the size of a fundus camera," Vision Res. **29**, 369-374 (1989).

14. D. van Norren and J. van de Kraats, "Imaging retinal densitometry with a confocal Scanning Laser Ophthalmoscope," Vision Res. **29**, 1825-1830 (1989).

16. D. van Norren and J. van de Kraats, "Spectral transmission of IOLs expressed as a virtual age," in press.

17. N. P. A. Zagers, J. van de Kraats, T. T. J. M. Berendschot, and D. van Norren, "Simultaneous measurement of foveal spectral reflectance and cone-photoreceptor directionality," Appl. Opt. **41**, 4686-4696 (2002).

Book Chapter

1. D. van Norren and J. van de Kraats, "Imaging retinal densitometry with a confocal Scanning Laser Ophthalmoscope," in *Scanning Laser Ophthalmoscopy and Tomography*, J. E. Nasemann and R. O. W. Burk, eds., Quintessenz, Munchen, Germany, 127-132 (1990).

Stellingen

Behorend bij het proefschrift
"Harvesting the weak angular reflections from the fundus of the human eye"
Jan van de Kraats

1. De verzwakking van licht in de oogmedia en de afzonderlijke delen daarvan, kan voor elke golflengte en voor elke leeftijd berekend worden met één formule. *Dit Proefschrift.*

2. Het glucose niveau in het bloed heeft geen invloed op de regeneratietijd van het visuele pigment.

3. De optische eigenschappen van een menselijke kegel zijn meer verwant aan die van een ouderwetse televisie antenne van het Yagi type, dan aan die van een optische golfpijp

4. De felle blauwe LEDs die nu op de markt komen, hebben een intensiteit die gevaarlijk kan zijn voor het netvlies. *Photonic Spectra feb 2007 p66-68.*

5. Het twee-spleten-experiment van Young kan maar tot één conclusie leiden, namelijk dat de ruimtelijke afmeting van een foton groter is dan de afstand tussen de spleten.

6. Het foton als quantum is een eigenschap die tot uiting komt in de interactie van licht met materie, en is niet een eigenschap van het licht zelf.

7. Dat CCD camera's met de hoogste gevoeligheid van het type EMCCD in tegenstelling tot hun oorspronkelijke broertjes minder lineair zijn, wordt door fabrikanten liefst verzwegen.

8. Met het gebruik van de menselijke huid als laser materiaal, kan na de periode van geestelijk verlichting in de 17de en 18de eeuw, in de 21ste eeuw een periode van fysieke verlichting worden gedacht. *Applied Physics Letters 2004 vol 85 number 7 p1289-1291.*

9. De opdracht "Onderzoek alles en behoud het goede" (*de Bijbel; 1 Tess. 5:21*) is ook van toepassing op de bron zelf.

10. Bij het zoeken van locaties voor windturbines moet bedacht worden dat zogenaamde horizonvervuiling in een bosrijke omgeving veel minder is dan in het vlakke polderland.

11. Een praktische aanwijzing voor het afstand houden in de file is het gelijk houden van de ruimte tot de voorganger en de ruimte tot de achterop komende auto.

12. Bij het uitbreken van een hongerperiode door bijvoorbeeld een oorlogssituatie, zal het geheugen van de boer niet bijdragen tot een ruimhartige verdeling van voedsel.

13. Het is moeilijk toegeven voor de natuurliefhebber, dat de mens niet altijd de schuldige is van een teruggang van een diersoort.

14. In het Romeinse leger trof decimeren 1 op de 10, niet 9 van de 10. *Wikipedia.nl*

15. De windturbine industrie in Nederland is ernstig beknot door zwalkend overheidsbeleid.

16. Het gebruik van Viagra in het weekeinde kan leiden tot een blauwe maandag. *Sildenafil (Viagra) and Ophthalmology Archives of Ophthalmology. Marmor 1999 vol:117 iss:4 p518.*

17. Internetdating vereist multiprocessor capaciteiten.

illumination
detection
total reflection seen by instrument
Anterior eye
media absorption (d_{LY}, d_{LO}, d_{RL}, Th_{water})
reflection from ILM
ILM reflex (R_{ILM})
macular pigment (d_{MP})
Receptor layer
Directional reflection from receptor discs
cone receptors (R_{disc}, rho, X_0)
non-directional reflection from deeper layers
Deeper layers
reflection from RPE
RPE (R_{rpe})
melanin (d_{mel})
blood (Th_{blood})
reflection from choroid
choriod (R_{cho})